Downloaded from orbit.dtu.dk on: Dec 18, 2017

Technical University of Denmark

Spatio-Temporal Encoding in Medical Ultrasound Imaging

Gran, Fredrik; Jensen, Jørgen Arendt; Nikolov, Svetoslav; Tomov, Borislav Gueorguiev

Publication date:
2005

Link back to DTU Orbit

Citation (APA):
Gran, F., Jensen, J. A., Nikolov, S., & Tomov, B. G. (2005). Spatio-Temporal Encoding in Medical Ultrasound Imaging.

DTU Library
Technical Information Center of Denmark

General rights
Copyright and moral rights for the publications made accessible in the public portal are retained by the authors and/or other copyright owners and it is a condition of accessing publications that users recognise and abide by the legal requirements associated with these rights.

- Users may download and print one copy of any publication from the public portal for the purpose of private study or research.
- You may not further distribute the material or use it for any profit-making activity or commercial gain
- You may freely distribute the URL identifying the publication in the public portal

If you believe that this document breaches copyright please contact us providing details, and we will remove access to the work immediately and investigate your claim.

Spatio-temporal encoding in medical ultrasound imaging

Fredrik Gran

July 1, 2005

Center for Fast Ultrasound Imaging
Ørsted·DTU
Technical University of Denmark
2800 Kgs. Lyngby
Denmark

SUBMITTED IN PARTIAL FULFILLMENT OF THE
REQUIREMENTS FOR THE DEGREE OF
DOCTOR OF PHILOSOPHY
AT
THE TECHNICAL UNIVERSITY OF DENMARK
JULY 2005

Signature of Author

THE AUTHOR RESERVES OTHER PUBLICATION RIGHTS, AND NEITHER THE THESIS NOR EXTENSIVE EXTRACTS FROM IT MAY BE PRINTED OR OTHERWISE REPRODUCED WITHOUT THE AUTHOR'S WRITTEN PERMISSION.

THE AUTHOR ATTESTS THAT PERMISSION HAS BEEN OBTAINED FOR THE USE OF ANY COPYRIGHTED MATERIAL APPEARING IN THIS THESIS (OTHER THAN BRIEF EXCERPTS REQUIRING ONLY PROPER ACKNOWLEDGEMENT IN SCHOLARLY WRITING) AND THAT ALL SUCH USE IS CLEARLY ACKNOWLEDGED.

© Copyright by Fredrik Gran 2005
All Rights Reserved

Contents

Contents **i**

Preface **v**

Acknowledgments **vii**

Abstract **ix**

List of Abbreviations **xi**

List of Symbols **xiii**

1 Introduction **1**

2 A linear description of ultrasound **5**
- 2.1 The linear wave equation 5
  - 2.1.1 The linearized equation of state 6
  - 2.1.2 The linearized continuity equation 7
  - 2.1.3 The linear inviscid force equation 8
  - 2.1.4 The velocity potential 9
  - 2.1.5 The wave equation 10
- 2.2 The Rayleigh integral 11
- 2.3 Spatial impulse responses 13
- 2.4 Summary 14

3 Ultrasound imaging **15**
- 3.1 Beamforming 15
  - 3.1.1 Delay and sum beamforming 16
  - 3.1.2 The Fourier relation for an imaging system 17
- 3.2 Conventional ultrasound imaging 18
  - 3.2.1 Linear array imaging 21
  - 3.2.2 Phased array imaging 22
- 3.3 Synthetic aperture ultrasound imaging 22
  - 3.3.1 The mono-static approach 24
  - 3.3.2 Synthetic transmit aperture ultrasound imaging 24
  - 3.3.3 Virtual sources 25
- 3.4 Summary 26

4 **Previous work on the topic of coded ultrasound** 29
4.1 Temporal encoding 29
4.1.1 The matched filter 30
4.1.2 The linear frequency modulated signal 32
4.1.3 Complementary code sequences 37
4.2 Spatial encoding 42
4.2.1 The general model 42
4.2.2 Hadamard encoding 43
4.2.3 Complementary code sequences revisited 44
4.2.4 Pseudo random code sequences 46
4.3 Summary 49

5 **Spatial encoding by means of frequency division** 51
5.1 Basic principle 51
5.2 Code and filter design 54
5.2.1 Linear phase waveforms 54
5.2.2 Narrow band linear frequency modulated signals 58
5.3 Signal to noise ratio 59
5.4 Applications 62
5.5 Frequency division ultrasound imaging 62
5.6 Summary 67
5.7 Conference paper: Multi Element Synthetic Aperture Transmission using a Frequency Division Approach 69
5.8 Journal paper: Frequency Division transmission imaging and synthetic aperture reconstruction 77
5.9 Conference paper: Spatio-temporal encoding using narrow-band linear frequency modulated signals in synthetic aperture ultrasound imaging 99
5.10 Journal paper: Directional velocity estimation using a spatio-temporal encoding technique based on frequency division for synthetic transmit aperture ultrasound 113

6 **Spatial encoding by means of code division** 133
6.1 Basic principles 134
6.2 The Maximum Likelihood Estimate of the wave propagation operator 136
6.3 Solving for the Maximum Likelihood Estimate 136
6.4 Mean square estimation error 137
6.5 Water tank experiments 138
6.6 Summary 143
6.7 Conference paper: A code division technique for multiple element synthetic aperture transmission 145
6.8 Conference paper: Identification of pulse echo impulse response for multi source transmission (Invited) 155
6.9 Journal paper: Spatial encoding using a code division technique for fast ultrasound imaging 163

7 **Co-authored contributions** 181
7.1 Conference paper: Fast color flow mode imaging using plane wave excitation and temporal encoding 183
7.2 Conference paper: Further development of synthetic aperture real-time 3d scanning with a rotating phased array 195

8 Conclusion **201**

Bibliography **203**

Preface

Someone once said: time flies when you are having fun. Indeed it does. When I started the journey which has taken me to where I am today, I could never have imagined that time would pass by so quickly. To illustrate this, during one of my first Wednesday meetings at CFU, I recall that the following statement was said

"... boxcar apodization both in transmit and receive will effect your lateral contrast ..."

Having no previous experience with the field of medical ultrasound, naturally, I did not understand a word of that sentence. There was nothing wrong with my capabilities of understanding the English language, but the meaning of the sentence was a complete mystery to me. It might seem trivial, but today, being able to understand what could have been meant by this collection of words, makes me realize how much I have learned during the years at CFU. I feel incredibly thankful to the people with whom I have been working, for teaching me about the wonderful world of ultrasound.

I hope you will enjoy reading this dissertation as much as I have
enjoyed working with medical ultrasound.

Fredrik Gran
Lyngby
July 2005

Acknowledgments

First of all I would like to thank my advisor Prof. Jørgen Arendt Jensen for making this research project possible, for providing the necessary equipment and the working environment for conducting the research associated with this project. I am also thankful for the guidance you have given me during this project and for proof-reading all my papers with criticism. Most of all I appreciate having been able to work independently, and mature into an independent researcher.

I would also like to thank Dr. Svetoslav Nikolov for being my ″second″ advisor, for always finding the time to help me with my problems work related or not, for helping me understand the mysterious world of beamforming and for being a good and helpful colleague.

Also Dr. Borislav Tomov, deserves a big Thank You for putting up with my complaining about hardware related issues and for always being helpful when the sampled signals were ″just not right″.

I would like to thank Dr. Kim Gammelmark, Dr.($\times 2$) Morten Høgholm, Dr. Malene Schlaikjer, Loise Kold Taylor and later also Jakob Kortbek and Niels Oddershede for creating a dynamic and interesting research group.

Special thanks goes to Jesper Udesen, who is beyond doubt, the person with whom I have discussed the most concerning ultrasound, signal processing and life in general during my years at CFU. Thanks for supporting me and keeping my motivation up when times where tough.

Thanks to Henrik Laursen for his assistance on computer related issues, and to Elna Sørensen for taking care of all administrative matters.

I would like to thank my parents for believing in me and always pretending to find my research interesting and/or comprehensible.

And last but not least, my fiancee Cecilia Adolfsson deserves my deepest admiration and respect for enduring my ups and downs during the course of this project, for being supportive and encouraging, and for setting my priorities straight when needed.

Thank you all!

Abstract

In this dissertation two methods for spatio-temporal encoding in medical ultrasound imaging are investigated.

The first technique is based on a frequency division approach. Here, the available spectrum of the transducer is divided into a set of narrow bands. A waveform is designed for each band, making it possible to transmit with several transmitters simultaneously and separate the signals at the receiver using a simple filtering operation. The separated signals can therefore be processed independently of each other. This facilitates transmission of more acoustic energy, which increases the signal to noise ratio and simultaneously the penetration depth so that the medical doctor can image deeper lying structures. The method is tested both experimentally and in simulation and has also evaluated for the purpose of blood flow estimation. The work presented is based on four papers which are also included in the dissertation.

The second method is based on encoding the transmitters with pseudo-random sequences. The signals can be separated after only one transmission using an estimation based technique. Broadband decoding can, therefore, be performed at the receiver after a single transmission. This increases the amount of data acquired in every transmission and can potentially reduce motion artifacts. The work presented utilizing this method is based on three papers which are included in the dissertation.

List of Abbreviations

CFU	Center for Fast Ultrasound imaging
XMT	Transmitter (Transmission)
RCV	Receiver
STA	Synthetic Transmit Aperture ultrasound imaging
SNR	Signal to noise ratio
FM	Frequency modulated
FIR	Finite Impulse Response
ADC	Analog to Digital Converter
MLE	Maximum Likelihood Estimator (or Estimate)
FWHM	Full Width Half Maximum
PSF	Point Spread Function

List of Symbols

c	The speed of sound
∇	The nabla operator, $\begin{pmatrix} \frac{\partial}{\partial x} & \frac{\partial}{\partial y} & \frac{\partial}{\partial z} \end{pmatrix}^T$
$\nabla\times$	The curl operator
$\nabla\cdot$	The divergence operator
∇^2	The Laplacian, $\nabla^2 = \nabla \cdot \nabla$
$E\left[(\cdot)\right]$	The expectancy value of $(\cdot)$
$(\cdot)^T$	The transpose of $(\cdot)$
$(\cdot)^H$	The complex conjugate transpose of $(\cdot)$
h	The scalar h
$\mathbf{h}$	The vector $\mathbf{h}$ (bold font)
$\mathbf{H}$	The matrix $\mathbf{H}$ (bold font, capital letters)
$\vec{r}$	The position vector $\vec{r} = \begin{pmatrix} x & y & z \end{pmatrix}^T$
$\mathcal{F}\left\{(\cdot)\right\}$	The Fourier transform of $(\cdot)$
$s(t)$	A time signal
$S(f)$	The Fourier transform of $s(t)$, $S(f) = \mathcal{F}\left\{s(t)\right\}$
$L(\vec{r})$	The low resolution image in the image point corresponding to $\vec{r}$
$H(\vec{r})$	The high resolution image in the image point corresponding to $\vec{r}$
$\star$	The convolution operator
$\otimes$	Kronecker product between matrices
$\widehat{s}$	The estimate of s
$(\cdot)^\dagger$	The generalized- or pseudo-inverse of $(\cdot)$
$\det\left\{(\cdot)\right\}$	The determinant of $(\cdot)$
$\mathbf{I}$	The identity matrix
$\delta(m)$	The discrete delta function
$\delta(t)$	The continuous delta function

CHAPTER
ONE

Introduction

Medical ultrasound is based on transmitting acoustic waves in the MHz range into the body of the patient. The reflected acoustic energy is measured by piezo-electric sensors. By processing the measured signals, spatial information can be extracted from the data.

By using an acoustic lens the waves can be focused in specific points of interest. Modern ultrasound scanners utilize transducer arrays, which consists of a set of small transducers gathered in an array. By applying different delays on different transducer elements, it is possible to steer the waves in arbitrary directions. This is termed electronic focusing.

In conventional ultrasound imaging, an acoustic beam is created by focusing the array in a point on a line in the direction which is supposed to be investigated. Ideally, a narrow beam is created, interrogating only a small region in space. The received signals are then processed as if structures along the beam is reflecting the acoustic waves. Hereby, an image line can be created along the transmitted acoustic beam. An image consisting of a number of image lines can be created after a number of consecutive transmissions illuminating different parts of space. Since the entire array is used, and the transmitted energy is focused in a single point in transmit, good SNR is attained. However, only a small part of space is interrogated in every transmission making the data acquisition rate slow.

In recent years it has become possible to realize ultrasound systems based on synthetic aperture techniques. Methods based on the concept of synthetic aperture were first developed for radar imaging systems. In radar, a single antenna is flying over the target and is simultaneously transmitting electro-magnetic radiation. The reflected signals are recorded, and by applying proper processing, a synthetic aperture with the same extent as that of the flight path can be created.

An ultrasound system based on synthetic transmit aperture could be realized by transmitting with only one element, record the received signals and beamform the signals. The purpose is to create an unfocused spherical wave which interrogates all directions of the tissue simultaneously. In the next transmission the active transmitter is moved to another spatial location on the array and the procedure is repeated. By using this approach, the entire transmitting array can be covered. If the target is stationary, combining data from the different transmissions makes it possible to steer the transmit beam in arbitrary directions. It is therefore possible to apply a specific transmit focus for each individual image point. This would not be possible in an conventional system, since the transmit focus is fixed for a given transmission.

However, the amount acoustic energy being transmitted in a given firing is still very small, due to the use of only a single transmitter. This will result in poor SNR. Moreover, motion will induce errors in the focusing if the object under investigation is moving very rapidly during the data acquisition. The data from different transmissions will be summed incoherently and motion artifacts will arise.

The purpose of this dissertation is to address these very problems. By utilizing spatial encoding in synthetic aperture imaging, it is possible to use several transmitters simultaneously. The purpose of encoding the transmitters, is that the received signals from the different transmitters can be separated. By doing this, the information corresponding to a specific transmitter can be processed without inter-transmitter interference.

The potential benefits from using spatial encoding is

- More information is acquired per time frame. This can reduce motion artifacts and provide better focusing under circumstances where rapid movement is present.
- More acoustic energy can be transmitted, which increases the SNR and effectively increases the penetration depth, facilitating imaging of deep lying objects.

This dissertation is divided into eight chapters where the first is this introduction. The following chapters are

Chapter Two: *A linear description of ultrasound* This chapter explains how to model an ultrasound system as a linear system. Using the concept of spatial impulse responses, the measured signal can be completely characterized by an impulse response. The spatial encoding methods which have been investigated during the course of this project, rely on the measured signal being considered as a linear transformation of the excitation signal. This chapter is therefore essential for the work presented in later chapters.

Chapter Three: *Ultrasound imaging* This chapter gives a brief review of existing imaging methods in medical ultrasound imaging. The chapter explains the concept of beamforming and the difference between conventional line based imaging and synthetic transmit aperture imaging.

Chapter Four: *Previous work on the topic of coded ultrasound* This chapter gives a brief overview of the work which has been carried out previously on the topic of coded ultrasound imaging. The chapter tries to describe some of the methods which have been investigated by other researchers. The purpose is to make it possible for the reader to realize how these theories differ from the ones which have been analyzed in this dissertation.

Chapter Five: *Spatial encoding by means of frequency division* Summarizes the work done on a method for spatial encoding based on a frequency division approach. The available transducer spectrum is divided into a number of narrow frequency bands with disjoint spectral support. The spatial encoding is achieved by designing waveforms with the same spectral support as the frequency bands. The same number of transmitters can, thus, be active simultaneously as the number of frequency bands, and the signals can be separated by matched- or bandpass filtering. The work is based on the results reported in the papers:

- **Multi Element Synthetic Aperture Transmission using a Frequency Division Approach.**
  Fredrik Gran and Jørgen Arendt Jensen
  Published in Proceedings IEEE Ultrason. Symp, pp 1942-1946, 2003
- **Frequency Division transmission imaging and synthetic aperture reconstruction.**
  Fredrik Gran and Jørgen Arendt Jensen
  Submitted to IEEE Transactions on Ultrasonics, Ferroelectrics and Frequency control, August 2004
- **Spatio-temporal encoding using narrow-band linear frequency modulated signals in synthetic aperture ultrasound imaging.**
  Fredrik Gran and Jørgen Arendt Jensen
  Accepted for publication, Proceedings of SPIE Medical Imaging meeting, Ultrasonic Imaging and Signal Processing, February 2005
- **Directional velocity estimation using a spatio-temporal encoding technique based on frequency division for synthetic transmit aperture ultrasound.**
  Fredrik Gran and Jørgen Arendt Jensen
  Submitted to IEEE Transactions on Ultrasonics, Ferroelectrics and Frequency control, June 2005

Chapter Six: *Spatial encoding by means of code division* In this chapter another method for spatial encoding is presented. Each transmitter is assigned a pseudo random code sequence and the signals are separated at the receiver using an estimation based approach. The chapter represents a summary of the work presented in the papers

- **A code division technique for multiple element synthetic aperture transmission.**
  Fredrik Gran, Jørgen Arendt Jensen and Andreas Jakobsson
  Published in the Proceedings of SPIE-Progress in biomedical optics and imaging 2004, vol 5373, pp 300-306
- **Identification of pulse-echo impulse responses for multi source transmission. (Invited)**
  Fredrik Gran and Jørgen Arendt Jensen
  Published in Conference Record of Thirty-Eighth Annular Asilomar Conference on Signals, Systems, and Computers, vol 1, pp 168-172, 2004
- **Spatial encoding using a code division technique for fast ultrasound imaging.**
  Fredrik Gran and Jørgen Arendt Jensen
  Submitted to IEEE Transactions on Ultrasonics, Ferroelectrics and Frequency control, May 2005

Chapter Seven: *Co-authored contributions* In this chapter co-authored publications are presented. A short introduction is given in the beginning of the chapter and the full papers are given in the following sections. The presented papers are:

- **Fast color flow mode imaging using plane wave excitation and temporal encoding.**
  Jesper Udesen, Fredrik Gran and Jørgen Arendt Jensen
  Accepted for publication Proceedings of SPIE Medical Imaging meeting, Ultrasonic Imaging and Signal Processing, 2005

- **Further development of synthetic aperture real-time 3d scanning with a rotating phased array.**
  Svetoslav Nikolov, Borislav Tomov, Fredrik Gran and Jørgen Arendt Jensen
  Published in Proceedings IEEE Ultrason. Symp., pp 1899-1902, 2003

Chapter Eight: *Conclusion* This chapter summarizes the findings in this dissertation and tries to give some suggestions to future directions of research.

CHAPTER

TWO

A linear description of ultrasound

Ultrasound imaging is based on transmitting acoustic energy into the body of a patient and listening for the reflected waves. The pressure is usually measured by an array of piezo-electric sensors which sample the wavefield spatially. In modern ultrasound scanners, temporal sampling is also applied to make it possible to utilize digital signal processing algorithms. The received and sampled signals are then processed to extract the spatial information contained in the sampled wavefield. Ultrasound systems are indeed very complicated, and to be able to extract the desired information, knowledge about the sampled wavefield has to be gathered. As a first step of characterizing the wavefield a model has to be derived.

Linear systems theory is very powerful since it allows the system under investigation to be completely characterized by an impulse response. Once the impulse response of the system has been obtained, the output for any arbitrary excitation can be predicted. It would therefore be advantageous to derive a linear model for the output when the geometry of the transducer is given.

This chapter is devoted to derive a model for describing the generated pressure from an ultrasound transducer as a linear system. Wherever possible, the assumptions and approximations associated with the model will be explained. However, to get full understanding of the acoustics, the interested reader is referred to the literature [1–3]. In [3] a comparison between the predicted acoustic field and the actual measured field is given.

2.1 The linear wave equation

To derive the linear wave equation first some variables have to be defined, and some assumptions have to be made. Consider the situation given in Fig. 2.1. Here a fluid with pressure P_0 and density ρ_0 experiences an acoustic disturbance which generates the local pressure P and the local density ρ. To derive the linear wave equation the following three equations have to be considered

- The linearized equation of state
- The linearized continuity equation
- The linearized inviscid force equation

A list of the different variables can be seen in table 2.1. Two important quantities which will be used during the derivation of the linear wave equation are: p, representing the difference between the local and the ambient pressure, and the condensation s, defined

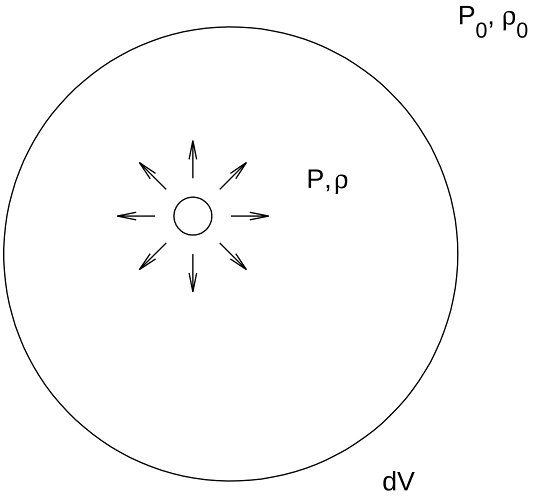

Figure 2.1: The figures indicates a fluid volume dV with an acoustic disturbance generating the pressure P and density ρ. The ambient pressure of the surrounding fluid is denoted P_0 and it's density ρ_0.

as the difference between the local and ambient density relative to the ambient density. The variable $\mathbf{u}$ represents the particle velocity in the fluid.

Variable	Explanation
P	The local pressure
P_0	The ambient pressure
ρ	The local density
ρ_0	The ambient density
$p = P - P_0$	Difference between local and ambient pressure
$s = \frac{\rho-\rho_0}{\rho_0}$	Condensation
$\mathbf{u}$	Particle velocity

Table 2.1: The variables used in the derivation of the linear wave equation.

2.1.1 The linearized equation of state

The equation of state describes the relationship between the pressure P and the density ρ. In the general case, the pressure can be written as a function of density

$$P(\rho).$$

However, using the Taylor expansion around the ambient density ρ_0 the pressure P be written

$$P(\rho) = P(\rho_0) + (\rho - \rho_0) \left.\frac{\partial P(\rho)}{\partial \rho}\right|_{\rho=\rho_0} + \cdots \tag{2.1}$$

where $P(\rho)$ is the local pressure and $P(\rho_0) = P_0$ is the ambient pressure. Linearizing (2.1) by dropping higher order terms the (linearized) equation of state emerges

$$P = P_0 + (\rho - \rho_0) \left.\frac{\partial P(\rho)}{\partial \rho}\right|_{\rho=\rho_0}. \tag{2.2}$$

Physically, this means that the difference between the local and ambient density must be small. By rearranging the terms in (2.2), this equation can be written

$$\underbrace{P - P_0}_{p} = \rho_0 \left.\frac{\partial P(\rho)}{\partial \rho}\right|_{\rho=\rho_0} \underbrace{\frac{\rho - \rho_0}{\rho_0}}_{s}$$

so that the difference in pressure p is proportional to the condensation s

$$p = \mathcal{B}s, \tag{2.3}$$

where

$$\mathcal{B} = \rho_0 \left.\frac{\partial P(\rho)}{\partial \rho}\right|_{\rho=\rho_0}$$

is the adiabatic bulk modulus.

2.1.2 The linearized continuity equation

The continuity equation describes the rate of change of mass in a fluid volume. If there is no mass created in the volume, the change of mass per time is equal to the net flow of mass into the volume per time. In Fig. 2.2 the projection of a small fluid volume $dV = dxdydz$ is displayed.

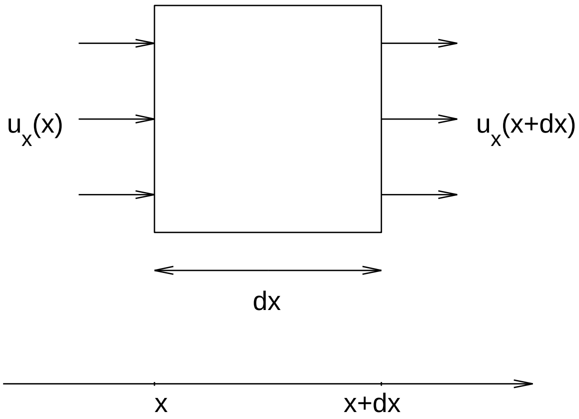

Figure 2.2: The projection of the small fluid volume in the x-direction. The particle velocity on the left side of the volume is $u_x(x)$ and the velocity on the right side is $u_x(x + dx)$

The net influx of mass into the fluid volume is

$$\left(\rho u_x - \left[\rho u_x + \frac{\partial(\rho u_x)}{\partial x}dx\right]\right) dydz = -\frac{\partial(\rho u_x)}{\partial x}dV \tag{2.4}$$

where $\rho u_x + \frac{\partial(\rho u_x)}{\partial x}dx$ is the linearized expression for ρu_x at the spatial location $x + dx$. Repeating the same calculation for all spatial directions and combining the results, yields the net influx of mass into the fluid volume as

$$-\nabla \cdot (\rho \mathbf{u})dV. \tag{2.5}$$

If no mass is created, the result in (2.5) is equal the rate of change of mass

$$\frac{\partial \rho}{\partial t}dV = -\nabla \cdot (\rho \mathbf{u})dV,$$

which implies that

$$\frac{\partial \rho}{\partial t} = -\nabla \cdot (\rho \mathbf{u}). \tag{2.6}$$

It shall be noted that (2.6) is non linear, since it involves both the instantaneous density and the particle velocity, which are both functions of space. However, by restricting the discussion to situations where the the condensation is much smaller than unity ($s \ll 1$) so that

$$\rho \approx \rho_0$$

the density ρ can be considered as a constant, leaving the expression

$$\frac{\partial \rho}{\partial t} = -\rho_0 \nabla \cdot \mathbf{u}.$$

The physical interpretation of $s \ll 1$ is that the density ρ is very close to the ambient density ρ_0. Therefore, the change in density due to the acoustic disturbance has to be very small. Finally, by using the relation between condensation and density specified in table 2.1, $\rho = \rho_0(1+s)$, the linearized continuity equation emerges

$$\frac{\partial s}{\partial t} + \nabla \cdot \mathbf{u} = 0. \tag{2.7}$$

2.1.3 The linear inviscid force equation

The force equation (Euler equation) states that the net forces $d\mathbf{f}$ acting on the fluid volume is equal to the acceleration $\mathbf{a}$ times the mass of the volume dm

$$d\mathbf{f} = \mathbf{a}\, dm. \tag{2.8}$$

In this derivation only external forces are considered. No attention to forces due to friction are analyzed, and viscosity is therefore ignored. The net forces on the fluid in the positive x-direction are

$$df_x = \left(P - \left[P + \frac{\partial P}{\partial x} dx \right] \right) dydz = -\frac{\partial P}{\partial x} dV \tag{2.9}$$

By writing the entire force vector $d\mathbf{f}$ for all spatial directions in analogy with (2.9) the net forces acting on the fluid volume can be written

$$d\mathbf{f} = -\nabla P dV.$$

The right hand side of (2.8) requires a bit more attention. Start by writing the acceleration of the fluid volume as

$$\mathbf{a} = \lim_{dt \to 0} \frac{\mathbf{u}(x+dx, y+dy, z+dz, t+dt) - \mathbf{u}(x,y,z,t)}{dt}$$

which can be simplified by writing

$$dx = u_x dt \qquad dy = u_y dt \qquad dz = u_z dt.$$

The first order Taylor expansion is now used to get the linearized expression of the particle velocity

$$\mathbf{u}(x+u_x dt, y+u_y dt, z+u_z dt, t+dt) =$$
$$\mathbf{u}(x,y,z,t) + \frac{\partial \mathbf{u}}{\partial x} u_x dt + \frac{\partial \mathbf{u}}{\partial y} u_y dt + \frac{\partial \mathbf{u}}{\partial z} u_z dt + \frac{\partial \mathbf{u}}{\partial t} dt.$$

Therefore, the acceleration is given by

$$\mathbf{a} = \frac{\partial \mathbf{u}}{\partial x}u_x + \frac{\partial \mathbf{u}}{\partial y}u_y + \frac{\partial \mathbf{u}}{\partial z}u_z + \frac{\partial \mathbf{u}}{\partial t} = (\mathbf{u}\cdot\nabla)\mathbf{u} + \frac{\partial \mathbf{u}}{\partial t},$$

and since $dm = \rho\, dV$ equation (2.8) is reduced to

$$-\nabla P = \rho\left((\mathbf{u}\cdot\nabla)\mathbf{u} + \frac{\partial \mathbf{u}}{\partial t}\right), \tag{2.10}$$

which like (2.6) is non-linear. Equation (2.10) can, however, be linearized by requiring that the condensation is much less than unity $s \ll 1$. This makes it possible to substitute ρ for ρ_0. Furthermore, by assuming that

$$|(\mathbf{u}\cdot\nabla)\mathbf{u}| \ll \left|\frac{\partial \mathbf{u}}{\partial t}\right|,$$

and realizing that P_0 is a constant with respect to time, so that

$$\frac{\partial P}{\partial t} = \frac{\partial}{\partial t}(P - P_0) = \frac{\partial p}{\partial t},$$

the linearized inviscid force equation emerges

$$-\nabla p = \rho_0\frac{\partial \mathbf{u}}{\partial t}. \tag{2.11}$$

2.1.4 The velocity potential

A peculiar result of the linear inviscid force equation (2.11) is a concept called the velocity potential. This abstraction is a convenient quantity which will be used in sequel to facilitate the derivations of the Rayleigh integral and the concept of spatial impulse responses. The velocity potential can be derived by using a basic result from vector analysis [1], stating that the curl of the gradient of any scalar function must vanish

$$\nabla\times\nabla g = 0. \tag{2.12}$$

To apply (2.12) on acoustics, the attention is turned to the linear inviscid force equation. Applying the curl operator on both sides of (2.11) results in

$$-\nabla\times\nabla p = \nabla\times\left(\rho_0\frac{\partial \mathbf{u}}{\partial t}\right).$$

Now, both sides are integrated with respect to time,

$$\int -\nabla\times\nabla p\, dt = \int \nabla\times\left(\rho_0\frac{\partial \mathbf{u}}{\partial t}\right)\, dt$$

The nabla operator and the integral operator are both linear operators. This implies that the operators can switch places without affecting the nature of the equation

$$-\nabla\times\nabla\int p\, dt = \rho_0\nabla\times\int\frac{\partial \mathbf{u}}{\partial t}\, dt,$$

where the left hand side must vanish due to (2.12), since $\int p\; dt$ is a scalar function of space. Moreover, $\int \frac{\partial \mathbf{u}}{\partial t}\, dt = \mathbf{u}$, and ρ_0 is a constant different from zero, so that

$$\nabla\times\mathbf{u} = 0. \tag{2.13}$$

The physical interpretation of (2.13) is that there is no rotational flow such as turbulence. When (2.13) is valid, the particle velocity can be written as the gradient of a (scalar) velocity potential

$$\mathbf{u} = \nabla \Phi, \tag{2.14}$$

where Φ is the velocity potential. Inserting (2.14) into (2.11) gives

$$-\nabla p = \rho_0 \frac{\partial}{\partial t} \left(\nabla \Phi \right) = \nabla \left(\rho_0 \frac{\partial \Phi}{\partial t} \right),$$

and

$$\nabla \left(p + \rho_0 \frac{\partial \Phi}{\partial t} \right) = 0. \tag{2.15}$$

If there is no acoustic excitation, the expression within brackets in (2.15) can be chosen to vanish [1],

$$p + \rho_0 \frac{\partial \Phi}{\partial t} = 0. \tag{2.16}$$

2.1.5 The wave equation

We are now equipped to derive the linear wave equation. By combining the linearized equation of state (2.3), the linearized continuity equation (2.7) and the linear inviscid force equation (2.11) this can be achieved. First, take the divergence of (2.11)

$$-\nabla \cdot \nabla p = \rho_0 \nabla \cdot \left(\frac{\partial \mathbf{u}}{\partial t} \right),$$

and change place on the divergence operator and the time derivative in the left hand side. Then, identifying $\nabla \cdot \nabla$ as the Laplacian operator ∇^2 results in

$$-\nabla^2 p = \rho_0 \frac{\partial}{\partial t} \left(\nabla \cdot \mathbf{u} \right).$$

Now, use the linearized continuity equation (2.7) and replace $\nabla \cdot \mathbf{u} = -\frac{\partial s}{\partial t}$

$$\nabla^2 p = \rho_0 \frac{\partial^2 s}{\partial t^2}.$$

Finally, the linearized equation of state is used to eliminate s, so that the linear wave equation emerges

$$\nabla^2 p = \frac{\rho_0}{\mathcal{B}} \frac{\partial^2 p}{\partial t^2}, \tag{2.17}$$

where $c = \sqrt{\frac{\mathcal{B}}{\rho_0}}$ is the speed of sound,

$$\nabla^2 p = \frac{1}{c^2} \frac{\partial^2 p}{\partial t^2}. \tag{2.18}$$

The general spherical wave solution to (2.18) is [1]

$$p(r,t) = \frac{1}{r} g \left(t - \frac{r}{c} \right) + \frac{1}{r} h \left(t + \frac{r}{c} \right) \tag{2.19}$$

where r is the radial distance form the point of origin, and g and h are arbitrary functions.

2.2 The Rayleigh integral

In this section the Rayleigh integral will be derived according to [2]. The linear wave equation does not directly provide tools for describing radiated fields from apertures or arrays. In ultrasound, however, this is of major interest. To arrive at the concept of spatial impulse responses (Section 2.3), the Rayleigh integral will be utilized. The Rayleigh integral describes how the shape and geometry of the active aperture affects the generated acoustic field. First, note that a causal spherical wave solution to the linear wave equation is

$$p(r,t) = \frac{1}{r} g\left(t - \frac{r}{c}\right). \tag{2.20}$$

By analyzing (2.16) under the constraint that the pressure is given by (2.20) it can be realized that the velocity potential just like the pressure, will have r^{-1} dependence and an argument depending on $t - \frac{r}{c}$. Now, we cunningly choose the velocity potential as

$$\Phi(r,t) = -c\frac{1}{r}\psi\left(t - \frac{r}{c} + \frac{a}{c}\right), \tag{2.21}$$

where ψ is an arbitrary function, and a is a constant which will explained in sequel. Consider a small oscillating sphere with radius a located at the origin, oscillating with the surface velocity $v_s(t)$, as depicted in Fig. 2.3. By combining (2.14) and (2.21) the particle velocity in the radial direction u_r can be written

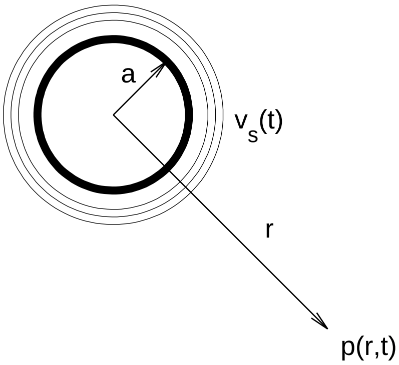

Figure 2.3: A small sphere with radius a, oscillating with the surface velocity $v_s(t)$

$$u_r(t) = \frac{c}{r^2}\psi\left(t - \frac{r}{c} + \frac{a}{c}\right) + \frac{1}{r}\dot{\psi}\left(t - \frac{r}{c} + \frac{a}{c}\right) \tag{2.22}$$

where $\dot{\psi}(f(r,t)) = \frac{\partial \psi(f(r,t))}{\partial f(r,t)}$ is the partial derivative with respect to the argument $f(r,t)$. At the boundary of the sphere $r = a$, the particle velocity must be equal to the surface velocity velocity of the sphere so that

$$\frac{c}{a^2}\psi(t) + \frac{1}{a}\dot{\psi}(t) = v_s(t). \tag{2.23}$$

If the discussion is restricted to a low-frequency approximation, $\frac{1}{a}\dot{\psi}(t) \ll \frac{c}{a^2}\psi(t)$, and (2.23) can be written

$$\frac{c}{a^2}\psi(t) = v_s(t), \qquad \psi(t) = \frac{a^2}{c}v_s(t).$$

Therefore, the velocity potential is

$$\Phi(r,t) = -\frac{a^2}{r} v_s \left(t - \frac{r}{c} + \frac{a}{c}\right).$$

If it assumed that the field point r is very far away compared to the radius of the sphere ($a \ll r$) then

$$\Phi(r,t) = -\frac{a^2}{r} v_s \left(t - \frac{r}{c}\right). \tag{2.24}$$

By combining (2.16) and (2.24) the pressure can be written

$$p(r,t) = \frac{\rho_0}{r} a^2 \frac{\partial}{\partial t} v_s \left(t - \frac{r}{c}\right). \tag{2.25}$$

To extend this formulation to an arbitrarily shaped source, consider an infinitely small sphere with surface area dS located at spatial position $\vec{r}_2$. The contribution to the pressure in the field point located at $\vec{r}_1$ can be written

$$dp(\vec{r}_1,t) = \frac{\rho_0}{4\pi} \frac{\frac{\partial}{\partial t} v_s \left(\vec{r}_2, t - \frac{|\vec{r}_1 - \vec{r}_2|}{c}\right)}{|\vec{r}_1 - \vec{r}_2|} dS, \tag{2.26}$$

where $|\vec{r}_1 - \vec{r}_2|$ is the distance from the oscillating sphere to the field point. To derive the total pressure generated by the source with surface S, the surface is decomposed into an infinite amount of point sources each with a pressure contribution to the field point $\vec{r}_1$ as given in (2.26). The total pressure is then the surface integral over all point sources on the surface

$$p(\vec{r}_1,t) = \frac{\rho_0}{4\pi} \int_S \frac{\frac{\partial}{\partial t} v_s \left(\vec{r}_2, t - \frac{|\vec{r}_1 - \vec{r}_2|}{c}\right)}{|\vec{r}_1 - \vec{r}_2|} dS. \tag{2.27}$$

The geometry is given in Fig. 2.4

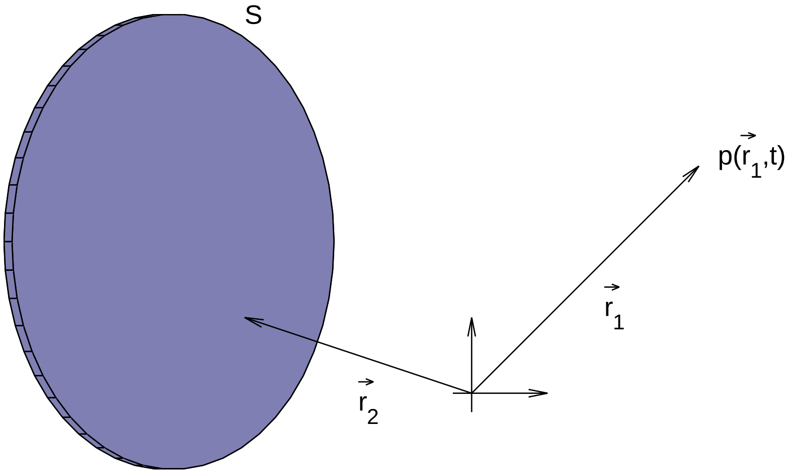

Figure 2.4: The pressure in field point $\vec{r}_1$ is calculated for an arbitrary source with surface S. The vector $\vec{r}_2$ points to the surface of the source and is used in the integration over the surface in (2.27)

2.3 Spatial impulse responses

Equation (2.27) is valid for a source in free space. In ultrasound, however, the transmitting transducer elements are mounted on the transducer. A common model for this situation is that the elements are fixed to a rigid wall. Because of mirroring effects, the radiated pressure from a source on a rigid wall will be twice the pressure from a source in free space [1]

$$p(\vec{r}_1,t) = \frac{\rho_0}{2\pi}\int_S \frac{\frac{\partial}{\partial t} v_s\left(\vec{r}_2, t - \frac{|\vec{r}_1-\vec{r}_2|}{c}\right)}{|\vec{r}_1-\vec{r}_2|}\, dS. \tag{2.28}$$

Since the integral operator and the differential operator both are linear, it is possible to move the differential operator outside the integral

$$p(\vec{r}_1,t) = \rho_0 \frac{\partial}{\partial t}\left(\int_S \frac{v_s\left(\vec{r}_2, t - \frac{|\vec{r}_1-\vec{r}_2|}{c}\right)}{2\pi|\vec{r}_1-\vec{r}_2|}\, dS\right). \tag{2.29}$$

The integrand can be expressed using a time convolution

$$v_s\left(\vec{r}_2, t - \frac{|\vec{r}_1-\vec{r}_2|}{c}\right) = v_s(\vec{r}_2,t) \star \delta\left(t - \frac{|\vec{r}_1-\vec{r}_2|}{c}\right),$$

so that (2.29) can be written

$$p(\vec{r}_1,t) = \rho_0 \frac{\partial}{\partial t}\left(\int_S v_s(\vec{r}_2,t) \star \frac{\delta\left(t - \frac{|\vec{r}_1-\vec{r}_2|}{c}\right)}{2\pi|\vec{r}_1-\vec{r}_2|}\, dS\right), \tag{2.30}$$

where $\delta(t)$ is the delta function and $\star$ is the convolution operator. By assuming the surface velocity to be constant over the source, $v_s(t)$ will no longer be spatially dependent and can be considered as a constant in the surface integral. Therefore, (2.30) can be written

$$p(\vec{r}_1,t) = \rho_0 \frac{\partial}{\partial t}\left(v_s(t) \star \int_S \frac{\delta\left(t - \frac{|\vec{r}_1-\vec{r}_2|}{c}\right)}{2\pi|\vec{r}_1-\vec{r}_2|}\, dS\right).$$

Moreover, since

$$\mathcal{F}\left\{\frac{\partial}{\partial t}\left(g(t)\star h(t)\right)\right\} = j2\pi f\ \left(G(f)H(f)\right) =$$

$$G(f)\left(j2\pi f\ H(f)\right) = \mathcal{F}\left\{g(t) \star \frac{\partial}{\partial t}\left(h(t)\right)\right\},$$

the pressure can take on the expression

$$p(\vec{r}_1,t) = \rho_0 \left(\frac{\partial v_s(t)}{\partial t}\right) \star \int_S \frac{\delta\left(t - \frac{|\vec{r}_1-\vec{r}_2|}{c}\right)}{2\pi|\vec{r}_1-\vec{r}_2|}\, dS, \tag{2.31}$$

where

$$h(\vec{r}_1,t) = \int_S \frac{\delta\left(t - \frac{|\vec{r}_1-\vec{r}_2|}{c}\right)}{2\pi|\vec{r}_1-\vec{r}_2|}\, dS, \tag{2.32}$$

is defined as the spatial impulse response. Moreover, if it assumed that the displacement of the baffle can be written as a convolution of the excitation waveform $x(t)$ and an impulse response $g(t)$, the surface acceleration is given by

$$\frac{\partial v_s(t)}{\partial t} = \frac{\partial^2}{\partial t^2}\left(x(t) \star g(t)\right) = x(t) \star \frac{\partial^2 g(t)}{\partial t^2} \tag{2.33}$$

so that (2.31) can be written

$$p(\vec{r}_1, t) = \rho_0 \frac{\partial^2 g(t)}{\partial t^2} \star h(\vec{r}_1, t) \star x(t). \tag{2.34}$$

2.4 Summary

In this chapter the concept of spatial impulse responses has been derived. Using this approach it is possible to model the output pressure from a given transducer geometry for any excitation waveform. The advantage of describing a system using linear theory is that the system can be fully characterized using an impulse response. Therefore, it is possible to determine the spectral support of the measured signal if the spectral support of the excitation waveform and the spatial impulse response is known.

The methods for spatial encoding which are analyzed in this dissertation, rely on the measured signal being a linear transformation of the input- or excitation signal. This chapter is therefore essential for understanding the theory of the spatial encoding techniques described in later chapters.

Of course, a complete analysis of the acoustics is not possible, as it is out of scope for this dissertation, however, the interested reader is referred to [3,4] for a thorough investigation.

CHAPTER

THREE

Ultrasound imaging

This chapter tries to give an overview of current beamforming techniques in medical ultrasound imaging. In ultrasound imaging the wave field is sampled by an array of transducer elements (sensors). Each sensor yields a time signal, and beamforming is the art of extracting spatial information from these time signals.

Medical ultrasound imaging mainly concerns near-field imaging, since the far-field starts at [1,5]

$$z \sim \frac{r^2}{\lambda} \tag{3.1}$$

where r is the radius the aperture and λ is the wavelength of the transmitted ultrasound. Typically $r \sim 1$ cm and $\lambda \sim 0.22$ mm[1] so that the far-field starts at ~ 45 cm, whereas imaging depths in the human body range from 0-30 cm. This means that the waves should be treated as originating from near-field sources. Imaging is therefore done by focusing the acoustic energy in a number of spatial points.

Modern ultrasound systems utilize transducer arrays. These probes consists of a number of transducer elements with the capability of applying sensor specific delays both for the transmitting aperture and the receiving aperture. Therefore, the ultrasonic waves can be focused in arbitrarily chosen points using the proper delays. Naturally, if only one transmission is carried out, only one transmit focus can be attained. This is termed *fixed focusing*. *Dynamic focusing* represents beamforming where the acoustic energy is focused in several spatial points. To achieve *dynamic focusing* for the transmitting aperture, the same number of transmissions as the number of focal points has to be carried out. For the receiving aperture, however, an arbitrary number of focal points can be chosen, and the data can be beamformed as many times as necessary using data from only one transmission.

3.1 Beamforming

Beamforming denotes the array signal processing carried out to extract spatial information contained in the field. The purpose (in the near-field case) is to enhance the signal propagating from a specific spatial location, while suppressing noise and waves propagating from other locations.

---

[1] Assuming a 7 MHz transducer and speed of sound 1540 m/s

3.1.1 Delay and sum beamforming

The concept of delay and sum beamforming is very simple. It is based on the principle of enhancing a given signal utilizing the geometrical information about the array relative to the source of interest [6]. This assumes that the speed of propagation of the wave-field is known.

Consider an array of M transducer elements located at the spatial locations $\{\vec{r}_m\}_{m=0}^{M-1}$. Assume that wave-field is generated by a point source at the spatial location $\vec{r}_0$ radiating the waveform $s(t)$. The generated wave-field can be written

$$f(\vec{r},t) = \frac{s\left(t - \frac{|\vec{r}-\vec{r}_0|}{c}\right)}{|\vec{r}-\vec{r}_0|}. \tag{3.2}$$

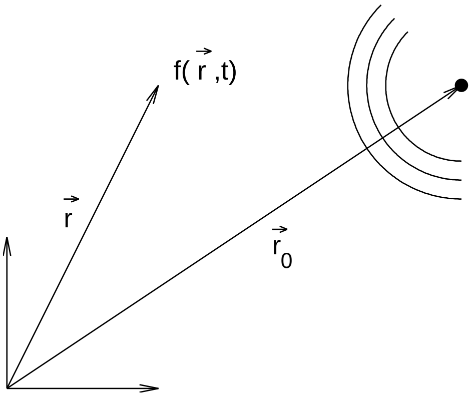

Figure 3.1: The wave-field as a function of space $\vec{r}$ and time t when the source is a single point source emitting spherical waves from the location $\vec{r}_0$.

The geometry of (3.2) can be seen in Fig. 3.1. The M sensors, sample the wave-field spatially such that M time signals emerges

$$y_m(t) = f(\vec{r}_m,t) = \frac{s\left(t - \frac{|\vec{r}_m-\vec{r}_0|}{c}\right)}{|\vec{r}_m-\vec{r}_0|}, \qquad m = 0,\ldots,M-1. \tag{3.3}$$

The delay and sum beamformer tries to sum the sensor signals in phase by applying a sensor specific delay to the time signal at every sensor. The beamformer output is

$$z(t) = \sum_{m=0}^{M-1} w_m y_m(t-\Delta_m), \tag{3.4}$$

where Δ_m is the sensor specific delay and w_m is a sensor specific weighting factor[2]. By combining (**??**) and (3.4) the beamformer output for this specific wave-field is given by

$$z(t) = \sum_{m=0}^{M-1} w_m \frac{s\left(t - \frac{|\vec{r}_m-\vec{r}_0|}{c} - \Delta_m\right)}{|\vec{r}_m-\vec{r}_0|}. \tag{3.5}$$

By examining (3.5) and choosing the delay as[3]

$$\Delta_m = \frac{|\vec{r}_0-\vec{r}_m|}{c} + \frac{|\vec{r}_0|}{c} \tag{3.6}$$

---

[2] In ultrasound this is denoted apodization. Apodize is Greek for "to remove the feet" [7]

[3] The additional term $\frac{|\vec{r}_0|}{c}$ is used to get the range information about the source.

the beamformed output can be written as the radiated waveform $s(t)$, delayed by the time corresponding to the travel-distance from the source to the origin of the system and multiplied by a spatially dependent factor

$$z(t) = s\left(t - \frac{|\vec{r}_0|}{c}\right) \sum_{m=0}^{M-1} w_m \frac{1}{|\vec{r}_m - \vec{r}_0|}. \tag{3.7}$$

The basic principle of the delay and sum beamformer is given in Fig. 3.2, where the propagating signal is arriving at the different sensors at different times. The propagating signal is enhanced by applying sensor specific delays to each sensor. By analyzing the delay given in (3.6) it can be seen that if the speed of sound (or more generally the speed of propagation) is not specified correctly, the beamformer output will be misadjusted. This results in a non-coherent summation of the data. Therefore, ideal focusing can not be attained. In medical ultrasound imaging, this is called phase aberrations and has been studied extensively by different researchers [8–12].

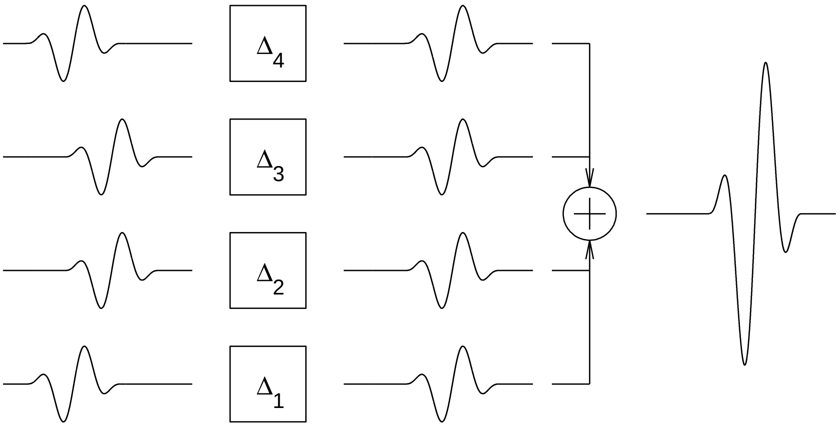

Figure 3.2: By applying proper delays on the individual sensors, the signals can be coherently summed and the propagating signal can be enhanced.

3.1.2 The Fourier relation for an imaging system

A very powerful and useful tool in imaging, is the Fourier relation between the aperture function $\{w_m\}_{m=0}^{M-1}$ and the observed wave-field. Consider a wave-field generated by a single monochromatic plane wave with temporal frequency ω_0 and wave-vector $\vec{k}_0$[4]

$$f(\vec{r}, t) = e^{j(\omega_0 t - \vec{k}_0 \cdot \vec{r})}. \tag{3.8}$$

This wave-field is sampled spatially by the array with sensors at the spatial positions $\{\vec{r}_m\}_{m=0}^{M-1}$

$$y_m(t) = e^{j(\omega_0 t - \vec{k}_0 \cdot \vec{r}_m)}. \tag{3.9}$$

---

[4] The ultrasound field has, as previously mentioned, not a plane wave characteristic, but point focusing can be regarded as straightening the curvature of the spherical wave so that it is experienced as a plane wave.

Now, assume that the beamformer is looking for plane waves with the wave-vector $\vec{k}$. [5] The delays applied on each sensor is then [6]

$$\Delta_m = -\vec{k} \cdot \vec{r}_m,$$

and the beamformer output becomes

$$z(t) = \sum_{m=0}^{M-1} w_m e^{j(\omega_0 t - \vec{k}_0 \cdot \vec{r}_m + \vec{k} \cdot \vec{r}_m)} = e^{j\omega_0 t} \sum_{m=0}^{M-1} w_m e^{j(\vec{k} - \vec{k}_0) \cdot \vec{r}_m}. \tag{3.10}$$

Now, define the spatial Fourier transform of the aperture as

$$W(\vec{k}) = \sum_{m=0}^{M-1} w_m e^{j\vec{k} \cdot \vec{r}_m}. \tag{3.11}$$

By comparing (3.10) and (3.11) the beamformed output can be written

$$z(t) = e^{j\omega_0 t} W(\vec{k} - \vec{k}_0). \tag{3.12}$$

Equation (3.12) reveals the relationship between the observed field and the incident field. It can be seen that the observed field will be "smoothed" by the spatial Fourier transform of the aperture function, with the peak value around the true wave-number $\vec{k}_0$.

In Fig. 3.3 the array response for a ten sensor linear array located at $y = 0$ for a field incident at 0° can be examined. The top left figure displays the array response when using a boxcar weighting function with $\lambda/2$ spacing between the sensors. The corresponding array response for the same array but with λ spacing can seen as the right top figure. The mainlobe is narrower for the right figure but displays secondary mainlobes at $\pm 90^\circ$ called grating lobes. The result is expected since the coarser sampling will move the grating lobes closer to the mainlobe and provide better resolution as the effective width of the aperture is doubled. The bottom left figure shows the array response when the spatial sampling distance is $\lambda/2$ but when the sensor weighting is a Hanning window. This response has compared to the response utilizing the boxcar weighting has a broader mainlobe but the sidelobe structure has been suppressed. If the Fourier transforms of the two weighting functions are considered, this can be explained. The amplitude spectrum of the boxcar function, has a narrower mainlobe, but more dominant sidelobe structure compared to Fourier transform of the Hanning weighting.

It should be noted that the derivation in (3.12) only is valid for beamforming the waves received from a plane wave. However, similar reasoning can be applied for the transmit field for the transmit focus, leaving a Fourier relation between the transmit aperture and the generated transmit field [7]. Combining these theories, the concept of "effective aperture" can be derived [13–15]. This concept provides a powerful tool for designing sparse arrays. The theory is, however, out of scope for this dissertation, and the interested reader is referred to the literature.

3.2 Conventional ultrasound imaging

A conventional B-mode image consists of a number of image lines. An image line is created by creating a narrow transmit- and receive beam, so that only a small part of space is interrogated. The image line is represented by the dashed line in Fig. 3.4.

---

[5] This wave-vector is not necessarily equal to the wave-vector of the field.

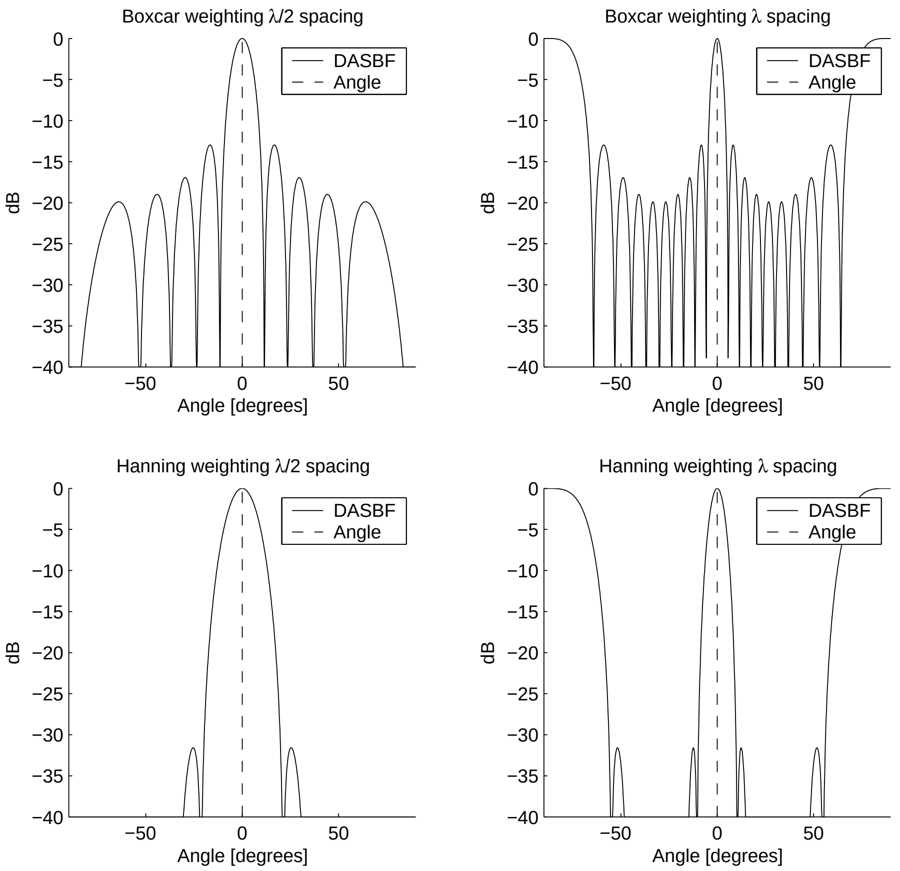

Figure 3.3: The array response for a field incident at $0°$. The top right plot shows the response for an array with $\frac{\lambda}{2}$ spacing and a boxcar sensor weighting. The right top plot is the same setup but with λ spacing between the sensors. The coarser spatial sampling results in grating lobes at $90°$ but provides also better resolution since the effective width of the aperture has doubled. In the bottom left plot the array response for the array with $\frac{\lambda}{2}$ spacing is again displayed, but with a Hanning weighting. The Hanning window has a broader main lobe but a less dominant sidelobe structure compared to the boxcar window [6]. In the right bottom plot the Hanning weighting was applied to the sensor with λ spacing.

In transmit, this is achieved by focusing the active transducer elements [6] in a specific spatial location specified by $\vec{r}_{focus}$. This means that the delays are adjusted so that the transmitted waves arrive simultaneously in this specific point. If several transmit foci are desired (dynamic transmit focusing) , the same number of transmissions have to be carried out as the number of foci.

The received signals from the active receiving aperture should thereafter be beamformed to produce an image. The geometry of the beamforming is depicted in Fig. 3.4. Assume that a scatterer is positioned at the spatial location $\vec{r}_p$. The time of flight from the center of the active transmitting array, located at $\vec{r}_a$, out to the point[7] and back to the q:th receiving element located at $\vec{r}_{rcv,q}$ is then

$$t_{pq} = \frac{|\vec{r}_p - \vec{r}_a|}{c} + \frac{|\vec{r}_{rcv,q} - \vec{r}_p|}{c}. \tag{3.13}$$

---

[6] represented by the gray elements in Fig. 3.4.

[7] This assumes that the center of the sub-array is transmitting at time point $t = 0$.

Summing data for the Q active receiving elements using the equation given in (3.13) will yield receive focus in the point specified by $\vec{r}_p$

$$z(\vec{r}_p) = \sum_{q=0}^{Q-1} w_q y_q(t_{pq}), \tag{3.14}$$

where $y_q(t)$ is the measured time signal on the q:th receiving transducer element. The distance from the center of the transmitting array to the point is represented by $|\vec{r}_p - \vec{r}_a|$ and the distance from the point and back to the q:th receiving element is given by $|\vec{r}_{rcv,q} - \vec{r}_p|$. Note how the delay line is changing as a function of spatial position $\vec{r}_p$. The transmit focus specified by $\vec{r}_{focus}$ is not explicitly used in the processing. However, the generated acoustic beam will only be narrow in the vicinity of the transmit focus, and the image quality will be poorer far away from this focal point. Dynamic transmit focusing is therefore beneficial for the image quality, but requires several transmissions per image line.

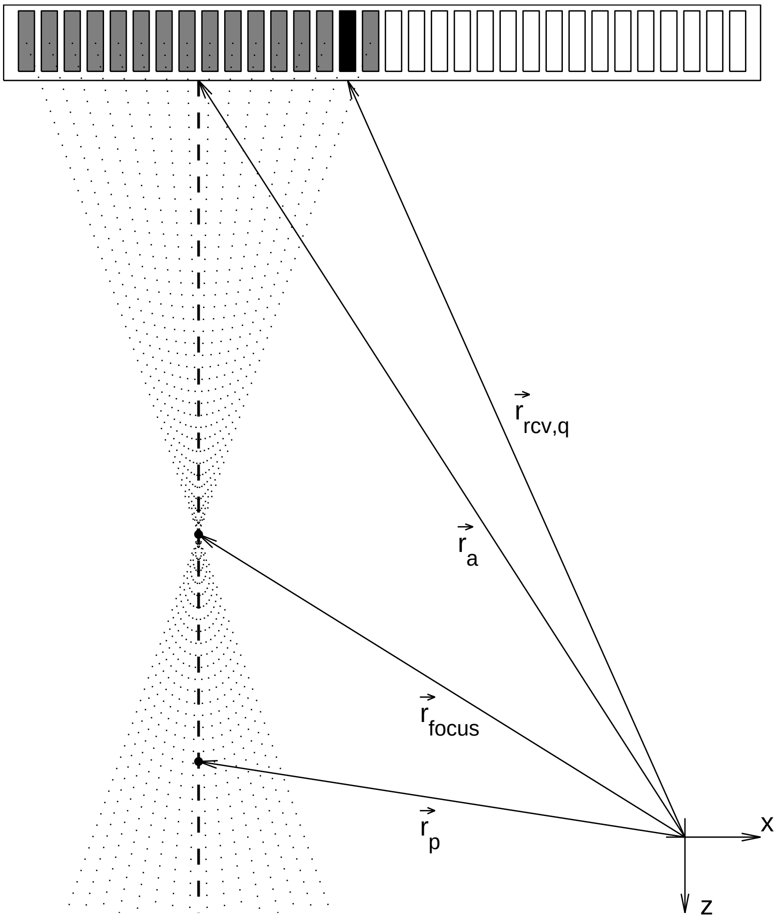

Figure 3.4: Conventional ultrasound imaging. The transducer is focused in a specific depth, and ideally, a narrow beam is created. The beam is indicated by the dashed line. Along the beam, an image line is created. The active transmitting sensors are indicated in gray and the receiving sensor of interest is indicated by black. The points on the line are beamformed using (3.14), where $\vec{r}_p$ is the spatial location of the image point, $\vec{r}_a$ the spatial location of the center of the active array and $\vec{r}_{rcv,q}$ the receiving sensor of interest

Conventional line based ultrasound imaging suffers from two drawbacks:

- Only one image line is created per transmission.
- The transmit focus is fixed in every transmission.

Because only one image line is created per transmission, the data acquisition rate will be slow. An ultrasound image consists of ∼100 image lines, implying that at least 100 transmissions have to be carried out before a complete image can be formed. Therefore, imaging of rapid moving objects, like the heart, will be problematic. Moreover, having access to only one transmit focus per transmission will cause problems when imaging objects far away from the transmit focal point. Here, the acoustic beam will broaden and poorer resolution will be attained. This can be compensated by applying dynamic transmit focusing. However, this requires several transmissions per image line and will worsen the problem concerning motion even more.

3.2.1 Linear array imaging

Linear array systems are widely used for diagnostic purposes and is very much in use in commercial ultrasound systems [5]. In a linear array system, a sub-array is used in every transmission. The active sensors are focused in a certain depth, and the reflected acoustic waves are recorded by some, or all of the transducer elements. After one transmission an image line is beamformed using either fixed or dynamic focusing. To generate more than one line, the active aperture is shifted one or several sensors, and the procedure is repeated. In this way several parallel lines are created. The principle of operation can be seen in Fig. 3.5.

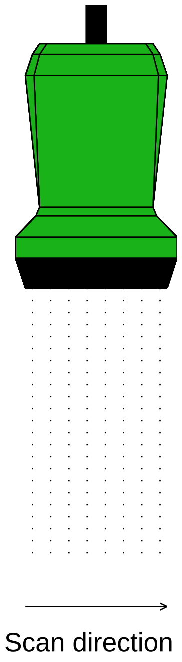

Figure 3.5: The principle of linear array imaging. A focused sub-array is used in every transmission, creating one image line. The active aperture is shifted and the procedure is repeated.

3.2.2 Phased array imaging

Phased array systems were developed for radar imaging, and have been adopted in the ultrasound community. The major advantage over linear array systems is that the beam is steered to the side, offering superior field of view. The image lines are defined on a polar grid, and an image line is created by steering the transmit beam in a certain direction and recording the reflected waves. The measured signals are then beamformed to yield an image line along this direction. Thereafter another direction is chosen and the procedure is repeated. By using this approach, the full array can be used both as the transmitting and the receiving aperture, unlike linear array imaging. The basic principle can be seen in Fig. 3.6.

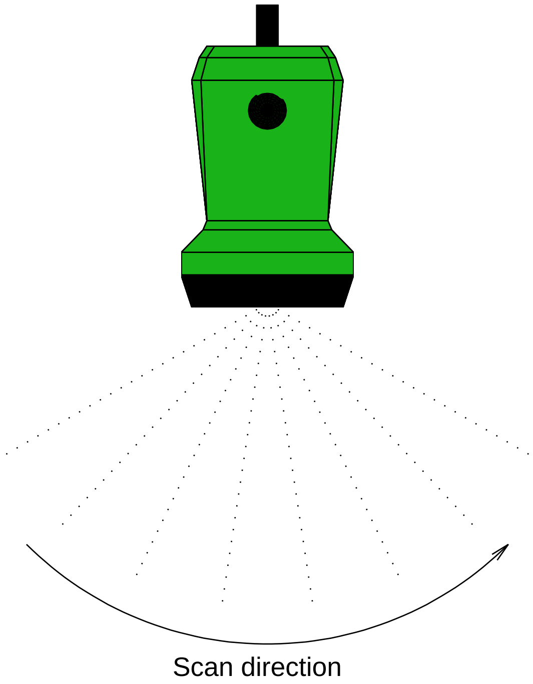

Figure 3.6: The principle of phased array imaging. The image lines are created by steering the beam in different directions. By doing so, image lines are created on a polar grid.

3.3 Synthetic aperture ultrasound imaging

The concept of synthetic aperture was originally developed, as for the phased array, for radar imaging systems [16–18]. In radar, the antenna could be mounted on an airplane while in operation. During flight, the antenna transmits electromagnetic radiation, and the reflected waves are received and recorded using the same antenna. By applying proper beamforming and signal processing techniques, an aperture can be synthesized which has the same extent as the flight path of the airplane. This offers superior resolution compared to the diffraction limit specified by the single antenna [8]. Ultrasound does suffer from some limitations compared to radar. The speed of sound is several orders of magnitude slower than the speed of light.[9] Moreover, the target is not discrete, as it is in many radar applications, but it is distributed over the entire imaging region.

---

[8] This can be explained by the Fourier relation for imaging systems: the larger the aperture the better resolution.

Several research groups have investigated the use of synthetic aperture techniques for ultrasound imaging. One way of applying the concept of synthetic aperture for synthesizing the transmitting aperture, is to use only one transducer element as the transmitting aperture. An unfocused spherical wave will then be created. One or several receiving elements will actively be listening for reflected waves from this wave-field which will be approximately spherical. In the next transmission, the transmitting aperture is shifted in space by exciting another transducer element, and the procedure is repeated. Using proper beamforming and under the assumption of stationarity, a transmitting aperture equal to that of both transducer elements can be synthesized by combining beamformed data from the two transmissions. This can, naturally, be extended to cover as many transmitting elements as required, as long as the assumption on stationarity is not violated. The principle of synthetic aperture imaging can be seen in Fig. 3.7.

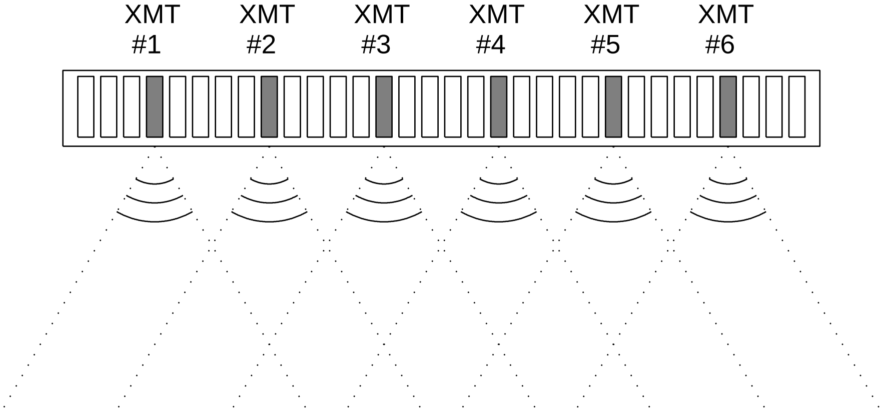

Figure 3.7: The principles of synthetic aperture imaging. A single transducer element is used in every transmission. A spherical wave is created, spreading the acoustic energy in all directions simultaneously, rather than focusing the acoustic energy in a narrow beam. Since the reflected echoes represent all directions of space, several receive lines can be beamformed in parallel. By combining data from different transmissions, a synthetic transmit beam can be created which can be focused in arbitrary chosen points simultaneously.

The transmitted acoustic field will have an approximately spherical nature, spreading the acoustic energy in all directions simultaneously. This should be compared to conventional imaging where it is desirable to focus acoustic energy in a narrow beam. By distributing the acoustic energy in all directions, several receive lines can be beamformed in parallel using dynamic receive focusing. The resolution of the resulting image will, of course, be poor since only one transmitting element is used. However, by combining data from several transmissions from different locations on the array, a larger transmitting aperture can be synthesized. By doing so, the transmit beam can be steered synthetically in any direction of interest, yielding dynamic transmit focusing. Compared to conventional ultrasound imaging it is possible to:

- attain dynamic transmit focusing and still maintain the number of transmissions per image on a reasonable level.

---

[9] The speed of sound in water is $\sim$1540 m/s, whereas the speed of light in vacuum is $\sim 300 \cdot 10^6$m/s!

- beamform several image lines in every transmission.

This will effectively provide means for faster data acquisition.

3.3.1 The mono-static approach

Synthetic aperture imaging comes in many forms. The method which is probably most identical to the original taken from the radar theory, is the method called the "mono-static approach" to synthetic aperture in ultrasound imaging. This has been investigated in [19–21]. In this approach one single transducer element acts as both the transmitter and the receiver, and the active element is slid across the array.

3.3.2 Synthetic transmit aperture ultrasound imaging

Synthetic transmit aperture ultrasound imaging is another method for creating a synthetic aperture. In this method, one transducer element is the active transmitter, and all transducer elements are listening for echoes from this element. Since the single element transmits a spherical wave in all directions, all receiving elements can be used to record data. This offers means for increasing the SNR compared to the mono-static approach. Extensive research has gone into this area [22–31], both in simulation and using different in-vivo applications such as tissue and blood flow imaging. The principle of the beamforming is depicted in Fig. 3.8. For this STA system, assume that data from K transmissions from different spatial locations on the aperture $\{\vec{r}_{xmt,k}\}_{k=0}^{K-1}$ are available. Assume that Q receiving elements are active in every transmission. Following the notation of [24], a spatial point $\vec{r}_p$ can be beamformed

$$H(\vec{r}_p) = \sum_{k=0}^{K-1} \underbrace{\sum_{q=0}^{Q-1} w_{kq} y_{kq}(t_{kpq})}_{L_k(\vec{r}_p)} \tag{3.15}$$

where $y_{kq}(t)$ is the received signal on the q:th receiving element located at $\vec{r}_{rcv,q}$ during the transmission when the k:th transmitting element is active. The aperture weighting function w_{kq} is applied on the receiving elements for the k:th transmission. The beamformed signals from the k:th transmission yields an image $L_k(\vec{r}_p)$, which is denoted *low resolution image*. The name refers to the small extent of the transmitting aperture[10] used for creating the image. By combining data from the K transmissions, a larger transmitting aperture can be synthesized and the *high resolution image* $H(\vec{r}_p)$ can be created.

The data from the different transmissions are beamformed by choosing the time point t_{kpq} corresponding to the time of flight from the k:th transmitting element out to the point of interest $\vec{r}_p$ and back to the q:th receiving element

$$t_{kpq} = \frac{|\vec{r}_p - \vec{r}_{xmt,k}|}{c} + \frac{|\vec{r}_{rcv,q} - \vec{r}_p|}{c}. \tag{3.16}$$

The distance $|\vec{r}_p - \vec{r}_{xmt,k}|$ is the distance from the k:th transmitter to the point of interest and $|\vec{r}_{rcv,q} - \vec{r}_p|$ is the distance from the point to the q:th receiving element. By summing data from different transmissions, both dynamic transmit and receive focusing can be attained.

---

[10] Which in fact is only one single transducer element.

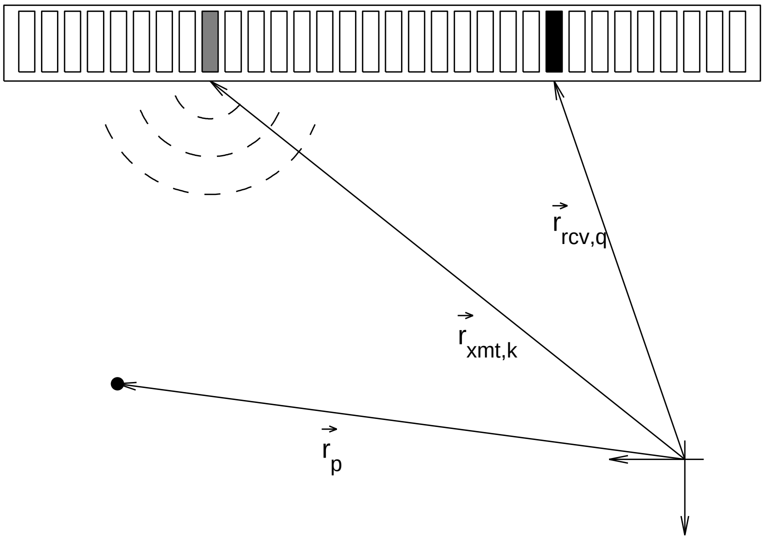

Figure 3.8: The transmitting location for the k:th transmitter is known as well as the location of the location of the q:th receiver. Defocused data is available for all transmitters. Therefore, it is possible to attain both dynamic transmit and receive focusing in any spatial point $\vec{r}_p$.

For the data to be summed coherently, no motion is allowed between successive transmissions. If motion is present, the low resolution images will not be combined in phase, resulting in a smearing of the PSF. This will influence the resolution and the contrast of the imaging system. Therefore, if rapid moving objects are to be imaged, only a few transmissions are affordable. Alternatively, methods can be applied where it is possible to acquire data from different transmitters simultaneously, e.g. spatial encoding of the transmitters.

Moreover, by using only one element in transmit severely limits the amount of acoustic energy transmitted in every emission. This decreases the SNR compared to a conventional focused system where several transducer elements are used. The use of virtual sources, briefly reviewed in section 3.3.3, has been suggested to partly compensate for this. Also, temporal encoding (explained in chapter 4) has been investigated for this purpose. By exciting several transmitters simultaneously, more acoustic energy can be transmitted, therefore, spatial encoding also offers an interesting alternative for increasing the SNR.

3.3.3 Virtual sources

One way of approaching a solution to the SNR problem in STA, is to use virtual sources. The principle of virtual sources is to group a number of transducer elements, apply appropriate focusing to create a spherical wave, and treat the focus point as a virtual transmitter. In this way, more acoustic energy is transmitted in every single transmission. This increases the SNR. The approach has been investigated by many research groups [32–36]. Combining virtual sources, temporal encoding (see chapter 4) and STA was investigated in [37–39] and a preclinical in-vivo study was conducted in [40, 41]. The position of the virtual source (the focal point) can be chosen to be positioned either behind or in front of the physical aperture. The position of the virtual source has to be considered in the beamforming, as was indicated in [42]. A schematic of a virtual source behind the transducer can be seen in Fig. 3.9 and a virtual source in front of the transducer can be seen in Fig. 3.10.

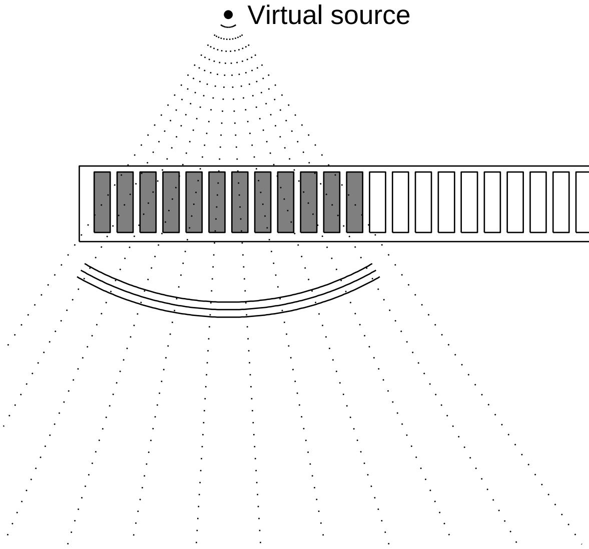

Figure 3.9: The virtual source positioned behind the actual transducer surface. The focusing generates a spherical wave.

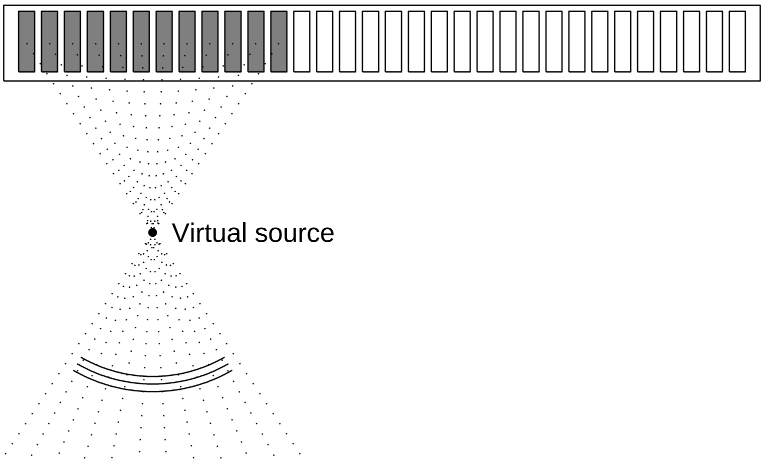

Figure 3.10: The virtual source is generated in the tissue. The source is brought "closer" to the tissue.

3.4 Summary

In this chapter the basics of ultrasound imaging has been reviewed. The array signal processing involved in beamforming and focusing has been explained. Conventional line based ultrasound imaging has been discussed. Linear array imaging and phased array imaging has been compared to ultrasound imaging using synthetic aperture techniques and the differences have been highlighted. STA has been explained in detail and plays a very important role in this dissertation. The reason for this is that the methods described in this dissertation concerning spatio-temporal encoding have been developed to combat the different problems associated with STA.

The benefits of using STA in ultrasound can be summarized as:

- Under stationarity, dynamic transmit and receive focusing can be achieved.
- Several image lines can be created from a single transmission, since the transmitted wave is spherical, interrogating all directions simultaneously.

STA, however, does suffer from drawbacks compared to traditional imaging:

- Only a small amount of acoustic energy is transmitted in every transmission, resulting in poor SNR.
- Rapid motion makes it problematic to focus the data coherently.

In chapter 4 previous work carried out on the topic of coded ultrasound for compensating for different problems in STA imaging is reviewed. In chapter 5 and chapter 6 the methods developed during this project for spatio-temporal encoding with the purpose of solving some of the problems concerning STA are presented.

CHAPTER

FOUR

Previous work on the topic of coded ultrasound

This chapter is intended to give a brief overview of some of the work which has been carried out previously on the topic of coded ultrasound imaging. The work presented in this chapter, however, does not represent a complete list of all existing work, as composing such a list would require a life time devoted to literature study. The main concepts of the ideas presented in this chapter are intended to give an introduction to coded ultrasound imaging. The results herein are based on findings reported by other researchers, and a reference to existing literature is given in the start of each section.

4.1 Temporal encoding

In a digital ultrasound system, factors playing important roles when it comes to SNR are

- The precision of the ADCs. (Determines the level of the quantization noise)
- Thermal noise.
- The amount of acoustic energy transmitted.

An easy way of changing the SNR is to manipulate the amount of acoustic energy which is being transmitted.

Normally, a short sinusoidal excitation waveform is used to attain good axial resolution and contrast. Such a waveform has, naturally, low energy. To compensate for this a number of transducer elements are focused in a specific point in the tissue, increasing the transmitted acoustic energy (see chapter 3, section 3.2).

In a STA system, only one transducer element is used in every transmission. Therefore, the transmitted acoustic energy will be low. Virtual sources have been suggested to partially compensate for this (described in chapter 3, section 3.3.3).

However, a straightforward approach of compensating for the low energy output, is to increase the excitation voltage. This will increase the transmitted energy and therefore increase the SNR. However, the voltage may not be increased to the limit, where it may generate a pressure amplitude in the tissue which could be harmful for the patient. These restrictions are generally set by the FDA [43].

Another way of increasing the transmitted energy is to increase the duration of the transmitted waveform. Choosing an excitation waveform with more oscillations, will increase the transmitted energy without increasing the excitation voltage. However, the bandwidth of the signal will also decrease, resulting in a poorer axial resolution.

Temporal encoding describes the theory of designing excitation waveforms with long duration without decreasing the bandwidth of the waveform. This can be achieved by e.g. frequency modulation (see section 4.1.2). However, even if the waveform exhibits a larger bandwidth, the resolution would still be poor if no attention was given to pulse compression.

Different methods for pulse compression exist, the matched filter, which will be analyzed in section 4.1.1, inverse filtering or deconvolution. The objective of pulse compression is to compress the longer waveform using signal processing, to yield the same axial resolution as with a short excitation waveform. Especially, the matched filter has been extensively analyzed in radar imaging systems, and has been adopted in medical ultrasound imaging.

4.1.1 The matched filter

The matched filter is used in many applications, joint time delay estimation and signal detection [6], pulse-compression [16] or noise suppression. To derive the matched filter, consider a deterministic signal $g(t)$ in additive noise $n(t)$

$$r(t) = g(t) + n(t), \tag{4.1}$$

where $g(t)$ has the Fourier transform $G(f)$ and $n(t)$ is a noise process with power spectral density $S_n(f)$. The noise process is assumed to be a stationary stochastic process with zero mean, and to have a power spectral density which is constant as a function of frequency

$$S_n(f) = P_n.$$

The measured signal $r(t)$ in (4.1) is filtered by a filter $h(t)$, so that

$$h(t) \star r(t) = \underbrace{h(t) \star g(t)}_{s(t)} + \underbrace{h(t) \star n(t)}_{v(t)}, \tag{4.2}$$

where $s(t)$ is the filtered signal part and $n(t)$ is the filtered noise part. The matched filter is defined as the filter, which maximizes the instantaneous peak signal power at time point t_0 compared to the filtered noise power (peak-power-SNR) [44]

$$SNR = \frac{|s(t)|^2_{t=t_0}}{E\ [|v(t)|^2\,]}. \tag{4.3}$$

The filtered noise power is given by [45]

$$E\left[\,|v(t)|^2\,\right] = \int S_n(f)|H(f)|^2\,df = P_n \int |H(f)|^2\,df \tag{4.4}$$

and the signal instantaneous peak power is

$$|s(t)|^2_{t=t_0} = \left| \int G(f)H(f)e^{j2\pi f t_0}\,df \right|^2 \tag{4.5}$$

The maximum of (4.3) with respect to the filter $h(t)$will clearly not be influenced by dividing the ratio with a positive scalar such as the signal energy

$$E_g = \int |G(f)|^2\,df. \tag{4.6}$$

The quantity which is to be maximized is, thus, given by

$$\frac{\left|\int G(f)H(f)e^{j2\pi f t_0}\,df\right|^2}{P_n\int |G(f)|^2\,df\cdot\int |H(f)|^2\,df}. \tag{4.7}$$

According to the Schwarz inequality

$$\left|\int G(f)H(f)e^{j2\pi f t_0}\,df\right|^2 \leq \int |G(f)|^2\;df\cdot\int |H(f)|^2\;df. \tag{4.8}$$

Equality of (4.8) occurs when

$$H(f) = K\,G^*(f)e^{-j2\pi f t_0}, \tag{4.9}$$

where K is an arbitrary scaling factor. Therefore, (4.3) is maximized when the transfer function of the filter is realized by (4.9). The impulse response of $h(t)$ will then be given by

$$h(t) = Kg(t_0 - t), \tag{4.10}$$

which is the time reversed version of $g(t)$ delayed by t_0. If the matched filter in (4.10) is chosen, the SNR specified in (4.3) will be

$$SNR = \frac{\left|\int |G(f)|^2\,df\right|^2}{P_n\int |G(f)|^2\,df} = \frac{E_g}{P_n}. \tag{4.11}$$

The matched filter also has another implication, consider the Fourier transform of the matched filtered signal part

$$\mathcal{F}\left\{g(t)\star g(t_0-t)\right\} = |G(f)|^2 e^{-j2\pi f t_0}. \tag{4.12}$$

By analyzing (4.12) it can be seen that the phase of the waveform is eliminated, since $G(f)G^*(f) = |G(f)|^2$. Therefore, the energy of the filtered signal will be concentrated around the time point t_0 even if the original waveform $g(t)$ was stretched in time. This property has made the matched filter a convenient and tractable solution for achieving pulse compression.

The SNR for an ultrasound system based on matched filtering

A comment to the SNR derived in 4.11 is that it may not always provide relevant information for ultrasound imaging. The matched filter receiver has been used extensively in radar imaging. However, in many radar applications the target (or) targets are discrete. In this case the matched filter provides an optimal detector [6]. In ultrasound imaging the ”target” is distributed all over the imaging region and can not be characterized as being discrete. Assume that the waveform $g(t)$ is transmitted, the received signal will then be

$$r(t) = h_{pe}(t)\star g(t) + n(t), \tag{4.13}$$

where $h_{pe}(t)$ is the linear process describing the interaction between the wave and the tissue and $n(t)$ is again the noise process. Since the tissue signal represents soft tissue, vessels, fat and other structures in the body, it is convenient to model $h_{pe}(t)$ as a stochastic signal. $h_{pe}(t)$ is assumed to be a white, Gaussian distributed stochastic process with zero mean. The auto-correlation function of $h_{pe}(t)$ is then

$$R_{pe}(\tau) = E\left[h_{pe}(t)h_{pe}(t+\tau)\right] = A\delta(\tau) \tag{4.14}$$

where A is the power spectral density of the process. Let the matched filter $g(-t)$ be applied

$$r(t) \star g(-t) = \underbrace{h_{pe}(t) \star g(t) \star g(-t)}_{s(t)} + \underbrace{n(t) \star g(-t)}_{v(t)}. \tag{4.15}$$

The SNR is now defined in a slightly different way

$$SNR = \frac{E\left[|s(t)|^2\right]}{E\left[|v(t)|^2\right]}. \tag{4.16}$$

The power of the filtered noise is still according to (4.11)

$$E\left[|v(t)|^2\right] = P_n E_g. \tag{4.17}$$

To evaluate the numerator of (4.16), consider the auto-correlation function of $s(t)$ in (4.15)

$$R_s(\tau) = E\left[s(t)s(t+\tau)\right] = R_{pe}(\tau) \star R_{gg}(\tau) \tag{4.18}$$

where $R_{gg}(\tau)$ is the auto-correlation function of $g(t) \star g(-t)$. By combining (4.14) and (4.18), the following expression for the auto-correlation function of $s(t)$ is derived

$$R_s(\tau) = AR_{gg}(\tau). \tag{4.19}$$

The numerator of (4.16) can be found by evaluating (4.20) in $\tau = 0$

$$R_s(0) = AR_{gg}(0) = AE_g^2. \tag{4.20}$$

Therefore the SNR will be

$$SNR = A\frac{E_g}{P_n}. \tag{4.21}$$

It can be seen that the SNR for a distributed target yields a very similar expression as when evaluating the peak-signal SNR for a discrete target.

4.1.2 The linear frequency modulated signal

In radar systems, frequency modulated signals have been used for temporal encoding since the 1950's. The waveform has been adopted in medical ultrasound systems and has been analyzed by many research groups. To explain frequency modulation, consider a complex exponential

$$g(t) = e^{j2\pi\theta(t)} \tag{4.22}$$

where $\theta(t)$ is the phase of the waveform as a function of time. The instantaneous frequency of (4.22) is given by [45]

$$f_i(t) = \frac{\partial\theta(t)}{\partial t}. \tag{4.23}$$

For a conventional sinusoid with center frequency f_c

$$g(t) = \sin\left(2\pi f_c t\right),$$

the instantaneous frequency will, thus, be

$$f_i(t) = f_c,$$

which is constant as a function of time. A frequency modulated signal is a signal where the instantaneous frequency changes over time. In particular, the **linear** frequency modulated signal (chirp) [1] has an instantaneous frequency which increases (or decreases) linearly over time. The phase function of the linear FM signal is therefore quadratic. The linear FM signal is defined as

$$g(t) = a(t)\sin\left(2\pi\left\{\left[f_c - \frac{B}{2}\right]t + \frac{B}{2T}t^2\right\}\right), \quad 0 \le t \le T, \tag{4.24}$$

where f_c is the center frequency, $a(t)$ is a time-dependent weighting function, T is the duration of the waveform and B is the bandwidth being swept. The instantaneous frequency of (4.24) is

$$f_i(t) = f_c - \frac{B}{2} + \frac{B}{T}t. \tag{4.25}$$

Equation (4.25) shows how the instantaneous frequency starts at $f_c - \frac{B}{2}$ at time point zero, and ends with the instantaneous frequency $f_c + \frac{B}{2}$ at time T. A linear FM signal can be seen in Fig. 4.1. The center frequency is 7 MHz, the bandwidth is 7 MHz, the duration is 20 μs and $a(t)$ was chosen to be a rectangular window.

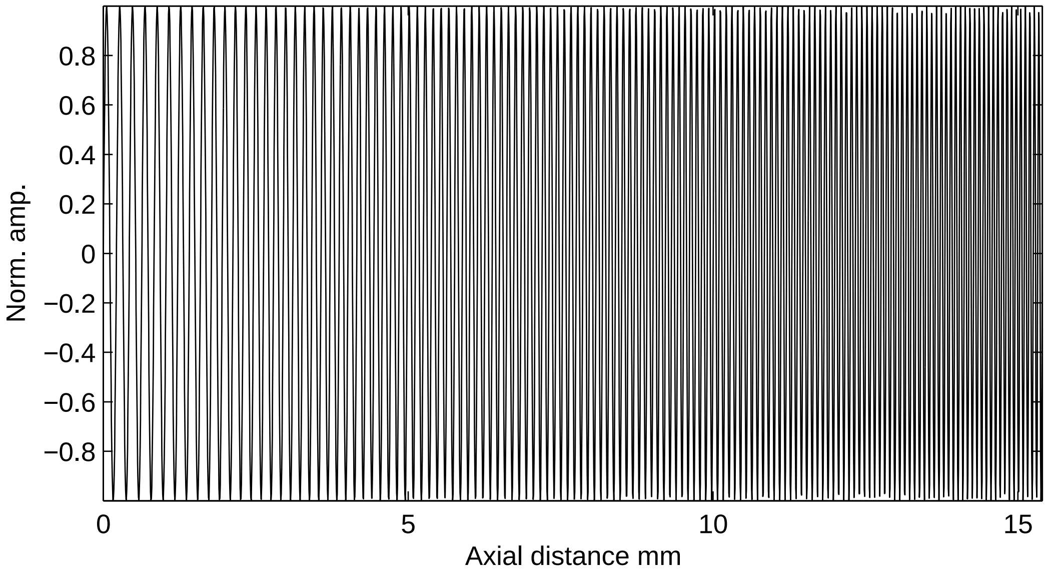

Figure 4.1: A linear FM signal with rectangular amplitude weighting. The center frequency is 7 MHz, the bandwidth 7 MHz and the duration 20 μs.

Pulse compression can be achieved by using a matched filter (4.10)

$$m(t) = g(-t). \tag{4.26}$$

---

[1] Some whales actually generate linear frequency modulated signals.

The envelope of the filtered output from the matched filter (4.26) for the waveform specified in Fig. 4.1 is depicted in Fig. 4.2. The level of the sidelobes is ~ -13 dB. This poses a problem for direct implementation of the linear FM signal and the corresponding matched filter in an ultrasound scanner. The dynamic range of an ultrasound system is $\geq$ 60 dB, which implies that an axial sidelobe structure of -13 dB would induce image artifacts. This will be obvious when objects with high contrast are imaged, like water filled cysts in surrounding tissue. The wall of the cyst would be reproduced at the location of the sidelobes, creating a ghost image of the wall inside the cyst. This degrades the image quality.

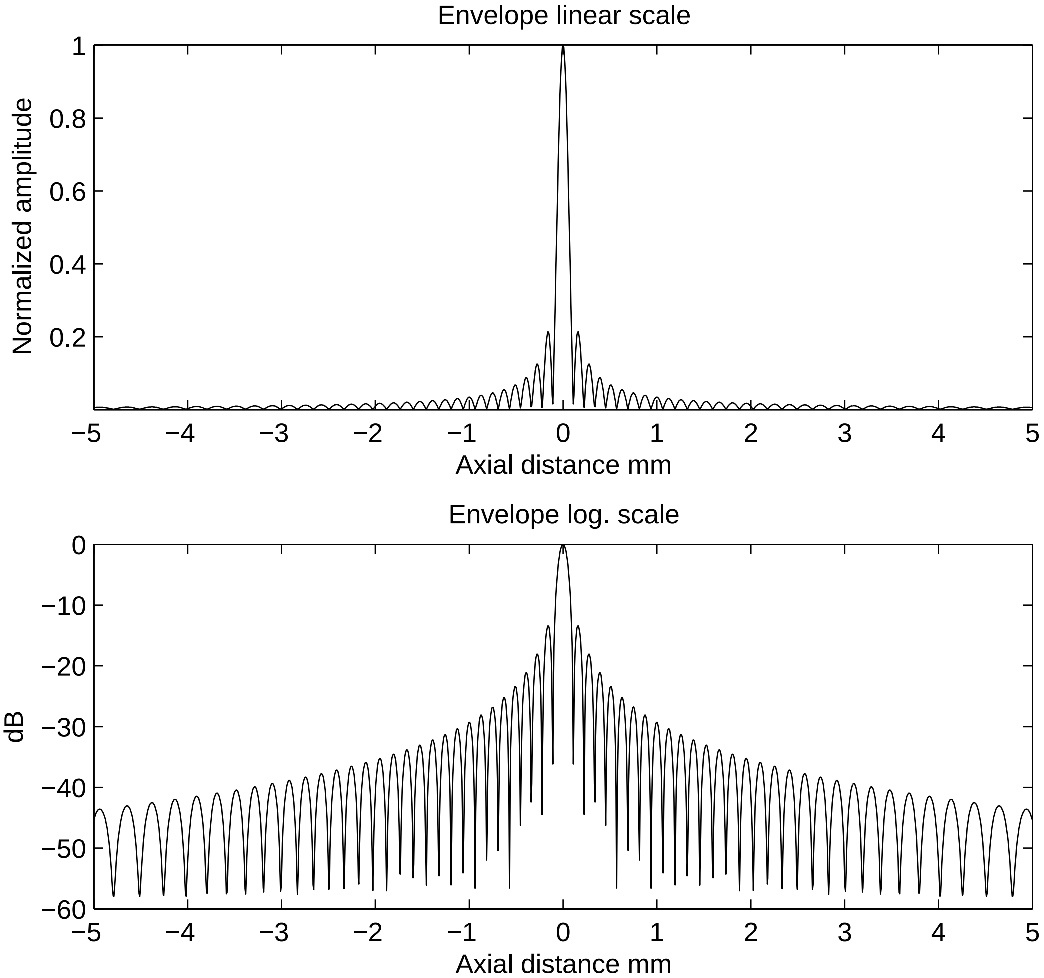

Figure 4.2: The filtered output for the linear FM signal. The top figure to is the envelope displayed on a linear scale, and the bottom figure is the envelope on a logarithmic scale. It can be seen that the level of the sidelobes is approximately -13 dB compared to the mainlobe.

Complications in ultrasound imaging

The theory and results presented in this section of the dissertation is based on the work reported by Misaridis [46–52]. According to the work reported, there are basically two problems with the linear FM signal and the corresponding matched filter. The problems concern axial contrast and can be explained by analyzing the spectrum of the linear FM signal in Fig. 4.3. The problems can be characterized as:

- The rectangular shape of the amplitude spectrum of the linear FM signal.
- The ripple in the passband of the amplitude spectrum.

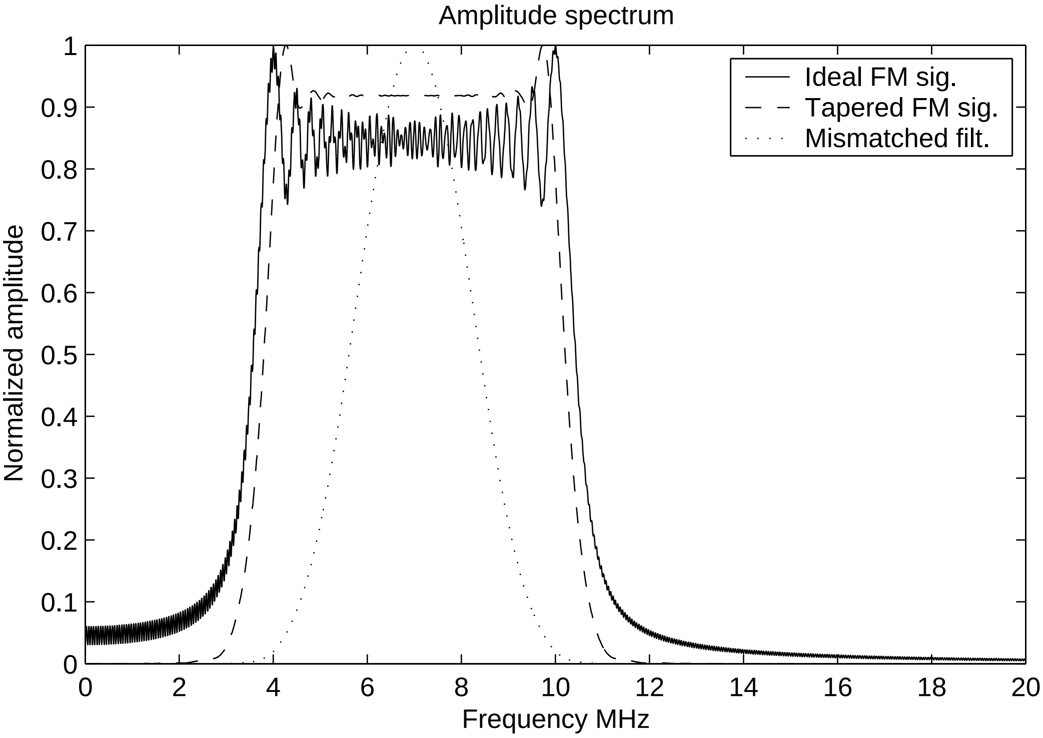

Figure 4.3: The solid line represents the linear FM signal with a center frequency of 7MHz and a bandwidth of 7 MHz when no amplitude weighting has been applied. A strong ripple can be seen in the passband of the signal. The dashed line represents the same linear FM signal when a Tukey window with 15% tapering has been applied. The ripple has been suppressed. The dotted line represents the mismatched filter when a Dolph-Chebyshev window with 80 dB relative sidelobe attenuation has been applied to the tapered linear FM signal.

The rectangular shape of the spectrum will result in a time response with sinc structure resulting in a high sidelobe structure. This can be verified by examining Fig. 4.2.

It can be shown that the ripple in the pass-band will result in "distant" sidelobes [49]. A replica of the filtered time response will then be generated at the location of these sidelobes, decreasing axial contrast.

A simple model for predicting the time response, is to model the spectrum of the signal as

$$\tilde{G}(f) = (a + b\cos(2\pi f t_0))\, G(f), \tag{4.27}$$

where $G(f)$ is the basic spectrum of the time response with unit gain, a is the amplification in the passband and b is the amplitude of the ripple. The time response of (4.27) can be written

$$\mathcal{F}^{-1}\left\{\tilde{G}(f)\right\} = \left(a\delta(t) + \frac{b}{2}\delta\left(t - t_0\right) + \frac{b}{2}\delta\left(t + t_0\right)\right) \star g(t). \tag{4.28}$$

Equation (4.28) shows that the time signal $g(t)$ will be replicated with an amplitude of $\frac{b}{2}$ a distance t_0 from the mainlobe.

Tapering of the excitation waveform

Tapering of the excitation waveform has been suggested for the purpose of reducing the ripple in the passband of the signal. However, the main idea of utilizing a longer waveform is to transmit more acoustic energy. Therefore, it is desirable to taper the signal as little as possible. A study of the effects of tapering in combination with mismatched filtering is given in [49]. A 7 MHz linear FM signal with a 7 MHz bandwidth, tapered using a Tukey window can be seen as the top plot in Fig. 4.4. The corresponding amplitude spectrum is depicted in Fig. 4.3 as the dashed line. Notice how the ripple in the passband is reduced.

Mismatched filtering to suppress axial sidelobes

Mismatched filtering has been suggested to suppress the rectangular shape of the filtered spectrum. Mismatched filtering means applying a temporal weighting on the matched filter. This has been suggested in radar imaging systems [17] and a study of mismatched filtering for ultrasound systems can be found in [49]. The mismatched filter is defined as

$$\tilde{m}(t) = g(-t) \cdot w(t), \tag{4.29}$$

where $g(t)$ is the transmitted waveform and $w(t)$ is the time window chosen to suppress the rectangular shape of $G(f)$. The Fourier transform of (4.29) is

$$\tilde{M}(f) = G^*(f) \star W(f). \tag{4.30}$$

A compression filter for the 7 MHz linear FM signal is shown in Fig. 4.4 as the bottom figure. The filter was mismatched using a Dolph-Chebyshev window with 80 dB relative sidelobe attenuation. Since the mismatching effectively reduces the amount of energy passed through the filter, the SNR will be effected. The expression for the SNR in (4.11) when applying the mismatched filter instead of the matched filter will be

$$SNR = \frac{\left|\displaystyle\int G(f)\tilde{M}(f)\,df\right|^2}{P_n \displaystyle\int |\tilde{M}(f)|^2\,df}. \tag{4.31}$$

For the example in Fig. 4.4, the decrease in SNR when using the mismatched filter will be $\sim$ 2 dB compared to using the matched filter.

The envelope of the mismatched filtered output of the 7 MHz tapered linear FM signal can be seen in Fig. 4.5. The axial sidelobe level is $\sim$ -60 dB compared to the matched filtered output in Fig. 4.2 where the sidelobe level is $\sim$ -13.5 dB. The SNR will be effected when applying temporal weighting on the transmitted waveform and the matched filter. Moreover, the spectrum of the mismatched filtered output will be narrower compared to when using the conventional matched filter. Therefore, the axial contrast will be improved at the cost of axial resolution. This can be seen by comparing Fig. 4.2 with Fig. 4.5.

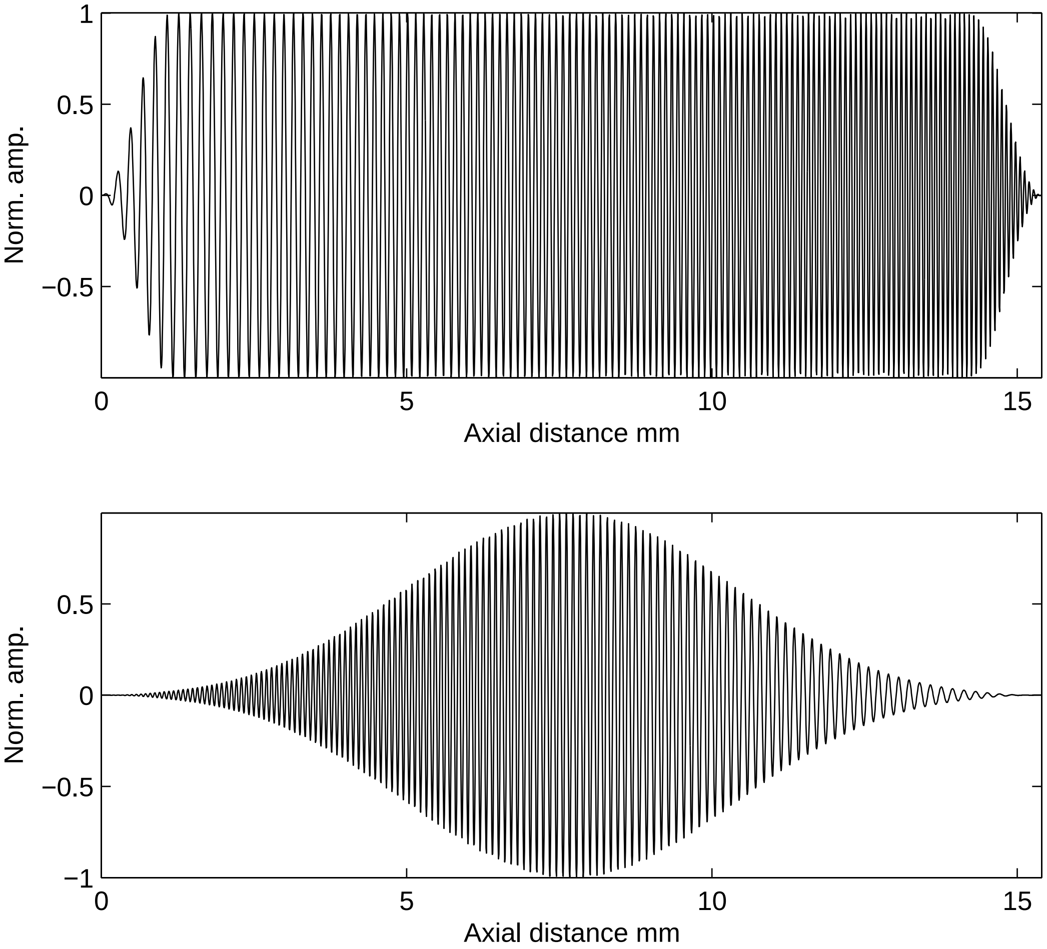

Figure 4.4: The 7 MHz linear FM signal with a bandwidth of 7 MHz. The excitation waveform has been tapered using a Tukey window with 15% tapering. The amplitude spectrum of this signal can be seen in Fig. 4.3 as the dashed line. The mismatched filter was generated by applying a Dolph Chebyshev window with 80 dB relative sidelobe attenuation on the time reversed version of the excitation waveform. The amplitude spectrum of the mismatched filter can be seen as the dotted line in Fig. 4.3.

4.1.3 Complementary code sequences

Complementary code sequences have been suggested as temporal encoding. A set of sequences of length N, $\{c_l(n)\}_{l=0}^{L-1}$ is said to be complementary if the set satisfies

$$\sum_{l=0}^{L-1} c_l(n) \star c_l(-n) = LN\delta(n). \tag{4.32}$$

A Golay complementary sequence is a special case with biphase elements [53, 54]. The work presented herein, explains how Golay coded excitation can be used for both temporal and spatial encoding. A typical set of complementary Golay sequences is given by (using vector notation)

$$\begin{aligned} \mathbf{c}_1 &= \begin{pmatrix} 1 & 1 \end{pmatrix}^T \\ \mathbf{c}_2 &= \begin{pmatrix} 1 & -1 \end{pmatrix}^T. \end{aligned} \tag{4.33}$$

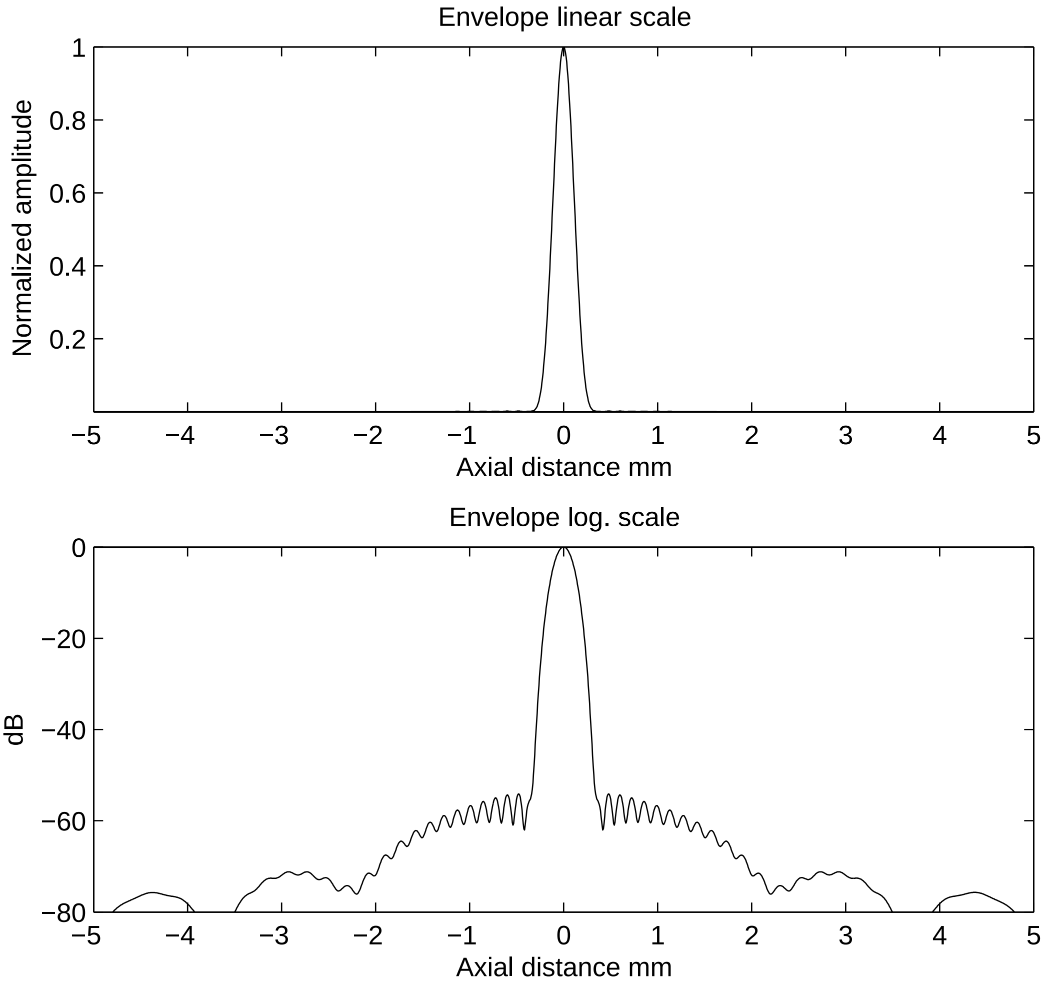

Figure 4.5: The envelope of the time signal resulting from the convolution between the excitation waveform and the mismatched filter. The top figure displays the envelope in linear scale, whereas the bottom figure shows the envelope in logarithmic scale. The axial sidelobes have been suppressed to a level of ∼-60 dB. The mainlobe has been widened compared to Fig. 4.2. Axial contrast will be improved on the cost of axial resolution and SNR.

Given one Golay pair $\{\mathbf{c}_1, \mathbf{c}_2\}$, another Golay pair $\{\tilde{\mathbf{c}}_1, \tilde{\mathbf{c}}_2\}$ of twice the length can be generated recursively using

$$\begin{aligned} \tilde{\mathbf{c}}_1 &= \begin{pmatrix} \mathbf{c}_1^T & \mathbf{c}_2^T \end{pmatrix}^T \\ \tilde{\mathbf{c}}_2 &= \begin{pmatrix} \mathbf{c}_1^T & -\mathbf{c}_2^T \end{pmatrix}^T. \end{aligned} \tag{4.34}$$

This procedure can be repeated to generate the desired length of the code sequence.

Two 16 bit codes generated using the recursive procedure in (4.34) starting from the base code given in (4.33) can be seen in Fig. 4.6. Calculating the matched filtered output for the two sequences given in Fig. 4.6, yields two cross-correlation functions with the same value at each lag but with opposite sign except at lag zero where the functions have the same sign. This property is displayed in Fig. 4.7. Summing the two filtered outputs produces a perfect delta function. Under ideal conditions, temporal coding using Golay sequences would result in ideal resolution and contrast.

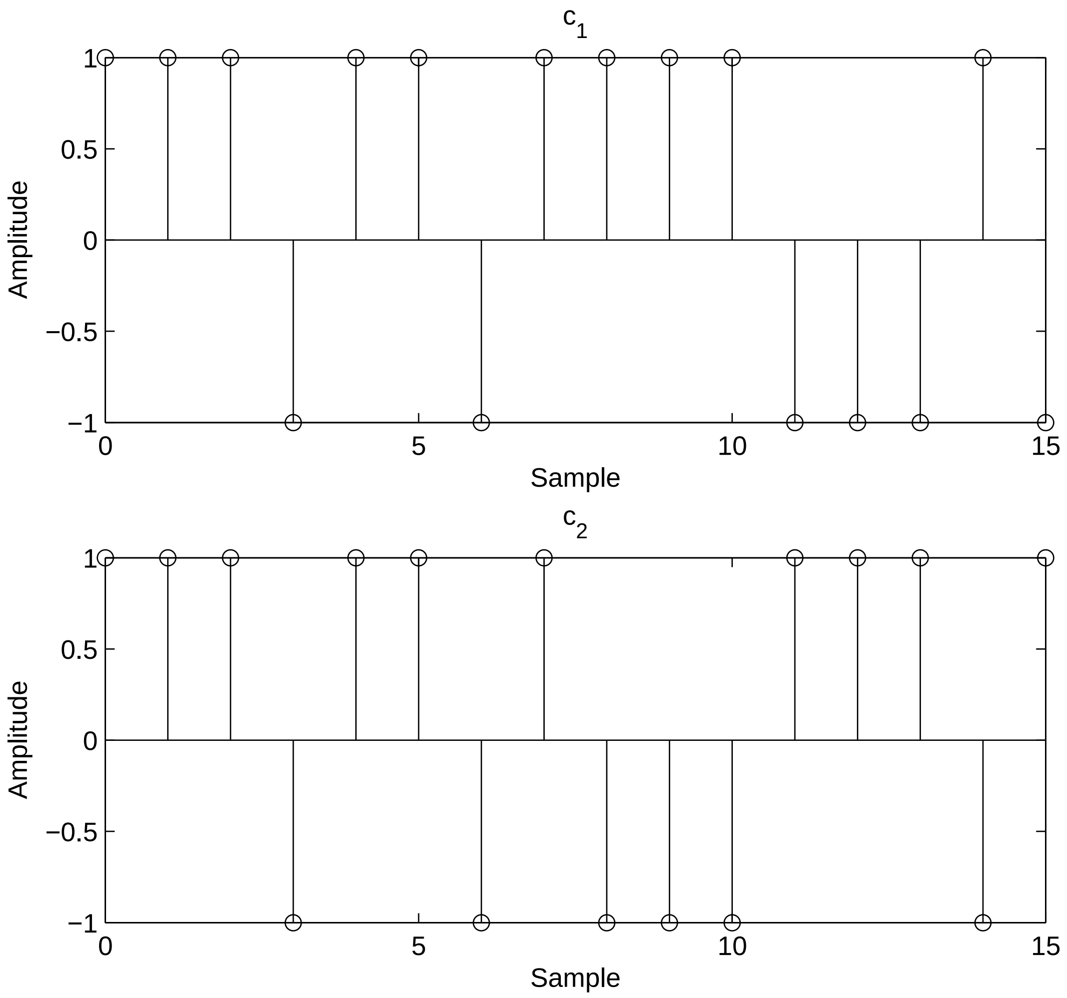

Figure 4.6: The top figure displays the first 16 bit Golay code generated from the base sequence given in (4.33), whereas the bottom figure displays the second code sequence. Together, the sequences form a complementary set.

Complications for ultrasound imaging

The property specified in (4.32) implies that the same number of transmissions have to be carried out as the number of sequences in the set, before pulse compression can be achieved. If (2.34) as assumed to be valid, and the (continuous) waveform $x(t)$ is transmitted from location $\vec{r}_{xmt,k}$, the generated field at spatial position $\vec{r}_{rcv,q}$ can be modeled as

$$\begin{aligned} p(\vec{r}_{rcv,q},t) = {} & x(t)\star \\ & \star\left(\sum_{p=0}^{P-1} s(\vec{r}_p)h(\vec{r}_{xmt,k},\vec{r}_p,t)\star h(\vec{r}_p,\vec{r}_{rcv,q},t)\star h_{tr}(t)\star a(\vec{r}_{xmt,k},\vec{r}_{rcv,q},\vec{r}_p,t)\right) \end{aligned} \tag{4.35}$$

The target consists of P scatterers and $s(\vec{r}_p)$ is the scatter strength of the p:th scatterer located at $vecr_p$, $h(\vec{r}_{xmt,k},\vec{r}_p,t)$ is the spatial impulse response between the transmitting element and the p:th scatterer, $h(\vec{r}_p,\vec{r}_{rcv,q},t)$ is the spatial impulse response between the p:th scatterer and the q:th receiving element, $h_{tr}(t)$ is the electro-mechanical impulse re-

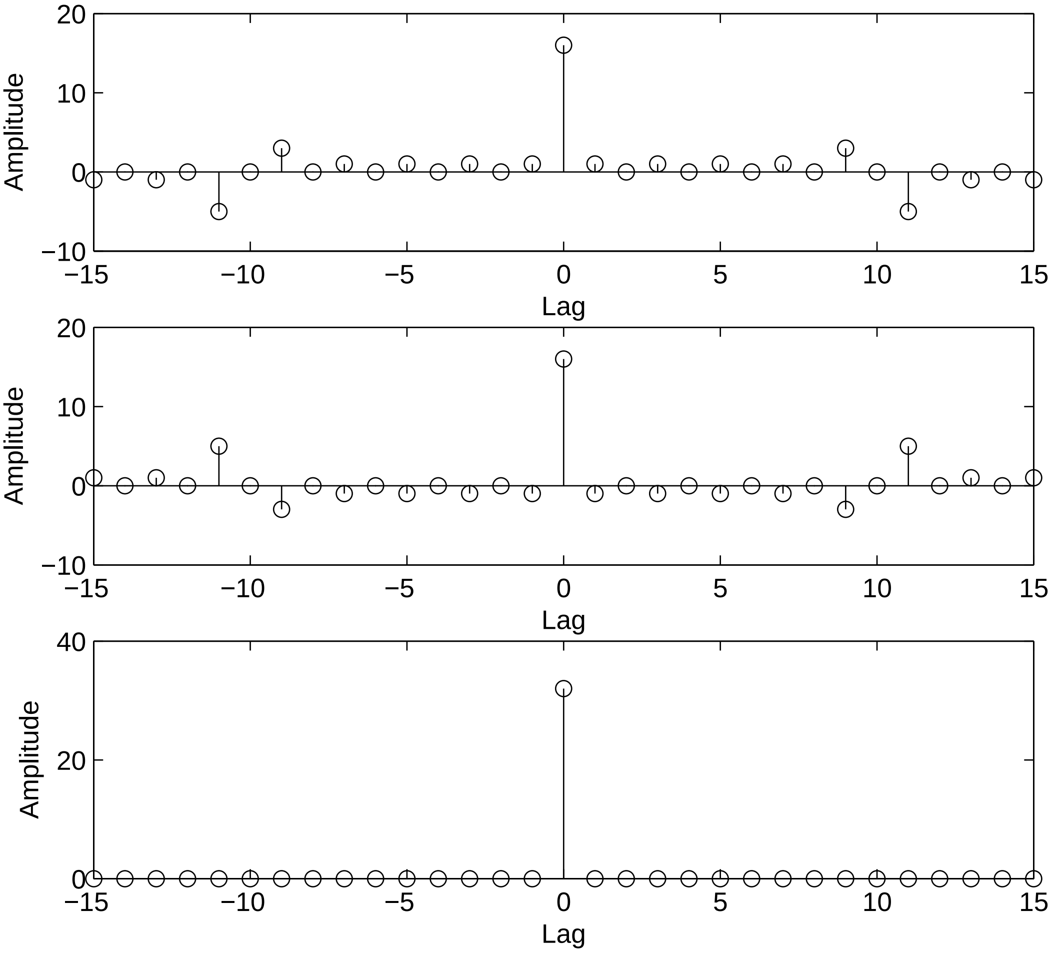

Figure 4.7: The matched filtered output for the two sequences are shown as the two top plots. The absolute value of the two functions are identical. Note how the value for each of the lags has opposite sign, except for lag zero. Here the two functions have the same sign. Adding the two filtered outputs results in a perfect delta function. Therefore, under ideal conditions a complementary set could achieve perfect resolution and contrast.

sponse of the transducer and $a(\vec{r}_{xmt,k}, \vec{r}_{rcv,q}, \vec{r}_p, t)$ is a filter accounting for depth dependent attenuation [55]. The expression within brackets of (4.35) can be written as a linear filter accounting for the propagation of the wave, such that the signal on the q:th receiver can be written

$$y_q(t) \quad = \quad x(t) \star h_{qk}(t). \tag{4.36}$$

Note that the spatial dependence of the transmitter located at $\vec{r}_{xmt,k}$ and the receiver located at $\vec{r}_{rcv,q}$ relative to the P scatterers has been totally incorporated in the sub-indexes qk. In this dissertation $h_{qk}(t)$ will be denoted the wave propagation operator.

Consider the Golay pair $\{c_1(n), c_2(n)\}$ as the excitation waveforms. The sampled version of (4.36) in the transmission when $c_1(n)$ is utilized is

$$y_{q,1}(n) \quad = \quad c_1(n) \star h_{qk,1}(n), \tag{4.37}$$

and the received and sampled signal is

$$y_{q,2}(n) \quad = \quad c_2(n) \star h_{qk,2}(n), \tag{4.38}$$

in the transmission when $c_2(n)$ is used. Note that the wave propagation operators for the different transmission have different sub-indexes. This represents motion between the transmissions. If there is no motion, $h_{qk,2}(n) = h_{qk,1}(n)$, and the two received signals can be correlated with the corresponding code sequence to yield

$$\begin{aligned} c_1(-n) \star y_{q,1}(n) &= c_1(-n) \star c_1(n) \star h_{qk,1}(n), && (4.39) \\ c_2(-n) \star y_{q,2}(n) &= c_2(-n) \star c_2(n) \star h_{qk,1}(n). && (4.40) \end{aligned}$$

Combining (4.39) and (4.40) then results in ideal compression in terms of axial resolution and contrast

$$c_1(-n) \star y_{q,1}(n) + c_2(-n) \star y_{q,2}(n) = 2L\delta(n) \star h_{qk,1}(n). \tag{4.41}$$

However, when motion between the transmissions is present, the decoding will suffer from motion artifacts. This makes Golay coding sensitive to imaging rapid moving objects.

Signal to noise ratio

Assume that a complementary set consisting of L sequences of length N is used to achieve the temporal encoding. Also, assume that the object under investigation is stationary during the data acquisition. The noise component influencing the l:th data acquisition is denoted $v_l(n)$. This process is modeled as a white, zero mean stochastic process with variance σ_v^2. Moreover, $v_l(n)$ is assumed to be independent from transmission to transmission. The filtered noise component from the L transmissions is given by

$$w(n) = \sum_{l=0}^{L-1} c_l(-n) \star v_l(n), \tag{4.42}$$

The noise power is

$$E\left[\left|\sum_{l=0}^{L-1} c_l(-n) \star v_l(n)\right|\right]. \tag{4.43}$$

The expression in (4.43) is the auto-correlation function of (4.42) evaluated at lag zero. Since the noise is independent from transmission to transmission, the autocorrelation of (4.42) is

$$R_w(m) = \sum_{l=0}^{L-1} R_{c_l}(m) \star R_v(m) = \sum_{l=0}^{L-1} R_{c_l}(m) \star \left(\sigma_v^2 \delta(m)\right) = \sigma_v^2 \sum_{l=0}^{L-1} R_{c_l}(m), \tag{4.44}$$

where $R_{c_l}(m)$ is the autocorrelation function of the l:th code sequence, and $R_v(m)$ is the auto-correlation function of the noise process. By evaluating (4.44) at $m = 0$ the noise power is obtained

$$R_w(0) = \sigma_v^2 LN. \tag{4.45}$$

The signal part of in the decoding problem is given by (4.32) with the maximum value LN. Therefore, the peak power SNR is given by

$$SNR = \frac{|LN|^2}{\sigma_v^2 LN} = \frac{LN}{\sigma_v^2} \tag{4.46}$$

4.2 Spatial encoding

Temporal encoding in ultrasound imaging aims at transmitting a long waveform while maintaining good axial resolution, by applying different signal processing algorithms. In contrast, the objective of spatial encoding is to excite several transmitters simultaneously using code sequences unique for each of the transmitters. The contributions to the received signal from the different transmitters, are separated utilizing the knowledge of these code sequences. By doing so, it is possible to process the data independently of the other transmitters although the data was acquired simultaneously. For STA, spatial encoding has the potential of

- Increasing the SNR for every transmission, since more acoustic energy can be transmitted compared to utilizing one single transmitter.
- Increasing the data acquisition rate.

The second point can be achieved in two ways. By actively utilizing several transmitters simultaneously, more acoustic energy is transmitted and a better SNR is attained in every data acquisition. Therefore, to yield the same overall SNR in the beamformed image as in the case of transmitting with only one transmitter, fewer transmissions can be afforded [2].

Secondly, imagine a scenario, where the information originating from the different transmitters can be decoded instantaneously at the receiver. In this case, fewer transmission can be carried out to obtain the same amount of information compared to the sequential data acquisition associated with STA. The principle of spatial encoding is depicted in Fig. 4.8.

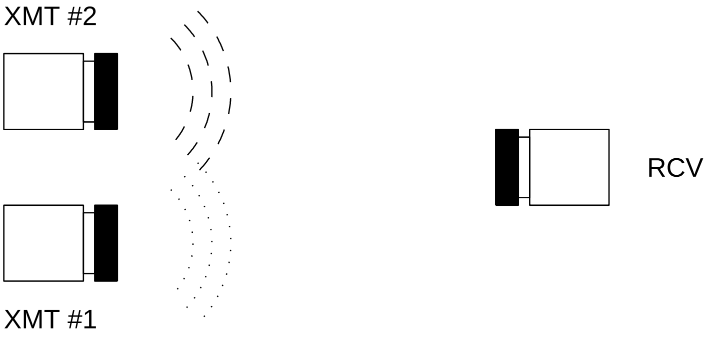

Figure 4.8: The principle of spatial encoding. Each active transmitter is assigned an individual code sequence. These code sequences are used to identify the transmitters. Knowledge about the code sequences makes it possible to distinguish signals originating from different transmitters.

4.2.1 The general model

The basic model is based on the equation given in (2.34). The wave propagation is assumed to be approximated by a linear process. Consider an ultrasound system with K

---

[2] This may, however, effect spatial resolution and contrast.

transmitters at spatial locations $\{\vec{r}_{xmt,k}\}_{k=0}^{K-1}$ and a single receiver located at $\vec{r}_{rcv,q}$. Assume that the k:th transmitter is excited using the waveform $x_k(t)$. Using the same definitions of the variables as in (4.36) the received signal can be modeled as

$$y_q(t) = \sum_{k=0}^{K-1} h_{qk}(t) \star x_k(t), \tag{4.47}$$

where $h_{qk}(t)$ is the wave propagating operator between the k:th transmitter and the q:th receiver, and is given by

$$h_{qk}(t) = \sum_{p=0}^{P-1} s(\vec{r}_p) h(\vec{r}_{xmt,k}, \vec{r}_p, t) \star h(\vec{r}_p, \vec{r}_{rcv,q}, t) \star h_{tr}(t) \star a(\vec{r}_{xmt,k}, \vec{r}_{rcv,q}, \vec{r}_p, t), \tag{4.48}$$

using the same definitions for the variables as used in 4.35.

4.2.2 Hadamard encoding

Hadamard encoding has been suggested as a method for spatial encoding in STA [56]. The transmitters are encoded using a conventional excitation waveform, but the waveform on each transmitter is premultiplied by an element of a row (or column) of a Hadamard matrix [3]. In the next transmission the waveforms are multiplied by the entries of the next row, and this procedure is repeated until all rows have been covered [4]. The signals from the different transmitters can then be decoded by adding and subtracting the received signals from the different transmissions.

For illustration purposes, consider the 2 × 2 Hadamard matrix

$$\mathbf{H}_2 = \begin{pmatrix} 1 & 1 \\ 1 & -1 \end{pmatrix}. \tag{4.49}$$

Now, consider a system with 2 active transmitters. In the first transmission, the first transmitter is assigned the excitation waveform $g(t)$, and so is the second transmitter. The received signal can be written using (4.47)

$$y_{q,1}(t) = h_{q1}(t) \star g(t) + h_{q2}(t) \star g(t). \tag{4.50}$$

In the second transmission the first transmitter is again excited using $g(t)$, whereas the second transmitter is excited using $-g(t)$. Under assumption of stationarity the received signal from the second transmission is

$$y_{q,2}(t) = h_{q1}(t) \star g(t) - h_{q2}(t) \star g(t). \tag{4.51}$$

Using the orthogonality of the Hadamard matrix, the signals corresponding to the two different transmitters can be decoded by

$$y_{q,1}(t) + y_{q,2}(t) = 2 \cdot h_{q1}(t) \star g(t), \tag{4.52}$$

$$y_{q,1}(t) - y_{q,2}(t) = 2 \cdot h_{q2}(t) \star g(t). \tag{4.53}$$

Of course this approach can be extended to encode an arbitrary number of transmitters, by just choosing a Hadamard matrix of appropriate dimension (2^k).

---

[3] Actually, any invertible matrix would do, but the Hadamard matrix has the advantage of being orthogonal and having binary entries. The decoding is then reduced to adding and subtracting different received signals.

[4] This number is equal to the number of active transmitters.

Signal to noise ratio

Assuming stationarity, and K active transmitters, the peak power SNR will be (after matched filtration with the basic pulse $g(t)$)

$$SNR = K\frac{E_g}{P_n}, \tag{4.54}$$

where E_g is the energy of $g(t)$ and P_n is the power spectral density of the noise.

Complications in ultrasound imaging

The main complication concerning Hadamard encoding in medical ultrasound imaging, is the assumption on stationarity. Even if the operator would hold the transducer absolutely still, the tissue would still be moving. This will result in errors when performing the decoding, creating image artifacts.

4.2.3 Complementary code sequences revisited

Orthogonal complementary sets of sequences can also be used to spatially encode the transmitters, and have been investigated by Chiao and Thomas [53]. The work reported herein is based on using orthogonal sets of Golay sequences. Two complementary sets of sequences $\{a_l(n)\}_{l=0}^{L-1}$ and $\{b_l(n)\}_{l=0}^{L-1}$ obeying (4.32) are said to be orthogonal if

$$\sum_{l=0}^{L-1} a_l(n) \star b_l(-n) = 0 \tag{4.55}$$

which means that the sum of the cross correlation functions between the sequences in the two sets must vanish. Therefore, if a certain set of Golay sequences is used to represent one specific transmitter, the inter-transmitter interference can be totally canceled. This can be illustrated by an example. Consider a system with two active transmitters, the first transmitter is represented by the complementary set $\{a_l(n)\}_{l=0}^{L-1}$ and the second transmitter is represented by the set $\{b_l(n)\}_{l=0}^{L-1}$. The sets both fulfill (4.32) and (4.55). Consider the l:th transmission, the received and sampled signal on the q:th receiving element is then

$$y_{q,l}(n) = h_{q1,l}(n) \star a_l(n) + h_{q2,l}(n) \star b_l(n). \tag{4.56}$$

By assuming stationarity, the wave propagating operators $h_{q1,l}(n), h_{q2,l}(n)$ are assumed to be time invariant and, therefore, the dependence on the transmission number l is removed

$$h_{qk,l}(n) = h_{qk}(n), \qquad l = 0, \ldots, L-1. \tag{4.57}$$

To extract the information from transmitter one, correlate the received signals with the corresponding code sequence and combine the result

$$\begin{aligned}\sum_{l=0}^{L-1} y_{q,l}(n) \star a_l(-n) &= \sum_{l=0}^{L-1} h_{q1}(n) \star a_l(n) \star a_l(-n) + \sum_{l=0}^{L-1} h_{q2}(n) \star b_l(n) \star a_l(-n) \\ &= h_{q1}(n) \star \underbrace{\left(\sum_{l=0}^{L-1} a_l(n) \star a_l(-n)\right)}_{=LN\delta(n)} + h_{q2}(n) \star \underbrace{\left(\sum_{l=0}^{L-1} b_l(n) \star a_l(-n)\right)}_{=0} \\ &= LNh_{q1}(n), \qquad (4.58)\end{aligned}$$

which is the wave propagating operator for the first transmitter. Repeating the procedure for the second set of code sequences $\{b_l(n)\}_{l=0}^{L-1}$ yields the wave propagating operator for the second transmitter.

Generation of orthogonal sets

In [53] a simple and efficient method for generating orthogonal sets of Golay sequences was proposed. Consider the matrix

$$\mathbf{G} = \begin{pmatrix} \mathbf{g}_{11} & \mathbf{g}_{12} \\ \mathbf{g}_{21} & \mathbf{g}_{22} \end{pmatrix} \qquad (4.59)$$

where

$$\begin{aligned}\mathbf{g}_{11} &= \begin{pmatrix} 1 & 1 \end{pmatrix}^T \\ \mathbf{g}_{12} &= \begin{pmatrix} -1 & 1 \end{pmatrix}^T \\ \mathbf{g}_{21} &= \begin{pmatrix} 1 & -1 \end{pmatrix}^T \\ \mathbf{g}_{22} &= \begin{pmatrix} -1 & -1 \end{pmatrix}^T.\end{aligned}$$

Note that $\{\mathbf{g}_{11}, \mathbf{g}_{12}\}$ make a complementary set and so do $\{\mathbf{g}_{21}, \mathbf{g}_{22}\}$. The set $\{\mathbf{g}_{11}, \mathbf{g}_{12}\}$ is orthogonal to the set $\{\mathbf{g}_{21}, \mathbf{g}_{22}\}$ with respect to (4.55). L orthogonal sets of complementary Golay sequences can be generated from

$$\mathbf{G} \otimes \mathbf{H}_{L/2}. \qquad (4.60)$$

Two sets of orthogonal four bit complementary Golay sequences can be seen in Fig. 4.9.

The auto-correlation functions of the two sets can be seen as the two left columns in Fig. 4.10 whereas the right column is the cross-correlation functions between the sequences of the two sets.

Complications for ultrasound imaging

Once again, for the decoding to work without errors, stationarity has to be assumed. It has previously been mentioned that rapid moving objects like the heart will introduce decoding errors resulting in image artifacts.

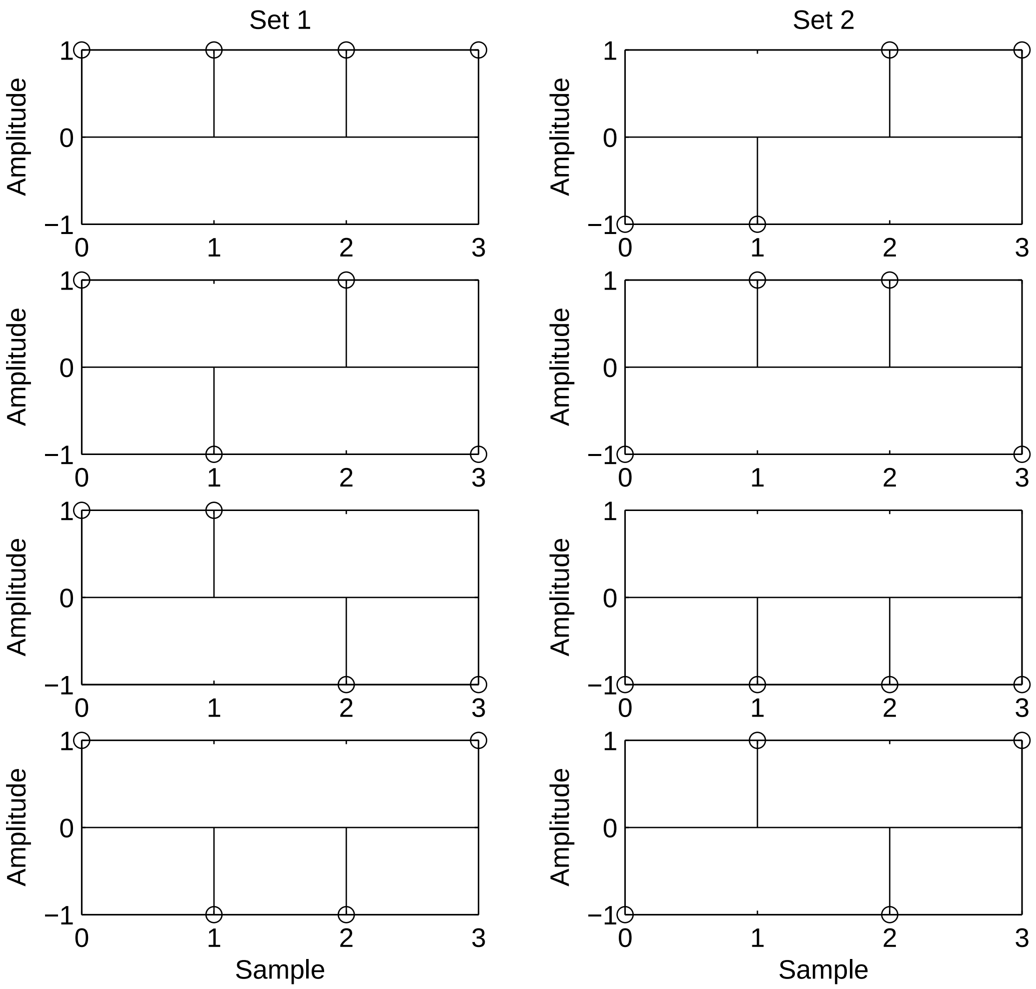

Figure 4.9: Two orthogonal sets of four bit complementary Golay sequences. The sequences were generated using (4.59) and(4.60).

4.2.4 Pseudo random code sequences

A technique using pseudo random sequences to encode the transmitters was proposed by Shen and Ebbini in [57,58]. The work has been further analyzed by Jeong and Ebbini in [59]. Each active transmitter is assigned an individual pseudo random code sequence. The reported results were based on M-sequences generated by a finite length shift register. The method is based on defining a grid of scatterers in the region of interest and estimating the scatter strength in these grid points. First a set of grid points is defined as (for a convex- or phased array system)

$$\vec{r}_p = \begin{pmatrix} r_p \cdot \sin(\theta_p) & r_p \cdot \cos(\theta_p) \end{pmatrix}^T, \qquad p = 0, \ldots, P-1. \tag{4.61}$$

The basic geometry can be seen in Fig. 4.11.

Let the transmitters be positioned at $\{\vec{r}_{xmt,k}\}_{k=0}^{K-1}$ and let each transmitter transmit the waveform $x_k(t)$. Assume that only a single scatterer with scatter strength $\vec{r}_p$ is present, positioned at $\vec{r}_p$. The received signal on the q:th receiving element can then be written

$$y_q(t) = s(\vec{r_p}) h_q(\vec{r}_p, t), \tag{4.62}$$

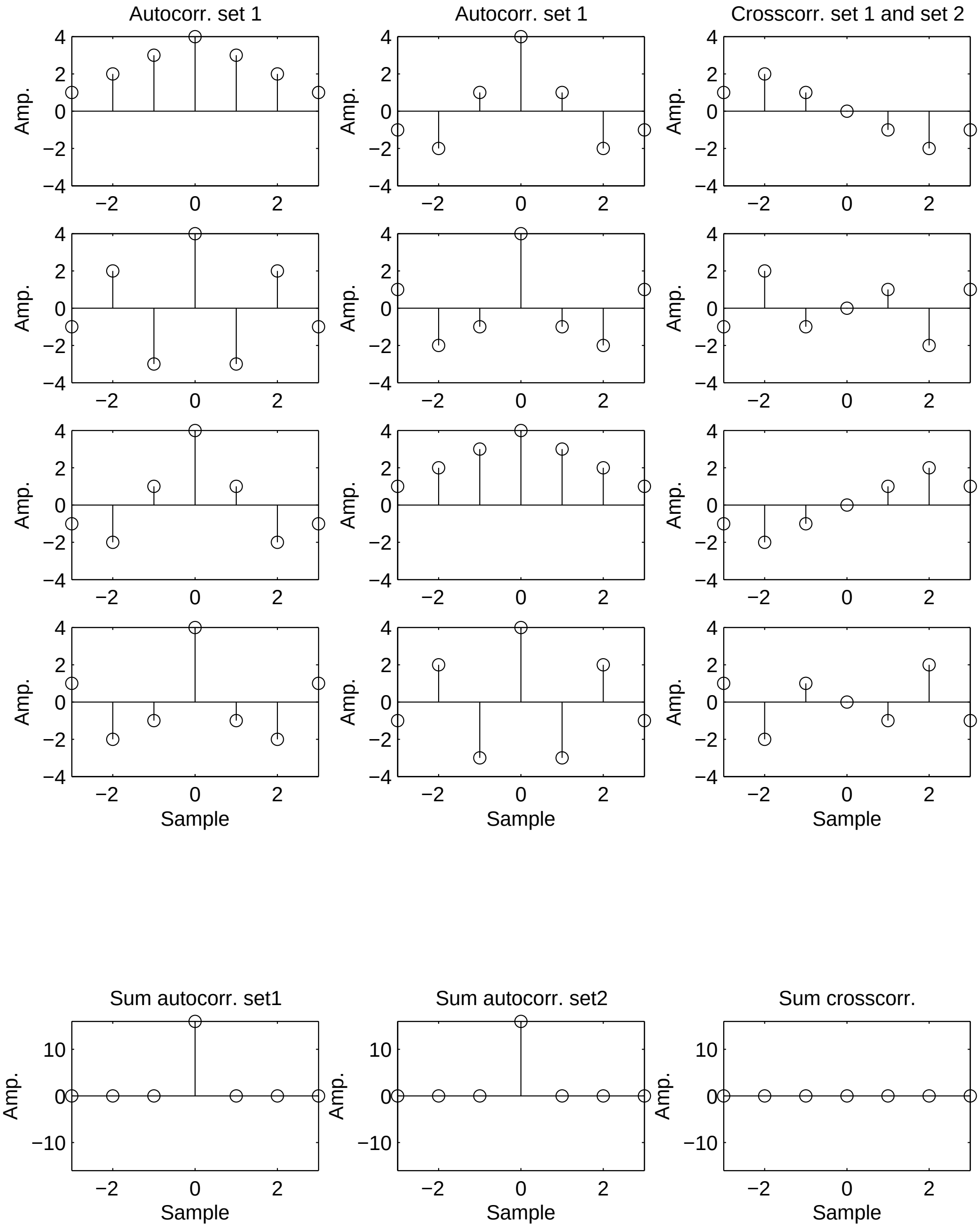

Figure 4.10: The auto-correlation functions of set one and set two and the cross-correlation functions between sequences of set one and set two. Note how the sum of the auto-correlation functions produce perfect delta functions whereas the sum of the cross-correlation functions vanish.

where

$$h_q(\vec{r}_p, t) = \sum_{k=0}^{K-1} h(\vec{r}_{xmt,k}, \vec{r}_p, t) \star h(\vec{r}_p, \vec{r}_{rcv,q}, t) \star h_{tr}(t) \star a(\vec{r}_{xmt,k}, \vec{r}_{rcv,q}, \vec{r}_p, t) \star x_k(t). \tag{4.63}$$

which in [57] was defined as the *spatio-temporal impulse response* for the q:th receiver. Sam-

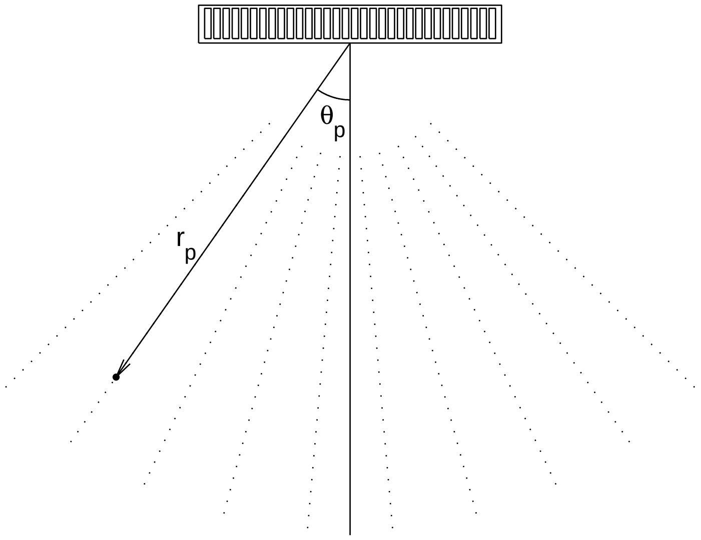

Figure 4.11: The geometry describing the grid points. The scatterers are assumed to be positioned on a grid corresponding to a convex- or phased array image grid. Each grid point is characterized by a radial distance from the center of the array r_p and an angle θ_p indicating the direction of the point.

pling of (4.62) makes it possible to write the received signal on vector form as

$$\mathbf{y}_q = s(\vec{r_p})\mathbf{h}_q(\vec{r}_p). \tag{4.64}$$

This formulation is extended by allowing all grid-points defined in (4.61) to reflect acoustic waves. By combining contributions from the scatterers in all grid points, makes it possible to write the total received and sampled signal as

$$\mathbf{y}_q = \mathbf{G}_q\mathbf{s}_q + \mathbf{v}_q, \tag{4.65}$$

where

$$\mathbf{s}_q = \begin{pmatrix} s(\vec{r}_0) & s(\vec{r}_1) & \ldots & s(\vec{r}_{P-1}) \end{pmatrix}^T$$

$$\mathbf{G}_q = \begin{pmatrix} \mathbf{h}_q(\vec{r}_0) & \mathbf{h}_q(\vec{r}_1) & \ldots & \mathbf{h}_q(\vec{r}_{P-1}) \end{pmatrix}^T,$$

and $\mathbf{v}_q$ is a noise process effecting the q:th receiver. The objective is now to try to estimate the scattering vector $\mathbf{s}_q$ which is most likely to generate the sampled time signal specified by $\mathbf{y}_q$. In the results reported, it is noted that $\mathbf{G}_q$ typically represents an under-determined linear system of equations. Therefore, an infinite number of solutions exists to the least squares estimation problem related to (4.65). However, by using the minimum-norm least-square estimator, a unique solution can be found [60]

$$\widehat{\mathbf{s}}_q = \mathbf{G}_q^H \left(\mathbf{G}_q\mathbf{G}_q^H\right)^\dagger \mathbf{y}_q. \tag{4.66}$$

The matrix $\mathbf{G}_q^H \left(\mathbf{G}_q\mathbf{G}_q^H\right)^\dagger$ is denoted the *Pseudo-Inverse Operator* (PIO). In [57,58] the design of the PIO is discussed. Therein, it is stated that this method is not diffraction limited.

Potentially, if a relevant solution to (4.66) can be found, a complete image can be formed after only one transmission, making the method "ultra" fast.

However, three complications trouble this method.

- The method relies on a fundamental assumption on the geometry of the object under investigation due to the pre-defined scattering grid.
- The spatio-temporal impulse responses have to obtained, either by modeling or measurements.
- The fact that the PIO typically does not have full column rank makes the estimation procedure troublesome.

First some comments regarding the statement of the method not being diffraction limited. It is indeed true that if a scatterer is positioned exactly in one of the grid points, and the PIO has full column rank, point resolution can be attained. However, a thorough analysis of performance for targets which do not coincide with the scattering grid is required. Also, tissue is a distributed medium and does not contain discrete targets like in radar imaging.

To form The PIO, the spatio-temporal impulse responses have to obtained, either by modeling or measurements. If modeling is used, it is uncertain if all effects which influence the wave-propagation can be accounted for, so that a sensible solution to (4.66) can be found. If the spatio-temporal impulse responses are to be measured, it is questionable in what medium such a measurement should be carried out. The properties of tissue, do indeed vary from patient to patient. Moreover, different objects in the body have different acoustic properties making it difficult to measure the spatio-temporal impulse responses in a meaningful way.

4.3 Summary

The purpose of this chapter has been to review recent findings on the topic of coded medical ultrasound imaging. Of course, a complete list is not available and , therefore, the interested reader is referred to the literature. In this chapter, both temporal- and spatial encoding techniques have been reviewed:

- Temporal encoding using the linear FM signal.
- Temporal encoding using complementary Golay sequences.
- Spatial encoding using Hadamard matrices.
- Spatial encoding using orthogonal sets of Golay sequences.
- Spatial encoding using pseudo-random sequences.

The purpose has been to give a foundation in coded ultrasound imaging. The basic principles of the reviewed methods have been explained, and expected benefits have been analyzed. Also, complications associated with the methods have been considered and discussed. This will facilitate the reading of the following chapters (Ch. 5 and Ch. 6), which summarize the work carried out on the topic of coded ultrasound imaging during the research project which this dissertation represents.

CHAPTER

FIVE

Spatial encoding by means of frequency division

This chapter summarizes the work which has been carried out during this project on a method for spatial encoding of the transmitters based on frequency division. The work has amounted to four papers:

- Multi Element Synthetic Aperture Transmission using a Frequency Division Approach.
  Fredrik Gran and Jørgen Arendt Jensen
  Published in Proceedings IEEE Ultrason. Symp, pp 1942-1946, 2003
- Frequency Division transmission imaging and synthetic aperture reconstruction.
  Fredrik Gran and Jørgen Arendt Jensen
  Submitted to IEEE Transactions on Ultrasonics, Ferroelectrics and Frequency control, August 2004
- Spatio-temporal encoding using narrow-band linear frequency modulated signals in synthetic aperture ultrasound imaging.
  Fredrik Gran and Jørgen Arendt Jensen
  Accepted for publication, Proceedings of SPIE Medical Imaging meeting, Ultrasonic Imaging and Signal Processing, February 2005
- Directional velocity estimation using a spatio-temporal encoding technique based on frequency division for synthetic transmit aperture ultrasound.
  Fredrik Gran and Jørgen Arendt Jensen
  Submitted to IEEE Transactions on Ultrasonics, Ferroelectrics and Frequency control, June 2005

The full papers are included as sections 5.7-5.10 at the end of this chapter. The papers are presented unedited. However, to better conform to the layout of this dissertation, the font size and layout has been changed in the papers which have not yet been published.

5.1 Basic principle

The idea behind spatial encoding of the transmitters by means of frequency division is to divide the ”acoustic channel” into a number of frequency bands with disjoint spectral support. One waveform is designed for each of the frequency bands. In a given transmission, each of the transmitters is assigned one of the waveforms. At the receiver, it is possible to distinguish between the signals originating from the different transmitters by using bandpass or matched filtering, even if the transmitters are active simultaneously.

To illustrate this, consider two time signals, $s(t)$ and $g(t)$, with the corresponding Fourier transforms $S(f)$ and $G(f)$. The signals $s(t)$ and $g(t)$ are said to have disjoint spectral support if

$$S(f) \cdot G(f) = 0. \tag{5.1}$$

The time domain representation of (5.1) is given by

$$\mathcal{F}^{-1}\Big\{S(f)G(f)\Big\} = s(t) \star g(t) = 0. \tag{5.2}$$

Now, consider the two processes

$$r_s(t) = h_s(t) \star s(t), \tag{5.3}$$

$$r_g(t) = h_g(t) \star g(t), \tag{5.4}$$

where $h_s(t)$ and $h_g(t)$ are two arbitrary stable filters with frequency responses $H_s(f)$ and $H_g(f)$ respectively. Then, the time signals $r_s(t)$ and $r_g(t)$ also have disjoint spectral support since,

$$\mathcal{F}\Big\{r_s(f) \star r_g(f)\Big\} = H_g(f)H_s(f)\underbrace{G(f)S(f)}_{=0} = 0. \tag{5.5}$$

Now, the principle behind spatial encoding based on frequency division emerges. If the passband of the transducer array can be divided into a number of narrow frequency bands, several transmitters can be active simultaneously without inter-transmitter interference. The information corresponding to the different transmitters can be separated at the receiver, even if the transmitters are effected by different linear processes. This can be realized by analyzing (5.5). In Fig. 5.1 the basic principle is displayed. The thick line represents the amplitude transfer function of the transducer. The transducer spectrum is divided into four frequency bands with disjoint spectral support[1]. The four frequency bands are displayed as the thin lines in Fig. 5.1.

Now, consider a more realistic situation with K transmitters and Q receivers. Let there be L different waveforms

$$x_l(t), l = 0, \ldots, L-1. \tag{5.6}$$

The k:th transmitter is transmitting the $l(k,n)$:th waveform during the n:th transmission. The received signal on the q:th receiver can be written as

$$r_q^n(t) = \sum_{k=0}^{K-1} h_{qk}(t) \star x_{l(k,n)}(t) + v_q^n(t) \tag{5.7}$$

where $v_q^n(t)$ is the noise effecting the q:th receiver during the n:th transmission. The function $h_{qk}(t)$ is the wave propagation operator as defined in (4.48). If the waveforms $x_l(t)$ have disjoint spectral support as specified in (5.2), the received signal after matched filtration with the $l(k,n)$:th waveform can be written

$$r_q^n(t) \star x_{l(k,n)}(-t) = h_{qk}(t) \star x_{l(k,n)}(t) \star x_{l(k,n)}(-t) + v_q^n(t) \star x_{l(k,n)}(-t). \tag{5.8}$$

---

[1] There will always be a certain amount of overlap between bands, since the signals are finite in time.

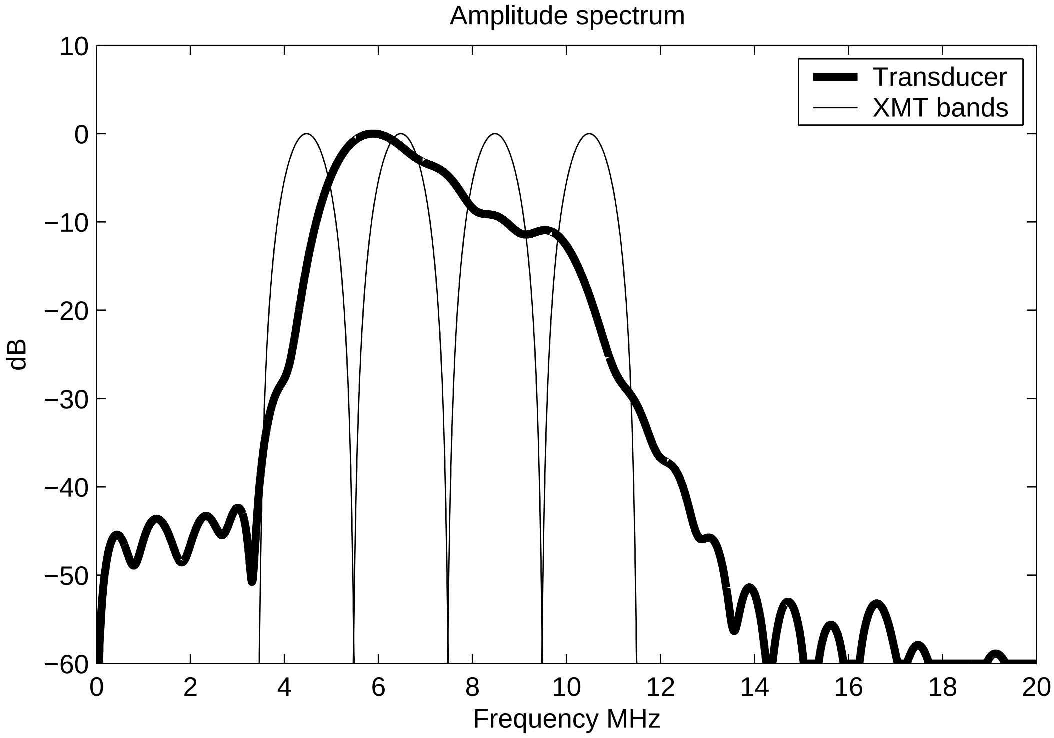

Figure 5.1: The basic principle of spatial encoding based on frequency division. The thick line represents the transducer transfer function. The four frequency bands are displayed as the thin curves. Since the frequency bands have approximately disjoint spectral support, the different signals can be separated using matched- or band pass filtration.

It is immediately realized that the decoding can be carried out instantaneously at the receiver. It is therefore possible to decode the received signals in only one transmission making the decoding insensitive to motion.

Using only one band for each transmitter would yield poor axial resolution, due to the limited bandwidth of each frequency band. To compensate for this, it is possible to distribute the data acquisition over a number of transmissions. By multiplexing the waveforms over the different transmitters for a number of transmissions, it is possible to synthesize a broadband excitation waveform for each transmitter.

Another practical complication arises when considering the shape of the spectra of the different waveforms. It is not possible to design waveforms with rectangular frequency responses, since this would require infinitely long waveforms. This means that the synthesized spectrum would exhibit ripples in the passband. This can be realized by summing the four frequency bands in Fig. 5.1. Ripples in the spectrum will degrade the resolution and contrast of the imaging system.

In the work presented in this dissertation this problem was solved by defining two overlapping sets of excitation signals, so that a smooth passband could be synthesized. The principle can be seen in Fig. 5.2. Signals from different sets must not be transmitted simultaneously, since these signals do not have disjoint spectral support.

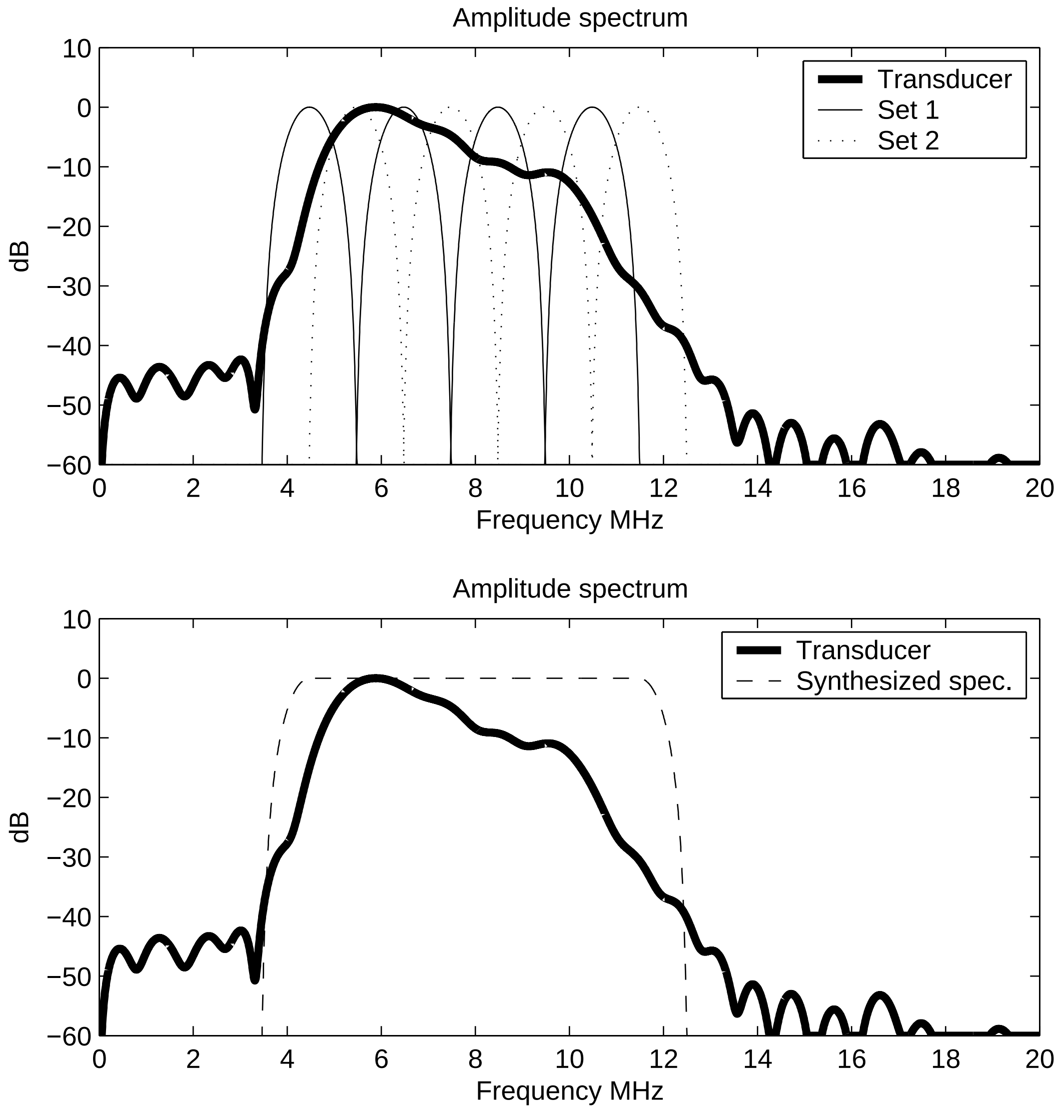

Figure 5.2: The top figure displays the two sets of signals. The solid lines represents the first set and the dotted lines represent the second set. Note that there is no overlap between neighboring bands within a set. Signals from different sets must not be transmitted simultaneously, since they have overlapping frequencies. The bottom figure displays the synthesized broadband spectrum.

5.2 Code and filter design

In this section some design considerations are reviewed which have been explored during the course of this project.

5.2.1 Linear phase waveforms

A very simple and attractive method for designing the waveforms is simply to design amplitude spectra with disjoint spectral support and appropriate frequency characteristic. To derive the excitation waveforms, linear phase FIR waveforms are generated using some optimization criteria. This was suggested in [61] (section 5.7). Assume that L waveforms have to be designed. The frequency spectra of these waveforms are specified by $X_l(f)$ and the matched filtered version of the waveforms is $|X_l(f)|^2$.

As mentioned earlier, two signal sets have to be generated. The sets must fulfill the following two criteria

- The signal within a set have to have disjoint spectral support.
- The two sets, when combined, must produce a smooth broadband spectrum.

One possibility of achieving these two properties, is to choose the desired spectra for the l:th waveform as

$$X_l(f) = \begin{cases} \sqrt{\frac{1}{2}\left(1+\cos\left(2\pi\frac{f-f_l}{B}\right)\right)}, & |f-f_l| \leq \frac{B}{2} \\ 0, & \text{otherwise,} \end{cases} \tag{5.9}$$

where B is the bandwidth and f_l is the center frequency of the l:th waveform. The matched filtered spectrum of the l:th waveform is then

$$|X_l(f)|^2 = \begin{cases} \frac{1}{2}\left(1+\cos\left(2\pi\frac{f-f_l}{B}\right)\right), & |f-f_l| \leq \frac{B}{2} \\ 0, & \text{otherwise.} \end{cases} \tag{5.10}$$

So, why is the spectrum specified (5.10) the desired spectrum? It turns out that if L signals are specified with the center frequencies

$$f_l = f_0 + \frac{B}{2}l, \quad l = 0, \ldots, L-1, \tag{5.11}$$

where f_0 is the center frequency of the first band, two sets of signals can be created with properties demonstrated in Fig. 5.2. This can be achieved by sorting all waveforms with odd index in set one and the waveforms with even index in set two. The waveforms in either of the sets will then have disjoint spectral support, and the two sets of signals, when combined, produce a spectrum with constant amplification in the passband.

Now, actual time signals have to be designed, so that the spectra of the signals give a good match to the desired spectra. One way of designing linear phase FIR waveforms is to use least squares optimization[2] [62]. The waveforms are calculated, so that the time representation of the waveform is the waveform which minimizes the error between the desired spectrum and the actual spectrum of the waveform, in the least square sense.

The separation filters are simply the corresponding matched filters of the excitation waveforms.

Complications

Two complications were noted during the development of the method in [61].

---

[2] Using the `firls` function in Matlab, ©1994-2005 by The MathWorks, Inc., 24 Prime Park Way, Natwick, MA 01760-1500.

- The amplitude of the waveform is not constant due to the linear phase constraint.
- Hardware problems were encountered when trying to transmit waveforms with great diversity in amplitude.

The first problem can be realized by looking at the time response of a signal designed using the approach based on the spectra given in (5.10) and least squares optimization compared to a linear FM signal. In Fig. 5.3, the top figure displays a linear FM signal with center frequency 7 MHz, bandwidth 2 MHz and duration 20 μs. A temporal Tukey-window with 15% tapering was applied. The bottom figure is a signal designed for frequency division, with the same center frequency, bandwidth and duration. Since the maximum excitation voltage is fixed in an ultrasound system, much less energy can be transmitted using the waveform designed for frequency division purposes compared to the linear FM signal. This will limit the SNR of the matched filtered output for the frequency division approach, and effectively remove the potential benefits from using spatial encoding to increase SNR.

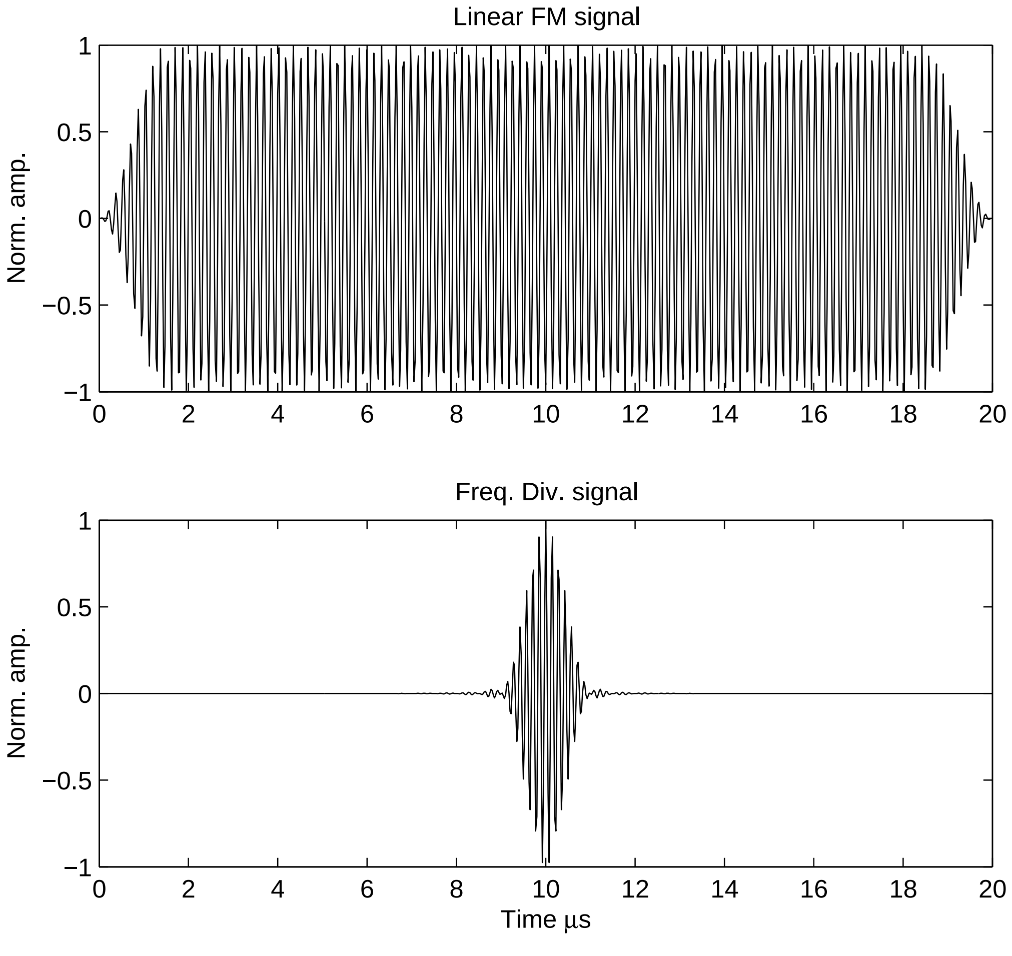

Figure 5.3: The top figure is a linear FM signal with center frequency 7 MHz, bandwidth 2 MHz and duration 20 μs. A temporal Tukey-window with 15% tapering was applied. The bottom figure is a signal designed for frequency division with the same center frequency, bandwidth and duration. When the amplitude is restricted, much less energy is transmitted using the waveform designed for frequency division purposes. This effects the SNR of the matched filtered output.

The second complication arose when the waveforms which exhibited great diversity in amplitude were implemented into a physical system [63] (RASMUS). It turned out that the system was not capable of transmitting the parts of the signal having very low amplitude. Therefore, the transmitted waveform did no longer possess the desired spectrum. In Fig. 5.4 the quantized excitation[3] waveform is shown in the top figure and the received signal is shown as the bottom figure. The received signal was created as the average of 32 measurements in a water tank, with a metal wire positioned at a depth of 42 mm relative to the transducer. A BK8804 linear array transducer was used to carry out the experiment. The duration of the excitation waveform was 20 μs, the bandwidth was 0.5 MHz and the center frequency was 5.4 MHz. It can be seen that the parts of the signal where the amplitude is low has been totally removed. This corresponds to applying a time window on the excitation waveform. The phenomena is more obvious in the top figure of Fig. 5.5 where the envelopes of the two signals are displayed. Moreover, the "window theory" is further verified by analyzing the spectrum of the excitation waveform and the received

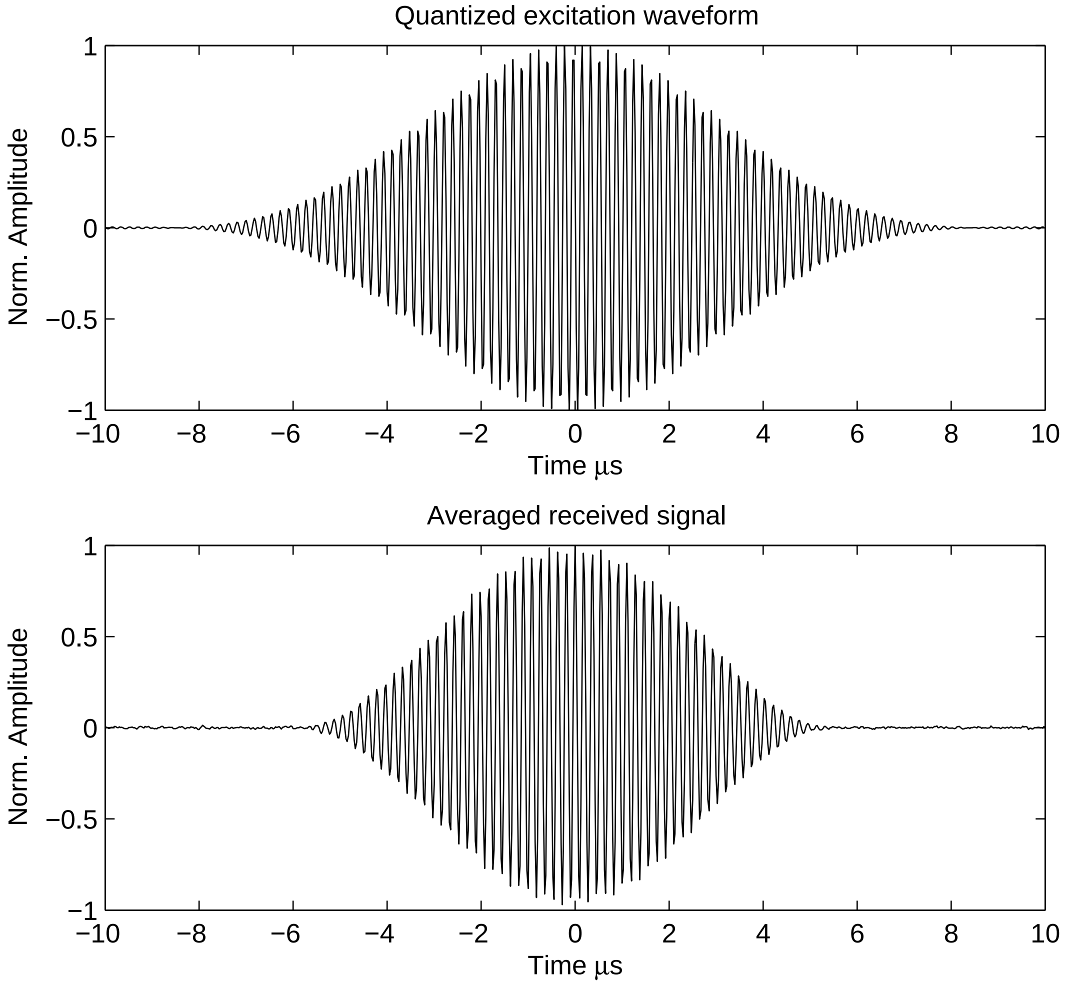

Figure 5.4: The top figure is the quantized excitation waveform. The center frequency is 5.4 MHz, bandwidth 0.5 MHz and has a duration of 20 μs. The time signal resulting from averaging 32 received signal generated using this excitation waveform with a wire target in water can be seen as the bottom figure.

---

[3] The RASMUS system has a waveform generator with a resolution of 12 bit.

signal, respectively. Applying a window on the excitation waveform corresponds to convolving the spectrum of the excitation waveform with the spectrum of the window. This would result in a smearing of the spectrum of the excitation waveform. By examining the bottom figure of Fig. 5.5 it can be concluded that it is indeed so. The spectrum of the received signal is widened compared to the spectrum of the excitation waveform. This results in that the property of disjoint spectral support amongst the signals in a given set is no longer valid. Therefore, the synthesis of a broadband pulse will be complicated, as the spectrum does no longer possess the desired shape.

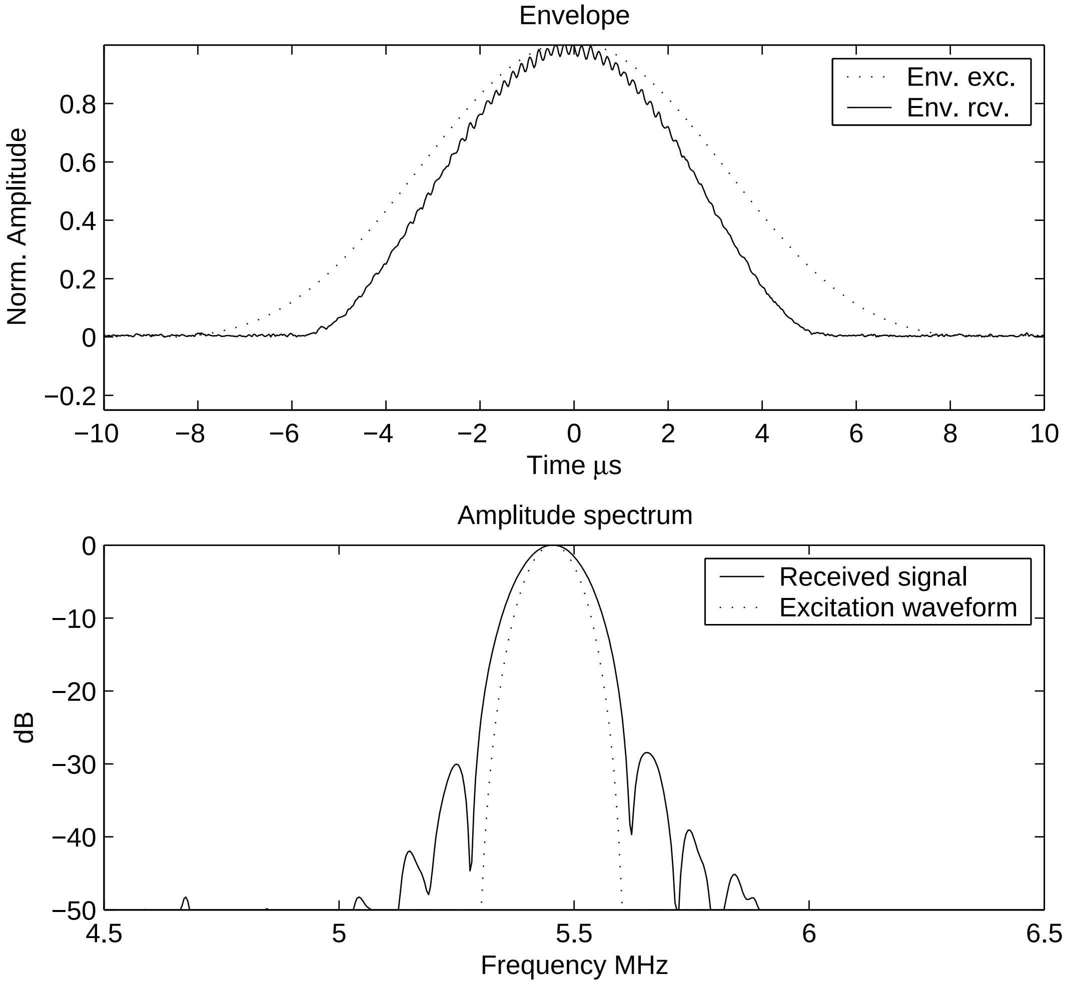

Figure 5.5: The top figure shows the envelope of the quantized excitation waveform and received signal, respectively. Seemingly, the received signal undergoes a transformation which can be regarded as windowing the excitation waveform. This is also verified when the spectra of the two signals are analyzed. The spectrum of the received signal is widened compared to that of the excitation waveform.

5.2.2 Narrow band linear frequency modulated signals

In [64, 65] (sections 5.8 and 5.9) the method was developed further. Herein, it was suggested to design the excitation waveforms as narrow band linear FM signals. The linear FM signal has the advantage of having constant amplitude during the entire waveform.

Therefore, no concern has to be given to exploiting the transmitting capabilities of the system to the maximum. The L linear FM signals are defined as

$$x_l(t) = a(t)\sin\left(2\pi\left\{\left[f_l - \frac{B}{2}\right]t + \frac{B}{2T}t^2\right\}\right), \quad \begin{array}{c} 0 \leq t \leq T, \\ l = 0, \ldots, L-1, \end{array} \tag{5.12}$$

where f_l is the center frequency of the l:th excitation waveform, B is the bandwidth of the waveforms, T is the duration and $a(t)$ is a temporal weighting applied to the waveform. The excitation waveforms are shown as the top figure of Fig. 5.6. The bandwidth of the signals where 2 MHz, the duration was 25 μs and the temporal weighting was chosen to be a Tukey window with 25% tapering. Note that the signals within a signal set no longer have disjoint spectral support. Therefore there will be inter-transmitter interference. To reduce the inter-transmitter interference, the separation filters are chosen to be

$$m_l(t) = x_l(-t) \star h_l(t), \qquad l = 0, \ldots, L-1, \tag{5.13}$$

which is the matched filter for the l:th waveform convolved with a filter $h_l(t)$. The purpose of $h_l(t)$ is to reduce inter-transmitter interference and to shape the spectrum of the filtered waveform, facilitating broadband synthesis. The desired amplitude spectrum of $h_l(t)$ is chosen to be

$$H_l(f) = \begin{cases} \frac{1}{2}\left(1 + \cos\left(2\pi\frac{f-f_l}{B}\right)\right), & |f - f_l| \leq \frac{B}{2} \\ 0, & \text{otherwise.} \end{cases} \tag{5.14}$$

and the corresponding time signal is derived as the linear phase FIR filter with a specific duration, which minimizes the error between the spectrum of the actual filter and the desired spectrum, in the least square sense. The separation filters for the two signal sets are shown as the bottom figure in Fig. 5.6. A measure for the inter-transmitter interference is to evaluate the ratio of the energy of the filtered excitation waveform and the energy of the filtered excitation waveform from the neighboring band in the same set

$$10\log_{10}\left\{\frac{\int \left|x_{l+2}(t) \star m_l(t)\right|^2 dt}{\int \left|x_l(t) \star m_l(t)\right|^2 dt}\right\}. \tag{5.15}$$

Using the matched filter as separation filter for the waveforms in Fig. 5.6, this ratio will be $\sim$ -41 dB. In contrast, the ratio will be $\sim$ -53 dB when using the filter designed using 5.13 and 5.14. The synthesized spectrum is displayed in Fig. 5.7 as the top figure, and the corresponding time signal convolved with the transducer impulse response is given as the bottom figure. The axial sidelobe structure is below -60 dB ensuring acceptable image quality

5.3 Signal to noise ratio

In this section, the effects on SNR when using the frequency division approach for spatial encoding will be discussed. First the SNR of a reference system will be derived. The reference system is a STA system with L transmitters. The transmitters are excited sequentially utilizing the excitation waveform $x_{ref}(t)$ with the energy E_{ref}. The received

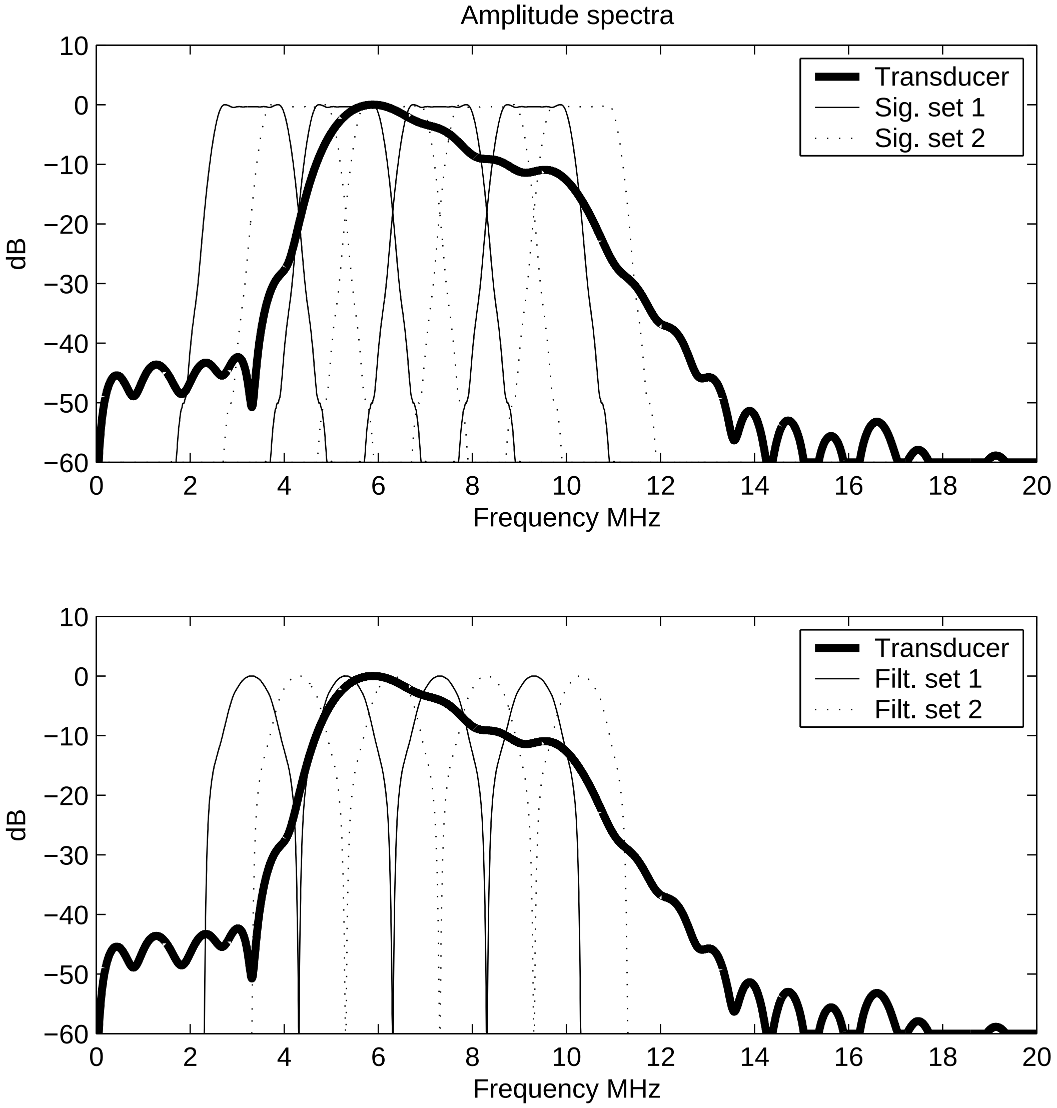

Figure 5.6: The spectra of the eight linear FM signals are displayed in the top figure. The first signal set is represented by the solid thin lines, and the second set is represented by the dotted lines. The corresponding spectra for the separation filters are given in the bottom figure.

signals are matched filtered using the time reversed excitation waveform[4]. The noise effecting the receivers is assumed to be white with power spectral density P_n and to be mutually uncorrelated from receiver to receiver and from transmission to transmission. The target is assumed to be a single point scatterer which is fully stationary during the data acquisition. The peak power SNR (4.3) for the beamformed data for a given receiver at the location of the scatterer is then

$$SNR_{ref} = \frac{L^2 E_{ref}^2}{L E_{ref} P_n} = \frac{L E_{ref}}{P_n}. \tag{5.16}$$

Now, consider a STA system realized using spatial encoding of the transmitters by utilizing frequency division. In this case only $L/2$ transmitters are used, since L transmis-

---

[4] No considerations to mismatched filtering will be taken in this analysis.

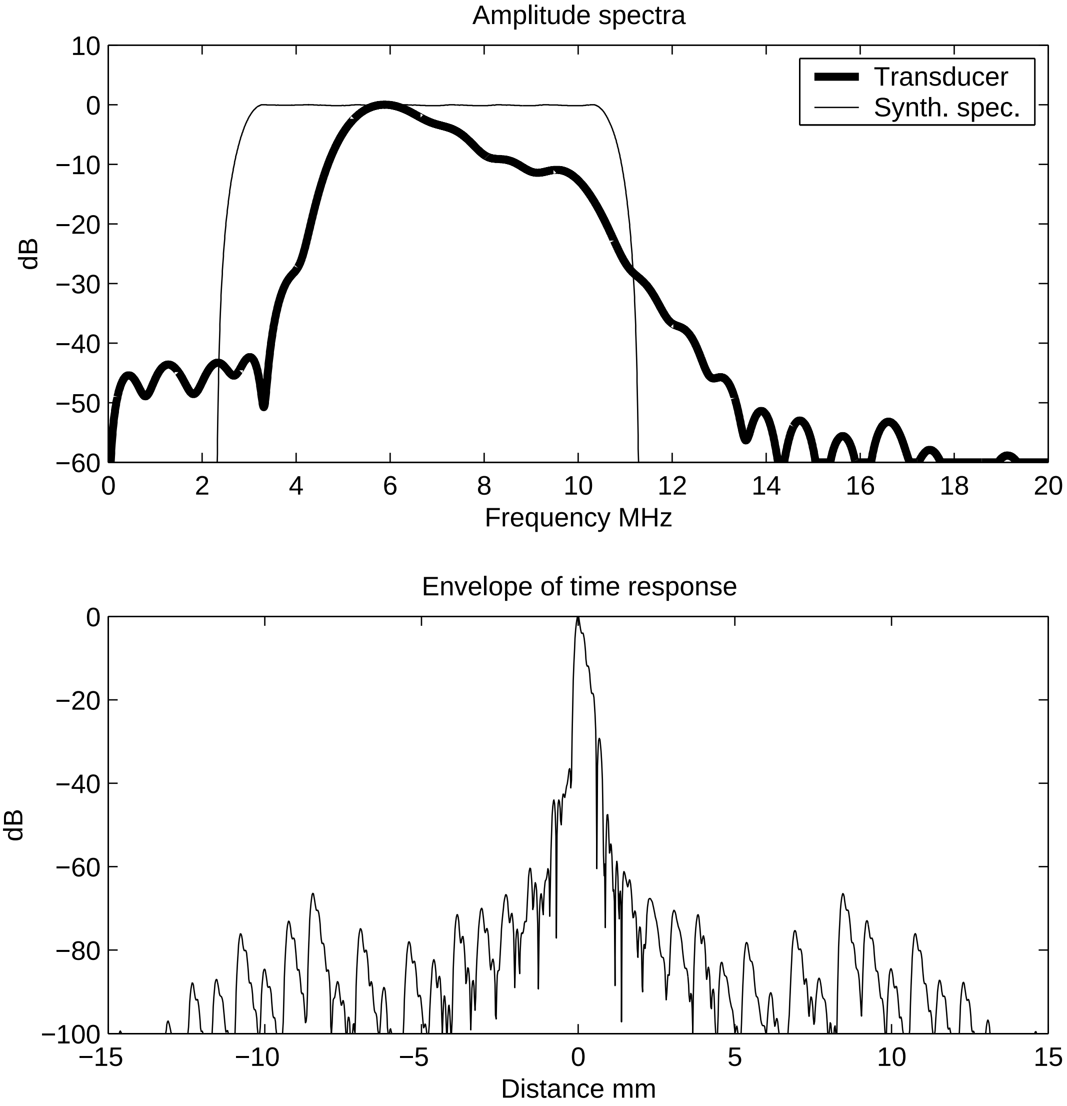

Figure 5.7: The synthesized broadband spectrum is given as the thin line, whereas the spectrum of the transducer is the thick line in the top figure. The bottom figure represents the envelope of the time response of the synthesized broadband pulse convolved with the impulse response of the transducer.

sions are required to synthesize the broadband pulse. The same number of transmissions are, therefore, carried out for both methods providing a fair comparison. However, all $L/2$ transmitters are active in every transmission, transmitting one of the waveforms in $\{x_l(t)\}_{l=0}^{L-1}$ all with the energy E_{fd}. The SNR in this case will be

$$SNR_{fd} = \frac{\left(\frac{L}{2}\right)^2 L^2 E_{fd}^2}{\frac{L}{2} L E_{fd} P_n} = \frac{L^2 E_{fd}}{2P_n}. \tag{5.17}$$

The term $L/2$ comes from beamforming data from $L/2$ transmitters and summing the data coherently, and the term L originates from broadband synthesis of L signals per transmitter.

The gain in SNR is therefore

$$G = \frac{SNR_{fd}}{SNR_{ref}} = \frac{L}{2}\frac{E_{fd}}{E_{ref}}. \tag{5.18}$$

The gain in SNR will, thus, be proportional to the number of active transmitters $L/2$. For a more detailed derivation of the SNR, see [64] (section 5.8).

5.4 Applications

It has been argued that spatial encoding based on Hadamard encoding or encoding the transmitters using orthogonal Golay sequences is sensitive to motion. Motion violates the assumption on stationarity and results in decoding errors[5]. When using frequency division to encode the transmitters, the decoding is not effected by motion, since the information can be decoded instantaneously. The beamforming will, however, just like STA be effected by the motion and the signals cannot be summed coherently. Since STA [29, 30, 66] has proven to yield a competent velocity estimator in blood flow imaging, it is interesting to apply frequency division to flow estimation problems. In [67] (section 5.10) a simulation study of flow estimation, utilizing frequency division encoding of the transmitters, was carried out.

5.5 Frequency division ultrasound imaging

To demonstrate the capabilities of spatio-temporal encoding based on frequency division for STA purposes, the method has been tested experimentally and compared to a STA system relying on only temporal encoding.

The measurement system consisted of a BK8804 linear array transducer and the RASMUS system [63]. Since RASMUS has 128 transmitting channels, the 128 central transducer elements of the existing 192 were used during transmission. The RASMUS system has 64 receiving channels which makes it possible to access 64 receiving elements in every data acquisition. However, by multiplexing, 128 receiving transducer elements can be synthesized.

Reference experiment: The reference experiment was carried out using a linear FM signal as excitation waveform. The duration was 20 μs, the center frequency was 7 MHz and the fractional bandwidth was 100%. A Tukey window with 15% tapering was applied on the excitation waveform. The mismatched filter was derived as the time reversed excitation waveform multiplied by a Dolph-Chebyshev window with 70 dB relative sidelobe attenuation.

In each transmission, one virtual source was used. By focusing 16 adjacent transducer elements 5 mm behind the face of the transducer a virtual source could be created. By acquiring data from two transmissions, 128 receiving elements were synthesized. The synthetic transmit aperture was created by sliding the virtual source across the array one transducer element at a time. The spatial distance between two virtual sources in the synthetic array, will therefore be equal to the pitch[6] of the transducer. In total 112 full data acquisitions were carried out[7].

---

[5] The author has, however, not found any report where the severeness of this problem is investigated.

The received signals were beamformed using a Hanning apodization for the synthesized 128 element receiving array. The result for the reference experiment in a water phantom with metal wires at different depths can be seen in Fig. 5.9. The axial and lateral projections of this image are given in Fig. 5.10 as the dotted curves. The dynamic range of the B-mode image is 50 dB. The axial and lateral resolution as a function of depth can be seen in Fig. 5.11 as the dotted lines.

The same experimental setup used on a tissue mimicking phantom with an attenuation of 0.5 dB/[cm·MHz] can be seen in Fig. 5.12. The penetration depth is approximately 90 mm.

Frequency division experiment: Four virtual sources were used in every transmission. A virtual source was created in the same way as in the reference experiment. This implied that 64 transmitting elements were used in every transmission. Eight waveforms were designed to cover the frequency band of the transducer. The bandwidth of the waveforms were 2 MHz and the duration was 25 μs. Further specifications of code and filter design can be found in [65] (section 5.9). The spectra of the waveforms and the corresponding separation filters can be seen in Fig. 5.8 and the center frequencies are given in table 5.1.

Signal set	f_0	f_1	f_2	f_3	
1	3.3000	5.4024	7.5048	9.6072	MHz
2	4.3512	6.4356	8.5560	10.658	MHz

Table 5.1: The center frequencies of the different waveforms in the two sets. In Fig. 5.8 the spectra for the first signal set is depicted as the solid curves whereas the dotted curves represents the spectra of the second signal set.

Since eight waveforms were used to synthesize a broadband pulse, the same number of transmissions had to be carried out for each set of four virtual sources. To make a fair comparison to the reference experiment, only 56 virtual source could therefore be covered in 112 transmissions. The synthetic transmit array was created by acquiring data eight times, covering all frequency bands for all active transmitters, and then sliding the active aperture two transducer elements. The distance between the virtual sources in the synthetic transmitting array was therefore two times the pitch of the transducer. The active elements for the different transmissions can be seen in table 5.2. All data acquisitions were repeated twice such that 128 receiving elements could be synthesized.

The received signal were beamformed using a Hanning apodization over the 128 receiving elements. The resulting B-mode image can be seen as the right image in Fig. 5.9. The axial and lateral projections are given as the solid curves in Fig. 5.10. The dynamic range of the B-mode image is 50 dB. The axial and lateral resolution for the frequency division experiment are given as the solid lines in Fig. 5.11. The frequency division imaging method displays better resolution but poorer contrast. This can be explained by the rect-

---

[6] Pitch, denotes the spatial distance between the centers of two adjacent transducer elements.

[7] The total number is actually 224 if the multiplexing in receive is accounted for.

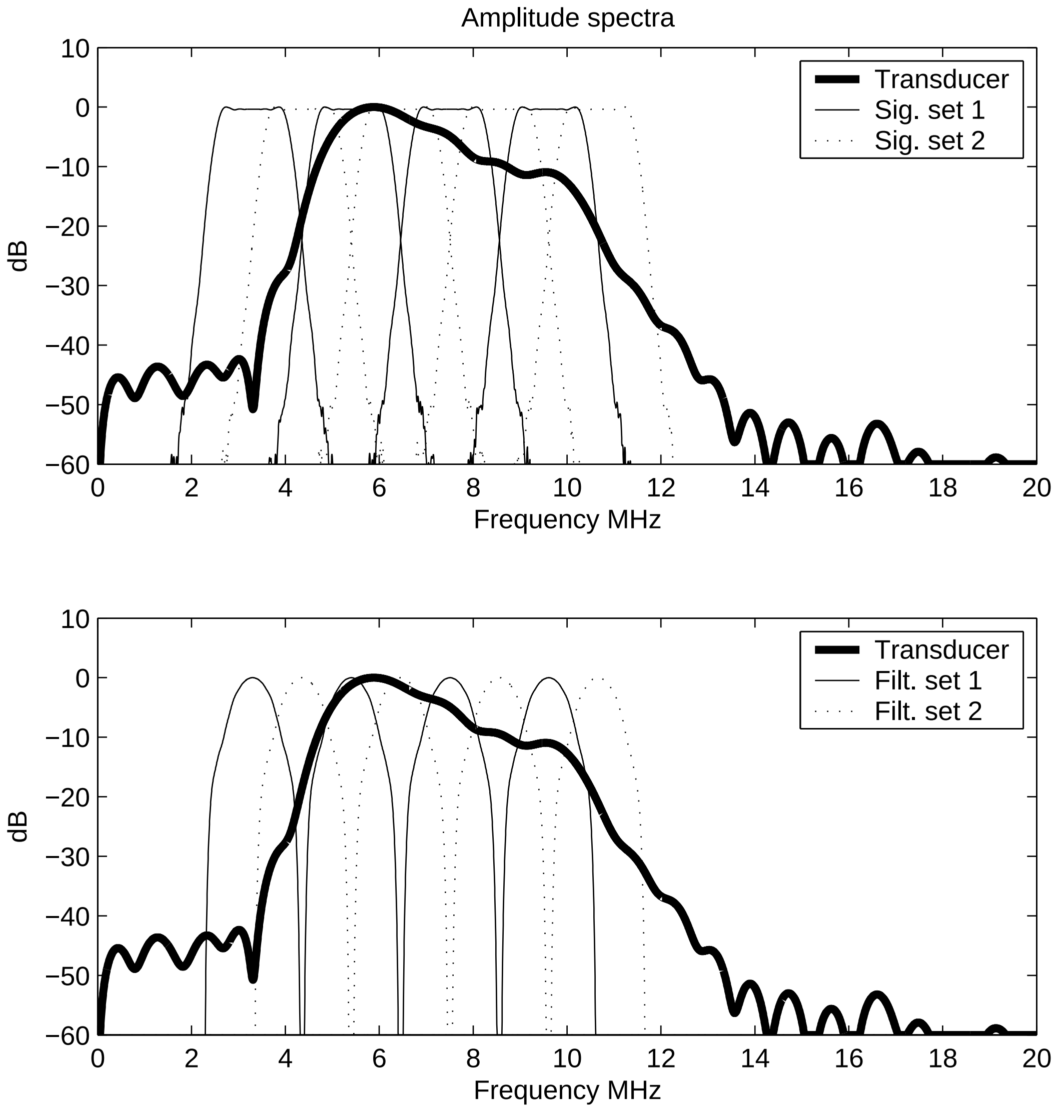

Figure 5.8: The amplitude spectra of the excitation waveforms and separation filters used in the experiments of the frequency division approach.

	virt. source no	1	2	3	4
XMT no					
1-8		1-16	29-44	58-73	86-101
9-16		3-18	31-46	60-75	88-103
⋮		⋮	⋮	⋮	⋮
105-112		27-42	55-70	84-99	112-127

Table 5.2: The transducer elements used for the different transmitters in the different transmissions. To make a fair comparison to the reference experiment, the synthetic transmit aperture is sampled with twice the spatial distance compared to that of the reference experiment. In this way both methods used 112 transmissions to form one complete image.

angular shape of the synthesized broadband spectrum, compared to the spectrum of the mismatched filtered linear FM signal which displays a Gaussian characteristic.

The frequency division approach was also tested for the tissue mimicking phantom and the result is displayed as the right image in Fig. 5.12. The penetration depth is approximately 110 mm. This is an increase of 20 mm compared to the reference experiment. Investigation of the improvement in SNR and penetration depth can be found in [64, 65] (sections 5.8 and 5.9).

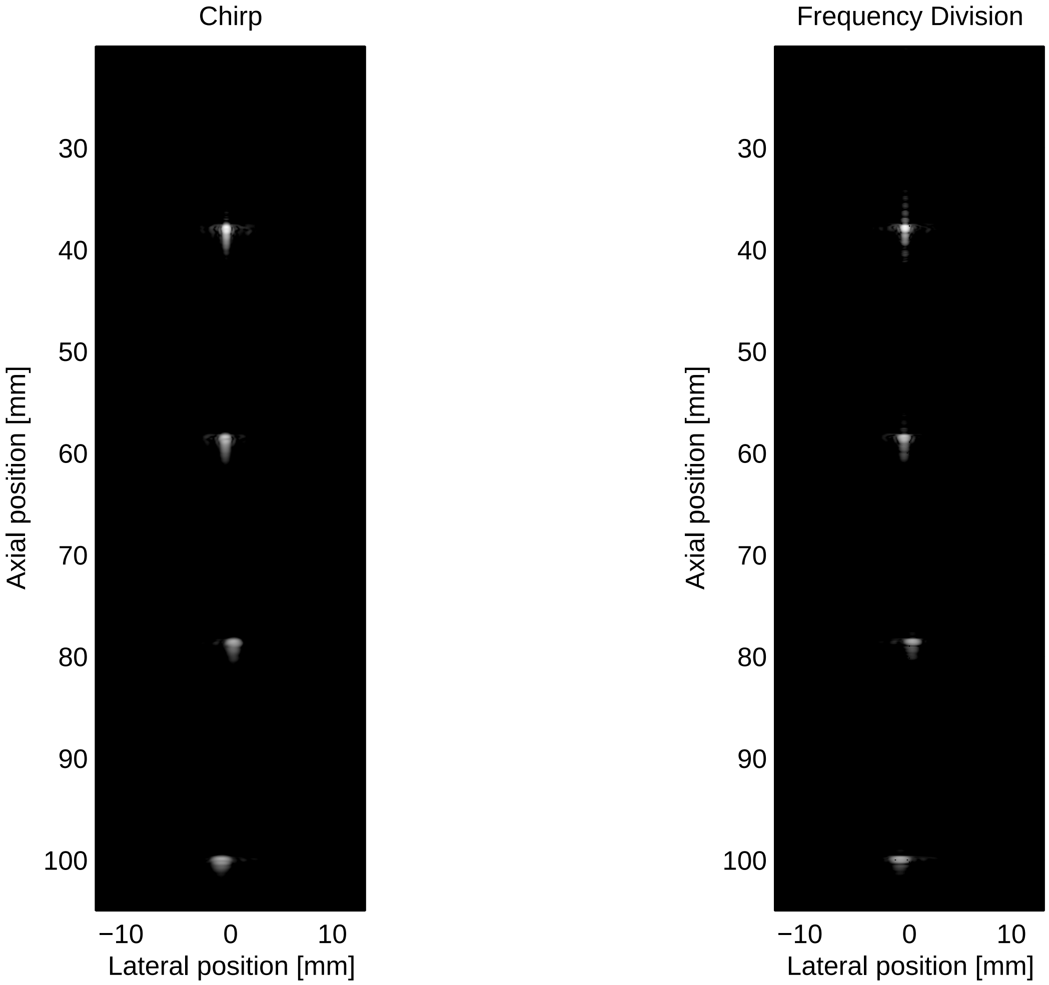

Figure 5.9: The figure to the left is the reference experiment. The excitation waveform is a 7 MHz linear FM signal with 15% tapering. The mismatched filter was generated by applying a Dolph-Chebyshev window on the matched filter with 70 dB relative sidelobe attenuation. The figure to the right is the proposed method based on frequency division encoding of the transmitters. Four transmitters were active simultaneously. In both cases a transmitter was created by focusing 16 transducer elements 5 mm behind the face of the transducer. In total 112 transmissions were carried out with both methods. The targets were four metal wires in a water bath, and the dynamic range in both images is 50 dB.

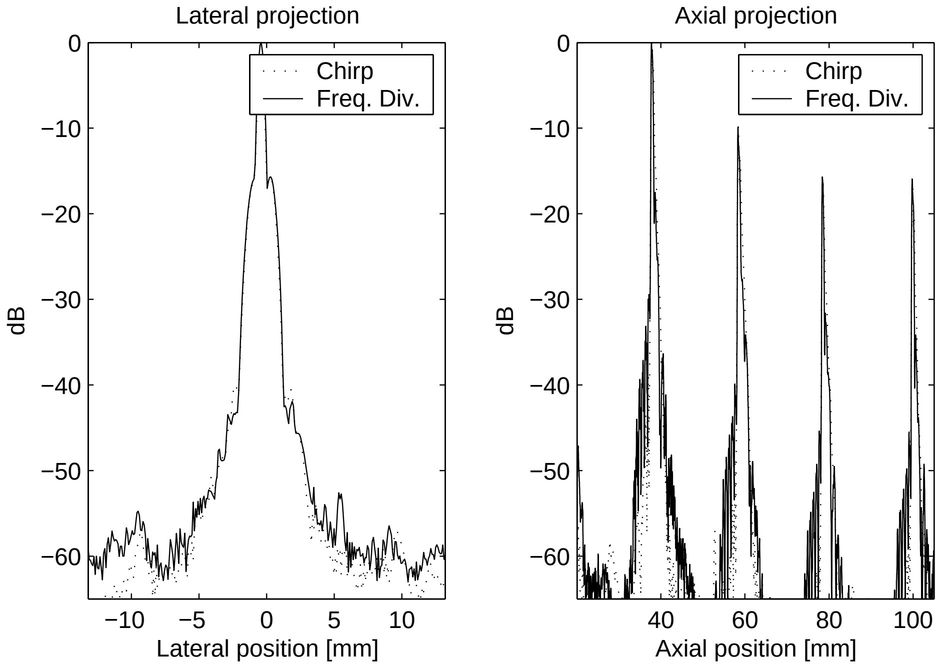

Figure 5.10: The axial and lateral projections of Fig. 5.9. The axial projections were calculated by taking the maximum value of each row in both images and the lateral projections by taking the maximum of each column.

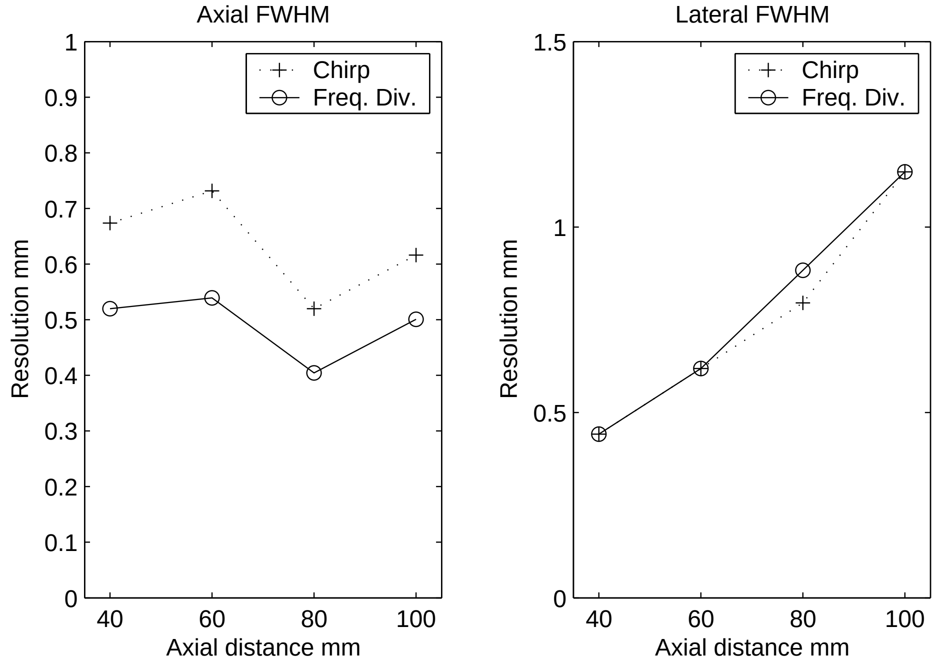

Figure 5.11: The axial and lateral resolution (FWHM) at the depths 40, 60, 80 and 100 mm. The data was obtained from the images shown in Fig. 5.9. The dotted line represents the conventional STA method with a linear FM signal as excitation, whereas the solid line represents the frequency division approach.

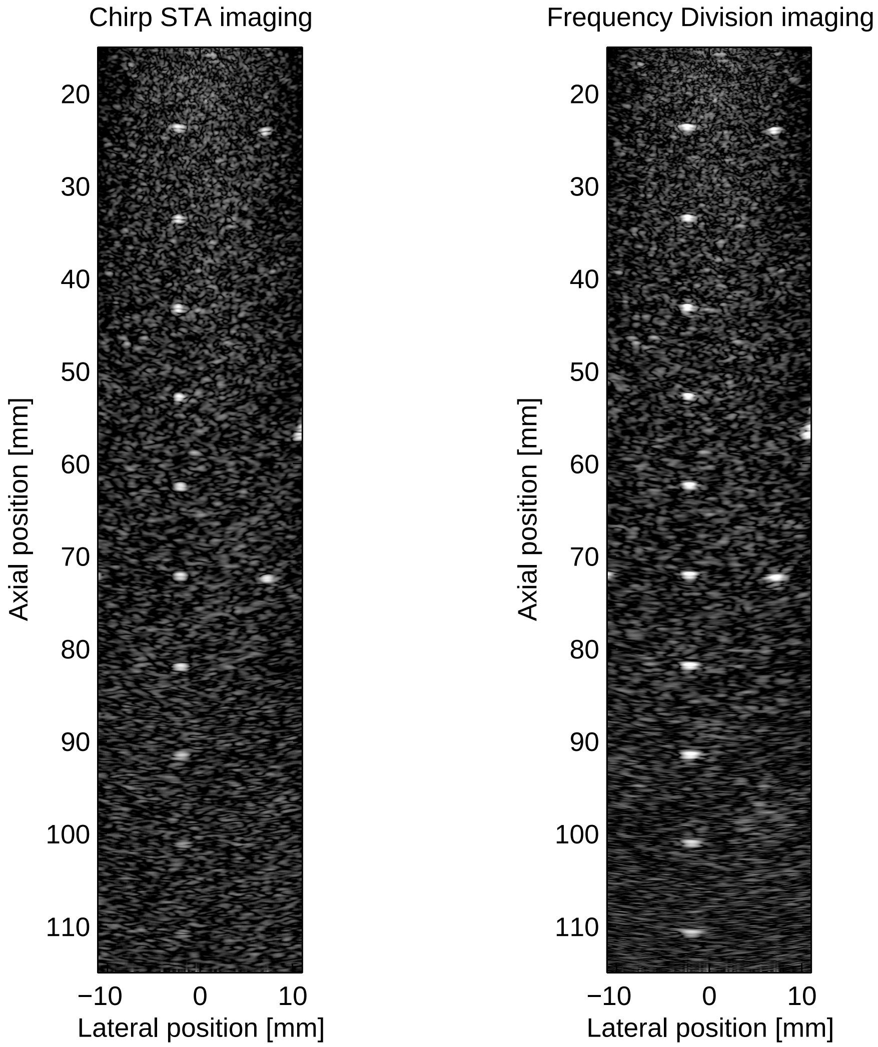

Figure 5.12: The result for the reference method and the frequency division approach in a tissue mimicking phantom. The attenuation in the phantom is 0.5 dB/[MHz·cm]. The distance between the metal wires is 10 mm. The same experimental setup was used as in Fig. 5.9. It can be seen that the frequency division approach exhibits approximately 2 cm better penetration compared to the conventional STA approach.

5.6 Summary

Spatial encoding offers an attractive solution for increasing the SNR. Especially for STA systems where the SNR is low due to the small amount of energy transmitted compared to a focused system. During this project a method for spatial encoding has been developed and investigated.

The spatial encoding is achieved by designing a number of waveforms with approximately disjoint spectral support. A specific transmitters can therefore be represented by assigning one of the waveforms to this transmitter. Several transmitters can therefore be excited simultaneously, and the decoding can be performed instantaneously at the receiver using matched filtering, and is therefore not influenced by motion between transmissions. To further increase the transmitted energy, the waveforms were designed as linear FM signals.

The method has been tested experimentally and improvement in SNR has been documented. The method displays comparable performance in terms of axial and lateral resolution and contrast compared to conventional STA imaging with a linear FM signal as excitation waveform. Future work includes invivo experiments and clinical evaluation of the method. Also, the method should be tested experimentally for blood flow estimation.

5.7 Conference paper: Multi Element Synthetic Aperture Transmission using a Frequency Division Approach

Published in Proceedings IEEE Ultrason. Symp, pp 1942-1946, 2003

Comments:

On page 1945 in the paper *Multi Element Synthetic Aperture Transmission using a Frequency Division Approach* it is stated that the energy of the frequency division waveforms is

$$E_s = \frac{a^2}{2} T_s,$$

where T_s is the duration of the waveforms and a is the amplitude of the waveforms. However, this assumes constant amplitude. The waveforms are designed as linear phase FIR waveforms, implying that this will **not** be true. Therefore the reader is requested to disregard from this statement, and use equation (20) on page 1945 to evaluate SNR.

Multi Element Synthetic Aperture Transmission using a Frequency Division Approach

Fredrik Gran and Jørgen Arendt Jensen

Center for Fast Ultrasound Imaging, Ørsted•DTU, Bldg. 348,
Technical University of Denmark, DK-2800 Kgs. Lyngby, Denmark

Abstract - In synthetic aperture imaging an image is created by a number of single element defocused emissions. A low resolution image is created after every emission and a high resolution image is formed when the entire aperture has been covered. Since only one element is used at a time the energy transmitted into the tissue is low.

This paper describes a novel method in which the available spectrum is divided into $2N$ overlapping sub-bands. This will assure a smooth broadband high resolution spectrum when combined. The signals are organized into two subsets in which all signals are fully orthogonal. The transmitting elements are excited so that N virtual sources are formed. All sources are excited using one subset at a time. The signals can be separated by matched filtration, and the corresponding information is extracted. The individual source information is hence available in every emission and the method can therefore be used for flow imaging, unlike space time encoding techniques such as Hadamard and Golay encoding. The frequency division approach increases the SNR by a factor of N^2 compared to conventional pulsed synthetic aperture imaging, provided that N transmission sources are used. Simulations and phantom measurements are presented to verify the method.

I INTRODUCTION

In conventional synthetic aperture imaging (STA) [1] an image is created by making a number of consecutive defocused transmissions from different locations of the aperture. The purpose is to form one image for every single element transmission. This is accomplished by beamforming the RF-lines originating from each transmission. However, the individual images have low resolution, since the corresponding transmission only covers a small part of the aperture. By adding the low resolution images, an image with higher resolution can be constructed. The main advantage of STA is that perfect focus can be attained for all points in the image, since RF-data from the individual defocused transmissions are available. The image has to be acquired over a number of emissions, and motion can therefore be a problem. Since only a small part of the aperture is used in every transmission, conventional STA provides a lower SNR than linear array imaging. The SNR can be increased by using several elements in transmit to form the spherical wave [2]. This can also be combined with a chirp excitation [3] to increase the SNR beyond that of a conventional image. The basic problem however, is that only part of the aperture can be used during transmission. This can be solved by using space time encoding [4] in which the full aperture can be used. These techniques, relies on the tissue to be stationary and can therefore not be used for flow imaging, where the SNR is most crucial.

In this paper we propose a novel method in which all transmitting sources can be excited at the same time and still be separated at the receiver, see Fig. 1. This is done by defining a set of narrow-band signals, which are disjoint in the frequency domain, enabling the receiver to separate the different signals. Since the individual signals are narrow-band, it is imperative to do a number of consecutive firings, so that each source transmits every signal in the set and thereby cover the entire bandwidth of the transducer. To synthesize a smooth broadband spectrum, it is necessary to define two sets of signals, which are overlapping but with signals mutually orthogonal within the sets, as will be shown in Section II. If the system consist of N sources, $2N$ signals have to be defined and $2N$ transmissions have to be made. The approach will improve the SNR, which will be shown in Section III, and data from all sources are available in every transmission unlike space time encoding making it suitable for flow imaging. In Section IV some simulation and experimental results are shown and concluding remarks are given in Section V.

II METHOD

The transmitting aperture is excited so that N virtual sources are formed. Each source must be assigned an unique signal in order to separate all signals at the receiver. This means that in every transmission there has to be at least N signals. Let

$$\{s_k(t)\}_{k=1}^{N} \leftrightarrow \{S_k(f)\}_{k=1}^{N} \tag{1}$$

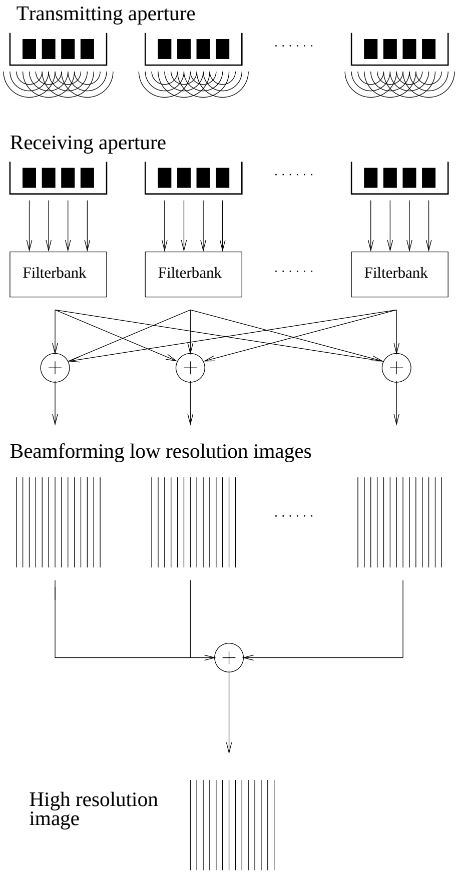

Figure 1: Frequency division synthetic aperture imaging

denote the signals, which are transmitted and their corresponding Fourier transforms. Under the assumption that the system is governed by the linear wave-equation, the response at the j:th receiver can be modeled as,

$$R_j^{(n)}(f) = \sum_{i=1}^{N} H_{ij}(f) S_{k(i,n)}(f), \tag{2}$$

where $H_{ij}(f)$ corresponds to the pulse echo frequency response between the i:th transmitting source and the j:th receiving element and $S_{k(i,n)}(f)$ is the signal transmitted on the i:th source at the n:th transmitting event. To be separable by a matched filter at the receiver, the signals have to have the following property,

$$S_k(f) S_l^*(f) = 0, \forall k \neq l, \tag{3}$$

where $S_l^*(f)$ is the complex conjugate of $S_l(f)$. This condition will automatically be fulfilled, if the signals do not overlap in the frequency domain , see Fig. 2. The signals will thus have to be band limited. Consider a frequency response function $S(f)$ which vanishes outside of $f_0 + \frac{f_B}{2} > f > f_0 - \frac{f_B}{2}$ where f_0 is the center frequency and f_B is the total bandwidth

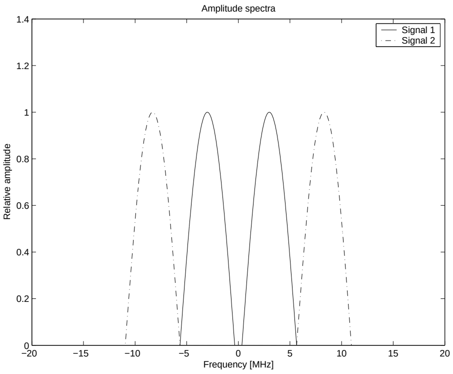

Figure 2: Two signal spectra, disjoint in the frequency domain

of the corresponding signal. A set of signals disjoint in the frequency domain can now be defined as

$$S_k(f) = S(f - (k-1) f_B), \, k = 1 \ldots N. \tag{4}$$

If the i:th source transmits signal with index $k(i,n)$ the filtered contribution at the j:th receiver will be,

$$R_{ij}^{(n)}(f) \quad = \quad R(f)_j^{(n)} S^*_{k(i,n)}(f) = H_{ij}(f) |S_{k(i,n)}(f)|^2. \tag{5}$$

Since the result from (5) is narrow-band, the system would yield a very poor resolution if only one transmission was made. Therefore it is necessary to transmit with all signals on all sources to synthesize a smooth broadband spectrum. The resulting received spectrum from the i:th source will then be given by,

$$R_{ij}^{tot}(f) \quad = \quad \sum_{n=1}^{N} R_{ij}^{(n)}(f) = H_{ij}(f) \sum_{n=1}^{N} |S_{k(i,n)}(f)|^2. \tag{6}$$

The variable $k(i,n)$ is both a function of transmitting source number i, and transmit event n. It is desirable that $\sum_{n=1}^{N} |S_{k(i,n)}(f)|^2$ is a smooth function under the bandwidth of the frequency response function $H_{ij}(f)$, so that the achieved image quality is as good as possible. However it is unrealistic to assume that $\{S_k(f)\}_{k=1}^{N}$ can be defined so that $\{|S_k(f)|^2\}_{k=1}^{N}$ are rectangular functions, instead the signal spectra have to be continuous as in Fig. 2. This makes it necessary to define a second set of signals overlapping the set given in (1). Let

$$\{s_k(t)\}_{k=N+1}^{2N} \leftrightarrow \{S_k(f)\}_{k=N+1}^{2N} \tag{7}$$

represent the second set of signals and their corresponding Fourier transforms. If the new set of signals is chosen such that

$$\{S_k(f)\}_{k=N+1}^{2N} = \{S_k(f - \frac{f_B}{2})\}_{k=1}^{N}, \tag{8}$$

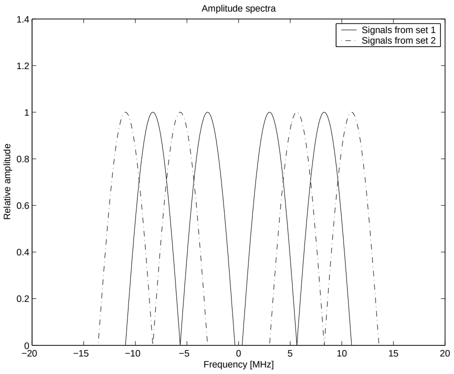

Figure 3: Two overlapping sets of spectra

the two different sets will overlap exactly. An example with 2 sources and 4 signals can be seen in Fig. 3. One can choose the functions $\{S_k(f)\}_{k=1}^{2N}$, so that $\sum_{k=1}^{2N}|S_k(f)|^2$ is a constant function on the interval $f_0 \leq f \leq f0 + f_B\frac{2N-1}{2}$. The total received signal for the $2N$ transmissions at the j:th receiver originating from the i:th source can now be written as

$$R_{ij}^{tot} = H_{ij}(f)\sum_{n=1}^{2N}|S_{k(i,n)}(f)|^2. \tag{9}$$

Since $\sum_{k=1}^{2N}|S_k(f)|^2$ is a smooth broadband function, the result from (9) will also be broadband and a good image quality can be attained. It is finally worth repeating that for a system consisting of N sources there will be $2N$ signals and thus $2N$ transmissions are necessary, since signals from the set given in (1) must not be transmitted at the same time as signals from the set given in (7). A typical firing scheme for a system with 4 sources is given in Table 1.

$k(i,n)$	n							
i	1	2	3	4	5	6	7	8
1	1	2	3	4	5	6	7	8
2	4	1	2	3	8	5	6	7
3	3	4	1	2	7	8	5	6
4	2	3	4	1	6	7	8	5

Table 1: Firing sequence for the total signal set

III SIGNAL-TO-NOISE RATIO

In this section the effects of the frequency division multi source communication technique will be discussed. Consider a setup where the received signals originates from one point scatterer. The noise is assumed to be white additive and to have a gaussian distribution. First a system which operates according to a conventional STA firing scheme will be analyzed. The system consists of N sources and for fair comparison $2N$ transmissions are made. Consider the data from one single source transmission yielding one low resolution image. The power of the noise in this low resolution image is then,

$$P_{lo}^{conv} = \int_{-\infty}^{\infty} P_0|H(f)|^2 df = P_0 E_h, \tag{10}$$

where P_0 is the power spectral density of the noise, $H(f)$ is the frequency response and E_h is the energy of the transmitted waveform. The total power of the noise for the $2N$ low resolution images is,

$$P_{hi}^{conv} = 2NP_0E_h, \tag{11}$$

assuming that the noise is uncorrelated from emission to emission. The peak output of the filtered transmitted signal in one low resolution image is [5]

$$y_{lo}^{conv}(t_{max}) = \int_{-\infty}^{\infty}|H(f)|^2 df = E_h. \tag{12}$$

The high resolution image will then give the peak output

$$y_{hi}^{conv}(t_{max}) = 2NE_h, \tag{13}$$

when all low resolution images are combined coherently. The *peak pulse signal to noise ratio* is then

$$SNR_{conv} = \frac{|y_{hi}^{conv}(t_{max})|^2}{P_{hi}^{conv}} = 2N\frac{E_h}{P_0}. \tag{14}$$

If the energy of each signal is denoted E_s for the frequency division case, the noise power of one low resolution image is given by

$$P_{lo}^{FD} = \sum_{k=1}^{2N}\int_{-\infty}^{\infty} P_0|S_k(f)|^2 df = 2NP_0E_s, \tag{15}$$

which gives that the noise power of the high resolution image is

$$P_{hi}^{FD} = 2N^2P_0E_s. \tag{16}$$

The total peak output of a low resolution image is

$$y_{lo}^{FD}(t_{max}) = \sum_{k=1}^{2N}\int_{-\infty}^{\infty}|S_k(f)|^2 df = 2NE_s, \tag{17}$$

and the peak output of the corresponding high resolution image is

$$y_{hi}^{FD}(t_{max}) = 2N^2E_s. \tag{18}$$

This gives

$$SNR_{FD} = \frac{|y_{hi}^{FD}(t_{max})|^2}{P_{hi}^{FD}} = 2N^2\frac{E_s}{P_0}. \tag{19}$$

This again assumes that the noise is uncorrelated from emission to emission and that the summing of the low resolution images is coherent. Therefore it can be stated that

$$\frac{SNR_{FD}}{SNR_{conv}} = N\frac{E_s}{E_h}. \tag{20}$$

If a normal pulsed STA system is analyzed as a reference, $E_h = \frac{a^2}{2}T_h$ and $E_s = \frac{a^2}{2}T_s$ where a is the amplitude and T_h and T_s are the duration of the corresponding waveforms. The duration of the waveforms are related to the bandwidths B_s and B_h as $T_s \sim \frac{1}{B_s}$ and $T_h \sim \frac{1}{B_h}$. The bandwidths are related as $B_s \sim \frac{B_h}{N}$ which gives,

$$\frac{E_s}{E_h} \quad = \quad N, \tag{21}$$

so that

$$\frac{SNR_{FD}}{SNR_{conv}} = N^2. \tag{22}$$

When a chirp excitation is used however, the duration of the chirp can be chosen to equal the durations of the frequency division signals. This reduces the gain in SNR to

$$\frac{SNR_{FD}}{SNR_{conv-chirp}} = N. \tag{23}$$

using 8 transmission sources will, thus increase the signal-to-noise ratio by 9 dB.

IV SIMULATIONS AND MEASUREMENTS

The method was tested using both simulations in Field II [6] and experiments on the experimental ultrasound scanner RASMUS [7]. Field II was used to simulate an ultrasound system with 64 transmitting and 128 receiving elements. The transmit aperture was organized so that 8 virtual sources were formed. The target was a single scatterer located 40 mm from the transducer surface. The transducer center frequency was 7 MHz with a kerf of 0.035 mm and pitch of 0.208 mm. First the conventional STA technique with a 1 cycle, 7 MHz sinusoid was used to simulate the point spread function (PSF) as a reference. The result can be seen in Fig. 4. The axial resolution was 0.21 mm (-3dB) and 0.31 mm (-6dB) respectively, and the lateral resolution was 0.41 mm (-3dB) and 0.62 mm (-6dB). The same setup was used for the frequency division approach with 16 bands starting from 1.5 MHz to 17.5 MHz. The PSF is given in Fig. 5. The axial resolution was 0.23 mm (-3dB) and 0.31 mm (-6dB) respectively, and the lateral resolution was 0.41 mm (-3dB) and 0.62 mm (-6dB). The experimental ultrasound scanning system RASMUS was used to verify the simulations. A wire phantom was used to measure the PSF. The wire was located 40 mm from the transducer surface. A BK8804 transducer was used with a center frequency of 7 MHz. The transmit and receiving aperture were identical to the simulated setups. The conventional STA technique can be seen in Fig. 8. The axial resolution was 0.25 mm (-3dB) and 0.38 mm (-6dB) respectively, and the lateral resolution was 0.71 mm (-3dB) and 1.06 mm (-6dB). The experiment was repeated using the frequency division approach with 16 bands starting from 1.5 MHz to 17.5 MHz. The PSF is given in Fig. 9. Axial resolution 0.21 mm (-3dB) and 0.29 mm (-6dB) respectively, and lateral resolution 0.52 mm (-3dB) and 0.73 mm (-6dB).

V CONCLUSION

A new method for STA imaging has been presented, where all elements can be excited at the same time and still be separated at the receiver. The method improves the *SNR* by a factor of $N\frac{E_s}{E_h}$ and makes information from all elements available in every transmission and is therefore suitable for flow imaging. Both simulations and experiments show that the method is realizable in an ultrasound system.

ACKNOWLEDGEMENT

This work was supported by grant 9700883, 9700563 and 26-01-0178 from the Danish Science Foundation and by B-K Medical A/S, Denmark.

VI REFERENCES

[1] S. I. Nikolov. *Synthetic aperture tissue and flow ultrasound imaging*. PhD thesis, Ørsted•DTU, Technical University of Denmark, 2800, Lyngby, Denmark, 2001.

[2] M. Karaman, P. C. Li, and M. O'Donnell. Synthetic aperture imaging for small scale systems. *IEEE Trans. Ultrason., Ferroelec., Freq. Contr.*, 42:429–442, 1995.

[3] K. L. Gammelmark and J. A. Jensen. Multi-element synthetic transmit aperture imaging using temporal encoding. In *Proc. SPIE: Progress in biomedical optics and imaging*, volume 3, pages 25–36, 2002.

[4] R. Y. Chiao, L. J. Thomas, and S. D. Silverstein. Sparse array imaging with spatially-encoded transmits. In *Proc. IEEE Ultrason. Symp.*, pages 1679–1682, 1997.

[5] S. Haykin. *Communication Systems*. John Wiley & Sons, Inc., 2001.

[6] J. A. Jensen. Field: A program for simulating ultrasound systems. *Med. Biol. Eng. Comp.*, 10th Nordic-Baltic Conference on Biomedical Imaging, Vol. 4, Supplement 1, Part 1:351–353, 1996b.

[7] J. A. Jensen, O. Holm, L. J. Jensen, H. Bendsen, H. M. Pedersen, K. Salomonsen, J. Hansen, and S. Nikolov. Experimental ultrasound system for real-time synthetic imaging. In *Proc. IEEE Ultrason. Symp.*, volume 2, pages 1595–1599, 1999.

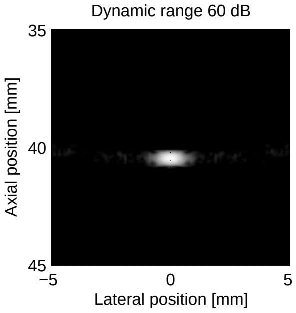

Figure 4: Simulated PSF for the STA system with 8 transmission centers

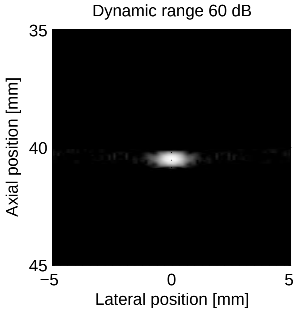

Figure 5: Simulated PSF for the FD system with 8 transmission centers

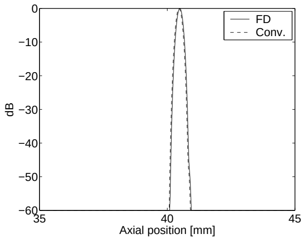

Figure 6: Axial projection of Fig. 4 and Fig. 5

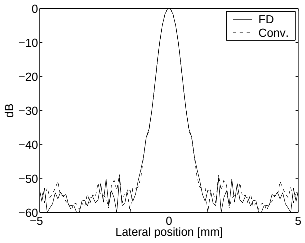

Figure 7: Lateral projection of Fig. 4 and Fig. 5

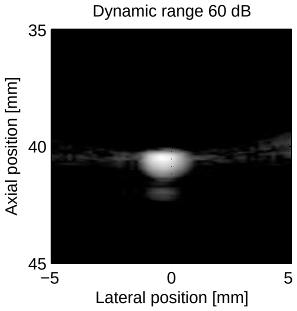

Figure 8: PSF for the STA system with 8 transmission centers

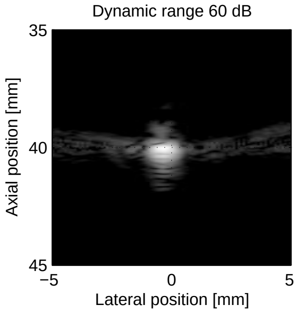

Figure 9: PSF for the FD system with 8 transmission centers

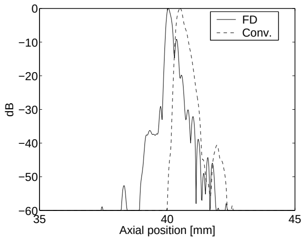

Figure 10: Axial projection of Fig. 8 and Fig. 9

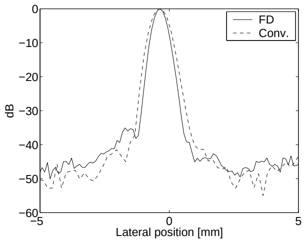

Figure 11: Lateral projection of Fig. 8 and Fig. 9

5.8 Journal paper: Frequency Division transmission imaging and synthetic aperture reconstruction

Submitted to IEEE Transactions on Ultrasonics, Ferroelectrics and Frequency control, August 2004

Frequency Division transmission imaging and synthetic aperture reconstruction

Fredrik Gran and Jørgen Arendt Jensen, *Senior Member, IEEE*

Abstract

In synthetic transmit aperture imaging only a few transducer elements are used in every transmission, which limits the signal to noise ratio. The penetration depth can be increased by using all transmitters in every transmission. In this paper a method for exciting all transmitters in every transmission and separating them at the receiver is proposed. The coding is done by designing narrow-band linearly frequency modulated signals, which are approximately disjoint in the frequency domain and assigning one waveform to each transmitter. By designing a filter bank consisting of the matched filters corresponding to the excitation waveforms, the different transmitters can be decoded at the receiver. The matched filter of a specific waveform will only allow information from this waveform to pass through, thereby separating it from the other waveforms. This means that all transmitters can be used in every transmission and the information from the different transmitters can be separated instantaneously. Compared to traditional synthetic transmit aperture (STA) imaging, where the different transmitters are excited sequentially, more energy is transmitted in every transmission and a better signal to noise ratio is attained. The method has been tested in simulation, where the resolution and contrast was compared to a standard synthetic transmit aperture system with a single sinusoid excitation. The resolution and contrast was comparable for the two systems. The method has also been tested using the experimental ultrasound scanner RASMUS. The resolution was evaluated using a string phantom. The method was compared to a conventional STA using both sinusoidal excitation and linear FM signals as excitation. The system using the FM signals and the frequency division approach yielded the same performance concerning both axial (of $\approx 3\ \lambda$) and lateral resolution (of $\approx 4.5\ \lambda$). A signal to noise ratio measurement showed an increase in signal to noise ratio of 6.5 dB compared to the system using the conventional STA method and FM signal excitation.

I. INTRODUCTION

Normal linear array images are made from a set of beamformed lines. Each line is created by transmitting a focused beam along a specific direction, and beamforming the received echoes from the receiving transducer elements using either fixed or dynamic focus. By applying this method one image line will be created per transmission, and relies on the object to be completely stationary.

In synthetic transmission aperture imaging (STA) [1], [2], only one element is utilized in every transmission. By this approach a spherical wave is created which excites the tissue spreading the acoustic energy in all directions in contrast to focusing the energy in a single point. Instead of beamforming only one line an entire image can be formed, since information from all directions is available. Perfect focus can, thus, be attained for every point in the image, since the origin for the emanating wave is known, as well as where the propagating wave was received. Since only a single element is used as the transmitting aperture, the resolution in the resulting image will be poor [3]. However, by transmitting from several different locations on the aperture and summing the individual images the full aperture can be synthesized. The major advantage for the STA approach is clearly the ability to produce perfect focusing for all points in the image. A major disadvantages however, is the poorer signal to noise ratio (SNR), which results from that

---

Fredrik Gran (fg@oersted.dtu.dk) and Jørgen A. Jensen (jaj@oersted.dtu.dk) are both from the Center for Fast Ultrasound Imaging, Ørsted•DTU, Building 348, Technical University of Denmark, 2800 Kgs. Lyngby, Denmark

only a single element is used at a time and the acoustic energy is distributed all over the tissue. Furthermore, the process of synthesizing the aperture rests on the assumption that the propagating medium is stationary, which can impose a problem in certain applications in medical ultrasound, e.g. flow imaging and imaging rapidly moving tissue.

The problem concerning SNR has been addressed previously in [4], [5], [6], [7], [8] where longer linear frequency modulated (FM) signals were transmitted, increasing the transmitted energy without increasing the instantaneous amplitude of the signals. Another way of increasing the SNR is by grouping a number of transducer elements and focusing close to the transducer surface. This can either be achieved by focusing in front or behind the transducer creating a defocused high energetic virtual source. This has previously been proposed in [9], [10], [11], [12] and have been studied further in . Recently a clinical study was made combining the use of virtual sources and linear FM signals and comparing the results to conventional convex array imaging [13]. By applying virtual sources a larger portion of the aperture is used, but the full aperture is still not utilized in every transmission. In [14], [15] an Hadamard encoding scheme was proposed, so that the full aperture can be excited at the same time. This approach, however, requires N transmissions in order to decode the information provided that N transmitters [1] are used. Another approach to spatio temporal coding was proposed in [16] using orthogonal Golay coded excitation. This method does also require more than one transmission before the information can be decoded making it subceptible to motion of the tissue.

In this paper a novel method for exciting the entire aperture is proposed. The different transmitters are coded using narrow-band signals, which are disjoint in the frequency domain. It is therefore possible to extract the received information from each transmitter by matched filtration, and each waveform thereby represents a physical location on the aperture. The principle of the Frequency Division (FD) approach compared to conventional STA can be seen in Fig. 1. Note that it is still required to transmit more than once if the full bandwidth of the transducer is to be covered, since the signals assigned to the different transmitters are narrow-band. The full bandwidth of the transducer can, however, be synthesized by assigning different signals to the transmitters from transmission to transmission and summing the filtered responses. The approach increases the SNR, since more energy is transmitted in every transmission, and makes new information from all locations on the aperture available in every transmission.

The outline of the paper is: in Section II the theory of the method will be described and analyzed. In Section III the beamforming involved in making the images will briefly be explained. Simulations will be shown in Section IV, where the FD imaging technique will be compared to a conventional STA system with a sinusoid excitation. In Section V some measurements using the experimental RASMUS scanner will be presented and in Section VI concluding remarks will be given.

II. THEORY

The principles and the underlying theory concerning the frequency division imaging approach will be presented. In Section II-A the system model and the assumptions on this model will be described, in Section II-B the theoretical design of the excitation waveforms is discussed, continued by a practical explanation in Section II-C. The impact on signal-to-noise-ratio will be analyzed in Section II-D.

A. System model and system assumptions

Consider an ultrasound system consisting of K transmitters and Q receivers. Let each transmitter be assigned an individual waveform $x_{p(k)}(t)$, where $p(k)$ represents the index of the waveform

---

[1] The term transmitter will be used to denote a transducer element or a virtual source

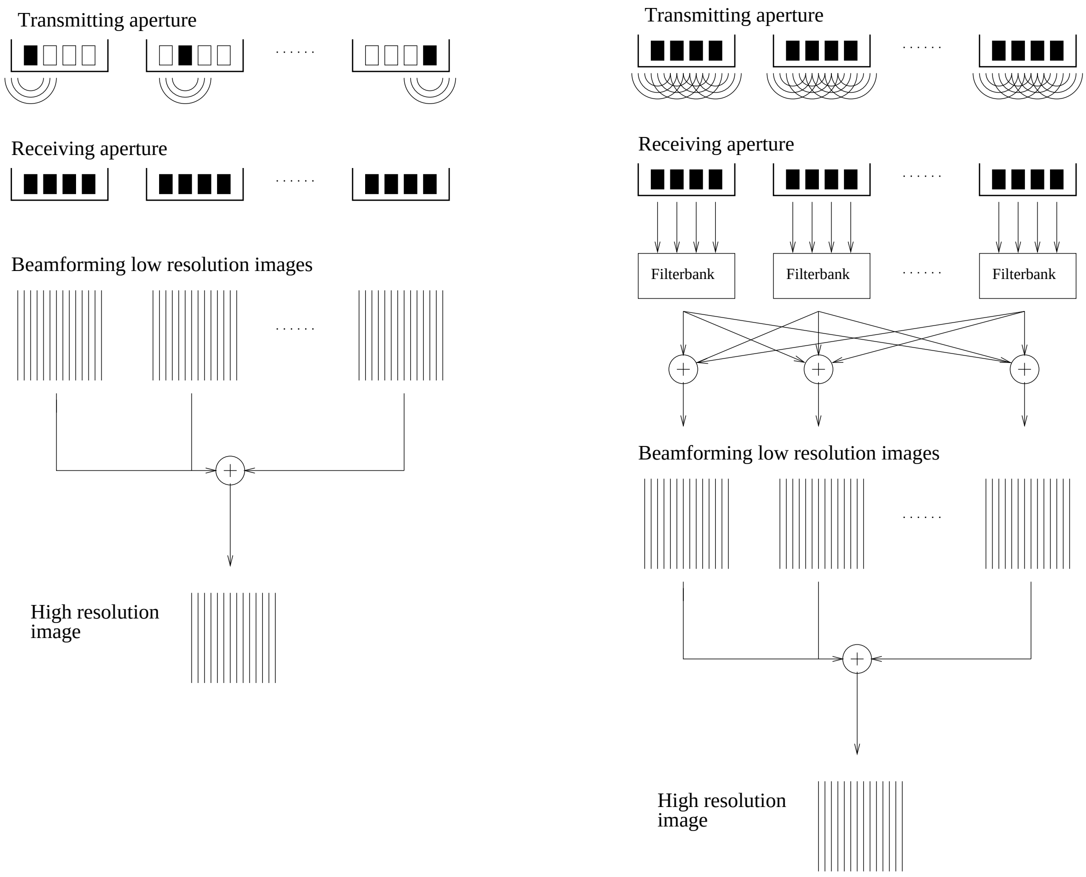
Transmitting aperture
Receiving aperture
Beamforming low resolution images
High resolution image
Transmitting aperture
Receiving aperture
Filterbank
Filterbank
Filterbank
Beamforming low resolution images
High resolution image

(a) Conventional STA approach

(b) Frequency Division approach

Fig. 1. The conventional STA approach 1(a) with sequential data acquisition, where only one transmitter is used in every transmission. The full aperture is synthesized in the beamforming. To the right the frequency division 1(b) approach where the full aperture is used in every transmission, and every transmitter only uses a narrow band of the available bandwidth. The signals are separated by a filterbank consisting of the matched filters corresponding to the excitation waveforms. The full spectrum of each transmitter is synthesized by transmitting several times and using different center frequencies every time.

on the k:th transmitter. If it is assumed that the system dynamics is linear the received signal at the q:th receiver $y_q(t)$ can be written as[2]

$$y_q(t) = \sum_{k=1}^{K} h_{kq}(t) \star x_{p(k)}(t), \tag{1}$$

where $h_{kq}(t)$ represents the impulse response between the k:th transmitter and the q:th receiver. This impulse response is a function of the location of the transmitter $\vec{r}_k$, the location of the receiver $\vec{r}_q$ and the location of the scatters $\vec{r}_m$. For M scatters this impulse response would be

$$h_{kq}(t) = \sum_{m=1}^{M} h(\vec{r}_k, \vec{r}_q, \vec{r}_m, t), \tag{2}$$

assuming that the medium is linear and consists of point scatters. The measured signal on the q:th receiver is, however, also influenced by the system noise

$$r_q(t) = y_q(t) + v(t), \tag{3}$$

---

[2] $\star$ denotes the convolution operator

where $v(t)$ is assumed to be a white, zero mean and gaussian distributed process.The network structure of this system can be viewed in Fig. 2. The Fourier transform of (1) is given by

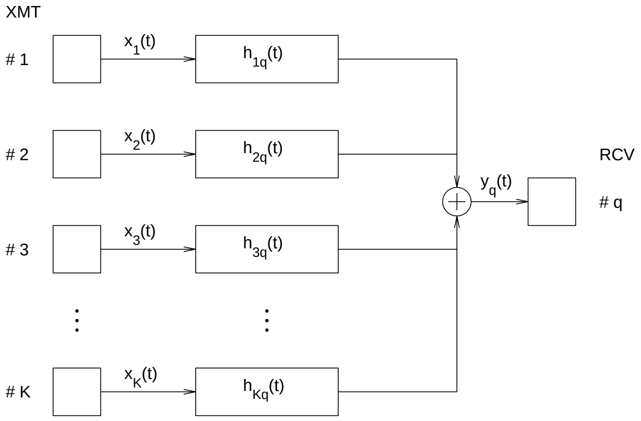

Fig. 2. The network structure of the input/output model of (1).

$$Y_q(f) = \sum_{k=1}^{K} H_{kq}(f) X_{p(k)}(f), \tag{4}$$

where $H_{kq}(f)$ and $X_{p(k)}(f)$ are the Fourier transforms of $h_{kq}(t)$ and $x_{p(k)}(t)$, respectively.

B. Designing the excitation waveforms

The information about the system carried by each individual waveform has to be extracted from (1). One way of achieving this is to design the waveforms such that they are approximately disjoint in the frequency domain. This condition can be written as

$$X_p(f)X_s^*(f) = \begin{cases} |X_p(f)|^2 & p = s \\ 0 & p \neq s \end{cases} \tag{5}$$

By dividing the available frequency band into a set of narrow bands and assigning one band to one specific transmitter, it is thus, possible to use several transmitters at the same time and still be able to separate them at the receiver. Such a set of signals for a system with four transmitters can be seen in Fig. 3. Each transmitter is now assigned an individual waveform. The received signal will be on the form as in (3), and the signal part of the received signal will be given by (1). If the attention is focused on the l:th transmitter, the only term of interest is basically the contribution from this transmitter. The contributions from the other transmitters are considered to be interference. Since the signals have virtually no overlap in the frequency domain, it is possible to filter out all the interference by simply applying a filter matched to the waveform representing the transmitter of interest. Since the noise is assumed to be white, the matched filter for the l:th transmitter is given by [17] $x_{p(l)}(-t)$, which has a frequency response $X^*_{p(l)}(f)$ [3]. The filtered version of (4) is then

$$\begin{aligned} Y_q(f)X^*_{p(l)}(f) &= \Big(\sum_{k=1}^{K} H_{kq}(f)X_{p(k)}(f)\Big)X^*_{p(l)}(f) \\ &= H_{lq}(f)|X_{p(l)}(f)|^2. \end{aligned} \tag{6}$$

---

[3] Z^* denotes complex conjugate of Z

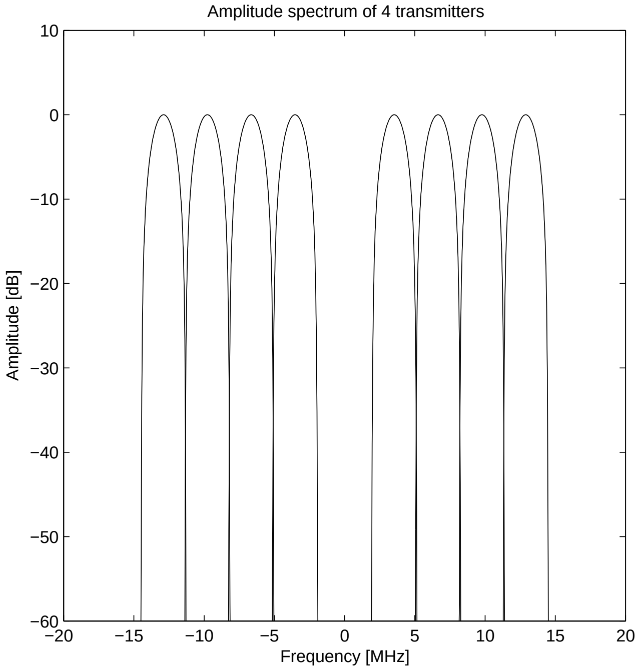

Fig. 3. A set of signals with the property specified in (5). The signals are weakly correlated and will remain so, even if subjected to phase shifts.

This result is independent of all other transmitters and can be treated as if transmitter l had been transmitting alone. The result in (6) however, does not excite the full bandwidth of the transfer function $H_{lq}(f)$ and will, thus, not provide the best achievable resolution. By acquiring data over a number of transmissions, and changing the transmitted waveforms for the transmitters to cover the full frequency band of the transducer, this problem can be solved. The total contribution from the l:th transmitter to the q:th receiver over N transmissions is now

$$\begin{aligned} Y_{lq}(f) &= \sum_{n=1}^{N} H_{lq}(f)|X_{p(l,n)}(f)|^2 \\ &= H_{lq}(f)\sum_{n=1}^{N}|X_{p(l,n)}(f)|^2. \end{aligned} \tag{7}$$

The sub index denoted by $p(l, n)$ is the number of the waveform transmitted on the l:th transmitter in the n:th transmitting event. By considering the different spectra in Fig. 3, it can clearly be seen that the summed frequency response do not produce a smooth function. This is unacceptable, if artifacts are to be avoided. If a second set of signals is designed which is a frequency shifted version of the first signal set, this problem can be circumvented. The requirement is that the summed matched filtered response results in a smooth spectrum which covers the full bandwidth of the transducer. The basic principle can be seen in Fig 4. If it is assumed that the transfer function between the l:th transmitter and the q:th receiver $H_{lq}(f)$ is band-limited, and that the summed spectrum of the N matched filtered waveforms is a constant function over this frequency band, then

$$Y_{lq}(f) = H_{lq}(f). \tag{8}$$

To cover the entire frequency band of the transducer for all transmitters the number of waveforms $P = 2K$, which means that $2K$ transmissions have to be made. It is imperative that signals from

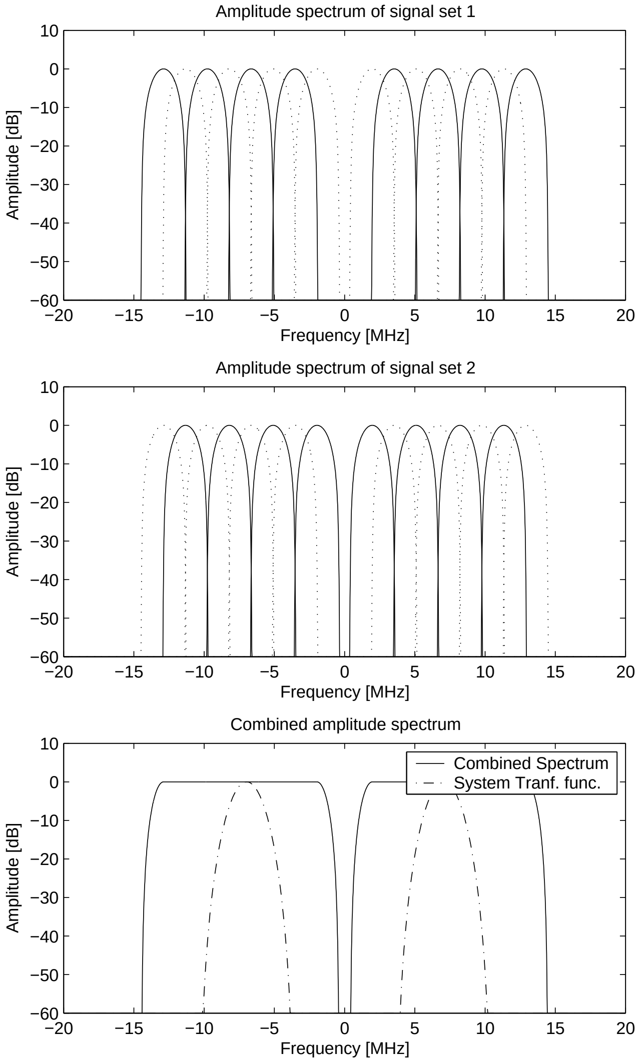

Fig. 4. The top most figure shows the amplitude spectrum of the first signal set and the middle figure shows the amplitude spectrum of the second signal set. The bottom figure shows the matched filtered and summed amplitude response for these two signal sets.

the first set are not transmitted at the same time as signals from the second set. This would destroy the orthogonality and it would not be possible to cancel the interference by matched filtering. Evidently some sort of pulsing strategy has to be devised. Let the set of P waveforms be denoted

$$\{x_p(t)\}_{p=1}^{P}, \tag{9}$$

where the waveforms from $p = 1$ to $p = K$ denotes the signals corresponding to the first signal set which are mutually orthogonal. The signals $p = K + 1$ to $p = 2K$ corresponds to the signals from the second set, which are also mutually orthogonal, but not orthogonal to the signals in the first set. For a system with 4 transmitters and thus, 8 different excitation waveforms a possible pulsing scheme is given in table I. The filtered and summed time (axial) response of the signals corresponding to the spectra in Fig. 4 can be examined in Fig. 5.

C. Design of narrow-band FM signals

Since an ultrasound system has a maximum excitation voltage, the limiting factor concerning the transmitted energy is the amplitude of the waveforms. It is therefore important to design

$p(k,n)$	n							
k	1	2	3	4	5	6	7	8
1	1	2	3	4	5	6	7	8
2	4	1	2	3	8	5	6	7
3	3	4	1	2	7	8	5	6
4	2	3	4	1	6	7	8	5

TABLE I

FIRING SEQUENCE FOR THE TOTAL SIGNAL SET

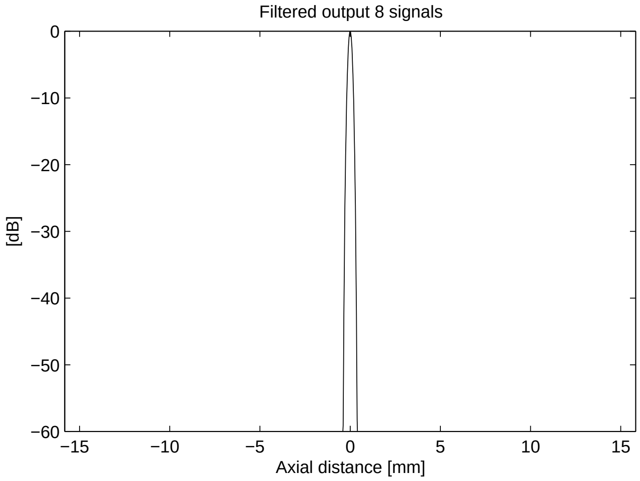

Fig. 5. The time response of the filtered and summed signals corresponding to Fig. 4 convolved with the impulse response of a 7 MHz transducer. Mutually orthogonal signals were summed to simulate simultaneous transmission

the waveforms such that the full excitation voltage can be applied over the full duration of the signal. The transmitted signals should thus, have long duration with fairly constant amplitude to maximize SNR, narrow bandwidth, and low sidelobes in the frequency domain to minimize inter-band interference. An obvious choice would be to use amplitude weighted narrow-band linear frequency modulated signals (chirps) with a very slow FM slope. A chirp with bandwidth B, center frequency f_p, duration T and temporal amplitude modulation function $a(t)$ is defined as

$$x_p(t) = a(t)\sin\Big\{2\pi(f_p - \frac{B}{2})t + 2\pi\frac{B}{2T}t^2\Big\},\ 0 \leq t \leq T. \tag{10}$$

The corresponding matched filter is simply the time reciprocal of the excitation waveform. For the examples in this paper the duration T of the waveforms is chosen to be 20 μs. The bandwidth of each individual waveform was 1 MHz. The signals were weighted using a Tukey window with 75% tapering to reduce ripple in the combined spectrum such that temporal sidelobes were minimized [8]. 16 waveforms were produced, organized in two subsets of 8 signals. The distance in the frequency domain between two adjacent signals in the same subset was chosen to be 1 MHz. This value was chosen in order to produce a smooth combined spectrum and get an acceptable inter-band interference level. The first signal in the first subset had a center frequency of 3.3 MHz, whereas the first signal in the second subset had a center frequency of 3.8 MHz. Two signals from the first subset can be seen in Fig. 6, where the top most figure is the signal corresponding to the smallest center frequency, whereas the bottom figure is the signal with the largest center frequency. The cross talk between two signals (the p:th and the s:th signal) will be defined as

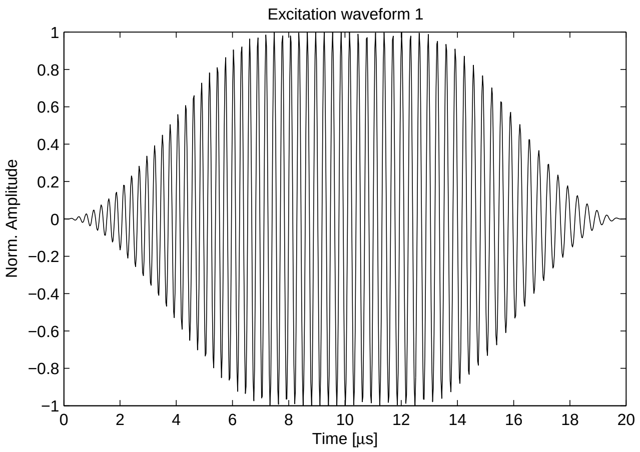

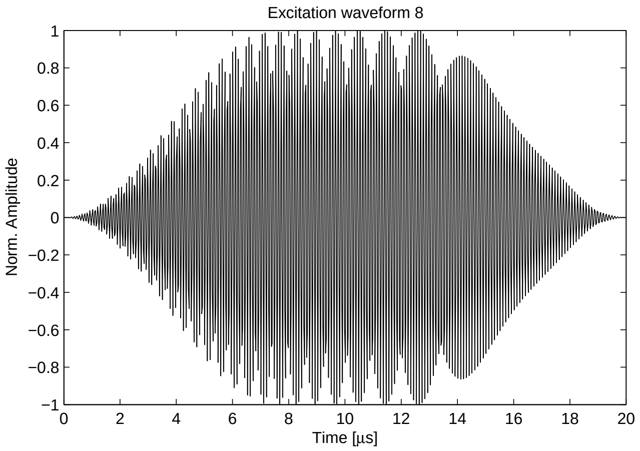

Fig. 6. The first (smallest center frequency, 3.3 MHz) and last (largest center frequency, 10.3 MHz) signals from the first signal subset.

$$\gamma_{p,s} = \frac{\int |x_p(t) \star x_s(t)|^2 dt}{\int |x_p(t) \star x_p(t)|^2 dt}. \tag{11}$$

The cross talk between two neighboring bands in the same signal subset, $\gamma_{p,p+1}$ was -46 dB. The inter-band interference produced a ripple in the combined spectrum with an amplitude of 0.1 dB. The resulting signal amplitude spectra can be seen in Fig. 7. The time response for the combined spectrum was computed and can be seen in Fig. 8. The temporal sidelobes at ±12 mm is a result of the ripple in the combined spectrum. The influence of these sidelobes will be analyzed using simulations in Section IV.

D. Signal to Noise Ratio

In this Section the influence on the peak signal-to-noise-ratio will be discussed. Consider a setup where the investigated object is a single point scatterer in an non-attenuating medium. The received signal will then simply be a timeshifted and scaled version of the transmitted waveform plus the system noise, which is assumed to be white, zero mean and Gaussian distributed. The noise is also assumed to be uncorrelated from transmission to transmission and from transducer element to transducer element. Consider first the conventional synthetic transmission aperture method with sequential data acquisition. The transmitted waveform is denoted $x(t)$ and its Fourier transform is $X(f)$ with energy E_{REF}. The received signal from one transmission will then be

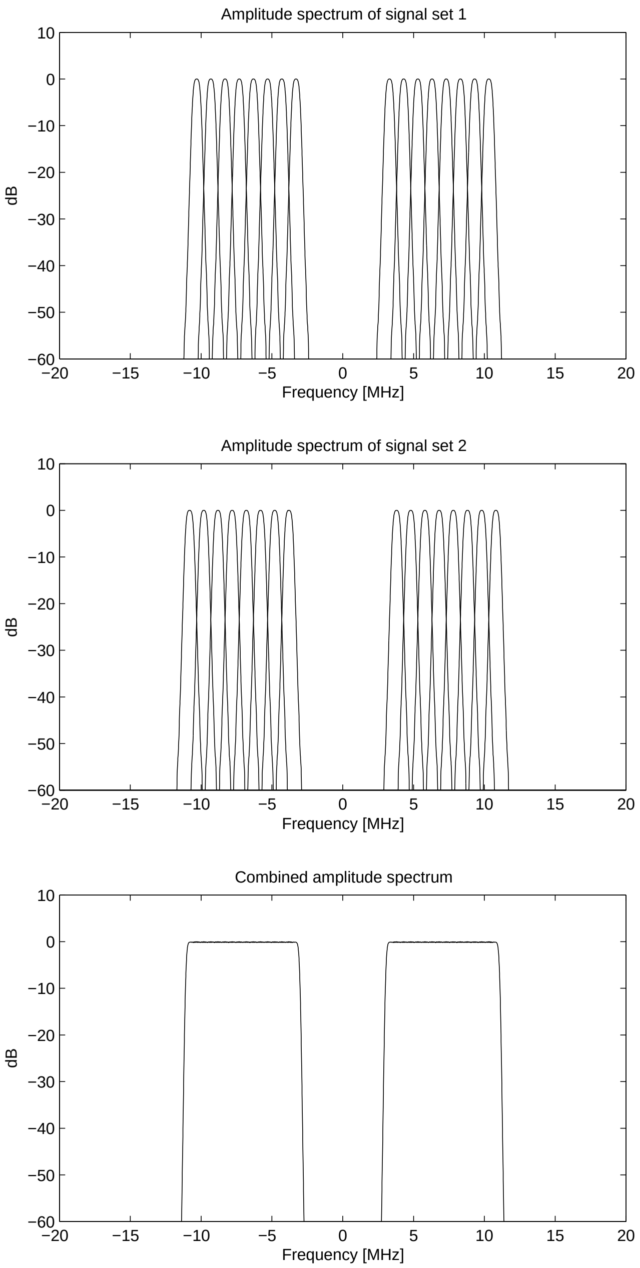

Fig. 7. The resulting amplitude spectra for the 16 narrow-band FM signals. The first waveform has a center frequency of 3.3 MHz, the bandwidth of the individual waveforms is 1 MHz.

(omitting time shift and scaling for simplicity)

$$r(t) = x(t) + v(t), \tag{12}$$

where $v(t)$ is the system noise with power P_v. The matched filtered output of (12) will be

$$r(t) \star x(-t) = x(t) \star x(-t) + v(t) \star x(-t). \tag{13}$$

The peak signal-to-noise-ratio is given by

$$SNR = \frac{\Big| x(t) \star x(-t)\big|_{t=t_{max}} \Big|^2}{E\big[|v(t) \star x(-t)|^2\big]}. \tag{14}$$

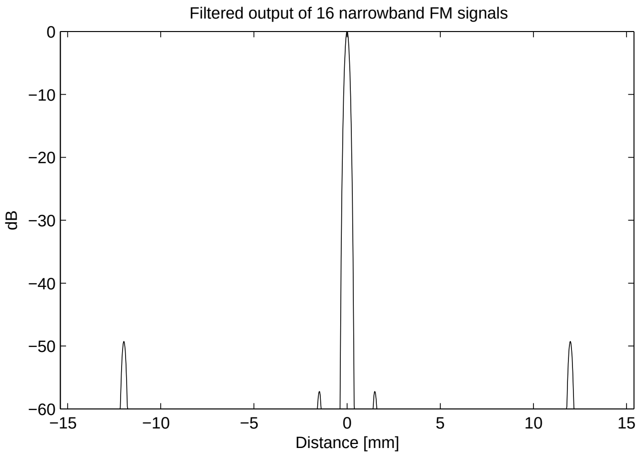

Fig. 8. The time response of the combined spectrum for the 16 signals. Signals from the two subsets were added to simulate simultaneous transmission.

The expression inside the absolute value of the numerator in (14) is given by [17]

$$x(t) \star x(-t)\big|_{t=t_{max}} = \int_{-\infty}^{\infty} |X(f)|^2 df = E_{REF}, \tag{15}$$

whereas the denominator will be

$$E\big[|v(t) \star x(-t)|^2\big] = \int_{-\infty}^{\infty} P_v |X(f)|^2 df = P_v E_{REF} \tag{16}$$

Assuming K transmitters, $2K$ transmissions are made for the sake of fareness compared to the FD approach. It it is assumed that the summing of the data originating from the different transmissions is coherent. The final signal-to-noise-ratio is then

$$SNR_{REF} = \frac{(2K)^2 E_{REF}^2}{2KP_v E_{REF}} = \frac{2KE_{REF}}{P_v}. \tag{17}$$

The attention is now turned to the FD imaging method. The narrow band waveforms $\{x_p(t)\}_{p=1}^{P}$ all have the energy E_{FD}. The response for one transmitter is constructed using $P = 2K$ transmissions. The received signal for one transmitter and one transmission is

$$r_p(t) = x_p(t) + v_p(t). \tag{18}$$

The matched filtered response is

$$r_p(t) \star x_p(-t) = x_p(t) \star x_p(-t) + v_p(t) \star x_p(-t), \tag{19}$$

giving the total response of

$$r_{mf}(t) = \sum_{p=1}^{2K} x_p(t) \star x_p(-t) + v_p(t) \star x_p(-t) \tag{20}$$

which in turn yields the filtered signal peak

$$\begin{aligned} \sum_{p=1}^{2K} x_p(t) \star x_p(-t)\big|_{t=t_{max}} &= \\ \sum_{p=1}^{2K} \int_{-\infty}^{\infty} |X_p(f)|^2 df &= 2KE_{FD}, \end{aligned} \tag{21}$$

and the filtered noise power

$$\begin{aligned} E\big[|\sum_{p=1}^{2K} v_p(t) \star x_p(-t)|^2\big] &= \\ \sum_{p=1}^{2K} \int_{-\infty}^{\infty} P_v |X_p(f)|^2 df &= 2KP_v E_{FD}. \end{aligned} \tag{22}$$

Once again coherent summing of the data from the different transmitters is assumed. The noise from transmission to transmission is also assumed to be uncorrelated, which gives the total signal-to-noise-ratio

$$SNR_{FD} = \frac{(2KK)^2 E_{FD}^2}{2KKP_v E_{FD}} = \frac{2K^2 E_{FD}}{P_v}. \tag{23}$$

The ratio of SNR's will, thus, be

$$\frac{SNR_{FD}}{SNR_{REF}} = K \frac{E_{FD}}{E_{REF}}. \tag{24}$$

III. BEAMFORMING

This section describes the beamforming, which has been applied to properly focus the data. When the data from one specific transmitter is available, either by applying the FD method and filtering out the data from a specific transmitter, or using only one transmitter at a time, it is possible to exactly determine where on the aperture the acoustic wave was transmitted, and where it was received. This allows the synthetic aperture focusing technique described in [2] to be applied.

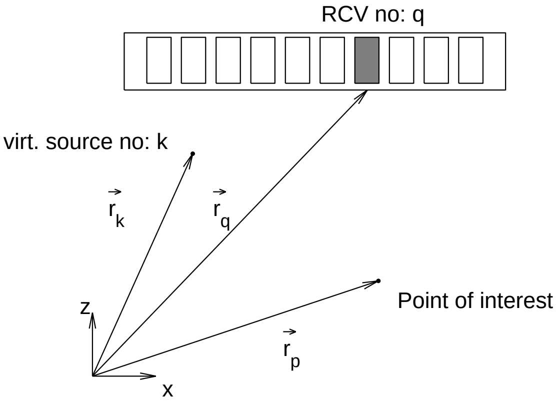

Fig. 9. Principles of synthetic aperture focusing for a point p for the k:th transmitter and the q:th receiver.

Since the system has access to defocused transmissions from all transmitters on the aperture, it is possible to focus in any arbitrarily chosen point of interest. The amplitude in a point p in the image is given by

$$H(\vec{r}_p) = \sum_{k=1}^{K} \sum_{q=1}^{Q} g_q h_{kq}(t_{pkq}), \tag{25}$$

where g_q is a weighting function (apodization) over the receiving aperture, and $h_{kq}(t)$ is the received (and possibly filtered) echo on the q:th receiver originating from the k:th transmitter. Here

t_{pkq} is the time corresponding to the geometrical travel distance from the k:th transmitter to the point p and back to the q:th receiver:

$$t_{pkq} = \frac{||\vec{r}_p - \vec{r}_k|| + ||\vec{r}_q - \vec{r}_p||}{c}, \tag{26}$$

where c is the speed of sound, and $\vec{r}_p - \vec{r}_k$ is the vector from the transmitter to the point p, and $\vec{r}_q - \vec{r}_p$ is the vector from the point p to the receiver as indicated in Fig. 9. Summing contributions from all transmissions for all receiving elements then gives both dynamic transmit and receive focusing.

IV. SIMULATIONS

The method was tested using the virtual ultrasound scanner software Field II [18], [19]. A 7 MHz, 128 element transducer was simulated. The kerf was 0.035 mm, pitch 0.208 mm and height 4.5 mm. The transmitting aperture was created by grouping and focusing 64 of the central transducer elements so that 8 virtual sources were formed. The bandwidth of the transducer limited the maximum number of active transmitters to 8, which in turn resulted in that only the 64 central elements were used, such that the spacing between the virtual sources would not become to large. Each virtual source consisted of 8 transducer elements which were focused 2.5 mm in front of the transducer surface. The receiving aperture used all 128 elements with a Hanning weighting. The sampling frequency was 120 MHz. The transducer impulse response was set to be a single cycle sinusoid at 7 MHz with a temporal Hanning weighting.

A. Frequency division excitation

All transmitters were used in every transmission. Two sets of signals were created. Each set consisted of 8 narrow band FM signals. The first band had a center frequency of 3.3 MHz and the spacing in the frequency domain was 1 MHz. The signals were 20 μs long. The target was 7 point scatterers starting at 30 mm from the transducer surface with a 5 mm spacing. The result can be seen in Fig. 10. The resolution as a function of depth can be seen in Table II. Note that the axial sidelobes, which occurred in the time response in Section II-C, are not present in the image in Fig 10.

	Axial res. mm		Lateral res. mm	
depth	-3dB	-6dB	-3dB	-6dB
30 mm	0.192	0.278	0.245	0.403
35 mm	0.189	0.272	0.270	0.429
40 mm	0.185	0.268	0.291	0.464
45 mm	0.184	0.265	0.334	0.522
50 mm	0.184	0.265	0.400	0.601
55 mm	0.184	0.264	0.449	0.653
60 mm	0.183	0.265	0.484	0.728

TABLE II

RESOLUTION AS A FUNCTION OF DEPTH, FREQUENCY DIVISION IMAGING

B. Sinusoidal excitation

As a reference a conventional synthetic aperture transmission scheme was used. One virtual source was used in every transmission. The excitation was a single cycle sinusoid with a center frequency of 7 MHz with a temporal Hanning weighting. The target was once again 7 point

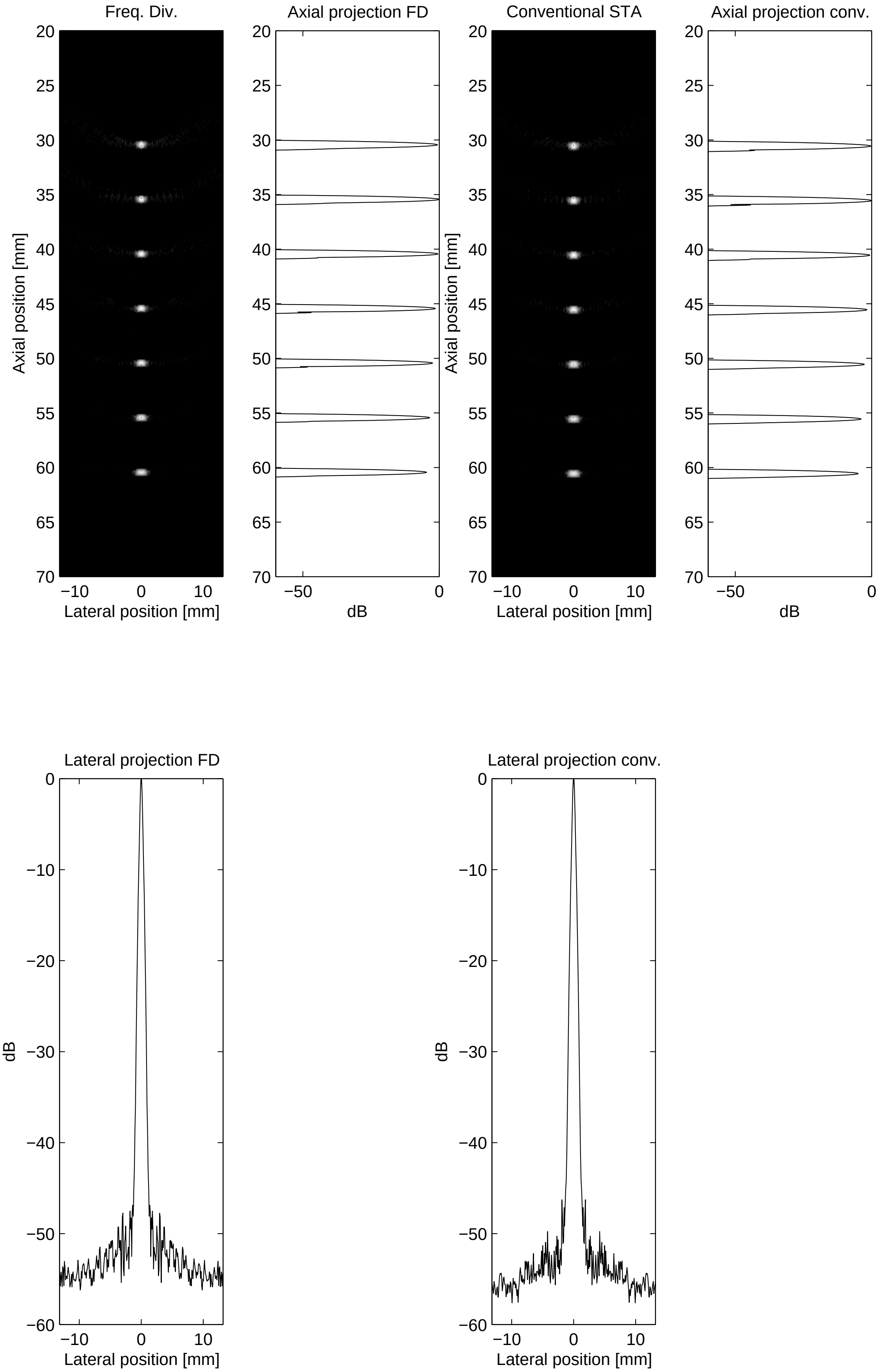

Fig. 10. The simulation of the response for the 7 point scatterers. The figures to the left shows the response for the frequency division method with 8 virtual sources and 16 bands. The figures to the right shows the response for a conventional synthetic aperture transmission approach using a single cycle sinusoid at 7 MHz as excitation.

	Axial res. mm		Lateral res. mm	
depth	-3dB	-6dB	-3dB	-6dB
30 mm	0.201	0.292	0.268	0.433
35 mm	0.196	0.286	0.274	0.446
40 mm	0.195	0.283	0.324	0.508
45 mm	0.194	0.282	0.377	0.575
50 mm	0.194	0.281	0.435	0.637
55 mm	0.194	0.281	0.473	0.712
60 mm	0.195	0.283	0.530	0.788

TABLE III

RESOLUTION AS A FUNCTION OF DEPTH, CONVENTIONAL STA IMAGING

scatterers starting at 30 mm from the transducer surface with a 5 mm spacing. The result can be seen in Fig. 10. The resolution as a function of depth can be seen in Table III. From Tables II and III it can be concluded that the frequency division approach yields the same resolution as a normal STA system with a sinusoid excitation. The lateral sidelobe level was also the same, below -45 dB.

V. EXPERIMENTS

The Frequency Division imaging method has been tested in an experimental setup and the results were compared to other methods. The ultrasound research scanner RASMUS [20] was used for the measurements, with a BK8804 7 MHz linear array transducer (B-K Medical A/S, Herlev, Denmark). The FD method was compared to a system which used a single cycle sinusoid excitation and to a system with a linear Frequency Modulated signal as excitation.

The transmitting and receiving aperture was the same for all three methods. 64 active elements were used as the transmitting aperture. The reason for using only the central 64 tranducer elements was the same as in Section IV. The transmitting elements were grouped and focused such that 8 virtual sources were formed. The focusing point was 2.5 mm in front of the transducer surface. Each virtual source was created by 8 transducer elements. The RASMUS system only has access to 64 elements as receiving aperture, but 128 receiving elements were emulated by multiplexing. The receiving aperture was weighted by a Hanning window. All three methods used the synthetic aperture focusing technique described in [2]. The main difference is that the FD method used all active elements in transmit, whereas the two other methods used only one virtual source at a time.

A. Sinusoid excitation

The excitation was in this case a single cycle sinusoid with a center frequency of 7 MHz corresponding to the center frequency of the transducer, with a temporal Hanning weighting.

B. Linear Frequency Modulated signal (Chirp)

The linear Frequency Modulated excitation waveform had a center frequency of 7 MHz, duration 20 μs, and a bandwidth of 75% of the center frequency. The waveform was tapered using a Tukey window with 10 % tapering. The compression filter was the corresponding matched filter version of the excitation waveform mismatched using a Chebyshev window with relative sidelobe attenuation of 70 dB. The temporal window applied to derive the mismatched filter is used in order to suppress axial sidelobes [8]. The excitation waveform and the corresponding mismatched filter can be seen in Fig. 11.

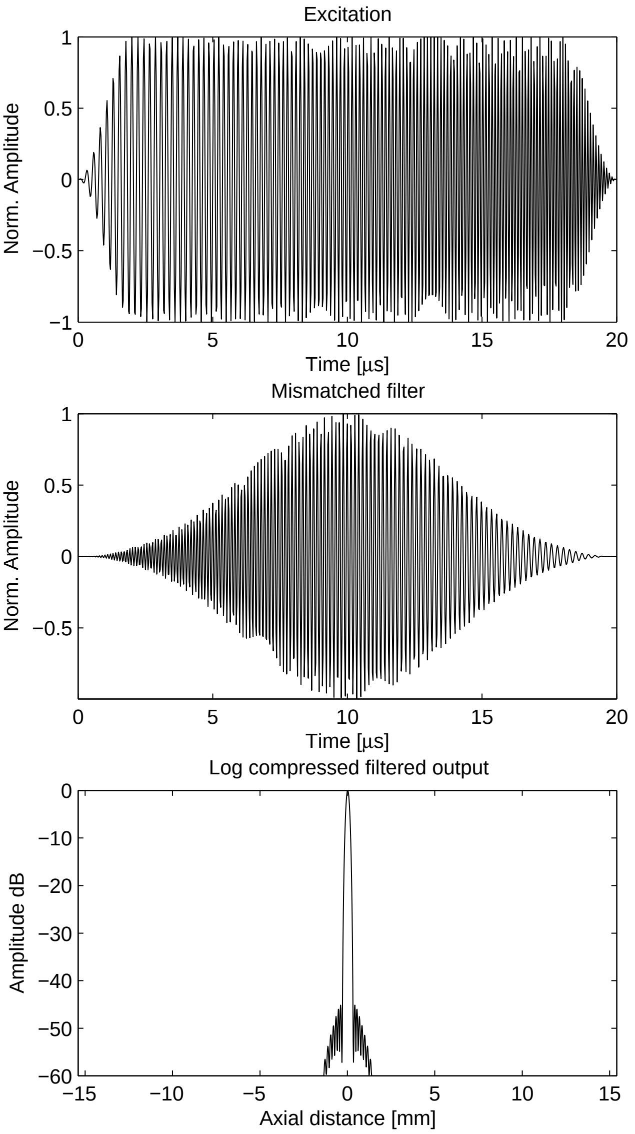

Fig. 11. The top most figure is the excitation waveform, the figure in the middle is the corresponding mismatched filter. The bottom figure is envelope of the filtered output. Note that the rangelobes will be further suppressed by the transducer impulse response.

C. Frequency Division imaging method

All virtual sources were excited in every transmission. This was done by assigning the waveforms derived in Section II-C to the different transmitters.

D. Phantom measurements

Three measurements were done using a string phantom from Dansk Fantomservice (Jylling, Denmark) to evaluate resolution. The result from the three measurements can be seen in Fig. 12. The frequency division approach improves the penetration depth by 3.5-4 cm compared to the system using the single cycle sinusoid excitation, whereas the penetration depth is improved by 1-2 cm compared to the system using the chirp excitation. The axial and lateral resolution as a function of depth can be seen in Tables IV and V for the frequency division approach and chirp excitation, respectively. The axial resolution is somewhat better for the setup using the chirp for depth 22-42 mm, whereas the frequency division approach has better axial resolution for depths

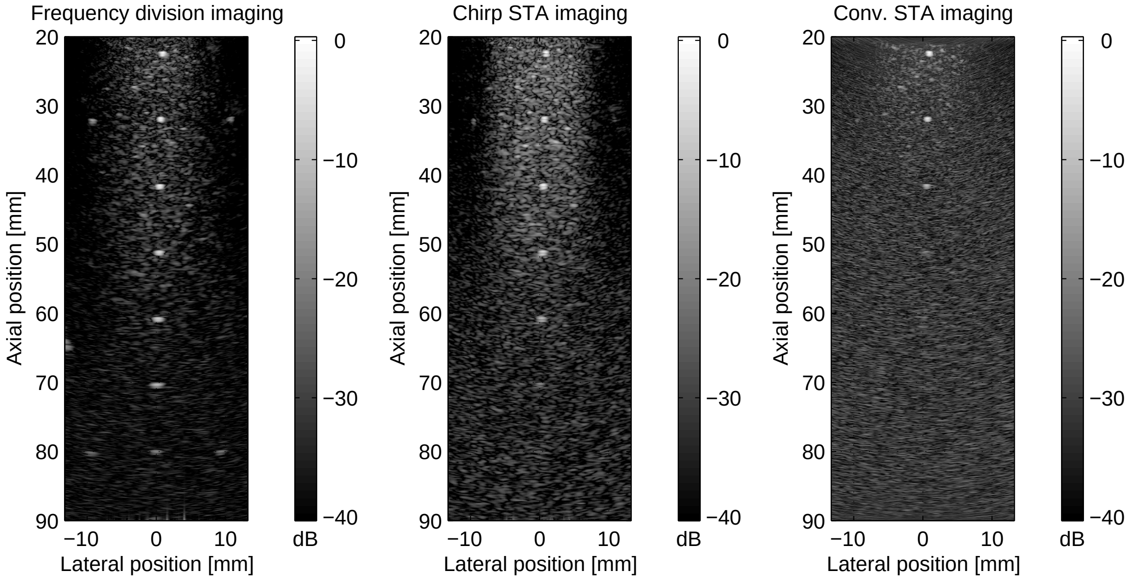

Fig. 12. The left most image is the image produced by the frequency division approach using 16 frequency bands. The image in middle is the image produced by the chirp specified in V-B The right image is the image resulting from a single sinusoid excitation with a center frequency of 7 MHz.

	Axial res. mm	Lateral res. mm
depth	-6dB	-6dB
22 mm	0.568	0.568
32 mm	0.590	0.567
42 mm	0.557	0.684
52 mm	0.520	0.851
62 mm	0.534	0.989

TABLE IV

RESOLUTION AS A FUNCTION OF DEPTH, FREQUENCY DIVISION IMAGING

52-62 mm. The lateral resolution is in all cases in favor of the setup using the chirp excitation, but the difference is so small, that it is concluded that the lateral resolution is comparable for the two different excitation schemes.

E. Signal to noise ratio measurement

The signal to noise ratio was also measured and compared to the results derived in Section II-D. The same setup was used as in the phantom measurements. However, the setup using a single sinusoid excitation was ignored and instead the chirp excitation was used as a reference. A speckle phantom from Dansk Fantom service M571 was used (90.6 % water, 9.4 % glycerol(85%), 0.2 % Na-benzonat, 0.1 % K_2-EDTA). Only speckle was measured. First 100 images were acquired using the setup with a chirp as excitation waveform. These images were added pair-wise to emulate the same number of transmissions as in the frequency division approach. Next, 50 images were acquired using the frequency division approach. The two equally large sets of images were averaged in order to get an estimate of the signal component in the images.

$$S(i,j) = \frac{1}{N}\sum_{n=1}^{N} H_n(i,j), \tag{27}$$

	Axial res. mm	Lateral res. mm
depth	-6dB	-6dB
22 mm	0.437	0.519
32 mm	0.450	0.561
42 mm	0.460	0.679
52 mm	0.633	0.830
62 mm	0.666	0.923

TABLE V

RESOLUTION AS A FUNCTION OF DEPTH, CHIRP STA IMAGING

where $H_n(i, j)$ is a sample in a specific high resolution image originating from one data acquisition (full image constructed from several firings). The resulting signal component was subtracted from the images to get an estimate of the noise component in the images.

$$N(i,j) = H_n(i,j) - S(i,j). \tag{28}$$

The signal to noise ratio for a specific depth was then computed for the center line in an image as

$$SNR(d) = \frac{\sum_{i=i_d-L+1}^{i_d} S(i,j_c)^2}{\sum_{i=i_d-L+1}^{i_d} N(i,j_c)^2} \tag{29}$$

where i_d corresponds to the row in the image which represents the depth d, i_c is the center line and L is the segment length over which the SNR estimate is computed. The segment length was chosen to be 200 samples, which corresponds to 3.85 mm in the phantom, assuming that the speed of sound is 1540 m/s.

The result can be seen in Fig. 13. The data originating from the measurement using the chirp was fitted to a straight line using linear regression. Since the number of transmitters is $K = 8$ and the ratio of signal energies $\frac{E_{FD}}{E_{chirp}} = 0.61$, according to (24), the gain in SNR should be 6.86 dB. The theoretical gain in SNR can be seen as the dotted line in Fig. 13. The theoretically computed gain in SNR agrees with the measured gain in SNR.

VI. CONCLUSION

A method for exciting several transmitters simultaneously and separating them in receive has been proposed. Compared to the traditional way of acquiring data in synthetic transmit aperture imaging, this method has the advantage, that it can use all transmitters in every transmission. This means that the transmitted energy will be increased, and that the signal to noise ratio will be increased. The major advantage of the approach is that the acquired information from the multiple transmitters, can be separated from each other instantaneously, once the data has been received. It is not necessary as in Hadamard or Golay coding, to use multiple transmissions before it is possible to decode the data. The proposed approach is, thus, not influenced by motion effects in the decoding step. Furthermore, a temporal coding concept has also been deployed, where the different narrow-band signals are linearly frequency modulated, such that the instantaneous frequency of the signals increases linearly with time. This enables the system to use the full excitation voltage for a longer time. These two factors combined means that the number of transmission can be decreased, and the same signal to noise ratio can be achieved, which is an advantage in cases of rapid tissue movement or in flow imaging. The method has been evaluated using the simulation

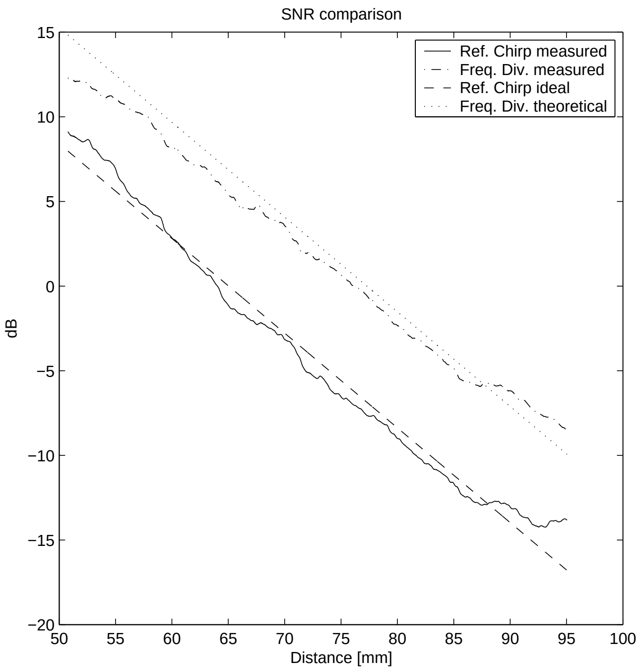

Fig. 13. The signal to noise ratio as a function of depth. The solid line is the measured SNR for the reference experiment using a chirp excitation. The dashed line is the same data but after linear regression has been applied. The dashed dotted line is the SNR measurement using the frequency division approach. The dotted line is the theoretical SNR for the frequency division approach using the chirp excitation as a reference.

tool Field II, where it was compared to traditional synthetic aperture acquisition using a single cycle sinusoid excitation. The resolution and contrast were found to be comparable in the two different situations. A measurement in an attenuating string phantom has also been performed. The frequency division approach was compared to a conventional STA acquisition approach using both a chirp and a sinusoidal excitation. The penetration depth was found to be increased by 1-2 cm compared to the chirp excitation and 3.5-4 cm compared to sinusoidal excitation. The setup using the sinusoidal excitation was excluded in the resolution comparison because of the poor penetration depth. Concerning axial and lateral resolution, the frequency division approach and the conventional STA using a chirp was found to yield approximately the same performance. A signal to noise ratio measurement was also performed. The frequency division approach was compared to the STA setup using a chirp excitation. The improvement in SNR was found to be approximately 6.5 dB, which agrees with the theoretically derived results.

ACKNOWLEDGMENT

This work was supported by grant 9700883, 9700563 and 26-01-0178 from the Danish Science Foundation and by B-K Medical A/S, Denmark.

REFERENCES

[1] S. Bennett, D. K. Peterson, D. Corl, and G. S. Kino, "A real-time synthetic aperture digital acoustic imaging system," in *Acoust. Imaging*, P. Alais and A. F. Metherell, Eds., 1982, vol. 10, pp. 669–692.

[2] S. I. Nikolov, *Synthetic aperture tissue and flow ultrasound imaging*, Ph.D. thesis, Ørsted●DTU, Technical University of Denmark, 2800, Lyngby, Denmark, 2001.

[3] J. W. Goodman, *Introduction to Fourier optics*, McGraw Hill Inc., New York, second edition edition, 1996.

[4] M. O'Donnell, "Coded excitation system for improving the penetration of real-time phased-array imaging systems," *IEEE Trans. Ultrason., Ferroelec., Freq. Contr.*, vol. 39, pp. 341–351, 1992.

[5] T. X. Misaridis, K. Gammelmark, C. H. Jørgensen, N. Lindberg, A. H. Thomsen, M. H. Pedersen, and J. A. Jensen, "Potential of coded excitation in medical ultrasound imaging," *Ultrasonics*, vol. 38, pp. 183–189, 2000.

[6] T. X. Misaridis, M. H. Pedersen, and J. A. Jensen, "Clinical use and evaluation of coded excitation in B-mode images," in *Proc. IEEE Ultrason. Symp.*, 2000, vol. 2, pp. 1689–1693.

[7] T. X. Misaridis and J. A. Jensen, "An effective coded excitation scheme based on a predistorted FM signal and an optimized digital filter," in *Proc. IEEE Ultrason. Symp.*, 1999, vol. 2, pp. 1589–1593.

[8] T. Misaridis, *Ultrasound imaging using coded signals*, Ph.D. thesis, Ørsted●DTU, Technical University of Denmark, Lyngby, Denmark, 2001.

[9] M. O'Donnell and L. J. Thomas, "Efficient synthetic aperture imaging from a circular aperture with possible application to catheter-based imaging," *IEEE Trans. Ultrason., Ferroelec., Freq. Contr.*, vol. 39, pp. 366–380, 1992.

[10] M. Karaman, P. C. Li, and M. O'Donnell, "Synthetic aperture imaging for small scale systems," *IEEE Trans. Ultrason., Ferroelec., Freq. Contr.*, vol. 42, pp. 429–442, 1995.

[11] C. Passmann and H. Ermert, "A 100-MHz ultrasound imaging system for dermatologic and ophthalmologic diagnostics," *IEEE Trans. Ultrason., Ferroelec., Freq. Contr.*, vol. 43, pp. 545–552, 1996.

[12] C. H. Frazier and W. D. O'Brien, "Synthetic aperture techniques with a virtual source element," *IEEE Trans. Ultrason., Ferroelec., Freq. Contr.*, vol. 45, pp. 196–207, 1998.

[13] M. H. Pedersen, K. L. Gammelmark, and J. A. Jensen, "Preliminary in-vivo evaluation of convex array synthetic aperture imaging," in *Proc. SPIE - Progress in biomedical optics and imaging*, 2004, pp. 33–43.

[14] R. Y. Chiao, L. J. Thomas, and S. D. Silverstein, "Sparse array imaging with spatially-encoded transmits," in *Proc. IEEE Ultrason. Symp.*, 1997, pp. 1679–1682.

[15] T. Misaridis and J. A. Jensen, "Space-time encoding for high frame rate ultrasound imaging," *Ultrasonics*, vol. 40, pp. 593–597, 2002.

[16] R. Y. Chiao and L. J. Thomas, "Synthetic transmit aperture using orthogonal golay coded excitation," in *Proc. IEEE Ultrason. Symp.*, 2000, pp. 1469–1472.

[17] S. Haykin, *Communication Systems*, John Wiley & Sons, Inc., 2001.

[18] J. A. Jensen and N. B. Svendsen, "Calculation of pressure fields from arbitrarily shaped, apodized, and excited ultrasound transducers," *IEEE Trans. Ultrason., Ferroelec., Freq. Contr.*, vol. 39, pp. 262–267, 1992.

[19] J. A. Jensen, "Field: A program for simulating ultrasound systems," *Med. Biol. Eng. Comp.*, vol. 10th Nordic-Baltic Conference on Biomedical Imaging, Vol. 4, Supplement 1, Part 1, pp. 351–353, 1996b.

[20] J. A. Jensen, O. Holm, L. J. Jensen, H. Bendsen, S. I. Nikolov, B. G. Tomov, P. Munk, M. Hansen, K. Salomonsen, J. Hansen, K. Gormsen, H. M. Pedersen, and K. L. Gammelmark, "Ultrasound research scanner for real-time synthetic aperture image acquisition," *IEEE Trans. Ultrason., Ferroelec., Freq. Contr.*, p. Submitted, 2003.

5.9 Conference paper: Spatio-temporal encoding using narrow-band linear frequency modulated signals in synthetic aperture ultrasound imaging

Accepted for publication, Proceedings of SPIE Medical Imaging meeting, Ultrasonic Imaging and Signal Processing, February 2005

Spatio-temporal encoding using narrow-band linear frequency modulated signals in synthetic aperture ultrasound imaging

Fredrik Gran and Jørgen Arendt Jensen

Center for Fast Ultrasound Imaging, Ørsted•DTU, Build. 348
Technical University of Denmark, DK-2800 Kgs. Lyngby, Denmark

ABSTRACT

In this paper a method for spatio-temporal encoding is presented for synthetic transmit aperture ultrasound imaging (STA). The purpose is to excite several transmitters at the same time in order to transmit more acoustic energy in every single transmission. When increasing the transmitted acoustic energy, the signal to noise ratio will increase. However, to focus the data properly using the STA approach, the transmitters have to be separated from each other. This is done by dividing the available spectrum into several subbands with a small overlap. Separating different transmitters can be done by bandpass filtering. Therefore, the separation can be done instantaneously without the need for further transmissions, unlike spatial encoding relying on Hadamard or Golay coding schemes, where several transmissions have to be made before the decoding can be done. Motion artifacts from the decoding can, thus, be avoided. To further increase the transmitted energy, the excitation waveforms are designed as linear frequency modulated (FM) signals. This makes it possible to maintain the full excitation amplitude during most of the transmission. The design of the separation filters will also be discussed. The method was tested using the experimental ultrasound scanner RASMUS and evaluated using a reference setup with a linear FM excitation waveform and STA beamforming. The point spread function (PSF) was measured on a wire phantom in water. A wire phantom with an attenuating medium was also measured, where the proposed method achieved approximately 2 cm improvement in penetration depth. The signal to noise ratio was also measured, where the gain was $\sim$ 7 dB in comparison to the reference.

Keywords: Spatial and temporal encoding, coded ultrasound imaging, synthetic transmit aperture ultrasound

1. INTRODUCTION

In synthetic transmit aperture ultrasound imaging (STA),[1, 2] one transmitting element is active in every transmission and one or several receiving elements are actively listening for echoes from only this transmitting element. Since only one element is active, the received echoes can be beamformed with dynamic receive focusing to yield several parallel created receive lines. A larger transmit aperture can be synthesized by changing the physical location of the active element in the next transmission, beamforming the echoes and combining the results from the two transmissions. This of course assumes that the object under investigation is fully stationary. The approach can be extended to cover a large amount of transmissions as long as this condition is not violated. STA therefore provides means for both dynamic transmit and receive focusing.

A problem concerning this method is, however, the low signal-to-noise ratio (SNR) due to the use of only one single transducer element. The use of virtual sources[3–6] has been suggested to increase the SNR. This method relies on using a focused sub-array, and treats the focus point as a virtual transmitting element. In[7–11] the use of linear frequency modulated signals (chirps) were suggested to increase the SNR. These signals make it possible to transmit longer signals with more energy by increasing (or decreasing) the instantaneous frequency of the signal linearly. By matched (or mismatched) filtration, the same axial resolution as with a short excitation waveform can be achieved.

Further author information: (Send correspondence to F. Gran)
F. Gran: E-mail: fg@oersted.dtu.dk, Telephone: +45 45 25 57 38

These approaches, however, still use only a relatively small part of the available aperture. By spatial encoding, several transmitters* can be excited simultaneously and separated at the receiver. In this way more acoustic energy can be transmitted with an increase in SNR as a result. Chiao et.al.[12] and later also Misaridis and Jensen[13] suggested to use Hadamard encoding to spatially encode the transmitters. The excitation waveforms on the individual transmitters are multiplied by the coefficients of a row (or column) of the Hadamard matrix of the same dimension as the number of transmitters. The decoding is done by adding and subtracting the echoes from transmissions which have been premultiplied by different rows of the Hadamard matrix. Naturally, the same number of transmissions have to be made as the number of active transmitters before the echoes can be decoded. This imposes a restriction on the object under investigation to be fully stationary in order for the decoding to be done without any artifacts. Chiao and Thomas[14] suggested another method for spatially encoding the transmitters using Golay codes. This method, however, also requires the same number of transmissions as number of active transmitters and suffers from the same drawbacks as Hadamard encoding.

In this paper developement of a method based on the results in[15] is described. The method is based on dividing the available transducer bandwidth into several sub-bands with very little overlap in the spectral domain. In every transmission each transmitter is assigned an individual band. Therefore, the information from a specific transmitter can be separated from the other transmitters instantaneously at the receiver with a simple filtering operation. The decoding requires, thus, only one transmission and no motion artifacts will be present in the decoding step. By changing the frequency bands for the different transmitters, transmitting several times and summing the results, a broad-band spectrum can be synthesized for each transmitter. The results reported were based on signals with linear phase and the separation was done using simple matched filtration. In this paper the excitation waveforms are narrow-band linear frequency modulated signals. This makes it possible to use the full transmit amplitude during most of the transmission. Consequently, more acoustic energy can be transmitted, which increases the SNR. The separation is also modified. It is still based on matched filtration, but with the slight modification that the matched filters are prefiltered with linear phase filters. This is done to make the spectrum of the filtered output more narrow, to decrease inter-transmitter interference.

The paper is organized as follows: In Section 2 the design of the excitation waveforms is presented and in Section 3 the design of the separation filters is explained. The effect on SNR is given in Section 4 and a brief discussion of the beamforming is given in Section 5. The experimental results are given in Section 6 followed by concluding remarks in Section 7.

2. DESIGN OF EXCITATION WAVEFORMS

Let the number active of transmitters be denoted K and let the system dynamics be fully linear. The interaction between the ultrasonic wave and the interrogated tissue is also considered to be fully linear. The sampled received signal in transmission p on the q:th receiving element can then be written

$$r_q^p(n) = \underbrace{\sum_{k=1}^{K} h_{qk}^p(n) \star x_{l(k,p)}(n)}_{s_q^p(n)} + v_q^p(n), \tag{1}$$

where $h_{qk}^p(n)$ represents the (linear) process which transforms the excitation waveform $x_{l(k,p)}$ transmitted on transmitter k before it is received on the q:th receiver in transmission number p. $l(k,p)$ indicates the waveform number which is transmitted on transmitter k in transmission p, and $\star$ denotes the convolution operator. The variable $v_q^p(n)$ represents the measurement noise and is assumed to be a white zero mean and Gaussian distributed process. The signal part of (1) is denoted $s_q^p(n)$. The Fourier transform of $s_q^p(n)$ is given by

$$S_q^p(f) = \sum_{k=1}^{K} H_{qk}^p(f) X_{l(k,p)}(f), \tag{2}$$

---

[*] The term transmitter can either represent a single transducer element or virtual source.

Set					
1	3.3000,	5.4024,	7.5048,	9.6072	MHz
2	4.3512,	6.4356,	8.5560,	10.6584	MHz

Table 1. The center frequencies of the different waveforms in the two sets.

where $H^p_{qk}(f)$ and $X_{l(k,p)}(f)$ denote the Fourier transform of $h^p_{qk}(n)$ and $x_{l(k,p)}(n)$, respectively. The objective is to design excitation waveforms such that the information represented by a specific transmitter can be distinguished by a standard filtering operation. This enables the use of several transmitters simultaneously and increases the transmitted acoustic energy in a single transmission and thus, increases the signal-to-noise ratio (SNR). It is also desirable to design signals with constant amplitude over a relatively long duration in time. To meet the first requirement narrow-band signals have to be designed. To meet the second requirement the linear frequency modulated signal (*chirp*) was chosen. This means that the excitation waveforms (in continuous time) are given by

$$x_l(t) = a(t)\sin\Big(2\pi\big(f_l - \frac{B}{2}\big)t + 2\pi\frac{B}{2T}t^2\Big), \quad 0 \le t \le T \tag{3}$$

where f_l is the center frequency of the l:th waveform, B is the bandwidth, T is the duration in time and $a(t)$ is a temporal weighting function. In this paper, four transmitters will be active simultaneously and for reasons which will be apparent in Section 3, eight excitation waveforms were generated. The duration of the waveforms were 25 μs with a bandwidth of 2 MHz. The temporal weighting was chosen to be a Tukey window with 35% tapering. This window was chosen in order to reduce ripple in the amplitude spectrum of the individual waveforms. The excitation waveforms were grouped in two sets and the center frequencies of the excitation waveforms is given in Table 1. The amplitude spectrums of the excitation waveforms can be seen in Fig. 1.

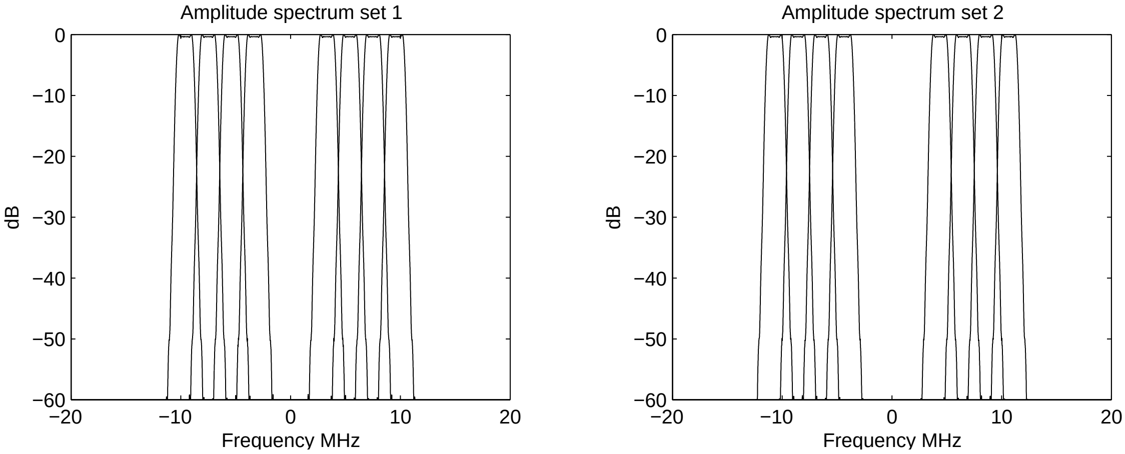

Figure 1. The two different sets of waveforms. All signals are linear frequency modulated signals with a Tukey window with 35% tapering. The bandwidth was 2 MHz and the duration of the waveforms was 25 μs.

3. DESIGN OF COMPRESSION FILTERS

The Fourier transform of the signal part for the p:th transmission is given in (2). In this transmission the k:th transmitter is represented by waveform number $l(k,p)$. To separate a specific waveform from the others, it is desirable to design filters $g_l(n)$, which have the Fourier transform $G_l(f)$ with the property

$$G_l(f)X_j(f) \approx 0, \quad l \neq j. \tag{4}$$

Since the excitation waveforms are relatively narrow band the interference from neighboring bands will be low. The matched filter, $g_l(n) = x_l(-n)$ would therefore be a good start. Furthermore, the matched filter will cancel the phase of the frequency modulated signal and thereby create a more narrow time response. To make the spectrum of the filtered output have a certain desired shape, to reduce the interference from other signals, a filter with appropriate frequency characteristics will be applied. Thus, the final filter will be

$$g_l(n) = x_l(-n) \star c_l(n), \tag{5}$$

with the corresponding Fourier transform

$$G_l(f) = X_l^*(f)C_l(f). \tag{6}$$

The filter $c_l(n)$ will, thus, have an amplitude shaping effect on the final spectrum of $g_l(n)$ and should not effect the phase at all. First a desirable spectrum $C_l(f)$ is specified, then the actual filter in the time domain $c_l(n)$ is chosen to be the linear phase FIR filter which minimizes the least squares criterion. This is given in Matlab by the function `firls`. The desired spectrum $C_l(f)$ is chosen to be

$$C_l(f) = \begin{cases} \frac{1}{2}\Big(1 + \cos(2\pi \frac{f-f_l}{B})\Big) & f_l - \frac{B}{2} \le f \le f_l + \frac{B}{2} \\ 0 & \text{otherwise.} \end{cases} \tag{7}$$

This spectrum was chosen because summed and appropriately frequency shifted versions of this spectrum produce a smooth bandpass spectrum. The length of $g_l(n)$ was chosen to be 500 samples corresponding to 15 μs. The amplitude spectrums of the filters can be seen in Fig. 2. In order to reduce multi-user interference it is imperative to separate the spectrums in the frequency domain by a sufficient amount. Since only a small part of the available bandwidth is used for every transmitter, poor axial resolution would result from only using one transmission for every set of transmitters. However, by transmitting several times for every set of transmitters and combining the resulting time signals, under assumption of stationarity, a broadband spectrum can be synthesized. Now, it becomes apparent why two sets of signals need to be generated. Since the excitation waveforms are separated in the frequency domain, the combined amplitude spectrum would experience ripples which would create artifacts. Hence, the second set of signals is transmitted to produce a smooth spectrum. The choice of shaping filter in (7) also becomes obvious since the sum of appropriately frequency shifted versions of this spectrum will produce a smooth function with constant amplification in the passband. The combined amplitude spectrum of the two sets of signals is given in Fig. 3. The figure to the left shows the filtered output for the different excitation waveforms (solid lines) whereas the thick solid line represents the transfer function of the measurement system combined with a BK8804 linear array transducer. The figure to the right shows the output when the signals have been convolved with the impulse response of the system,

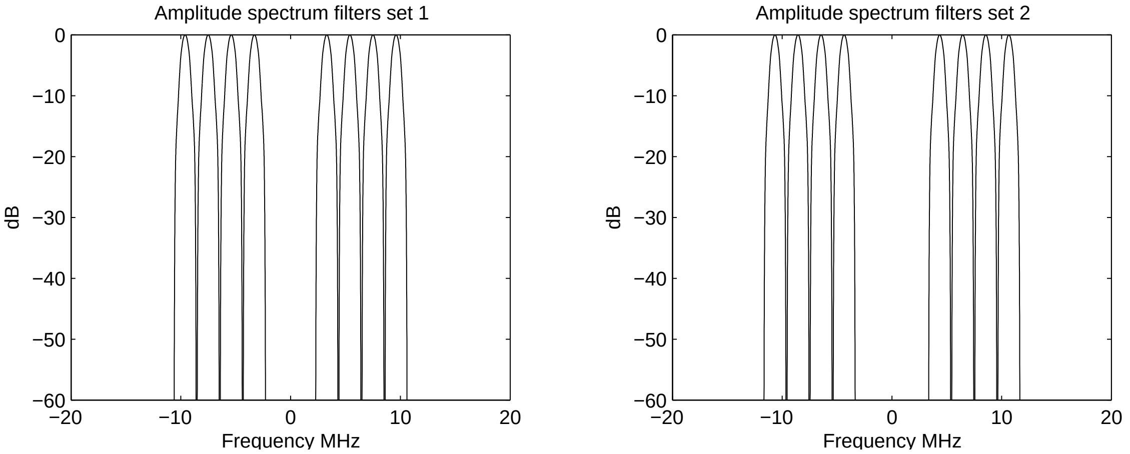

Figure 2. The amplitude spectrum of the filters after the amplitude shaping filters have been applied.

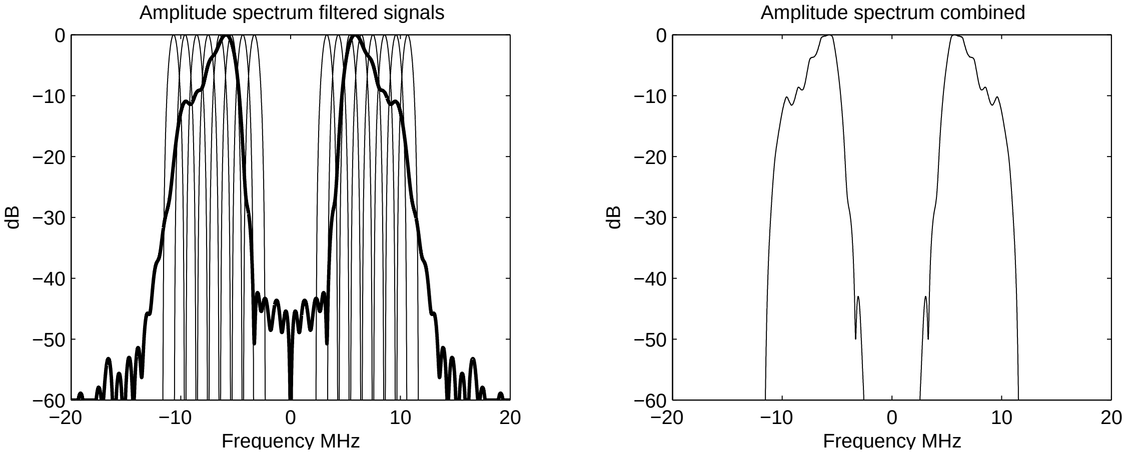

Figure 3. The figure on the left shows both sets of filtered signals (solid lines), the solid thick line represents the transfer function of the transducer and the measurement system. The figure to the right shows the result when the signals have been transmitted, filtered and combined to synthesize a broadband spectrum.

summed to emulate simultaneous transmission, then filtered and finally combined to synthesize a broadband spectrum. The time response corresponding to the spectrum given in the right figure in Fig. 3 is given in Fig. 4 (the speed of sound was assumed to be 1540 m/s).

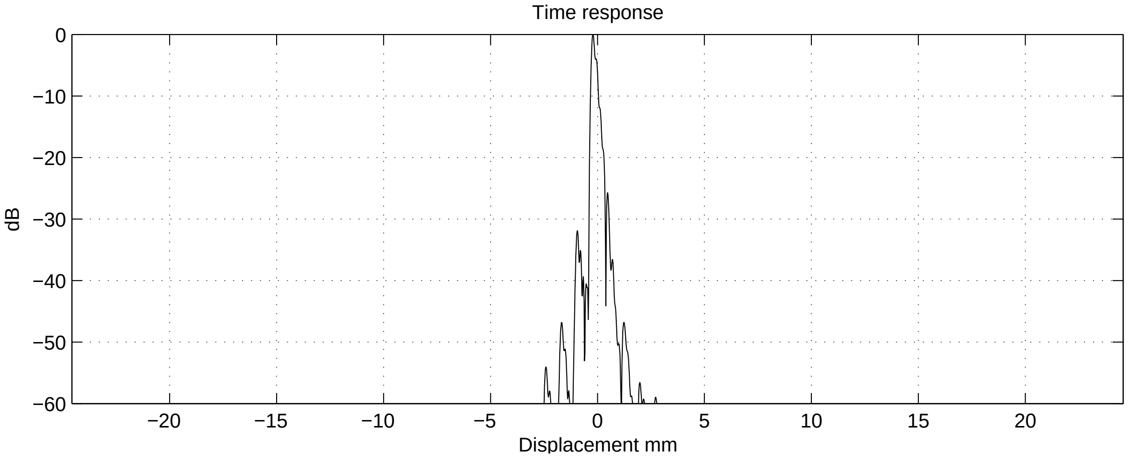

Figure 4. The time response resulting from the convolution between the excitation waveforms and the system impulse response

4. GAIN IN SIGNAL-TO-NOISE-RATIO

The increase in (peak) signal-to-noise-ratio is directly proportional to the transmitted energy. Naturally, the increase in SNR will be dependent on the number of active transmitters and the energy of the transmitted waveforms. Based on the previous findings[15] the expected increase in SNR is (in dB)

$$G = 10\log_{10}\Big(K\frac{E_{freq.div.}}{E_{ref}}\Big), \tag{8}$$

where K denotes the number of active transmitters in every transmission, $E_{freq.div.}$ is the energy of the transmitted waveforms used for the frequency division approach and E_{ref} is the energy of the waveform transmitted for the reference setup using a standard sequential STA firing scheme. In this paper the quantity in (8) will be ≈6.49 dB when compared to the setup using the chirp excitation and consecutive excitation of the transmitters.

5. BEAMFORMING

This section describes the beamforming, which has been applied to properly focus the data. When the data from one specific transmitter are available, either by applying the frequency division method and filtering out the data from a specific transmitter, or using only one transmitter at a time, it is possible to exactly determine where on the aperture the acoustic wave was transmitted, and where it was received. This allows the synthetic aperture focusing technique described in[2] to be applied.

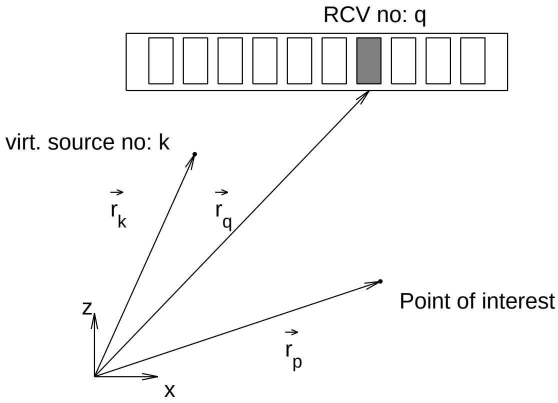

Figure 5. Principles of synthetic aperture focusing for a point p for the k:th transmitter and the q:th receiver.

Since the system has access to defocused transmissions from all transmitters on the aperture, it is possible to focus in any arbitrarily chosen point of interest. The amplitude in a point p in the image is given by

$$H(\vec{r}_p) = \sum_{k=1}^{K}\sum_{q=1}^{Q} g_q r_{qk}(t_{pqk}), \tag{9}$$

where g_q is a weighting function (apodization) over the receiving aperture, and $r_{qk}(t)$ is the filtered output on the q:th receiver originating from the k:th transmitter. Here, t_{pqk} is the time corresponding to the geometrical travel distance from the k:th transmitter to the point p and back to the q:th receiver

$$t_{pqk} = \frac{||\vec{r}_p - \vec{r}_k|| + ||\vec{r}_q - \vec{r}_p||}{c}, \tag{10}$$

where c is the speed of sound, and $\vec{r}_p - \vec{r}_k$ is the vector from the transmitter to the point p, and $\vec{r}_q - \vec{r}_p$ is the vector from the point p to the receiver as indicated in Fig. 5. Summing contributions from all transmissions for all receiving elements then gives both dynamic transmit and receive focusing.

6. EXPERIMENTAL RESULTS

In this Section the experiments which were carried out to verify the method will be described. In Section 6.1 the experimental system will be described along with the different experimental setups. In Section 6.2 the parameters associated with the reference experiments will be discussed and in 6.3 the setup for the proposed method will be explained. In Section 6.4 the (peak) signal-to-noise ratio is measured.

6.1. Measurement setup

The experimental ultrasound scanner RASMUS[16] was used for the experiments. The system has 128 individually programmable transmit channels, which can send arbitrarily shaped waveforms with a precision of 12 bits at a sampling rate of 40 MHz. The system has access to 64 receive channels simultaneously, but by means of 2-to-1 multiplexing 128 receiving transducer elements can be accessed. A BK8804 transducer was used for both the reference experiments and the experiments concerning the proposed method. Two phantoms were tested. The first phantom is a wire phantom in a water bath. The wire is positioned at a depth of 42 mm. The second phantom is a tissue mimicking phantom from Dansk Fantomservice consisting of 94 ml glycerol (85%), 100 ml rodalon (5%) and 806 ml distilled water with metal wires inside. The attenuation is 0.5 dB/[MHz·cm].

6.2. Reference experiment

The reference experiment was done by exciting one transmitter at a time, filtering the received signals and beamforming the echoes using the approach described in Section 5. A transmitter denotes a virtual source which consisted of 16 neighboring transducer elements. The elements were focused 5 mm in front of the transducer surface. The transmitters were excited consecutively using transducer element 1-16 in the first transmission, element 2-17 in the second transmission and so on. This means that there will be λ spacing also between the virtual sources. In total 112 transmissions were made. The excitation waveform was a 20 μs chirp with a center frequency of 7 MHz. The bandwidth was 100% relative to the center frequency. The excitation waveform was tapered using a Tukey window with 10% tapering. The compression filter was the time reversed excitation waveform with a temporal Chebychev window with 70 dB relative sidelobe attenuation. The temporal weighting on the filter was applied to reduce temporal sidelobes and increase axial contrast.[11] The experimental results for the reference experiment is given for the water phantom in the three left plots in Fig. 7, where the dynamic range for the B-mode image is 45 dB and 60 dB for the axial and lateral projections. The axial and lateral projections are also given as the dotted lines in Fig. 8, where it is compared to the proposed method using the frequency division approach. The result for the tissue mimicking phantom can be seen in Fig. 9 where a penetration depth of 80 mm is attained. The axial and lateral resolution at full width half maximum (FWHM) in the tissue mimicking phantom is given as a function of depth in Fig. 10 where it is compared to the frequency division approach.

6.3. Frequency Division

The excitation waveforms and the separation filters for the frequency division approach are specified in Sections 2 and 3, respectively. Since four transmitters were active at a time, eight waveforms were generated. Each transmitter consisted of 16 transducer elements focused 5 mm in front of the transducer. In total 64 elements were active in every transmission. Since eight transmissions were made for every set of transmitters, only half of the virtual sources could be used compared to the setup in Section 6.2. The virtual array consisted of virtual sources with twice the inter-source spacing compared to the reference setup. The reason for this was to make the same number of transmissions for both setups, to make a fair comparison concerning the penetration depth. The active elements for the different transmissions can be seen in Table 2. The excitation waveform with center frequency 7.5 MHz and the corresponding separation filter are given in Fig. 6. The result for the water phantom can be seen in the three right plots in Fig. 7 where the dynamic range for the B-mode image is 45 dB and 60 dB for the axial and lateral projections. The solid lines in Fig. 8 represents the axial and lateral projections compared to the reference experiment (dotted line). It can be seen that the axial sidelobe level is ~ -40 dB, compared to the reference experiment where the sidelobe level is ~ -45 dB. The lateral plot shows a slight advantage to the reference method in terms of lateral contrast. This is, however, expected since the frequency division approach

virt. source no	1	2	3	4
XMT no				
1-8	1-16	29-44	58-73	86-101
9-16	3-18	31-46	60-75	88-103
⋮	⋮	⋮	⋮	⋮
105-112	27-42	55-70	84-99	112-127

Table 2. The transducer elements used for the different transmitters in the different transmissions.

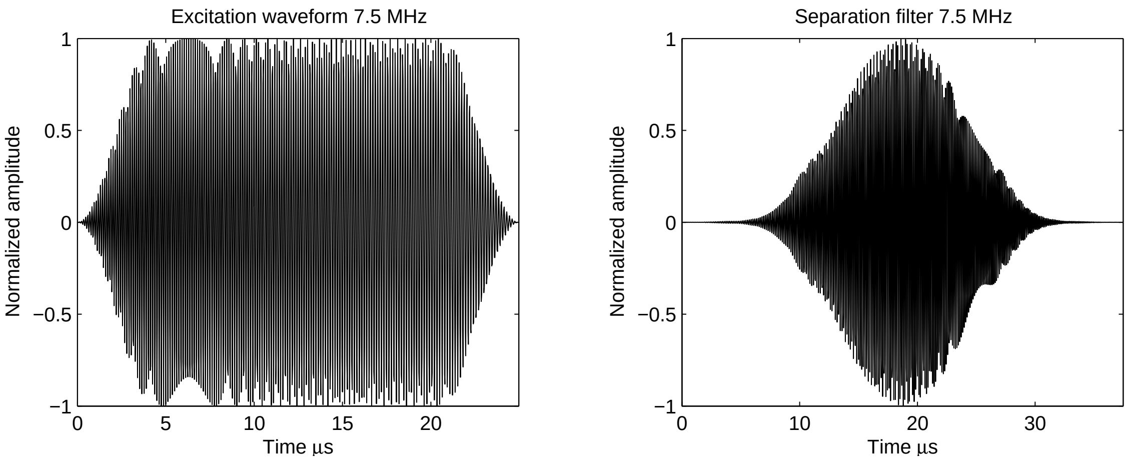

Figure 6. One of the excitation waveforms and the corresponding separation filter used in frequency division approach. The excitation waveform has a center frequency of 7.5 MHz and a bandwidth of 2 MHz. The duration of the excitation waveform is 25 μs. A Tukey window with 35% tapering was applied. The separation filter was the corresponding matched filtered convolved with the linear phase filter specified in (7).

operates at half the spatial sampling rate of the virtual array. The tissue mimicking phantom exhibits a larger penetration depth for the frequency division approach compared to the reference. The penetration depth is at least 100 mm, which is an increase of 20 mm. This corresponds to an increase in SNR of ∼7 dB. In Fig. 10 the axial and lateral resolution at FWHM can be seen as a function of depth compared to the reference experiment. It should be noted that the axial resolution is improved for all depths of the image, whereas the lateral resolution is approximately the same for both methods.

6.4. Peak signal to noise ratio

The gain in SNR was also measured. The experiments on the tissue mimicking phantom were the basis for the signal part of the beamformed images. The noise part of the images was generated by creating a noise field in Matlab for every set of received echoes in the experiments. The noise fields were then filtered and beamformed in exactly the same way as the echoes from the experiments. The SNR was evaluated at the positions where the metal wires occurred. The filtered and beamformed noise variance was estimated by choosing an area of 3mm×4mm around the position of the wire in the corresponding noise image

$$\hat{\sigma}^2(n_x, n_y) = \frac{1}{N_x N_y} \sum_{i=n_x}^{n_x+N_x} \sum_{j=n_y}^{n_y+N_y} n^2(i - \frac{N_x}{2}, j - \frac{N_y}{2}) \tag{11}$$

where (n_x, n_y) denotes the wire position in samples, $N_x \times N_y$ the area over which the variance should be estimated in samples and $n(i, j)$ the filtered and beamformed noise image. The SNR is then estimated as

$$SNR(n_x, n_y) = \frac{|s(n_x, n_y)|^2}{\hat{\sigma}^2(n_x, n_y)}, \tag{12}$$

where $s(n_x, n_y)$ is the amplitude in the wire phantom at the position of the wire. The gain in SNR for the proposed method was then calculated by computing the ratio between the SNR for the frequency division approach and the SNR for the approach using a chirp excitation. The gain (in dB) is then

$$G = 10 \log_{10}\Big(\frac{SNR_{freq.div.}}{SNR_{chirp}}\Big) \tag{13}$$

The resulting plot can be seen in Fig. 11 were the theoretical gain as a function of depth as given in Section 4 is shown as the dashed line and the measured gain is given as the solid line. The improvement in SNR in Fig. 11 also explains the improved penetration depth.

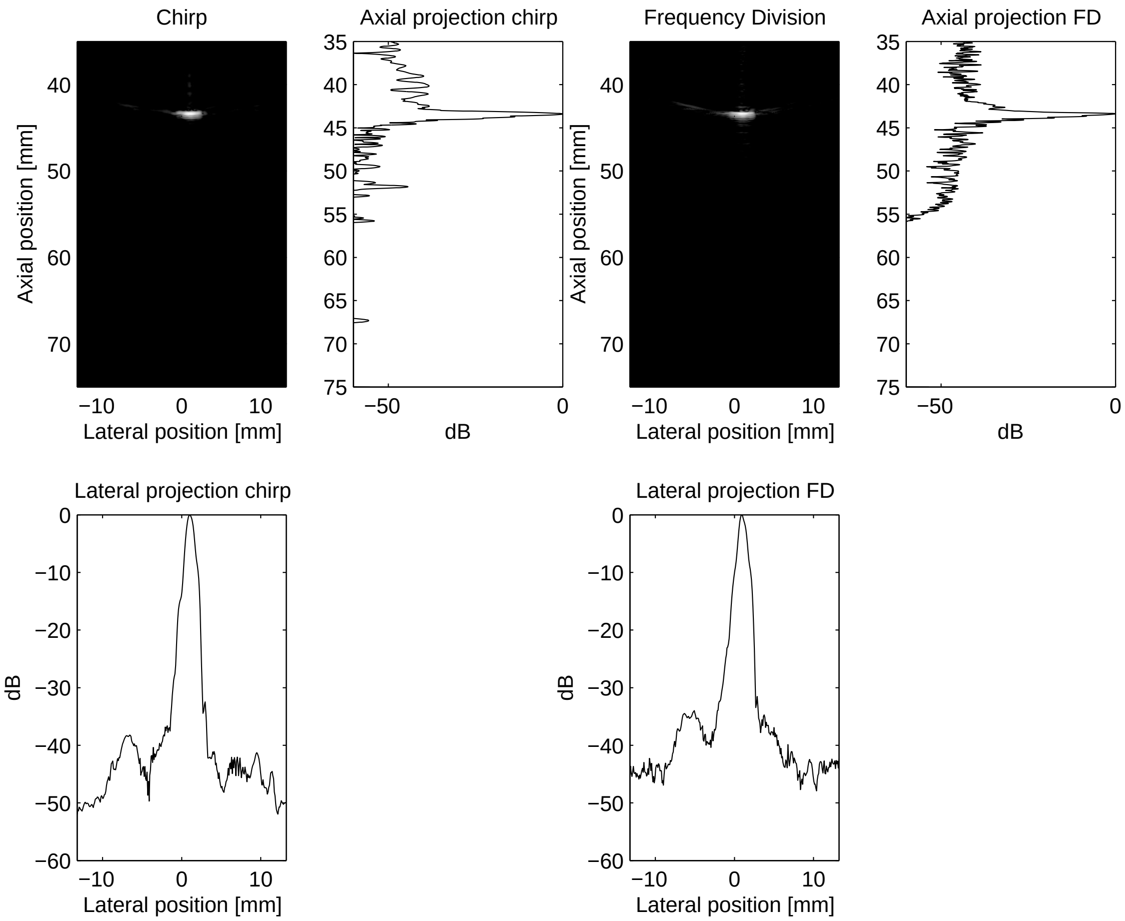

Figure 7. The PSF in the water phantom. The figure on the left shows the reference experiment whereas the figure on the right shows the PSF for the frequency division approach. The axial sidelobe level is ∼5 dB worse in the frequency division approach, resulting in slightly poorer axial contrast.

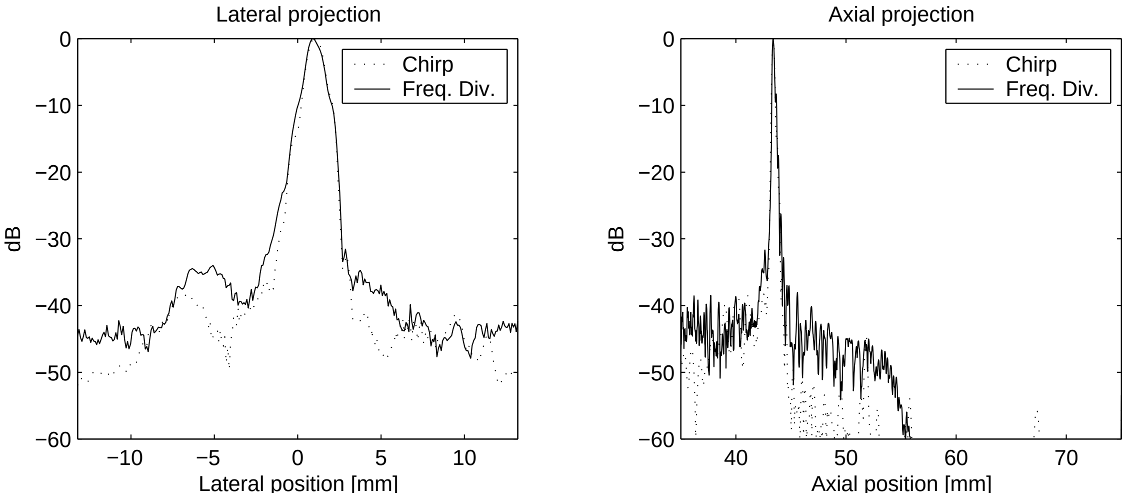

Figure 8. The lateral and axial projections of the PSFs in Fig. 7. The frequency division approach exhibits somewhat poorer axial contrast with axial sidelobe level of ∼ -40 dB, whereas the reference experiment has an axial sidelobe level of ∼ -45 dB. The lateral contrast is also somewhat poorer for the frequency division approach.

7. CONCLUSION

A new method for spatio-temporal encoding based on previous findings[15] has been proposed. The method has the advantage of providing means for spatial (and temporal) encoding where the

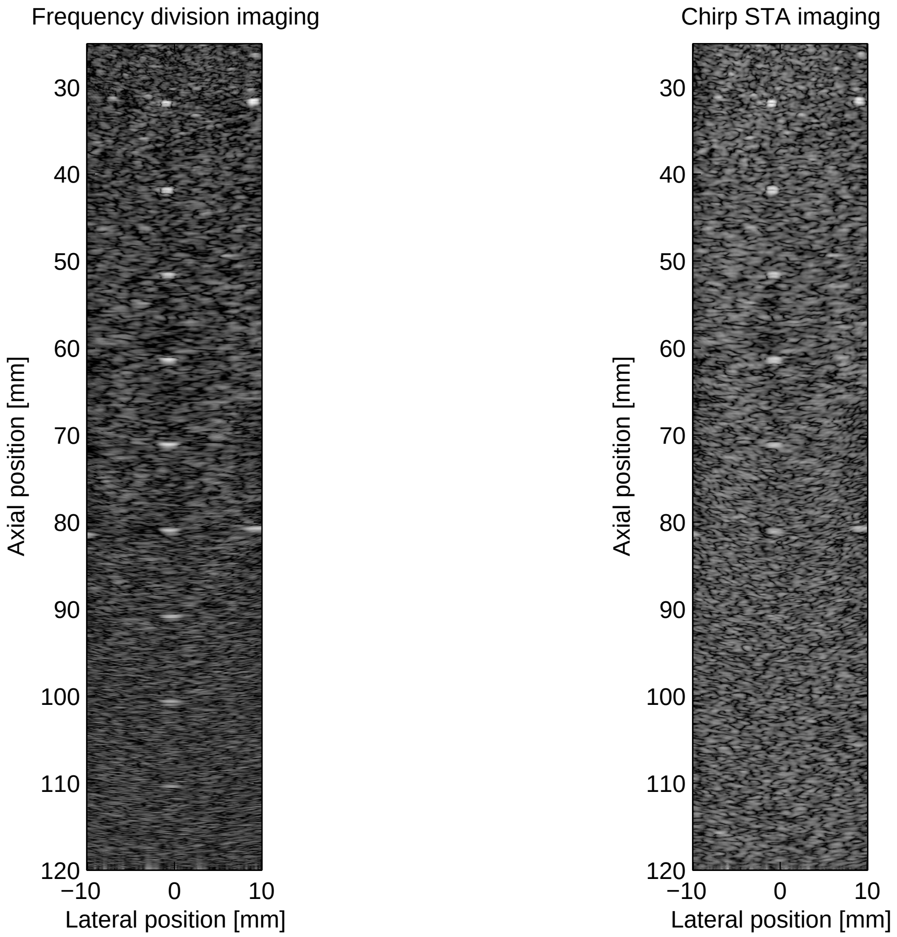
Frequency division imaging
Chirp STA imaging
Axial position [mm]
Lateral position [mm]
30
40
50
60
70
80
90
100
110
120
−10
0
10

Figure 9. The result of the experiments on the tissue mimicking phantom. The dynamic range is 40 dB. The figure on the left shows the output of the frequency division approach. The figure to the right is generated when a conventional linear FM signal is used as excitation waveform. The improvement in penetration depth is approximately 20 mm for the frequency division approach.

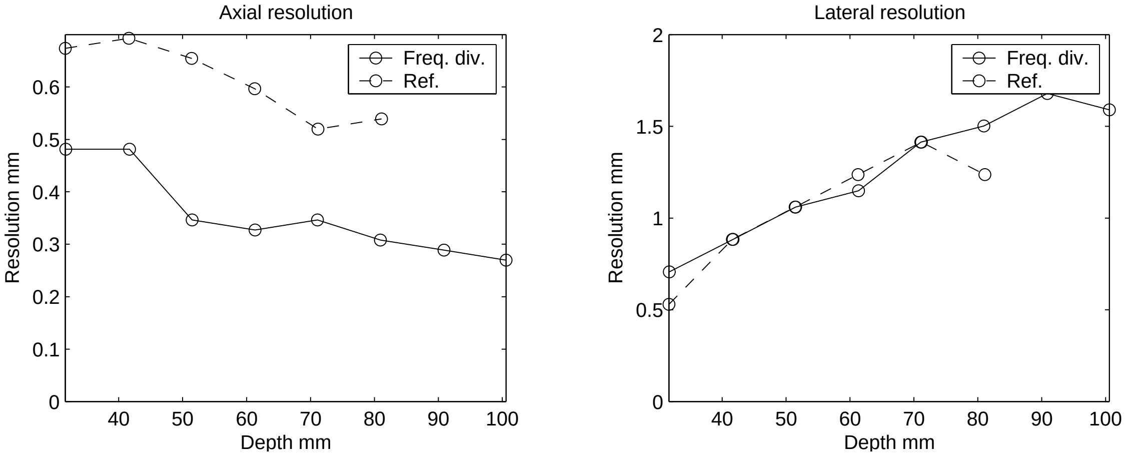

Figure 10. The FWHM resolution as a function of depth. The plot on the left is the axial resolution where the frequency division approach attains a better resolution throughout the entire medium whereas the lateral resolution is approximately the same for both methods. The resolution plots for the reference experiment terminates at 80 mm, since no wire could be distinguished beyond this point.

information can be decoded after only one transmission. Motion artifacts in the decoding step can

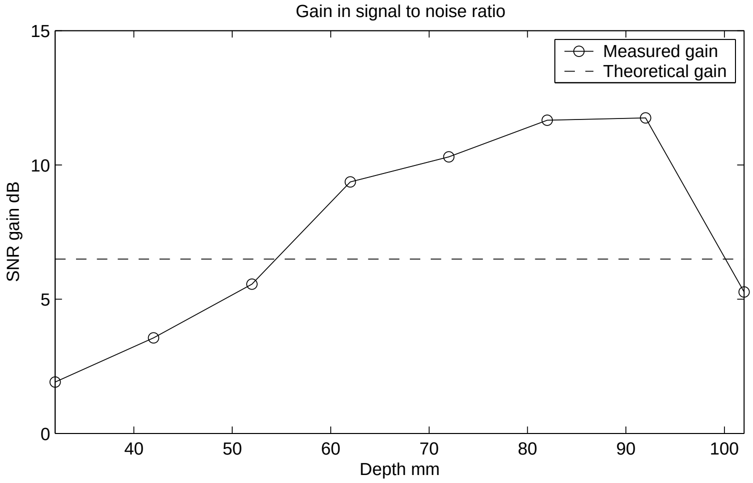

Figure 11. Gain in peak signal to noise ratio in dB. The solid line indicates the measured gain in signal to noise ratio, whereas the dashed line indicates the theoretical gain. It can be seen that an improvement of the SNR is attained for all depths of the image.

hereby be avoided. The method was compared and evaluated using a conventional STA excitation scheme with a linear FM signal as excitation waveform. The PSF was measured in a water phantom where the axial sidelobe level was found to be 5 dB higher for the frequency division approach compared to the reference PSF. A tissue mimicking phantom was used for evaluating axial and lateral resolution as a function of depth in presence of attenuation. The penetration depth could also be evaluated. It was concluded that a better axial resolution was attained for the proposed method throughout the entire phantom. The lateral resolution however, was comparable to the reference experiment. The improvement in penetration depth was approximately 20 mm, which corresponds to an increase in SNR by 7 dB. This agrees with the theoretically expected gain in SNR. The SNR was also measured, and it was concluded that the SNR was improved for all depths in the image compared to the reference setup.

ACKNOWLEDGMENTS

This work was supported by grants 9700883, 9700563 and 26-01-0178 from the Danish Science Foundation and by B-K Medical A/S, Denmark. The authors would like to thank Dr. Kim Gammelmark for providing the system transfer function.

REFERENCES

1. S. Bennett, D. K. Peterson, D. Corl, and G. S. Kino, “A real-time synthetic aperture digital acoustic imaging system,” in *Acoust. Imaging*, P. Alais and A. F. Metherell, eds., **10**, pp. 669–692, 1982.
2. S. I. Nikolov, *Synthetic aperture tissue and flow ultrasound imaging.* PhD thesis, Ørsted•DTU, Technical University of Denmark, 2800, Lyngby, Denmark, 2001.
3. M. O’Donnell and L. J. Thomas, “Efficient synthetic aperture imaging from a circular aperture with possible application to catheter-based imaging,” *IEEE Trans. Ultrason., Ferroelec., Freq. Contr.* **39**, pp. 366–380, 1992.
4. M. Karaman, P. C. Li, and M. O’Donnell, “Synthetic aperture imaging for small scale systems,” *IEEE Trans. Ultrason., Ferroelec., Freq. Contr.* **42**, pp. 429–442, 1995.
5. C. Passmann and H. Ermert, “A 100-MHz ultrasound imaging system for dermatologic and ophthalmologic diagnostics,” *IEEE Trans. Ultrason., Ferroelec., Freq. Contr.* **43**, pp. 545–552, 1996.
6. C. H. Frazier and W. D. O’Brien, “Synthetic aperture techniques with a virtual source element,” *IEEE Trans. Ultrason., Ferroelec., Freq. Contr.* **45**, pp. 196–207, 1998.

7. M. O'Donnell, "Coded excitation system for improving the penetration of real-time phased-array imaging systems," *IEEE Trans. Ultrason., Ferroelec., Freq. Contr.* **39**, pp. 341–351, 1992.
8. T. X. Misaridis, K. Gammelmark, C. H. Jørgensen, N. Lindberg, A. H. Thomsen, M. H. Pedersen, and J. A. Jensen, "Potential of coded excitation in medical ultrasound imaging," *Ultrasonics* **38**, pp. 183–189, 2000.
9. T. X. Misaridis, M. H. Pedersen, and J. A. Jensen, "Clinical use and evaluation of coded excitation in B-mode images," in *Proc. IEEE Ultrason. Symp.*, **2**, pp. 1689–1693, 2000.
10. T. X. Misaridis and J. A. Jensen, "An effective coded excitation scheme based on a predistorted FM signal and an optimized digital filter," in *Proc. IEEE Ultrason. Symp.*, **2**, pp. 1589–1593, 1999.
11. T. Misaridis, *Ultrasound imaging using coded signals.* PhD thesis, Ørsted•DTU, Technical University of Denmark, Lyngby, Denmark, 2001.
12. R. Y. Chiao, L. J. Thomas, and S. D. Silverstein, "Sparse array imaging with spatially-encoded transmits," in *Proc. IEEE Ultrason. Symp.*, pp. 1679–1682, 1997.
13. T. Misaridis and J. A. Jensen, "Space-time encoding for high frame rate ultrasound imaging," *Ultrasonics* **40**, pp. 593–597, 2002.
14. R. Y. Chiao and L. J. Thomas, "Synthetic transmit aperture using orthogonal golay coded excitation," in *Proc. IEEE Ultrason. Symp.*, pp. 1469–1472, 2000.
15. F. Gran and J. A. Jensen, "Multi element synthetic aperture transmission using a frequency division approach," in *Proc. IEEE Ultrason. Symp.*, pp. 1942–1946, 2003.
16. J. A. Jensen, O. Holm, L. J. Jensen, H. Bendsen, H. M. Pedersen, K. Salomonsen, J. Hansen, and S. Nikolov, "Experimental ultrasound system for real-time synthetic imaging," in *Proc. IEEE Ultrason. Symp.*, **2**, pp. 1595–1599, 1999.

5.10 Journal paper: Directional velocity estimation using a spatio-temporal encoding technique based on frequency division for synthetic transmit aperture ultrasound

Submitted to IEEE Transactions on Ultrasonics, Ferroelectrics and Frequency control, June 2005

Directional velocity estimation using a spatio-temporal encoding technique based on frequency division for synthetic transmit aperture ultrasound

Fredrik Gran and Jørgen Arendt Jensen, *Senior Member, IEEE*

Abstract

This paper investigates the possibility of flow estimation using spatio-temporal encoding of the transmissions in synthetic transmit aperture imaging (STA). The spatial encoding is based on a frequency division approach. In STA, a major disadvantage is that only a single transmitter (denoting single transducer element or a virtual source) is used in every transmission.

The transmitted acoustic energy will be low compared to a conventional focused transmission where a large part of the aperture is used. By using several transmitters simultaneously the transmitted energy can be increased. However, to focus the data properly, the information originating from the different transmitters must be separated. To do so, the pass band of the transducer is divided into a number of sub-bands with disjoint spectral support. At every transmission, each transmitter is assigned one of the sub-bands. In receive, the signals are separated using a simple filtering operation. To attain high axial resolution, broad-band spectra must be synthesized for each of the transmitters. By multiplexing the different waveforms on different transmitters over a number of transmissions this can be accomplished. To further increase the transmitted energy, the waveforms are designed as linear frequency modulated signals. Therefore, the full excitation amplitude can be utilized during most of the transmission.

The method has been evaluated for blood velocity estimation for several different velocities and incident angles. The program Field II was used. A 128 element transducer with a center frequency of 7 MHz was simulated. 64 transmitting elements were used as the transmitting aperture and 128 elements were used as the receiving aperture. Four virtual sources were created in every transmission. By beamforming lines in the flow direction, directional data was extracted and correlated. Hereby, the velocity of the blood was estimated. The pulse repetition frequency was 16 kHz. Three different setups were investigated with flow angles of 45, 60 and 75 degrees with respect to the acoustic axis. Four different velocities were simulated for each angle at 0.10, 0.25, 0.50 and 1.00 m/s. The mean relative bias with respect to the peak flow for the three angles was less than 2% , 2% and 4%, respectively.

I. INTRODUCTION

Synthetic transmit aperture (STA) can be used for velocity estimation in ultrasound imaging [1–5]. The method is based on correlating data acquired with exactly the same emission sequence. To synthesize a large transmit aperture, several transmissions have to be carried out from different locations on the transmitting aperture. Beamforming the received signals from one transmission results in a low resolution image with poor resolution and contrast. The synthesis of a larger transmit aperture is achieved by summing data from different transmissions yielding a high resolution image. This improves the resolution and contrast, and therefore also the image quality.

If the object under investigation is moving very rapidly only a small number of transmissions is affordable. Having a large number of transmissions to generate a high resolution image, would

Fredrik Gran (fg@oersted.dtu.dk) and Jørgen A. Jensen (jaj@oersted.dtu.dk) are both from the Center for Fast Ultrasound Imaging, Ørsted•DTU, Building 348, Technical University of Denmark, 2800 Kgs. Lyngby, Denmark

yield poor performance of the velocity estimator, since the movement results in a smearing of the point spread function (PSF). When the number of transmissions per data set is small, the signal-to-noise-ratio (SNR) will, however, drop. Virtual sources have been suggested to partly compensate for this [6–9]. Temporal encoding in form of a linear frequency modulated signal has also been suggested to increase the SNR [10–17].

Spatial encoding has previously been suggested as means of increasing SNR for STA when the number of transmissions per high resolution image is low. Chiao et. al. [18] suggested that a Hadamard space-time encoding scheme could be used to encode the transmitters[1]. The method relies on exciting the transmitters simultaneously with the same excitation waveforms. The encoding is based on pre-multiplying the waveform on each transmitter by a row (or column) of the Hadamard matrix of the same dimension as the number of transmitters (2^k). The next transmission is premultiplied by the next row, and this procedure is repeated until all rows have been covered. Under the assumption of stationarity the echoes originating from the different transmitters can be extracted by summing and subtracting the received signals from the different transmissions. The decoding is therefore dependent on data being stationary from transmission to transmission for the decoding to work properly. In flow estimation the target is not stationary, and it has been argued that this would degrade the method making it unsuitable for flow imaging.

Chiao and Thomas suggested in [19] to use complementary codes (orthogonal Golay sequences) to encode the transmitters. Here the transmitters are assigned a specific binary code sequence for each transmitter, and correlation receivers are applied to separate the signals. From one transmission the inter-code cross correlation is not zero, but by summing the result from different transmission utilizing different code sequences, the inter-code cross-correlation can be made to vanish. Using the same procedure, perfect auto-correlation properties can be achieved for the combined auto-correlation functions. This approach also assumes stationarity, since data from different transmissions have to be combined.

In this paper a method for spatial encoding developed in [20–22] is evaluated for blood flow estimation as suggested in [23]. To focus the data properly, the information originating from the different transmitters must be separated. To do so, the pass band of the transducer is divided into a number of sub-bands with disjoint spectral support. At every transmission, each transmitter is assigned one of the sub-bands. In receive, the signals are separated using a simple filtering operation. The decoding can be performed instantaneously at the receiver making the decoding process insensitive to motion. To attain high axial resolution, broad-band spectra must be synthesized for each of the transmitters. This can be accomplished by multiplexing the different waveforms on different transmitters over a number of transmissions. While the decoding is insensitive to motion, the synthesis of the broadband spectra may, however, exhibit motion artifacts as further detailed in Section VI. To further increase the transmitted energy, the waveforms are designed as linear frequency modulated signals.

The paper is organized as follows: in Section II the spatial coding is described, in Section III the beamforming which was applied to create directional flow data is explained. In Section IV the estimation procedure for finding the velocity of the blood is given. The simulation setup is described in Section V, and in Section VI the effects of motion on the broadband synthesis is analyzed. In VII the simulation results are presented and discussed. Concluding remarks are given in Section VIII

II. SPATIAL ENCODING USING FREQUENCY DIVISION

Spatial encoding using frequency division has been shown to improve the SNR for stationary objects (tissue mimicking phantoms) [21,22]. To separate the signals originating from the different transmitters, narrow-band signals with disjoint spectral support [2] are designed. To exploit the full excitation voltage of the system, the signals are designed as linear frequency modulated signals

---

[1] The general term transmitter will be used to represent a virtual source or a single transducer element. In [18] this was called phase center.

$$s_i(t) = b(t) \sin\left(2\pi\left[\left(f_i - \frac{B}{2}\right)t + \frac{B}{2T}t^2\right]\right),\ 0 \le t \le T, \tag{1}$$

where f_i is the center frequency of the i:th waveform, B is the bandwidth, T is the duration of the waveform and $b(t)$ is a temporal weighting applied to the waveform. The compression and separation filters for each individual waveform are given by

$$m_i(t) = s_i(-t) \star h_i(t), \tag{2}$$

where $\star$ denotes the convolution operator and $h_i(t)$ an additional filter applied to shape the synthesized broadband spectrum. Consider the filtered i:th waveform

$$r_i(t) = s_i(t) \star m_i(t) = s_i(t) \star s_i(-t) \star h_i(t), \tag{3}$$

with the Fourier transform

$$\mathcal{F}\left\{r_i(t)\right\} = |S_i(f)|^2 H_i(f), \tag{4}$$

where $S_i(f)$ is the Fourier transform of $s_i(t)$ and $H_i(f)$ is the Fourier transform of $h_i(t)$. The spectrum $H_i(f)$ is chosen such that the combined spectrum for the different signals produce a smooth broadband spectrum. In this paper, $H_i(f)$ was chosen to be

$$H_i(f) = \begin{cases} \frac{1}{2}\left(1 + \cos(2\pi\frac{f-f_i}{B})\right) & |f - f_i| \le \frac{B}{2} \\ 0 & \text{otherwise.} \end{cases} \tag{5}$$

as these spectra combined, $\sum_i H_i(f)$ give a broadband spectrum with a smooth pass-band. The filters $h_i(t)$ were designed as linear-phase FIR filters where the filter coefficients were optimized using least-squares error minimization [3]. In this paper, eight waveforms were generated. The duration was $25\mu s$, the bandwidth 2 MHz and the function $b(t)$ was chosen to be a Tukey-window with 35% tapering. The Tukey window is defined as

$$b(t) = \begin{cases} \frac{1}{2}\left(1 + \cos\left[2\pi\frac{t-\frac{\alpha}{2}T}{\alpha T}\right]\right) & 0 \le t \le \frac{\alpha T}{2} \\ 1 & \frac{\alpha T}{2} \le t \le (1-\frac{\alpha}{2})T \\ \frac{1}{2}\left(1 + \cos\left[2\pi\frac{t-(1-\frac{\alpha}{2})T}{\alpha T}\right]\right) & (1-\frac{\alpha}{2})T \le t \le T \end{cases} \tag{6}$$

where T is the duration of the window and $\alpha = 0.35$ is the amount of tapering applied. The center frequencies can be seen in Table I. To reduce inter-signal interference caused by overlapping frequencies, the waveforms were grouped in two sets. The first signal set consisted of the signals with odd index, and the second set of the signals with even index. This makes it possible to encode four transmitters simultaneously, but it requires eight transmissions before a broadband spectrum can be synthesized for each transmitter. The two signal-sets can be seen in Fig. 1. The filters $h_i(t)$ were specified to be FIR filters with a duration of $18.75\mu s$. The synthesized broadband time signal for one transmitter can be seen in Fig. 2. The majority of the axial sidelobes are below -60 dB, with exception for the near sidelobes which are at ~-50 dB. This is acceptable in a STA system used for flow estimation, since the short transmission sequence used to synthesize the transmitting aperture will cause the lateral sidelobes to have a level of ~-40 dB.

---

[2] This is only an approximation. The waveforms will in practice not have disjoint spectral support, since this would require that infinite code sequences were used.

[3] Using the function `firls` in Matlab, ©1994-2005 by The MathWorks, Inc., 24 Prime Park Way, Natwick, MA 01760-1500

i	f_i [MHz]
1	3.3000
2	4.3512
3	5.4024
4	6.4536
5	7.5048
6	8.5560
7	9.6072
8	10.6584

TABLE I
THE CENTER FREQUENCIES OF THE DIFFERENT WAVEFORMS.

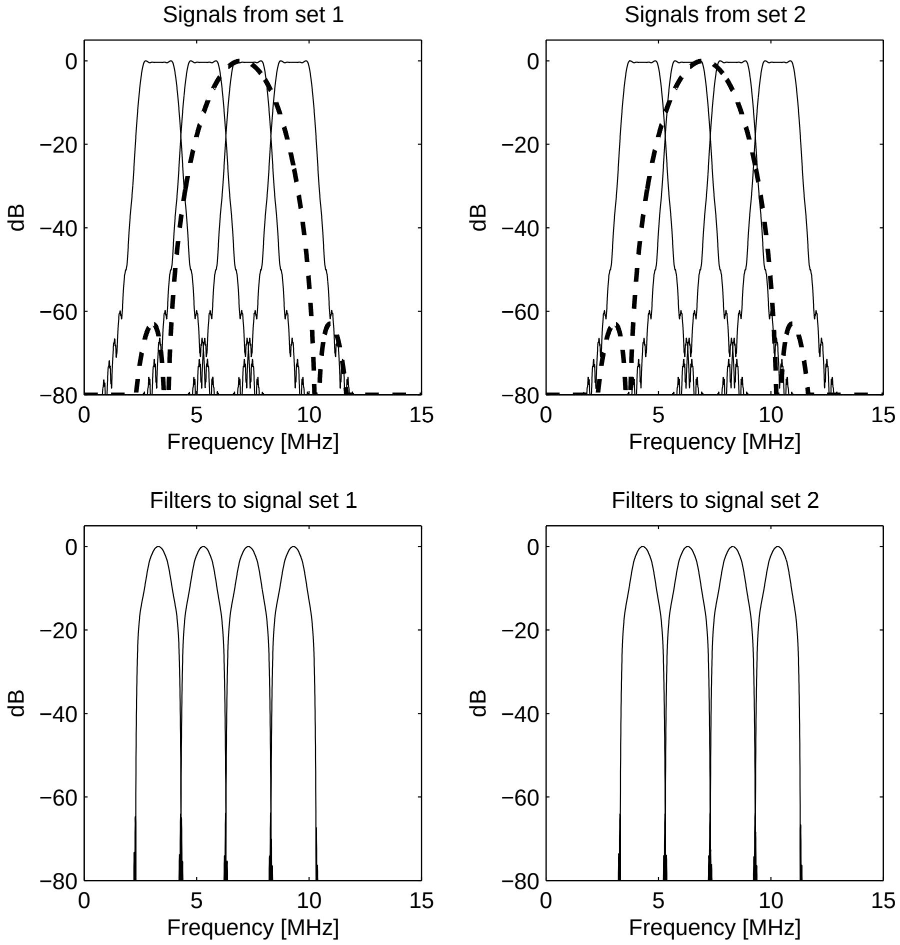

Fig. 1. The spectra for the two sets of excitation signals can be seen as the top figure. The corresponding separation filters are given as the two bottom figures. Note how the FIR filters $h_i(t)$ effect the frequency characteristic of the matched filters. The FIR filters reduce the inter-transmitter interference and shapes the filtered spectrum of each transmitter.

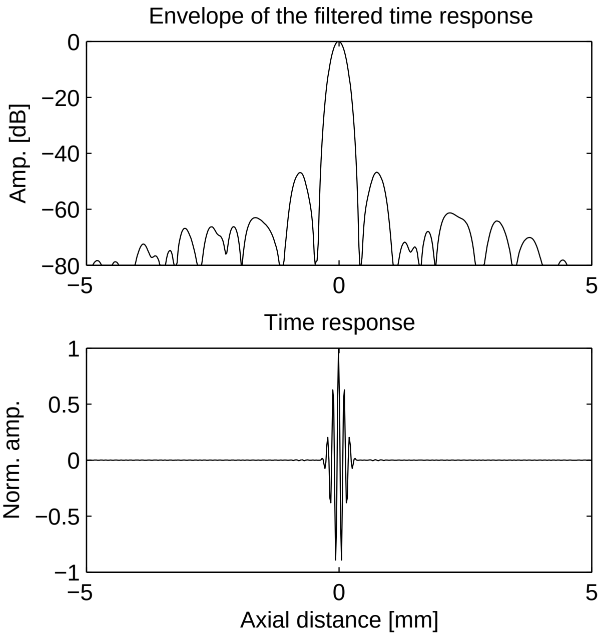

Fig. 2. The time response of a synthesized broadband pulse. After eight transmissions, broadband pulses can be synthesized for each transmitter. The axial sidelobe level is below -60 dB except for the near sidelobes which have a level of ∼-50 dB. The top figure displays the log compressed envelope of the time signal, whereas the bottom figure displays the actual time response on a linear scale.

III. BEAMFORMING

This section describes the beamforming which has been applied to properly focus the data. When a broadband excitation signal has been synthesized for every transmitter on the aperture, it is possible to beamform the synthesized broadband data as if only one transmitter was active in every transmission. This allows the synthetic aperture focusing technique described in [24] to be applied.

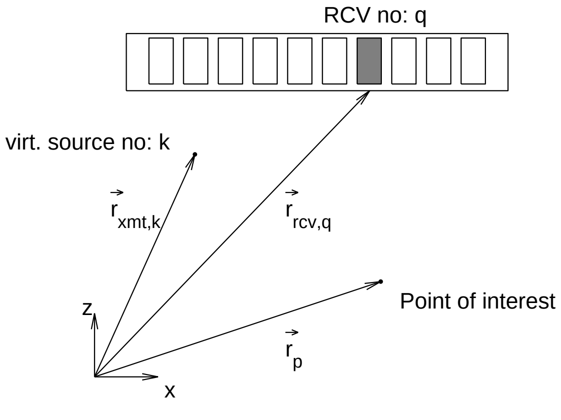

Fig. 3. Principles of synthetic aperture focusing for a point $\vec{r_p}$ for the k:th transmitter and the q:th receiver.

Since the system has access to defocused transmissions from all transmitters on the aperture, it is possible to focus the acoustic energy on any arbitrarily chosen point of interest. The amplitude in a point $\vec{r}_p$ in the image is given by

$$\mathbf{H}(\vec{r}_p) = \sum_{k=1}^{K} \sum_{q=1}^{Q} a_q(t_{pkq}) r_{kq}(t_{pkq}), \tag{7}$$

where $a_q(t_{pkq})$ is a weighting function (apodization) over the receiving aperture which ideally would be changing with spatial coordinates to keep a constant F-number. However, in this paper the apodization is constant over space and is chosen as a Hanning window over all 128 receiving elements. The time signal $r_{kq}(t)$ is the received synthesized broadband echo on the q:th receiver, originating from the k:th transmitter. Here t_{pkq} is the time corresponding to the geometrical travel distance from the k:th transmitter to the point $\vec{r}_p$ and back to the q:th receiver:

$$t_{pkq} = \frac{||\vec{r}_p - \vec{r}_{xmt,k}|| + ||\vec{r}_{rcv,q} - \vec{r}_p||}{c}, \tag{8}$$

where c is the speed of sound, and $\vec{r}_p - \vec{r}_{xmt,k}$ is the vector from the transmitter to the point $\vec{r}_p$, and $\vec{r}_{rcv,q} - \vec{r}_p$ is the vector from the point $\vec{r}_p$ to the receiver as indicated in Fig. 3. The beamformed data resulting from one transmission is denoted *low-resolution* image, and the result of summing a number of low-resolution images to synthesize a larger aperture results in a *high-resolution* image. Summing contributions from all transmissions for all receiving elements gives both dynamic transmit and receive focusing.

To obtain directional data suitable for finding the velocity of the moving particles, lines were beamformed in the direction of the flow [25, 26]. The principle can be seen in Fig. 5. Correlating successive lines, the spatial shift between the data can be found and, thus, the velocity. The spatial distance between data points in the directional data was chosen to be $\Delta x = \lambda/10$. Moreover, it has previously been shown that automatic detection of the flow angle is possible [5,27]. Therefore, the angle of the flow was assumed to be known.

IV. VELOCITY ESTIMATOR

The velocity of the moving blood scatterers was found using a cross-correlation velocity estimator [28, 29]. No stationary signal was present, therefore stationary echo-canceling was ignored. Since four transmitters were used, eight transmissions had to be carried out before broad band spectra could be synthesized for each transmitter. The velocity was found by correlating lines which had been beamformed in the direction of the flow. To find the velocity, lines obtained using the same transmission were correlated. A line in the l:th high resolution image is denoted $h_l(n)$, and the corresponding line in the next high resolution image obtained with the same transmission sequence is denoted $h_{l+1}(n)$. The cross-correlation between the lines is

$$R(m) = \frac{1}{N} \sum_{n=0}^{N-1} h_l(n) h_{l+1}(n+m), \tag{9}$$

where N is the length of the lines in samples. The spatial shift between two high resolution lines was found by finding the peak in the cross-correlation function

$$m_{max} = \arg\max_{m} R(m). \tag{10}$$

To get a more precise result, quadratic interpolation was performed using the samples $(m_{max} - 1, m_{max}, m_{max} + 1)$. The maximum lag [4] resulting from the interpolation is given by [29, 30]

$$\begin{aligned} m_v = m_{max} - &\\ &\frac{R(m_{max}+1) - R(m_{max}-1)}{2\left(R(m_{max}+1) - 2R(m_{max}) + R(m_{max}-1)\right)} \end{aligned} \tag{11}$$

---

[4] may be fractional

The velocity was found

$$v_{max} = \frac{m_v \Delta x}{T_h}, \tag{12}$$

where Δx is the spatial distance between samples in the high resolution lines, and T_h is the time period between two successive high resolution images obtained with the same transmission sequence [5].

V. SIMULATION SETUP

The method has been evaluated using the simulation tool Field II [31, 32]. A 128 element linear array transducer was used with the parameters shown in Table III. The central 64 transducer elements were utilized as the transmitting aperture, and 128 elements were active as the receiving aperture. Four virtual sources were created [6–9, 33]. A virtual source was created by focusing 16 transducer elements 5 mm behind the face of the transducer. The purpose was to emulate a high energy virtual spherical source. The basic principle can be seen in Fig. 4. The different waveforms were multiplexed for the different transmitters over eight transmissions. The transmission sequence used for the velocity estimation can be seen in Table II.

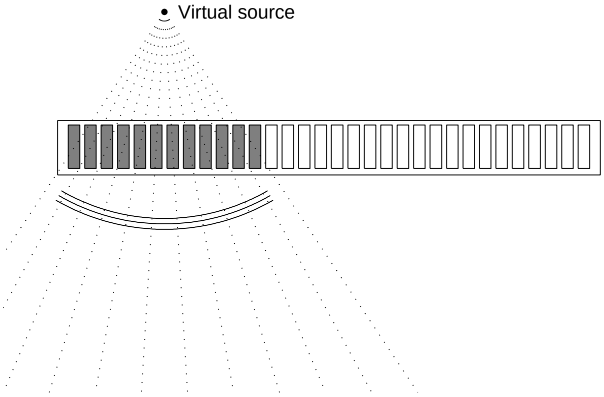

Fig. 4. The virtual source is created using 16 adjacent transducer elements. The focal point was chosen to 5 mm behind the face of the transducer (F-number 1.5). Hereby, a high energy virtual spherical wave was created.

The pulse repetition frequency was 16 kHz, and therefore 2000 high resolution images suitable for velocity estimation were created every second. The vessel was created as a cylinder with a radius of 5 mm, at a depth of 30 mm to the center of the vessel relative to the transducer. The length of the vessel was 20 mm, and enough point scatterers were positioned inside the vessel to ensure that 10 scatterers occupied a resolution cell [6]. The flow was laminar with a parabolic flow profile

$$v(r) = v_{max}\left(1 - \left(\frac{r}{R}\right)^2\right), \tag{13}$$

where v_{max} is the peak velocity, R is the radius of the vessel, and r is the location in the vessel where the velocity should be evaluated. The parameters for the simulation can be seen in Table III.

---

[5] In this paper $T_h = 8/f_{pr}$, since eight emissions were used to create a high resolution image.

[6] A resolution cell was assumed to be $\lambda \times \lambda \times \lambda$.

XMT no Em. no	1	2	3	4
1	1	3	5	7
2	2	4	6	8
3	7	1	3	5
4	8	2	4	6
5	5	7	1	3
6	6	8	2	4
7	3	5	7	1
8	4	6	8	2

TABLE II

THE TRANSMISSION SEQUENCE USED FOR THE FLOW ESTIMATION, XMT NO DENOTES THE TRANSMITTER OF INTEREST AND EM. NO THE EMISSION NUMBER.

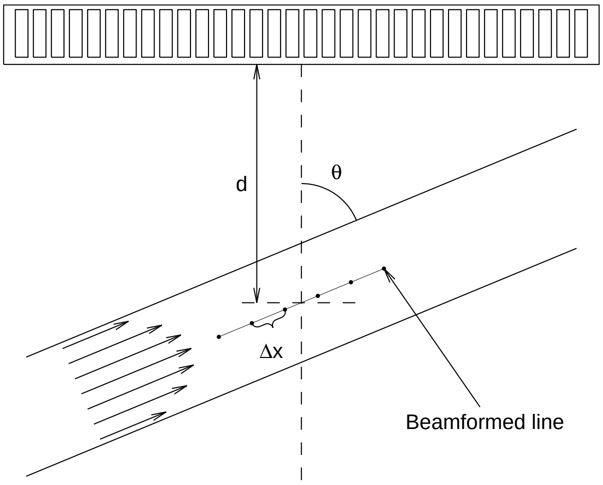

Fig. 5. The vessel is positioned at a depth d= 30 mm below the transducer. The angle of the flow with respect to the central axis of the transducer is indicated by θ. The radius of the vessel was 5 mm. To acquire directional data, points along the direction of the flow were beamformed. The direction of the flow was assumed to be known.

VI. MOTION EFFECTS BROADBAND SYNTHESIS

Section II stated that broadband spectra can be synthesized for each transmitter, as long as all frequency bands are covered for all transmitters. The synthesis will suffer from artifacts if the object under investigation is exhibiting movement during the data acquisition. This will affect the synthesized broadband pulse and therefor also the point spread function (PSF). It will also degrade the SNR compared to the maximum achievable using this method.

In this section simulations of the synthesized broadband pulse are presented, where it is possible to evaluate the degradation of the axial PSF for velocities 0.10, 0.25, 0.50 and 1.00 m/s in relation to a target which is not moving. In Fig. 6 the synthesized broadband pulse can be seen for different axial velocities. The amplitude of the synthesized pulse is decreasing and the axial resolution is degraded. Compensating for the motion can potentially restore the resolution as shown in [34].

To evaluate the SNR consider the following very simple model of the received signal

$$r(t) = p(t) \star h(t) + v(t) \tag{14}$$

Variable	Parameter	Unit
f_{pr}	16	kHz
f_0	7	MHz
λ	0.2200	mm
pitch	0.2080	mm
height	4.5	mm
No xmt elem.	64	
No rcv elem.	128	
No virt. sources	4	
Focal depth	-5	mm
Δx	1/10	λ
Line length	20	λ
Vessel radius	5	mm
Depth of vessel	30	mm

TABLE III
DIFFERENT PARAMETERS USED IN THE SIMULATION.

where $p(t)$ is the transmitted and filtered waveform given as any of the waveforms in Fig. 6, and $h(t)$ is a function representing the interaction between the wave and the interrogated tissue [7]. The function $h(t)$ is modelled as a Gaussian distributed, white process with zero mean. The variable $v(t)$ is the filtered measurement noise and is assumed to be independent of the signal. The SNR is then given as

$$SNR = \frac{E\left[\left|p(t) \star h(t)\right|^2\right]}{E\left[\left|v(t)\right|^2\right]}, \tag{15}$$

where $E\big[(\cdot)\big]$ is the expectancy value of $(\cdot)$. Now, consider the autocorrelation of $p(t) \star h(t)$

$$R_{ph}(\tau) = R_p(\tau) \star R_h(\tau) \tag{16}$$

where $R_p(\tau)$ and $R_h(\tau)$ are the autocorrelation functions of $p(t)$ and $h(t)$ respectively. By using the fact that $h(t)$ is modelled as a white Gaussian distributed process with zero mean, the autocorrelation function of $h(t)$ can be written

$$R_h(\tau) = S_h \delta(\tau), \tag{17}$$

where S_h is the power spectral density of $h(t)$. Combining (16) and (17) gives

$$R_{ph}(\tau) = S_h R_p(\tau). \tag{18}$$

The nominator in (15) is (18) evaluated at $\tau = 0$. Equation (18) evaluated at $\tau = 0$ gives

$$R_{ph}(0) = S_h R_p(0) = S_h \cdot E_p, \tag{19}$$

where E_p is the energy of $p(t)$. The decrease in SNR for a moving target with the synthesized broadband pulse having energy E_{mov}, compared to a stationary target with a synthesized broadband pulse with energy E_{stat} is (in logarithmic scale)

$$10 \log_{10}\left(\frac{E_{mov}}{E_{stat}}\right), \tag{20}$$

---

[7] This assumes that the movement is uniform over the target function and purely axial to the transmitter and the receiver of interest.

since the variance of the filtered noise is assumed to be the same for the two situations as well as the power spectral density of $h(t)$. Equation (20) is evaluated as a function of velocity for the synthesized broadband pulses in Fig. 7.

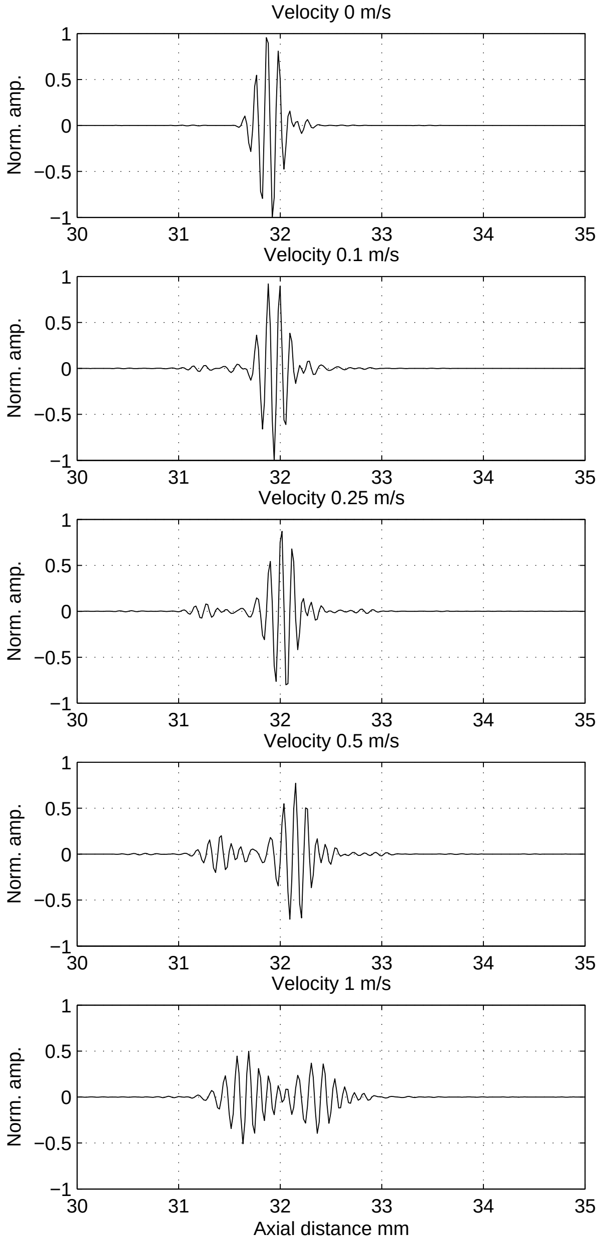

Fig. 6. The synthesized broad band pulse as a function of velocity. The target is a single point scatterer located at a depth of 30 mm on the central axis of the transducer. The synthesized pulse is valid for the second virtual source and the 64:th receiving element. The amplitude is normalized with respect to the maximum velocity of the stationary target (0 m/s).

VII. SIMULATION RESULTS

The directional lines were beamformed and extracted. Succeeding high resolution lines acquired using the same transmission sequence were correlated. To improve the estimates, ten successive estimates for the cross-correlation function were averaged, so that 80 transmissions were used to

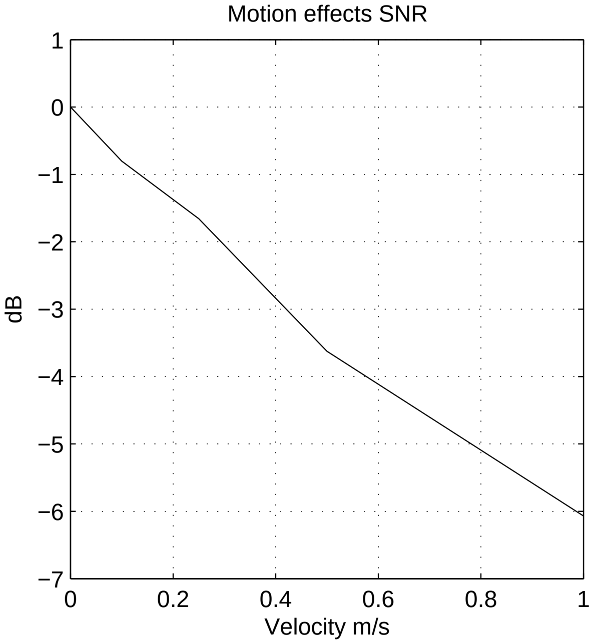

Fig. 7. The SNR as a function of velocity. The SNR is decreased by 6 dB when the target is moving with a velocity of 1 m/s.

Angle	Velocities	Unit
45°	0.10, 0.25, 0.50, 1.00	m/s
60°	0.10, 0.25, 0.50, 1.00	m/s
75°	0.10, 0.25, 0.50, 1.00	m/s

TABLE IV

THE FLOW ANGLES AND VELOCITIES INCLUDED IN THE STUDY.

generate one velocity estimate. The peak of the averaged cross correlation function was found, and thereby the velocity was estimated. Table IV shows the angles and velocities which were investigated. To evaluate performance, bias and standard deviation were calculated for the estimates of the velocity for the different simulation setups. For each setup, 22 full velocity [8] estimates were used to calculate the bias and standard deviation. The mean of the velocity estimates is given by

$$\overline{v}(z) = \frac{1}{M}\sum_{m=0}^{M-1}\widehat{v}_m(z), \tag{21}$$

where $\widehat{v}_m(z)$ is the m:th estimate for the velocity. The total number of estimates are given by M. The bias for the estimates is given by (as a function of depth)

$$b(z) = \overline{v}(z) - v(z), \tag{22}$$

where $\widehat{v}(z)$ is the estimate for the velocity at the depth z and $v(z)$ is the true velocity for this depth. The standard deviation for the estimates is given by

$$\sigma(z) = \sqrt{\frac{1}{M}\sum_{m=0}^{M-1}\Big[\widehat{v}_m(z) - \overline{v}(z)\Big]^2}. \tag{23}$$

---

[8] Each velocity estimate was based on 10 succeeding high resolution images.

The mean relative bias and the mean relative standard deviation are given by the mean bias and standard deviation relative to the peak velocity in the vessel. Mean relative bias (in percent):

$$\bar{b}_{rel} = \frac{1}{v_{max}} \left(\frac{1}{Z} \sum_{z=0}^{Z-1} b(z) \right) \cdot 100\%. \tag{24}$$

where the samples $z = 0, \ldots, Z-1$ are the samples within the vessel. Mean relative standard deviation (in percent):

$$\overline{\sigma}_{rel} = \frac{1}{v_{max}} \sqrt{\left(\frac{1}{Z} \sum_{z=0}^{Z-1} \sigma^2(z) \right)} \cdot 100\%. \tag{25}$$

where z is the sample index indicating where in the vessel the standard deviation is evaluated, and $z = 0, \ldots, Z-1$ are the samples within the vessel. The results for the velocity estimation for 45° for the four different velocities can be seen in Fig. 8-11. The corresponding mean relative bias for the different velocities is depicted in Fig. 14 as the solid line. The bias is below 2% in all four simulations. The standard deviation depicted in Fig. 15 as the solid line is significantly higher for the simulation with a peak velocity of 1 m/s. This can be explained by examining Fig. 11 which displays several false peaks in the velocity estimation. The result for the velocity estimation for 60° for the simulation with a peak velocity of 1m/s can be seen in Fig. 12. The mean relative bias for the four different velocities at 60° is shown in Fig. 14 as the dashed line. The bias is below 2% in all four simulations. The mean relative standard deviation given in Fig. 15 tends to drop for higher velocities. It should, however, be noted that the absolute standard deviation is higher for the higher velocities. The result for the velocity estimation for 75° for the simulation with peak velocity of 1 m/s can be seen in Fig. 13. The mean relative bias for the different velocities is given in Fig. 14 as the dotted line. The bias is below 4% in all four simulations. The mean relative standard deviation given in Fig. 15 tends again to drop for higher velocities. However, once again the absolute standard deviation is higher for the higher velocities.

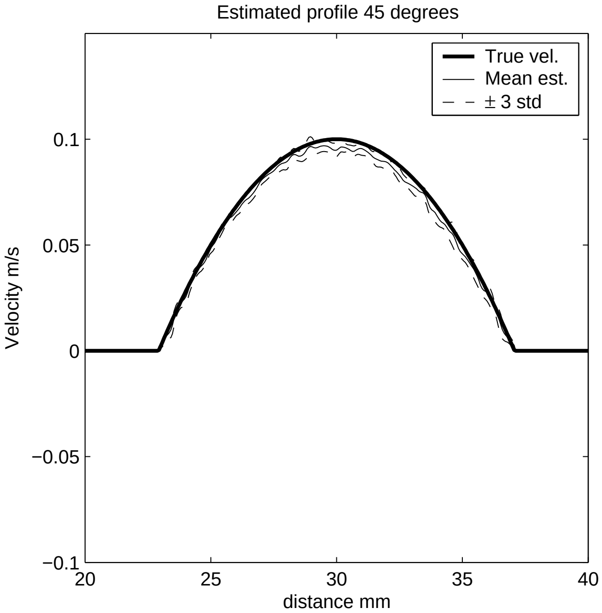

Fig. 8. The estimated velocity as a function of depth. The angle of the flow relative to the central axis of the transducer was 45°. The flow had a parabolic velocity distribution over the vessel with peak velocity 0.1 m/s.

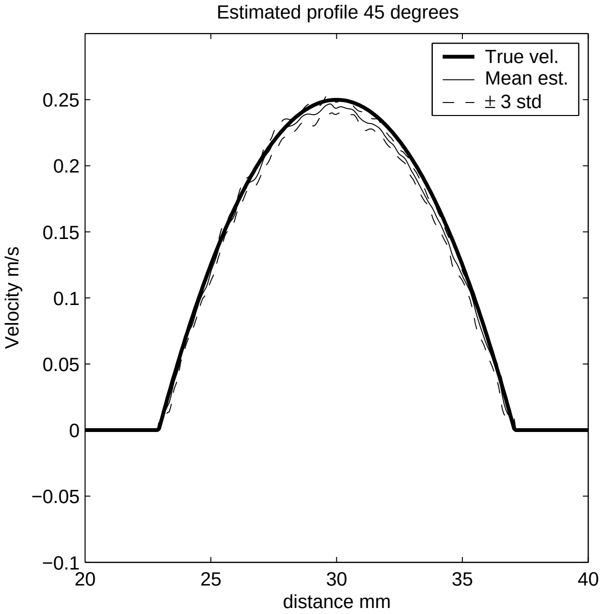

Fig. 9. The estimated velocity as a function of depth. The angle of the flow relative to the central axis of the transducer was 45°. The flow had a parabolic velocity distribution over the vessel with peak velocity 0.25 m/s.

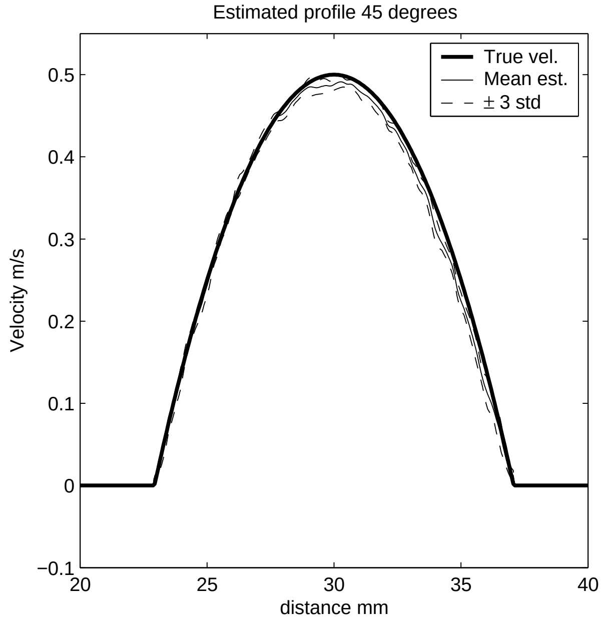

Fig. 10. The estimated velocity as a function of depth. The angle of the flow relative to the central axis of the transducer was 45°. The flow had a parabolic velocity distribution over the vessel with peak velocity 0.50 m/s.

VIII. CONCLUSION

This paper has investigated the feasibility to use spatial encoding of the transmits by means of frequency division for velocity estimation. A simulation study was carried out where a vessel with a radius of 5 mm was scanned at a depth of 30 mm. Several different velocities were tested, 0.1, 0.25, 0.50 and 1.00 m/s. Three angles were scanned per velocity 45°, 60° and 75°. The mean bias

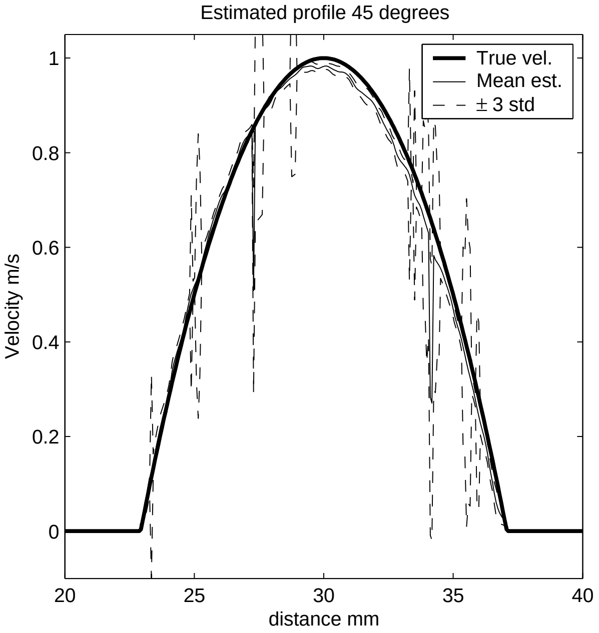

Fig. 11. The estimated velocity as a function of depth. The angle of the flow relative to the central axis of the transducer was 45°. The flow had a parabolic velocity distribution over the vessel with peak velocity 1.00 m/s.

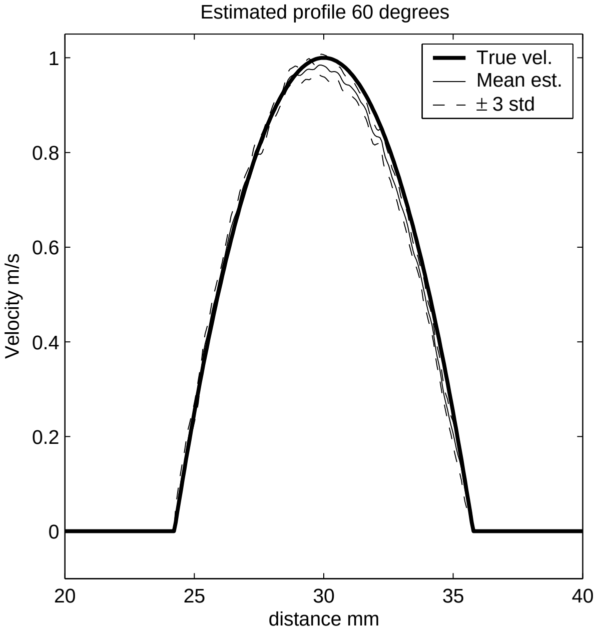

Fig. 12. The estimated velocity as a function of depth. The angle of the flow relative to the central axis of the transducer was 60°. The flow had a parabolic velocity distribution over the vessel with peak velocity 1.00 m/s.

relative to the peak velocity was for 45° less than 2%, for 60° less than 2% and for 75° less than 4%. It is therefore concluded that it is possible to estimate blood velocities using spatial encoding of the transmitters based on frequency division. This makes it possible to exploit the benefits of using spatial encoding in blood flow estimation, which would not be possible with e.g. Hadamard

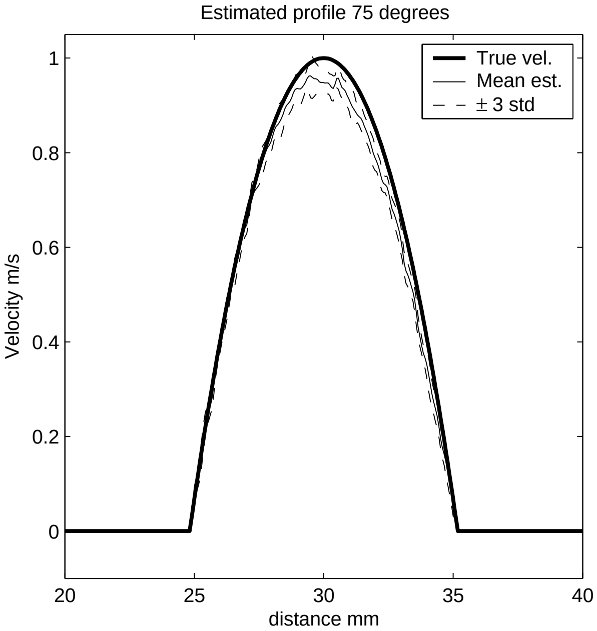

Fig. 13. The estimated velocity as a function of depth. The angle of the flow relative to the central axis of the transducer was 75°. The flow had a parabolic velocity distribution over the vessel with peak velocity 1.00 m/s.

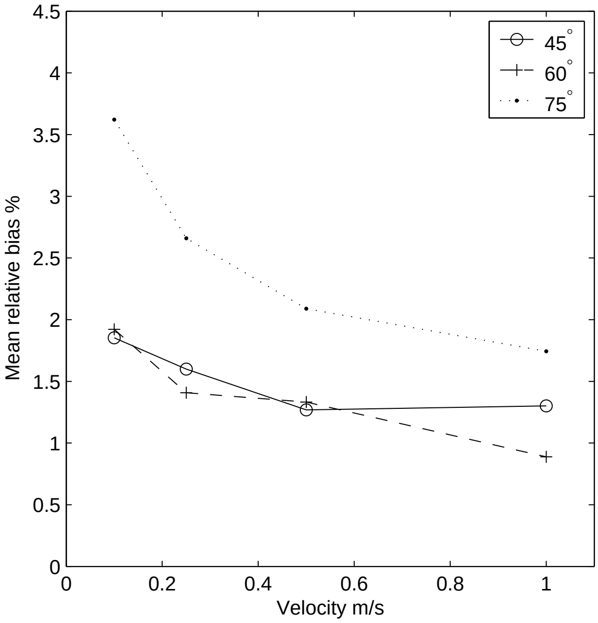

Fig. 14. The mean relative bias as a function of velocity. The solid line represents the results for 45°, the dashed 60° and the dotted 75°.

encoding.

ACKNOWLEDGMENT

This work was supported by grant 9700883, 9700563 and 26-01-0178 from the Danish Science Foundation and by B-K Medical A/S, Denmark.

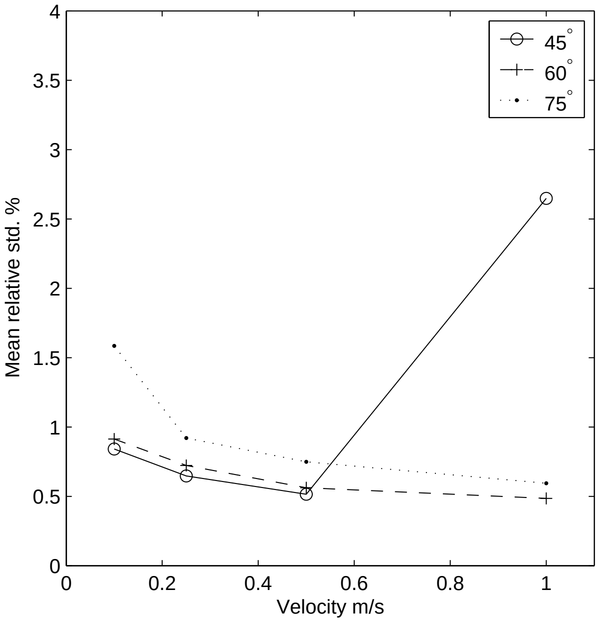

Fig. 15. The mean relative standard deviation as a function of velocity. The solid line represents the results for 45°, the dashed 60° and the dotted 75°.

REFERENCES

[1] S. I. Nikolov and J. A. Jensen, "Velocity estimation using synthetic aperture imaging," in *Proc. IEEE Ultrason. Symp.*, 2001, pp. 1409–1412.

[2] J. A. Jensen and S. I. Nikolov, "Transverse flow imaging using synthetic aperture directional beamforming," in *Proc. IEEE Ultrason. Symp.*, 2002, pp. 1488–1492.

[3] S. I. Nikolov and J. A. Jensen, "In-vivo synthetic aperture flow imaging in medical ultrasound," *IEEE Trans. Ultrason., Ferroelec., Freq. Contr.*, pp. 848–856, 2003.

[4] J. A. Jensen and S. I. Nikolov, "A method for real-time three-dimensional vector velocity imaging," in *Proc. IEEE Ultrason. Symp.*, 2003, pp. 1582–1585.

[5] J. A. Jensen, "Velocity vector estimation in synthetic aperture flow and B-mode imaging," in *IEEE International Symposium on Biomedical imaging from nano to macro*, 2004, pp. 32–35.

[6] M. O'Donnell and L. J. Thomas, "Efficient synthetic aperture imaging from a circular aperture with possible application to catheter-based imaging," *IEEE Trans. Ultrason., Ferroelec., Freq. Contr.*, vol. 39, pp. 366–380, 1992.

[7] M. Karaman, P. C. Li, and M. O'Donnell, "Synthetic aperture imaging for small scale systems," *IEEE Trans. Ultrason., Ferroelec., Freq. Contr.*, vol. 42, pp. 429–442, 1995.

[8] C. H. Frazier and W. D. O'Brien, "Synthetic aperture techniques with a virtual source element," *IEEE Trans. Ultrason., Ferroelec., Freq. Contr.*, vol. 45, pp. 196–207, 1998.

[9] M. H. Bae and M. K. Jeong, "A study of synthetic-aperture imaging with virtual source elements in B-mode ultrasound imaging systems," in *IEEE Trans. Ultrason., Ferroelec., Freq. Contr.*, 2000, vol. 47, pp. 1510–1519.

[10] M.I. Skolnik, *Introduction to Radar Systems*, McGraw-Hill, New York, 1980.

[11] M.I. Skolnik, *Radar Handbook*, McGraw-Hill, New York, second edition, 1990.

[12] M. O'Donnell, "Coded excitation system for improving the penetration of real-time phased-array imaging systems," *IEEE Trans. Ultrason., Ferroelec., Freq. Contr.*, vol. 39, pp. 341–351, 1992.

[13] T. X. Misaridis and J. A. Jensen, "An effective coded excitation scheme based on a predistorted FM signal and an optimized digital filter," in *Proc. IEEE Ultrason. Symp.*, 1999, vol. 2, pp. 1589–1593.

[14] T. Misaridis and J. A. Jensen, "Use of modulated excitation signals in ultrasound, Part I: Basic concepts and expected benefits," *IEEE Trans. Ultrason., Ferroelec., Freq. Contr.*, pp. 192–207, 2005.

[15] T. Misaridis and J. A. Jensen, "Use of modulated excitation signals in ultrasound, Part II: Design and performance for medical imaging applications," *IEEE Trans. Ultrason., Ferroelec., Freq. Contr.*, pp. 208–219, 2005.

[16] T. Misaridis and J. A. Jensen, "Use of modulated excitation signals in ultrasound, Part III: High frame rate imaging," *IEEE Trans. Ultrason., Ferroelec., Freq. Contr.*, pp. 220–230, 2005.

[17] R. Y. Chiao and X. Hao, "Coded excitation for diagnostic ultrasound: a system developer's perspective," *IEEE Trans. Ultrason., Ferroelec., Freq. Contr.*, vol. 52, pp. 160–170, 2005.

[18] R. Y. Chiao, L. J. Thomas, and S. D. Silverstein, “Sparse array imaging with spatially-encoded transmits,” in *Proc. IEEE Ultrason. Symp.*, 1997, pp. 1679–1682.

[19] R. Y. Chiao and L. J. Thomas, “Synthetic transmit aperture using orthogonal golay coded excitation,” in *Proc. IEEE Ultrason. Symp.*, 2000, pp. 1469–1472.

[20] F. Gran and J. A. Jensen, “Multi element synthetic aperture transmission using a frequency division approach,” in *Proc. IEEE Ultrason. Symp.*, 2003, pp. 1942–1946.

[21] F. Gran and J. A. Jensen, “Frequency division transmission and synthetic aperture reconstruction,” *IEEE Trans. Ultrason., Ferroelec., Freq. Contr.*, vol. Submitted for publication, 2004.

[22] F. Gran and J. A. Jensen, “Spatio-temporal encoding using narrow-band linearly frequency modulated signals in synthetic aperture ultrasound imaging,” in *Proc. SPIE - Progress in biomedical optics and imaging*, 2005, p. Accepted for publication.

[23] J. A. Jensen, “Simulation of advanced ultrasound systems using field II,” in *IEEE International Symposium on Biomedical imaging from nano to macro*, 2004, pp. 636–639.

[24] S. I. Nikolov, *Synthetic aperture tissue and flow ultrasound imaging*, Ph.D. thesis, Ørsted●DTU, Technical University of Denmark, 2800, Lyngby, Denmark, 2001.

[25] J. A. Jensen, “Directional velocity estimation using focusing along the flow direction: I: Theory and simulation,” *IEEE Trans. Ultrason., Ferroelec., Freq. Contr.*, pp. 857–872, 2003.

[26] J. A. Jensen and R. Bjerngaard, “Directional velocity estimation using focusing along the flow direction: II: Experimental investigation,” *IEEE Trans. Ultrason., Ferroelec., Freq. Contr.*, pp. 873–880, 2003.

[27] N. Oddershede and J. A. Jensen, “Experimental investigation of synthetic aperture flow angle estimation,” in *Proc. SPIE - Progress in biomedical optics and imaging*, 2005, p. Accepted for publication.

[28] O. Bonnefous, “Statistical analysis and time processes applied to velocity measurement,” in *Proc. IEEE Ultrason. Symp.*, 1989, pp. 887–892.

[29] J. A. Jensen, *Estimation of Blood Velocities Using Ultrasound: A Signal Processing Approach*, Cambridge University Press, New York, 1996.

[30] S. G. Foster, *A pulsed ultrasonic flowmeter employing time domain methods*, Ph.D. thesis, Dept. Elec. Eng., University of Illinois, Urbana, Ill., 1985.

[31] J. A. Jensen and N. B. Svendsen, “Calculation of pressure fields from arbitrarily shaped, apodized, and excited ultrasound transducers,” *IEEE Trans. Ultrason., Ferroelec., Freq. Contr.*, vol. 39, pp. 262–267, 1992.

[32] J. A. Jensen, “Field: A program for simulating ultrasound systems,” *Med. Biol. Eng. Comp.*, vol. 10th Nordic-Baltic Conference on Biomedical Imaging, Vol. 4, Supplement 1, Part 1, pp. 351–353, 1996b.

[33] S. I. Nikolov and J. A. Jensen, “Virtual ultrasound sources in high-resolution ultrasound imaging,” in *Proc. SPIE - Progress in biomedical optics and imaging*, 2002, vol. 3, pp. 395–405.

[34] K. L. Gammelmark and J. A. Jensen, “Duplex synthetic aperture imaging with tissue motion compensation,” in *Proc. IEEE Ultrason. Symp.*, 2003, pp. 1569–1573.

CHAPTER

SIX

Spatial encoding by means of code division

Increasing the SNR is one potential benefit from utilizing spatial encoding. Another is to increase the amount of information acquired in every transmission. When using the frequency division approach, each transmitter only uses a very small part of the available bandwidth. To synthesize broadband spectra for each transmitter, several transmissions are required. In this chapter, a method for broadband spatial encoding is presented. The purpose is to excite several transmitters simultaneously, and separate the broadband signals in receive after only one transmission. The approach has been inspired by methods developed for multiuser channel estimation in tele-communication applications [68]. Here, several users share the same communication channel. To properly reconstruct the information which was sent, the channel has to estimated. To do this, pilot or training sequences are transmitted from each user. By utilizing the knowledge of the training sequences and the received signals, the channel can be estimated.

In ultrasound imaging, the problem formulation is very similar. A pulse or code sequence is transmitted, and an acoustic wave is generated. During the propagation of the acoustic wave, some of the acoustic energy will be reflected. The reflected waves will be distorted depending on the acoustic properties and the geometry of the object under investigation. The purpose of the imaging system is to extract the information carried by the reflected waves. The problem can be formulated as a channel estimation problem, where the transmitted waveform is the ”pilot sequence”, and the objective is to estimate the ”channel” representing the information about the tissue.

During this project an approach has been developed to show that the basic concept is a fruitful idea. The theory has been analyzed and the method has been tested both in simulation and in experiments. Technical and theoretical challenges still remain to be solved, however, vast areas of the tele-communication literature remains unchartered and maybe a solution lies herein.

This chapter is a summary of the work presented in the papers:

- A code division technique for multiple element synthetic aperture transmission
  Fredrik Gran, Jørgen Arendt Jensen and Andreas Jakobsson
  Published in the Proceedings of SPIE-Progress in biomedical optics and imaging 2004, vol 5373, pp 300-306
- Identification of spatial impulse responses for multi source transmission (Invited)
  Fredrik Gran and Jørgen Arendt Jensen
  Published in Conference Record of Thirty-Eighth Annular Asilomar Conference on Signals,

Systems, and Computers, vol 1, pp 168-172, 2004

- Spatial encoding using a code division technique for fast ultrasound imaging. **Fredrik Gran** and Jørgen Arendt Jensen
  Submitted to IEEE Transactions on Ultrasonics, Ferroelectrics and Frequency control, May 2005

The full papers are given at the end of this chapter in sections 6.7-6.9. The papers are presented unedited. However, the font size and the layout of the yet unpublished paper, has been changed to better conform with the layout of this dissertation. The page numbers of the papers which have already been published are the page numbers in the corresponding proceedings.

6.1 Basic principles

Consider an ultrasound system with K transmitters at the spatial locations $\vec{r}_{xmt,k}$. Each transmitter is assigned an individual code sequence $x_k(t)$. The model for the received signal on the q:th receiving element located at $\vec{r}_{rcv,q}$ is once again

$$y_q(t) = \sum_{k=0}^{K-1} h_{qk}(t) \star x_k(t), \tag{6.1}$$

where

$$h_{qk}(t) = \sum_{p=0}^{P-1} s(\vec{r}_p) h(\vec{r}_{xmt,k}, \vec{r}_p, t) \star h(\vec{r}_p, \vec{r}_{rcv,q}, t) \star h_{tr}(t) \star a(\vec{r}_{xmt,k}, \vec{r}_{rcv,q}, \vec{r}_p, t), \tag{6.2}$$

with the same definitions of the variables as in (4.47). A block diagram of the model in (6.1) is found in Fig. 6.1.

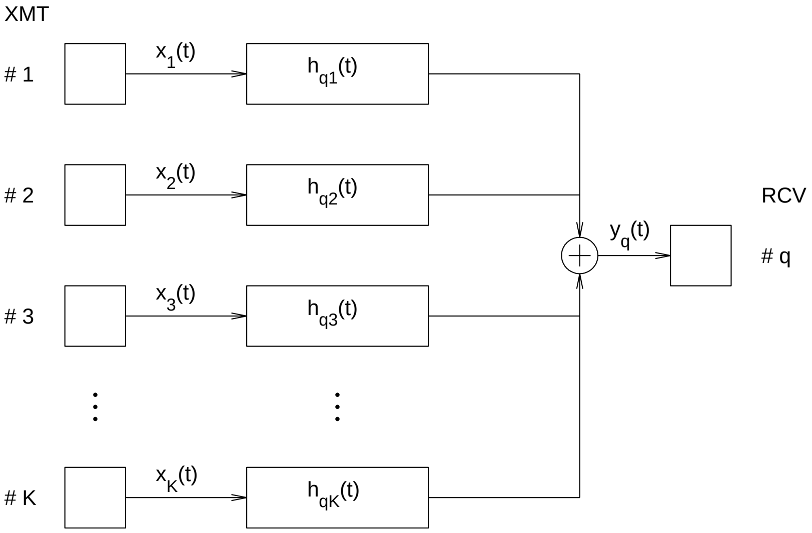

Figure 6.1: The received signal on the q:th receiver is a linear combination of the contributions from the K transmitters. The contribution from a specific transmitter is modeled as a linear process.

The sampled received signal under the influence of noise can be written as the sampled version of (6.1) plus a noise process

$$r_q(n) = y_q(n) + v_q(n) = \sum_{k=0}^{K-1} h_{qk}(n) \star x_k(n) + v_q(n), \tag{6.3}$$

where $y_q(n)$ is the sampled version of $y_q(t)$, $h_{qk}(n)$ is the sampled version of $h_{qk}(t)$ with duration L samples and $x_k(n)$ is the sampled code sequence with duration N samples. The variable $v_q(n)$ is a discrete time stochastic process, modeling the measurement noise. The noise is assumed to have zero mean and a Gaussian probability distribution. By writing the received signal on the q:th receiver as a column vector[1]

$$\mathbf{r}_q = \begin{pmatrix} r_q(0) & r_q(1) & \dots & r_q(M-1) \end{pmatrix}^T \tag{6.4}$$

the convolution between $h_{qk}(n)$ and $x_k(n)$ can be written as a matrix operation

$$\mathbf{r}_q = \sum_{k=0}^{K-1} \mathbf{X}_k \mathbf{h}_{qk} + \mathbf{v}_q. \tag{6.5}$$

Here, $\mathbf{h}_{qk}$ is the column vector representing the wave propagation operator between the k:th transmitter and the q:th receiver and $\mathbf{v}_q$ is the noise process written as a column vector

$$\begin{aligned} \mathbf{h}_{qk} &= \begin{pmatrix} h_{qk}(0) & h_{qk}(1) & \dots & h_{qk}(L-1) \end{pmatrix}^T && (6.6) \\ \mathbf{v}_q &= \begin{pmatrix} v_q(0) & v_q(1) & \dots & v_q(M-1) \end{pmatrix}^T. && (6.7) \end{aligned}$$

The matrix $\mathbf{X}_k$ is given by

$$\mathbf{X}_k = \begin{pmatrix} x_k(0) & 0 & \cdots & 0 \\ x_k(1) & x_k(0) & \ddots & 0 \\ \vdots & \ddots & \ddots & \vdots \\ x_k(N-1) & \ddots & \ddots & x_k(0) \\ 0 & x_k(N-1) & \ddots & x_k(1) \\ \vdots & \ddots & \ddots & \vdots \\ 0 & 0 & \cdots & x_k(N-1) \end{pmatrix}, \tag{6.8}$$

so that $\mathbf{X}_k\mathbf{h}_{qk}$ is a column matrix corresponding to the convolution between $h_{qk}(n)$ and $x_k(n)$. The equation given in (6.5) can be written using a more compact notation

$$\mathbf{r}_q = \underbrace{\begin{pmatrix} \mathbf{X}_0 & \mathbf{X}_1 & \dots & \mathbf{X}_{K-1} \end{pmatrix}}_{\mathbf{X}} \underbrace{\begin{pmatrix} \mathbf{h}_{q0} \\ \mathbf{h}_{q1} \\ \vdots \\ \mathbf{h}_{qK-1} \end{pmatrix}}_{\mathbf{h_q}} + \mathbf{v}_q. \tag{6.9}$$

This notation will be used for further analysis.

---

[1] M is the duration of the received signal in samples

6.2 The Maximum Likelihood Estimate of the wave propagation operator

The model for the received signal given in (6.9) is linear in $\mathbf{h}_q$. The Maximum Likelihood Estimate for $\mathbf{h}_q$ is found by maximizing the conditional probability distribution of receiving $\mathbf{r}_q$ given $\mathbf{h}_q$ and $\mathbf{X}$

$$\widehat{\mathbf{h}}_q^{MLE} = \arg\max_{\mathbf{h}_q} p\left(\mathbf{r}_q|\mathbf{h}_q, \mathbf{X}\right), \tag{6.10}$$

where $p\left(\mathbf{r}_q|\mathbf{h}_q, \mathbf{X}\right)$ is the conditional probability distribution of receiving $\mathbf{r}_q$ given $\mathbf{h}_q$ and $\mathbf{X}$.

When the variables, $\mathbf{h}_q$ and $\mathbf{X}$ are given, the only part of (6.9) which is stochastic is the noise $\mathbf{v}_q$. The noise is assumed to have zero mean

$$E\left[\mathbf{v}_q\right] = \mathbf{0}, \qquad q = 0, \ldots, Q-1, \tag{6.11}$$

and a covariance matrix given by

$$E\left[\mathbf{v}_q\mathbf{v}_q^T\right] = \mathbf{Q}_v, \qquad q = 0, \ldots, Q-1, \tag{6.12}$$

The noise process is as mentioned earlier, assumed to have a Gaussian probability distribution, so that the probability distribution of the noise is

$$p(\mathbf{v}_q) = \frac{1}{\sqrt{\det\left\{2\pi\mathbf{Q}_v\right\}}} \times \exp\left\{-\frac{1}{2}\mathbf{v}_q^T\mathbf{Q}_v^{-1}\mathbf{v}_q\right\}. \tag{6.13}$$

Thus, the distribution $p\left(\mathbf{r}_q|\mathbf{h}_q, \mathbf{X}\right)$ can be written

$$p\left(\mathbf{r}_q|\mathbf{h}_q, \mathbf{X}\right) = \frac{1}{\sqrt{\det\left\{2\pi\mathbf{Q}_v\right\}}} \times \exp\left\{-\frac{1}{2}(\mathbf{r}_q - \mathbf{X}_k\mathbf{h}_{qk})^T\mathbf{Q}_v^{-1}(\mathbf{r}_q - \mathbf{X}_k\mathbf{h}_{qk})\right\}. \tag{6.14}$$

Combining (6.10) and (6.14) yields the well known linear set of equations [69]

$$\left(\mathbf{X}^T\mathbf{Q}_v^{-1}\mathbf{X}\right)\widehat{\mathbf{h}}_q^{MLE} = \mathbf{X}^T\mathbf{Q}_v^{-1}\mathbf{r}_q. \tag{6.15}$$

When the noise is temporally white with variance σ_v^2, (6.15) reduces to

$$\left(\mathbf{X}^T\mathbf{X}\right)\widehat{\mathbf{h}}_q^{MLE} = \mathbf{X}^T\mathbf{r}_q. \tag{6.16}$$

6.3 Solving for the Maximum Likelihood Estimate

The question is: when does a unique solution to (6.16) exist [2]? When the signal matrix $\mathbf{X}$ has full column rank, $\mathbf{X}^T\mathbf{X}$ is invertible and the unique solution to (6.16) is

$$\widehat{\mathbf{h}}_q^{MLE} = \left(\mathbf{X}^T\mathbf{X}\right)^{-1}\mathbf{X}^T\mathbf{r}_q. \tag{6.17}$$

By analyzing the dimensions of the signal matrix $\mathbf{X}$, a peculiar implication emerges. The dimensions of $\mathbf{X}$ is

$$\dim\left\{\mathbf{X}\right\} = M \times KL, \tag{6.18}$$

---

[2] The noise is for this discussion assumed to be white.

where M is the length of the received signal $\mathbf{r}_q$ in samples. Since the received signal $\mathbf{r}_q$ is a linear combination of the the code sequences convolved with the corresponding wave propagation operators, the length of $\mathbf{r}_q$ is determined by

$$M = L + N - 1. \tag{6.19}$$

For the signal matrix to have full column rank, the columns have to make a linear independent set of vectors. Therefore, a fundamental requirement for a unique solution to (6.16) is that

$$\begin{array}{rcl} L + N - 1 & \geq & KL \\ & \Downarrow & \\ N & \geq & (K-1)L + 1, \end{array} \tag{6.20}$$

which sets a lower limit on the code length N. The code sequences must, thus, be chosen so that the columns of $\mathbf{X}$ make a linear independent set of vectors. Therefore, the code sequences must at least fulfill the requirement specified in (6.20).

6.4 Mean square estimation error

To evaluate the mean squared estimation error, assume that the model in (6.9) is correct, that the noise is white with variance σ_v^2 and that $\mathbf{X}$ has full column rank. The ML estimate of the wave propagation operators is then

$$\widehat{\mathbf{h}}_q^{MLE} = \left(\mathbf{X}^T\mathbf{X}\right)^{-1}\mathbf{X}^T\mathbf{r}_q = \left(\mathbf{X}^T\mathbf{X}\right)^{-1}\mathbf{X}^T\left(\mathbf{X}\mathbf{h}_q + \mathbf{v}_q\right). \tag{6.21}$$

By elimination this expression can be reduced to

$$\widehat{\mathbf{h}}_q^{MLE} = \mathbf{h}_q + \left(\mathbf{X}^T\mathbf{X}\right)^{-1}\mathbf{X}^T\mathbf{v}_q. \tag{6.22}$$

The estimate is unbiased since,

$$E\left[\widehat{\mathbf{h}}_q^{MLE}\right] = E\left[\mathbf{h}_q + \left(\mathbf{X}^T\mathbf{X}\right)^{-1}\mathbf{X}^T\mathbf{v}_q\right] \tag{6.23}$$

$$= \mathbf{h}_q + \left(\mathbf{X}^T\mathbf{X}\right)^{-1}\mathbf{X}^T\underbrace{E\left[\mathbf{v}_q\right]}_{=0}. \tag{6.24}$$

The estimation error can be defined as

$$\mathbf{e}_q = \left(\mathbf{X}^T\mathbf{X}\right)^{-1}\mathbf{X}^T\mathbf{v}_q, \tag{6.25}$$

and the covariance matrix of the estimation error is given by

$$\begin{aligned} E\left[\mathbf{e}_q\mathbf{e}_q^T\right] &= E\left[\left(\mathbf{X}^T\mathbf{X}\right)^{-1}\mathbf{X}^T\mathbf{v}_q\mathbf{v}_q^T\mathbf{X}\left(\mathbf{X}^T\mathbf{X}\right)^{-1}\right] \\ &= \left(\mathbf{X}^T\mathbf{X}\right)^{-1}\mathbf{X}^T E\left[\mathbf{v}_q\mathbf{v}_q^T\right]\mathbf{X}\left(\mathbf{X}^T\mathbf{X}\right)^{-1} \\ &= \sigma_v^2\left(\mathbf{X}^T\mathbf{X}\right)^{-1}\mathbf{X}^T\mathbf{X}\left(\mathbf{X}^T\mathbf{X}\right)^{-1} \\ &= \sigma_v^2\left(\mathbf{X}^T\mathbf{X}\right)^{-1}. \end{aligned} \tag{6.26}$$

According to [68], the optimum mean squared estimation error is attained when the codes have zero cross-correlation and ideal auto-correlation

$$\sum_{n=0}^{N-1} x_k(n)x_l(n+m) = \left\{ \begin{array}{cc} 0 & k \neq l, \\ E_x\delta(m) & k = l \end{array} \right. , \tag{6.27}$$

where E_x is the energy of the code sequences. In this case the matrix $\mathbf{X}^T\mathbf{X}$ is diagonal

$$\begin{array}{rcl} \mathbf{X}^T\mathbf{X} & = & E_x\mathbf{I} \\ & \Downarrow & \\ \left(\mathbf{X}^T\mathbf{X}\right)^{-1} & = & \frac{1}{E_x}\mathbf{I}. \end{array} \tag{6.28}$$

Combining (6.26) and (6.28) results in

$$E\left[\mathbf{e}_q\mathbf{e}_q^T\right] = \frac{\sigma_v^2}{E_x}\mathbf{I}, \tag{6.29}$$

which can be interpreted as if the estimation error acts as a white noise process with the variance $\frac{\sigma_v^2}{E_x}$. Ideally, if code sequences with the property specified by (6.27) could be designed, the SNR of the estimated data would be E_x times better than that of the raw RF data. In the papers [65,70,71] the issue of code design to attain the best possible SNR has not been addressed. Here, the objective was to produce a model which had a unique solution to (6.16). This was achieved by exciting the transmitters using transmitter specific pseudo-random code sequences[3] with the proper length.

6.5 Water tank experiments

The objective has been to demonstrate that the idea actually works in practice. For this purpose, the method was implemented into the research scanner RASMUS [63]. In this study two transmitters were active simultaneously and a metal wire in a water bath was scanned. A BK8804 linear array transducer was used in the experiments. Two pseudo-random binary sequences were generated in Matlab using the `randn` function. If the value specified by the random number generator was below zero, the sequence was given the value minus one, otherwise the sequence was given the value plus one. To limit the bandwidth of the transmitted signal, the code sequences were convolved with a four cycle sinusoid with a temporal Hanning weighting before transmission. The transmitted waveforms where, thus,

$$\begin{array}{l} s_1(n) = x_1(n) \star c(n) \\ s_2(n) = x_2(n) \star c(n) \end{array} \tag{6.30}$$

where $x_1(n)$ and $x_2(n)$ are the two binary code sequences and $c(n)$ is defined as

$$c(n) = a(n)\sin\left(2\pi f_0 \frac{n}{f_s}\right), \quad 0 \leq n \leq \frac{4f_s}{f_0} \tag{6.31}$$

where f_s is the sampling frequency, f_0 is the center frequency, which in this case was 5 MHz and $a(n)$ is a discrete temporal Hanning window. The code sequences were sampled such that there was no overlap between consecutive sinusoids. The experimental system has a sampling frequency of 40 MHz and the code sequences were sampled at 0.6 MHz. The code sequences and the transmitted waveforms can be seen in Fig. 6.2. In the estimation procedure, the sinusoidal waveform $c(n)$ is treated as a part of the wave propagation operator.

---

[3] Generated by the `randn` function in Matlab.

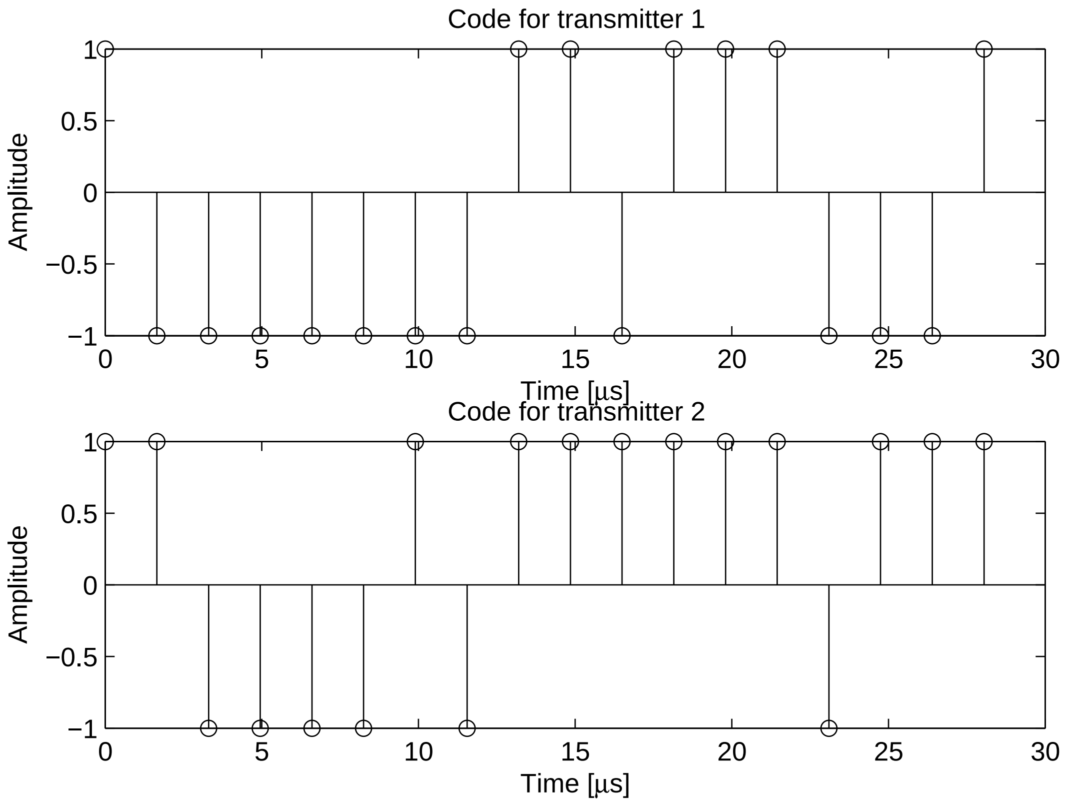

Figure 6.2: The two binary 18 bit pseudo random code sequences. The first code is assigned to the first transmitter and the second transmitter is assigned the second code sequence.

The actual transmitted waveforms given by (6.30) are shown in Fig. 6.3.

In all experiments, a BK8804 linear array transducer was used. The target was a metal wire, positioned at a depth of 42 mm relative to the transducer. The surrounding medium was demineralized water.

Two sets of experiments were carried out

- The decoding based on MLE was tested by exciting two transmitters simultaneously and considering the received signal on a single transducer element. The decoded echoes were compared to the echoes acquired by exciting the transmitters separately.
- The PSF was measured for a system based on the MLE decoder and was compared to the PSF of a conventional STA system with sequential data acquisition.

In the first set of experiments, the first transmitter was created by exciting transducer element 43 and 44 and the second transmitter was created by using transducer element 63 and 64. The active receiver was the 64:th transducer element.

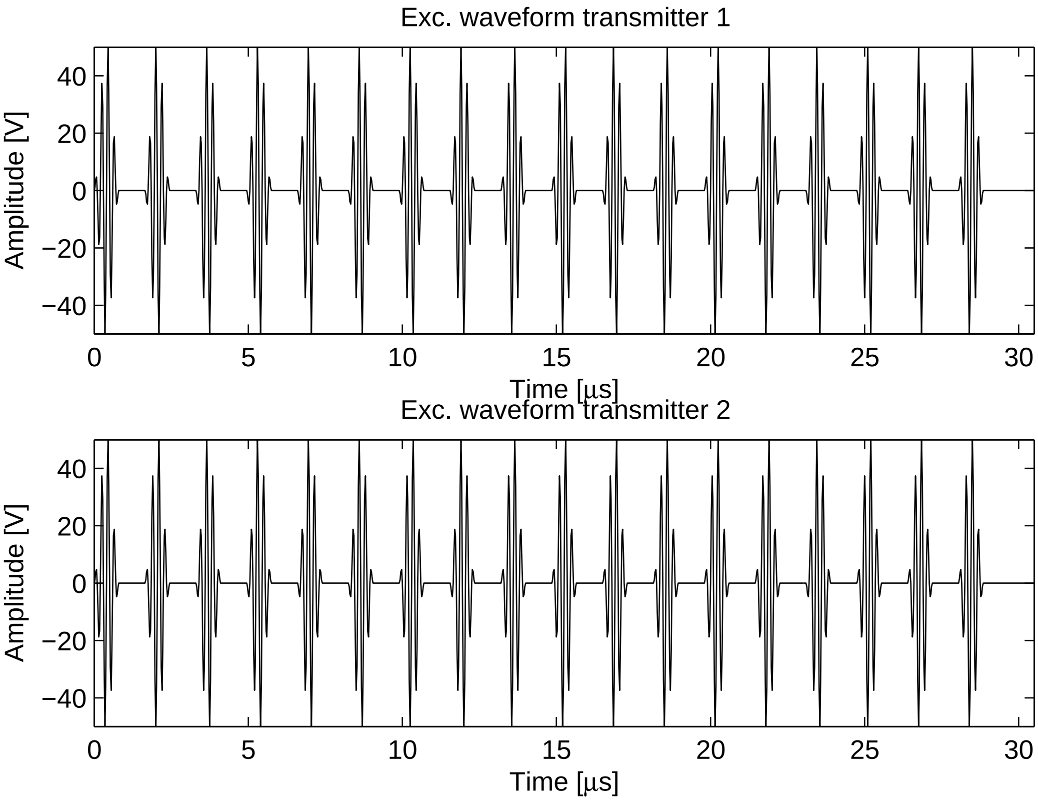

Figure 6.3: The two binary 18 bit pseudo random code sequences convolved with the waveform $c(n)$. The center frequency of $c(n)$ was 5 MHz, had a duration of four cycles and a temporal Hanning window was applied.

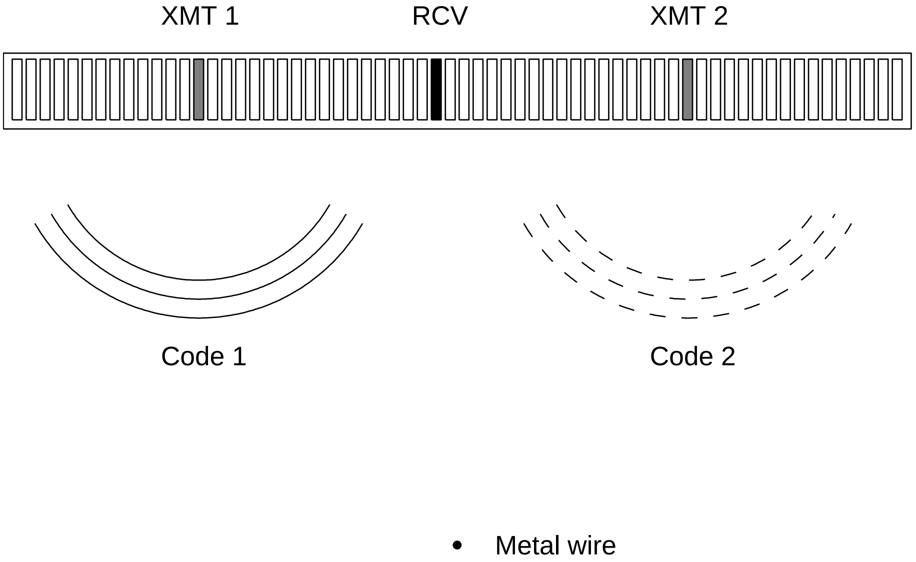

Figure 6.4: The measurement setup for the first experiment. Two active transmitters and one active receiver. For the coded case, the transmitters are active simultaneously and the signals are separated using a Maximum Likelihood Estimator.

Reference experiment: To get a reliable reference of the signals which should be estimated, 500 transmissions were performed with each of the transmitters. The first transmitter was used during the first 500 transmissions with $c(n)$ as excitation waveform. The second transmitter was used during the remaining 500 transmissions also using $c(n)$ as excitation waveform. All signals were matched filtered using the time reversed version of $c(n)$. The echoes were averaged to reduce the noise. The results for the two transmitters are given as the solid lines in Fig. 6.5 and Fig. 6.6. One realization of the experiment is depicted as the dotted line in Fig. 6.6.

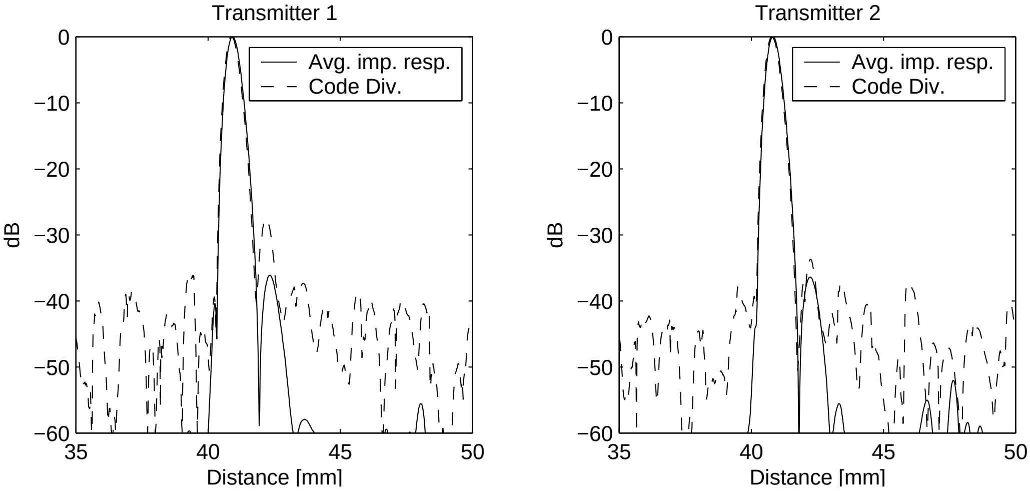

Figure 6.5: The solid lines in the two figures represents the envelope of the averaged response for the two different transmitters using $c(n)$ as excitation waveform. To reduce the noise 500 realizations of the received signal was averaged for each transmitter. The dashed line represents the envelope of the decoded signals from one transmission using the approach described in this chapter. The code sequences in Fig. 6.2 and the waveforms in Fig. 6.3 were used to encode the transmitters.

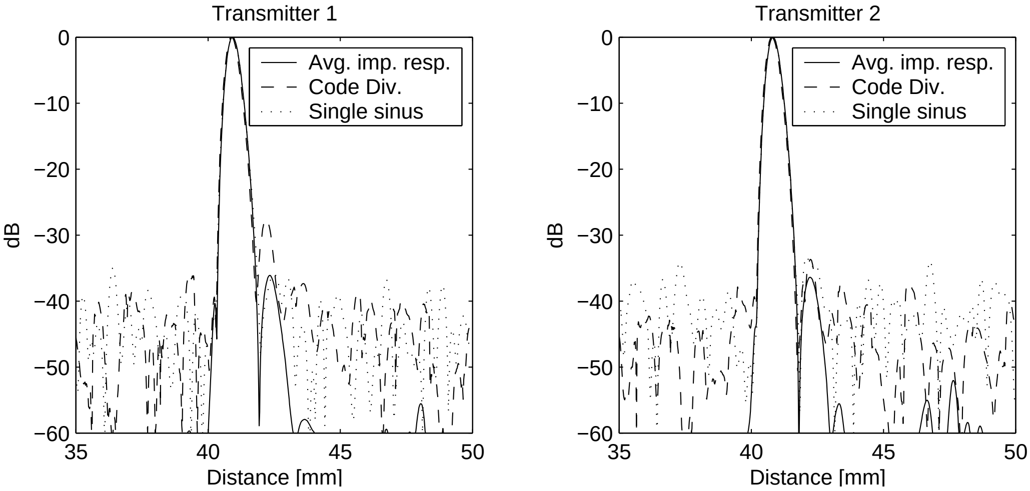

Figure 6.6: The solid and dashed lines represent the averaged reference signals and the decoded signals respectively. The dotted lines show the envelope of the received signals using one realization of the reference experiment per transmitter. The noise level is on the same order of magnitude as the estimation error in the decoded signals.

Coded excitation: The transmitters were excited using the two waveforms depicted in Fig. 6.3. Transmitter one was assigned waveform number one and transmitter two waveform number two. The two transmitters were excited simultaneously and the received signal on the 64:th receiving element was recorded. To separate the signals corresponding to the two different transmitters, the decoding procedure described in Section 6.2 was utilized. The resulting signals were matched filtered using the time reversed version of $c(n)$. The result from this experiment can be seen in Fig. 6.5 and Fig. 6.6 as the dashed line. The signals are separated in only one transmission. In contrast, other methods for spatially encoding the transmitters, like Hadamard or Golay encoding, would require two transmissions before the two different signals could be distinguished. For the method described in Chapter 5, four transmissions would be required.

In the second set of experiments, the PSF of a imaging system utilizing the MLE decoder is compared to the PSF of a system based on sequential STA data acquisition. In this case the reference image was created by sliding the active transmitter over the transmitting aperture. By doing so, transducer element one and two were active in the first transmission and element three and four were active in the second transmission. This was repeated until the 128 available transducer elements had been covered. In total 64 transmissions were carried out. When the signals from one transmission had been recorded, they were matched filtered using the time reversed version of $c(n)$.

The PSF for the spatially encoded approach was created by using two transmitters in every transmission. In the first transmission transmitter one was created from element one and two and transmitter two was created using element 65 and 66. The two transmitters were encoded with the waveforms in Fig. 6.3. The received signals were decoded and matched filtered. In the next transmission, transmitter one was created using transducer element three and four, and transmitter two using element 67 and 68. The received signals were again recorded, decoded and matched filtered. This procedure was repeated until all elements in the array had been covered. In total, 32 transmissions were carried out.

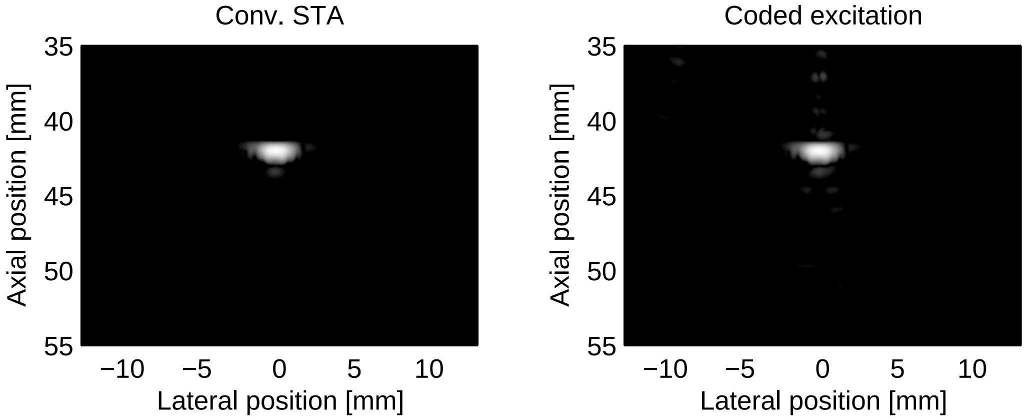

Figure 6.7: The PSFs of the reference experiment (left image) and the spatially encoded experiment (right image). the dynamic range is 50 dB. The images show very small differences, indicating that the spatial encoding is capable of distinguishing between the two signals which are decoded in every transmission.

In both experiments 128 receiving elements were used. However, the RASMUS system only has 64 receiving channels. By multiplexing, 128 receiving elements can be synthesized. Both sets of data were beamformed using the STA approach described in chapter 3. The apodization on the receiving elements where chosen to be a Hanning window. The PSF for the reference experiment can be seen as the left figure in Fig. 6.7 and the axial and lateral projections are given as the solid lines in Fig. 6.8. The PSF for the spatial encoded experiment is given as the right figure in Fig. 6.7 and the axial and lateral projections are depicted as the dotted lines in Fig. 6.8.

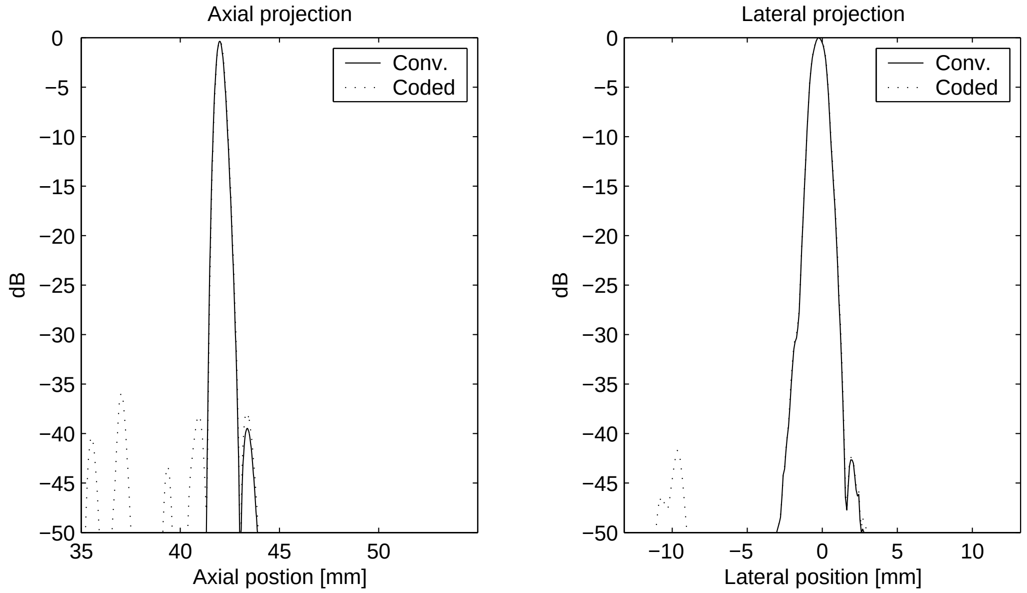

Figure 6.8: The axial and lateral projections of the PSF from the reference experiment are given as the solid lines. The dotted lines represent the axial and lateral projections of the PSF from the spatially encoded experiment. The projections are created by taking the maximum value of each row of the image matrix (axial projection) and maximum of each column (lateral projection) respectively. The main parts of the signals match perfectly, however, the spatially encoded experiment displays some axial and lateral artifacts resulting from the decoding.

6.6 Summary

In this chapter a method for spatial encoding has been presented. Compared to the method described in Chapter 5 based on frequency division, Hadamard or Golay encoding, the signals originating from the different transmitters can be decoded after only one transmission. The method can potentially provide means for fast acquisition of ultrasound data. However, the method is nowhere as complete as the frequency division approach. Theoretical challenges still remain. For a unique solution to the estimation problem to exist, a minimum code duration is required. This is problematic in ultrasound, because the transmitting array is also used as the receiver. For this method to be practical, a solution to the code duration problem has to be found. Another challenge is the code design. Ideally, great improvement in SNR is expected if the code sequences are designed properly. In [72] (section 6.9) the discrepancy between the theoretical limit and the achieved gain in SNR was traced to the choice of the code sequences.

6.7 Conference paper: A code division technique for multiple element synthetic aperture transmission

Published in the Proceedings of SPIE-Progress in biomedical optics and imaging 2004, vol 5373, pp 300-306

A Code Division Technique for Multiple Element Synthetic Aperture Transmission

[a]Fredrik Gran, [a]Jørgen Arendt Jensen and [b]Andreas Jakobsson

[a]Center for Fast Ultrasound Imaging, Technical University of Denmark
DK-2800 Kgs. Lyngby, Denmark
[b]Department of Electrical Engineering, Karlstad University
SE-651 88 Karlstad, Sweden

ABSTRACT

In conventional synthetic transmit aperture imaging (STA) the image is built up from a number of low resolution images each originating from consecutive single element firings to yield a high resolution image. This lowers the frame rate and may result in motion artifacts. This paper, describes a method in which all transmitting centers can be excited at the same time and separated at the receiver to yield a full image in only one transmission. Hereby the benefits from traditional STA can be utilized and a high frame rate can be maintained, which thereby prevents motion artifacts. The different centers are excited using mutually orthogonal codes. The signal at the receiver is a linear combination of the transmitted signals convolved with the corresponding pulse-echo impulse response. The pulse-echo impulse responses for the different elements are modeled as finite impulse response channels and estimated using a maximum likelihood technique. The method was verified using simulations in Field II. A 7 MHz transducer was simulated with 128 receiving elements and 64 transmitting elements divided into subapertures so that 4 virtual transmission centers were formed. The point spread function was simulated and the axial resolution was 0.23 mm (-3 dB) and 0.31 mm (-6 dB), lateral resolution 0.53 mm (-3 dB) and 0.71 mm (-6 dB) and maximum lateral sidelobe level less than 44 dB. Conventional STA is given as a reference with the same aperture setup using 4 emissions excited with a single cycle sinusoid at 7 MHz. The axial resolution is here 0.23 mm (-3 dB) and 0.31 mm (-6 dB), lateral resolution 0.53 mm (-3 dB) and 0.71 mm (-6 dB) and maximum lateral sidelobe level less than 44 dB.

Keywords: Joint channel estimation, coded ultrasound, synthetic aperture ultrasound.

1. INTRODUCTION

In conventional synthetic transmit aperture ultrasound an image is acquired over several defocused transmissions. Only a small part of the aperture is utilized in every transmission. For every transmission a different point of origin for the created spherical wave is chosen, so that the full spatial range of the aperture is covered. In the beamforming the entire aperture is synthesized to yield the full resolution of the system. It is possible to exactly determine the point of origin and the point of reception for every transmitter-receiver pair. Therefore it is possible to delay the received signals, so that perfect focusing can be attained for all points in the image. The drawbacks associated with this method is inherit from the sequential acquisition approach. If the tissue is moving, motion artifacts can arise. The fact that only a small part of the aperture is used in every defocused transmission also causes problems concerning signal to noise ratio (SNR). If the active transmitting aperture is small, the energy transmitted will be lower compared to using the full aperture and therefore a poorer SNR will be attained. Problems concerning SNR have been addressed in[1–5] , were a longer linear frequency modulated chirp is transmitted as compared to the conventional pulsed case. In this way it is possible to transmit more energy, which increases the SNR, without increasing the peak amplitude of the signal. Methods for exciting the entire aperture have been presented[6–8] , were the different transmitters are encoded via Hadamard or Golay schemes. Another approach has been given in[9] , utilizing signals orthogonal in the frequency domain

---

Further author information: (Send correspondence to F. Gran)
F. Gran: E-mail: fg@oersted.dtu.dk, Telephone: +45 45 25 57 38

for encoding the different transmitters. These techniques, however, have to use several emissions and cannot create a new image after every transmission. In this paper, a novel approach for coded ultrasound imaging will be presented. The transmitters are encoded with mutually orthogonal pseudo-random sequences. The information carried by each individual waveform is extracted at the receiver, and a full image can be created after every transmission. This provides a higher frame rate. The energy of the waveforms transmitted can be controlled by manipulating the length of sequences. First the system model will be explained and the estimation technique for decoding the signals will be analyzed. The beamforming associated with the method will be outlined and finally some simulation results will be presented, where the new method is compared to a standard STA system.

2. SYSTEM MODEL

Consider an ultrasound system with K transmitters and Q receivers. If it is assumed that the dynamics of the system is linear, it is possible to represent the response from the k:th transmitter and the q:th receiver using a linear transfer function. This transfer function includes all processes that effects the received signal, e.g. transducer, propagating medium and scattering. Since the tissue attenuates the transmitted signal exponentially over depth[10] , it is reasonable to assume that the received signal vanishes after a given time interval. Therefore the impulse response between a given transmitter-receiver pair is modeled as a finite impulse response (FIR). The network structure of this model can be viewed in Fig. 1.

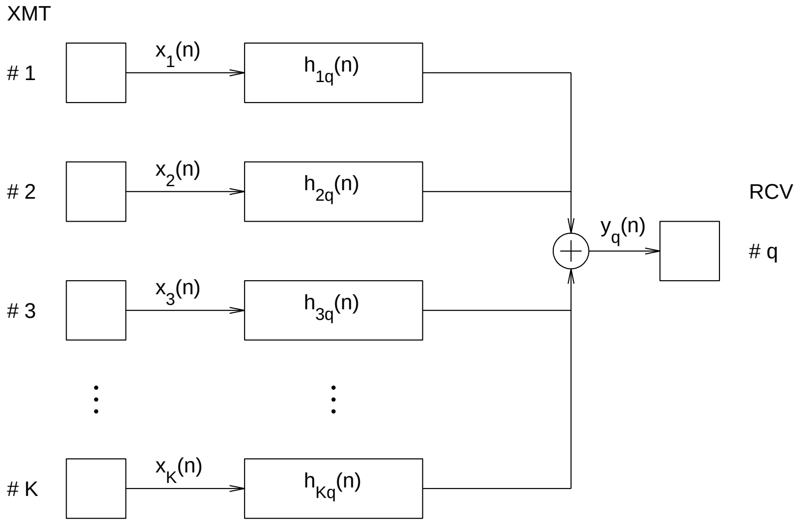

Figure 1. Linear system model for K transmitters and the q:th receiver

The signal transmitted on the k:th transmitter is denoted $x_k(n)$ and the received signal on the q:th receiver is denoted $y_q(n)$. The corresponding impulse response for this transmitter-receiver pair is denoted $h_{kq}(n)$. Therefore, the received signal at the q:th receiver can be written

$$y_q(n) = \sum_{k=1}^{K} h_{kq}(n) * x_k(n) + w(n), \tag{1}$$

where $*$ denotes the convolution operator and $w(n)$ is the system noise. $w(n)$ is assumed to be white, zero mean and gaussian distributed with variance σ_w^2. Equation (1) can be written using matrix operations

$$\mathbf{y}_q = \sum_{k=1}^{K} \mathbf{X}_k \mathbf{h}_{kq} + \mathbf{w}, \tag{2}$$

where $\mathbf{y}_q$ is an $N \times 1$ vector representing the sampled received signal

$$\mathbf{y}_q = \left[\begin{array}{cccc} y_q(0) & y_q(1) & \cdots & y_q(N-1) \end{array} \right]^T. \tag{3}$$

Further, the $M \times 1$ vector $\mathbf{h}_{kq}$ represents the impulse response for the k:th transmitter and the q:th receiver

$$\mathbf{h}_{kq} = \left[\begin{array}{cccc} h_{kq}(0) & h_{kq}(1) & \cdots & h_{kq}(M-1) \end{array} \right]^T, \tag{4}$$

and the matrices $\{\mathbf{X}_k\}_{k=1}^{K}$ are $N \times M$ matrices given by

$$\mathbf{X}_k = \begin{pmatrix} x_k(0) & 0 & \cdots & 0 \\ x_k(1) & x_k(0) & \ddots & 0 \\ \vdots & \ddots & \ddots & \vdots \\ x_k(L-1) & \ddots & \ddots & x_k(0) \\ 0 & x_k(L-1) & \ddots & x_k(1) \\ \vdots & \ddots & \ddots & \vdots \\ 0 & 0 & \cdots & x_k(L-1) \end{pmatrix}, \tag{5}$$

such that $\mathbf{X}_k\mathbf{h}_{kq}$ represents the convolution of the signal $\mathbf{x}_k = \left[\begin{array}{cccc} x(0) & x(1) & \cdots & x(L-1) \end{array} \right]^T$ and $\mathbf{h}_{kq}$. Finally, $\mathbf{w}$ is given by the time series $\mathbf{w} = \left[\begin{array}{cccc} w(0) & w(1) & \cdots & w(N-1) \end{array} \right]^T$. It is possible to write equation (2) on a more compact form using block matrices. Let $\mathbf{X} = \left[\begin{array}{cccc} \mathbf{X}_1 & \mathbf{X}_2 & \cdots & \mathbf{X}_K \end{array} \right]$ and let $\mathbf{h}_q = \left[\begin{array}{cccc} \mathbf{h}_{1q}^T & \mathbf{h}_{2q}^T & \cdots & \mathbf{h}_{Kq}^T \end{array} \right]^T$. Then equation (2) can be written as

$$\mathbf{y}_q = \mathbf{X}\mathbf{h}_q + \mathbf{w}. \tag{6}$$

Equation (6) is the equation which will be used for describing the system model further on in the paper.

3. CHANNEL ESTIMATION

The purpose of the ultrasound system is to measure the reflection coefficient as the ultrasound wave travels through the tissue and reflects the sound wave. In the model given in Fig. 1 this information is contained in the FIR functions between every transmitter-receiver pair. The system has to be capable of extracting the information carried by the individual waveforms $x_1(n)$, $x_2(n)$, $\cdots x_K(n)$, and thereby isolating the received signal on one element emanating from one specific transmitter in order to beamform the image. The task is therefore, to estimate the impulse responses in the vector $\mathbf{h}_q$ from the model given in equation (6). The Maximum Likelihood Estimate (MLE) of $\mathbf{h}_q$ can be derived by considering the conditional probability of receiving $\mathbf{y}_q$ given a set of parameters representing the impulse responses $\mathbf{h}_q$. This probability is given by[11]

$$p(\mathbf{y}_q|\mathbf{h}_q) = \frac{1}{\sqrt{(2\pi\sigma_w^2)^N}} \exp\Big(-\frac{||\mathbf{y}_q - \mathbf{X}\mathbf{h}_q||^2}{2\sigma_w^2}\Big), \tag{7}$$

since $\mathbf{w}$ is assumed to be a zero-mean, gaussian distributed, white process. The Likelihood function (7) has to be maximized with respect to $\mathbf{h}_q$, so that the most probable estimate is chosen. When considering the solution to

$$\arg\max_{\mathbf{h}_q} p(\mathbf{y}_q|\mathbf{h}_q), \tag{8}$$

one can equally well consider the solution to the problem

$$\arg\min_{\mathbf{h}_q} \log(p(\mathbf{y}_q|\mathbf{h}_q)). \tag{9}$$

The minimum of the log-likelihood function is found by differentiating $\log(p(\mathbf{y}_q|\mathbf{h}_q))$ with respect to $\mathbf{h}_q^H$ * and setting it to zero:

$$\frac{\partial}{\partial \mathbf{h}_q^H} \log(p(\mathbf{y}_q|\mathbf{h}_q)) = \mathbf{X}^H\mathbf{X}\mathbf{h}_q - \mathbf{X}^H\mathbf{y}_q = 0. \tag{10}$$

The maximum likelihood estimate of $\mathbf{h}_q$ is hence, given by solving the linear equation system

$$\mathbf{X}^H\mathbf{X}\mathbf{h}_q = \mathbf{X}^H\mathbf{y}_q \tag{11}$$

$$\Downarrow$$

$$\widehat{\mathbf{h}}_q = (\mathbf{X}^H\mathbf{X})^{-1}\mathbf{X}^H\mathbf{y}_q. \tag{12}$$

Clearly, for the parameters in $\mathbf{h}_q$ to be identifiable the matrix $\mathbf{X}^H\mathbf{X}$ has to be invertible. This is true if $\mathbf{X}$ has full column rank[12] . The dimensions of $\mathbf{X}$ is $N \times KM$, for $\mathbf{X}$ to have full column rank the KM columns have to be linear independent. By choosing the transmitted sequences mutually orthogonal with durations such that $N \geq KM$, this can be accomplished. It is now possible to excite all transmitters at the same time and separate the information at the receiver.

4. BEAMFORMING

In Section 3 it was shown that several transmitters can be excited at the same time and the information carried by each individual waveform can be extracted. Since every waveform represents a specific transmitter it is also possible to determine the source of origin for the acoustic wave. If every receiver is treated individually it is therefore possible to exactly determine where the sound wave was transmitted and where it was received. This allows the synthetic aperture focusing technique described in[13] to be applied.

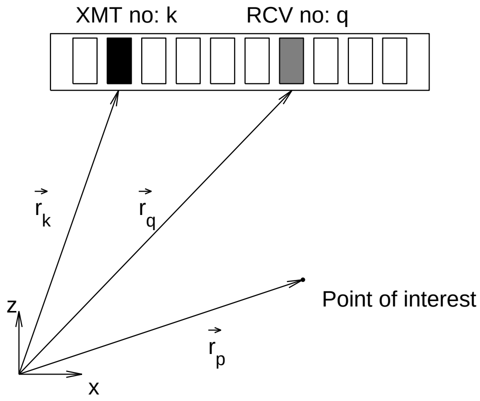

Figure 2. Priciples of synthetic aperture focusing for a point p for the k:th transmitter and the q:th receiver

Since the system has access to defocused transmissions from all transmitters on the aperture, it is possible to focus in any arbitrarily chosen point of interest. The amplitude in a point p in the image is given by

$$H(p) = \sum_{k=1}^{K}\sum_{q=1}^{Q} g_q h_{kq}(t_{pkq}), \tag{13}$$

where g_q is a weighting function over the receiving aperture. Here t_{pkq} is the time corresponding to the geometrical travel distance from the k:th transmitter to the point p and back to the q:th receiver

$$t_{pkq} = \frac{||\vec{r}_p - \vec{r}_k|| + ||\vec{r}_q - \vec{r}_p||}{c}, \tag{14}$$

---

[*] $(\cdot)^H$ denotes the conjugate transpose of $(\cdot)$

where c is the speed of sound, and $\vec{r}_p - \vec{r}_k$ is the vector from the transmitter to the point p, and $\vec{r}_q - \vec{r}_p$ is the vector from the point p to the receiver as indicated in Fig. 2.

5. SIMULATIONS

The method was verified using the virtual software scanner Field II[14] . A B-K Medical BK8804 transducer with 7 MHz center frequency was simulated. This transducer has a pitch of 0.208 mm, a kerf of 0.035 mm, and the height of the elements is 4.5 mm. The sampling frequency was 120 MHz. There was 64 elements in transmit grouped and focused, so that 4 defocused virtual sources were formed[15] . 16 elements were used to form one virtual source by focusing the elements 5 mm in front of the transducer surface. 128 elements were used in the receiving aperture. The central part of the aperture was used in both transmit and receive. In Fig. 3 the impulse responses from the four different virtual sources to the center receiving element can be examined. The object was a point scatter positioned at a depth of 50 mm. Initially, a simulation was performed with a delta function as excitation waveform, using a standard synthetic transmit aperture approach were the transmitters were excited sequentially. The result is given in Fig. 3 as the solid black line. Next the Code Division approach was applied using pseudo random sequences generated by the Matlab command `randn` with a duration of 12.5 μs. The transmitters were excited at the same time and was separated at the receiver using the approach described in Section 3. The result of this simulation is given as the dotted line in Fig. 3. The same simulation was repeated but with additive gaussian distributed white noise with a SNR of 30 dB. The result is given as the solid gray line in Fig. 3.

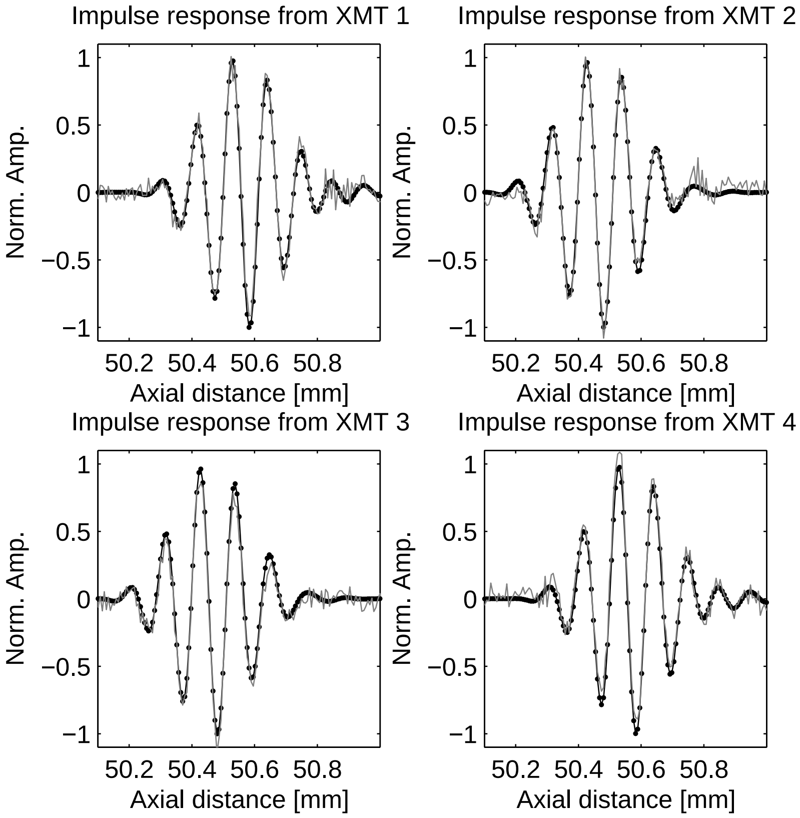

Figure 3. The impulse responses for the different virtual sources to the central receiving element. The solid line is the true impulse response, the dotted line is the estimated impulse response and the solid gray line is the estimated impulse response with a SNR of 30 dB

The average RMS error for the the impulse response estimates for the noise free case was $7.49 \cdot 10^{-11}\%$ which is close to the machine precision. The average RMS error for the the impulse response estimates with a SNR of 30 dB was 26.8%. A simulation of the point spread function (PSF) was also performed. The same system setup was used as before. First the normal synthetic transmit aperture approach was used with a single cycle sinusoid excitation at 7 MHz with temporal Hanning weighting. The beamforming described in Section 4 was applied and the result can be seen to the right in Fig. 4. The top figure is the PSF, whereas the two lower ones are the axial and lateral projections. The same simulation was repeated using the Code Division approach, where all four virtual sources were excited at the same time using pseudo random sequences with a duration of 12.5 μs. The components originating from the different virtual sources were separated and the resulting RF-data was beamformed as described in Section 4. The result can be seen on the left in Fig. 4. For both the Code Division approach and the normal STA approach the axial resolution was 0.23 mm (-3 dB) and 0.31 mm (-6 dB), lateral resolution 0.53 mm (-3 dB) and 0.71 mm (-6 dB) and maximum lateral sidelobe level less than 44 dB.

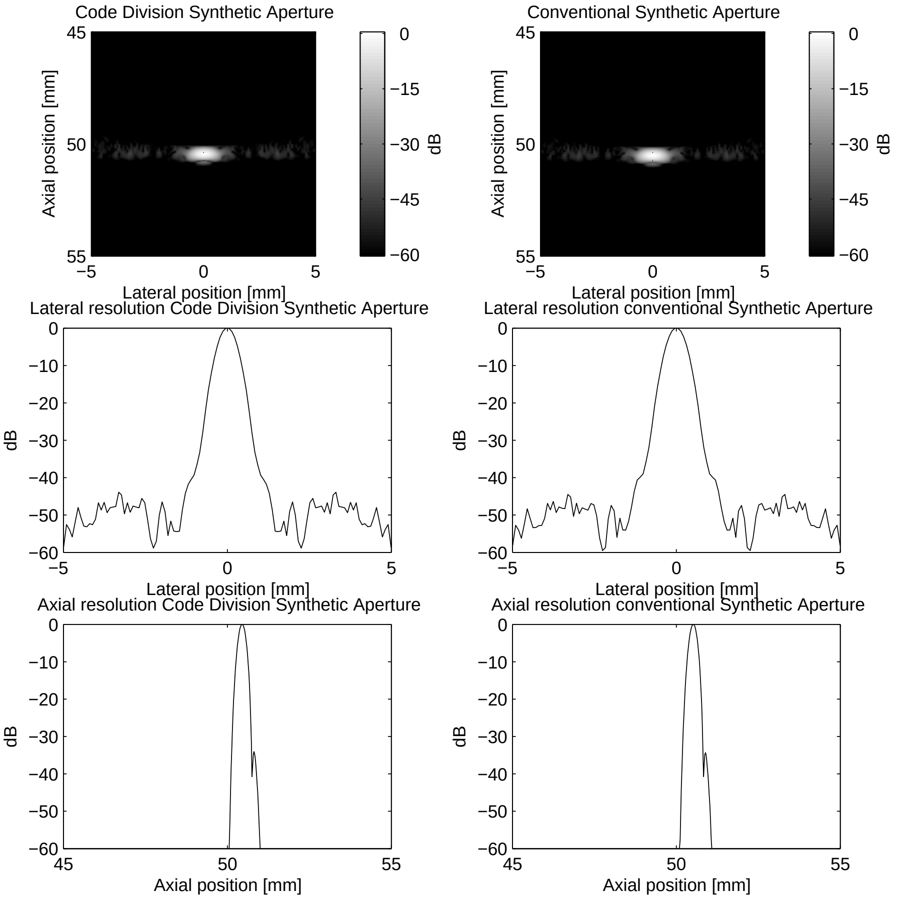

Figure 4. The figures on the left indicate the simulations from the code division approach, whereas the figures on the right indicate the simulations for the normal STA case.

6. CONCLUSION

A new method for exciting all transmitters at the same time has been proposed. A decoding scheme has been presented, enabling the extraction of the individual impulse responses for every transmitter-receiver pair.

Simulations have indicated that the impulse responses estimated exhibit negligible discrepancy from the true impulse responses. The approach has also been proven robust to additive, white, gaussian distributed noise. The performance of the method has been tested by imaging the PSF and comparing it to the PSF produced by a normal STA approach with a single cycle sinusoid excitation. The performance of the Code Division approach was comparable to that of the normal STA case. The limitations of this method are encountered for a system with many transmitters, since the requirement of the signal matrix $\mathbf{X}$ to have full rank will implicitly require that long codes have to be transmitted. This is impractical in a pulsed ultrasound system. Future work will therefore go into solving the problems concerning identifiability of the impulse response parameters.

ACKNOWLEDGMENTS

This work was supported by grant 9700883, 9700563 and 26-01-0178 from the Danish Science Foundation and by B-K Medical A/S, Denmark.

REFERENCES

1. M. O'Donnell, "Coded excitation system for improving the penetration of real-time phased-array imaging systems," *IEEE Trans. Ultrason., Ferroelec., Freq. Contr.* **39**, pp. 341–351, 1992.
2. T. X. Misaridis, K. Gammelmark, C. H. Jørgensen, N. Lindberg, A. H. Thomsen, M. H. Pedersen, and J. A. Jensen, "Potential of coded excitation in medical ultrasound imaging," *Ultrasonics* **38**, pp. 183–189, 2000.
3. T. X. Misaridis, M. H. Pedersen, and J. A. Jensen, "Clinical use and evaluation of coded excitation in B-mode images," in *Proc. IEEE Ultrason. Symp.*, **2**, pp. 1689–1693, 2000.
4. T. X. Misaridis and J. A. Jensen, "An effective coded excitation scheme based on a predistorted FM signal and an optimized digital filter," in *Proc. IEEE Ultrason. Symp.*, **2**, pp. 1589–1593, 1999.
5. T. Misaridis, *Ultrasound imaging using coded signals.* PhD thesis, Ørsted•DTU, Technical University of Denmark, Lyngby, Denmark, 2001.
6. R. Y. Chiao and L. J. Thomas, "Synthetic transmit aperture using orthogonal golay coded excitation," in *Proc. IEEE Ultrason. Symp.*, pp. 1469–1472, 2000.
7. R. Y. Chiao, L. J. Thomas, and S. D. Silverstein, "Sparse array imaging with spatially-encoded transmits," in *Proc. IEEE Ultrason. Symp.*, pp. 1679–1682, 1997.
8. T. Misaridis and J. A. Jensen, "Space-time encoding for high frame rate ultrasound imaging," *Ultrasonics* **40**, pp. 593–597, 2002.
9. F. Gran and J. A. Jensen, "Multi element synthetic aperture transmission using a frequency division approach," in *Proc. IEEE Ultrason. Symp.*, pp. 1942–1946, 2003.
10. J. A. Jensen, *Estimation of Blood Velocities Using Ultrasound: A Signal Processing Approach*, Cambridge University Press, New York, 1996.
11. H. L. V. Trees, *Detection, Estimation and Modulation Theory, Part I: Detection, estimation, and linear modulation theory*, Wiley, 1971.
12. S. H. Friedberg, A. J. Insel, and L. E. Spence, *Linear Algebra*, Prentice-Hall International Editions, 1992.
13. S. I. Nikolov, *Synthetic aperture tissue and flow ultrasound imaging.* PhD thesis, Ørsted•DTU, Technical University of Denmark, 2800, Lyngby, Denmark, 2001.
14. J. A. Jensen, "Field: A program for simulating ultrasound systems," *Med. Biol. Eng. Comp.* **10th Nordic-Baltic Conference on Biomedical Imaging, Vol. 4, Supplement 1, Part 1**, pp. 351–353, 1996b.
15. C. H. Frazier and W. D. O'Brien, "Synthetic aperture techniques with a virtual source element," *IEEE Trans. Ultrason., Ferroelec., Freq. Contr.* **45**, pp. 196–207, 1998.

6.8 Conference paper: Identification of pulse echo impulse response for multi source transmission (Invited)

Published in Conference Record of Thirty-Eighth Annual Asilomar Conference on Signals, Systems, and Computers, vol 1, pp 168-172, 2004

Identification of pulse echo impulse responses for multi source transmission

Fredrik Gran and Jørgen Arendt Jensen

Center for Fast Ultrasound Imaging, Ørsted•DTU, Bldg. 348,
Technical University of Denmark, DK-2800 Kgs. Lyngby, Denmark

Abstract— In this paper a method for acquiring data from several simultaneously transmitting elements in synthetic transmit aperture (STA) ultrasound imaging is proposed. Several transmitters are excited simultaneously using pseudo-random sequences. The received signal at a given time point and receiver is a mixture of the information corresponding to several transmitters. There is, thus, no direct way of determining which information corresponds to which transmitter, preventing proper focusing. In this paper we decode the received signal by estimating the pulse echo impulse responses between every transmitter and receiver pair, using a least squares estimator. The decoding is done instantaneously, making information from several transmitters available after only one transmission. This limits the influence of motion artifacts both in the decoding step and when the STA focusing scheme is applied. The method is evaluated using the simulation tool Field II. Three point spread functions are simulated where axial movement of 1 m/s is present. The axial resolution for the moving scatterer is 0.249 mm (-3dB) and 0.291 mm (-6dB), which is compared to a standard STA transmission scheme with sequential excitation of the transmitters using a chirp excitation. The axial resolution was in this case 0.260 mm (-3dB) and 0.611 mm (-6dB). Also a blood vessel is simulated with an angle of 45° to the acoustic axis with a peak flow of 1 m/s. The velocity is estimated with a mean bias of 2.57% and a mean standard deviation of 0.505% relative to the peak velocity of the flow.

I. INTRODUCTION

In traditional synthetic transmit aperture imaging (STA) one transmitter is active at a time. All receivers are actively listening for echoes from this specific transmitter. The single transmitter is creating a spherical wave, spreading the acoustic energy in all directions simultaneously. This makes it possible to create several image lines in every transmission. By transmitting several times from different locations on the aperture, the full aperture can be synthesized. This makes it possible to attain perfect dynamic transmit- and receive focusing, assuming constant wave propagation velocity.

The drawbacks of this method are, however, poor signal-to-noise ratio (SNR), due to the use of only one transmitter in every transmission, and the method assumes stationarity for coherent summing of the data to synthesize a large aperture. The problem concerning SNR has been addressed previously in [1–4], where it was suggested to create a high energy virtual source by grouping and focusing several transducer elements close to the transducer surface. This can be achieved either by focusing in front or behind the transducer. It has also been proposed [5–9] to use longer linear frequency modulated signals (chirps) to increase the transmitted energy without increasing the maximum amplitude of the transmitted waveform.

Spatial encoding has also been proposed to increase the transmitted energy and thereby increase the SNR. In [10, 11] several transmitters were excited at the same time using an Hadamard encoding scheme. If N transmitters are used simultaneously, N transmissions have to be made for decoding the sequence. Since the decoding is based on several transmissions, tissue motion will degrade the decoding process. In [12] Golay encoding was proposed to spatially encode the transmitters. However, this approach suffers from the same limitations as the Hadamard encoding scheme.

In this paper the latter of the two problems is addressed. A method for spatial encoding using pseudo-random sequences is proposed. This has been suggested previously in [13,14] where pseudo random codes were used to excite several of the transmitters simultaneously. The received signal was then modeled as the weighted sum of the system impulse response for certain scatterer positions. A fixed grid of scatterers is defined and the weights (scatterer strengths) in the image are estimated. In this paper, however, several transmitters are excited simultaneously and are decoded instantaneously at the receiver by estimating the pulse echo impulse response between the transmitters and the receivers. The impulse responses are modeled as FIR filters and no scatter map is defined, which means that no assumptions on the geometry is made. The decoded echoes are then beamformed using a synthetic transmit aperture focusing technique. The principle can be seen in Fig. 1 compared to conventional STA in Fig. 2. The outline of the paper is as follows: in Section II, the theory of the proposed method will be explained and in Section III the beamforming algorithm associated with the method is described. In Section IV a simulation study evaluates the point spread function (PSF) for the proposed method. Additionally a flow simulation is presented where the velocity of the flow is estimated. Finally, concluding remarks are given

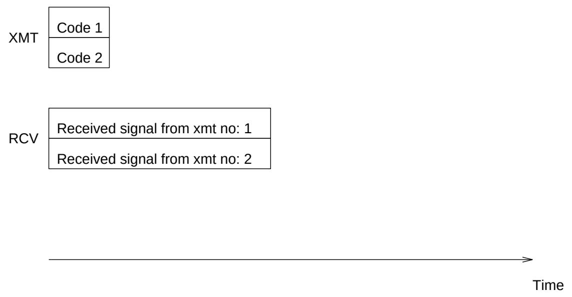
XMT
Code 1
Code 2
RCV
Received signal from xmt no: 1
Received signal from xmt no: 2
Time

Fig. 1. The principle for the proposed method. Two different transmitters are excited simultaneously , yielding a higher effective pulse repetition frequency and a higher frame rate.

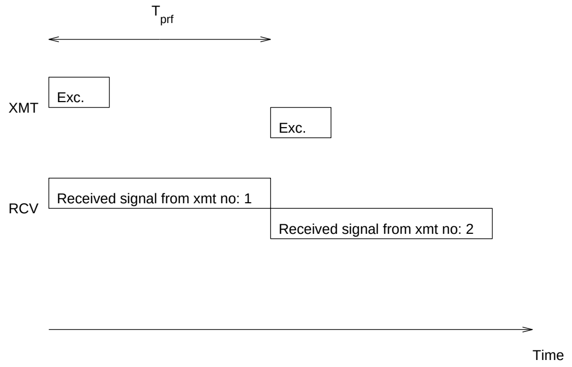
T_prf
XMT
Exc.
Exc.
RCV
Received signal from xmt no: 1
Received signal from xmt no: 2
Time

Fig. 2. The conventional synthetic transmit aperture approach. Every transmitter has access to the system separately, giving a lower pulse repetition frequency.

in Section V.

II. THEORY

Consider a system with K transmitters and Q receivers. Each transmitter is assigned a specific code $x_k(n)$ of length M generated from a white, zero mean process with gaussian probability distribution. It assumed that the system dynamics is linear, and the impulse response between the k:th transmitter and the q:th receiver is modeled by an FIR filter of order N. The impulse response between a given transmitter and receiver pair accounts for all phenomena that effect the transmitted waveform seen from the receiver. This impulse response, thus, represents the transducer impulse response, as well as interaction with tissue, scattering and attenuation. The sampled received signal on the q:th receiving element can then be written

$$y_q(n) = \sum_{k=1}^{K} \mathbf{h}_{qk}^H \mathbf{x}_k(n) + v_q(n) \tag{1}$$

where $\mathbf{h}_{qk} = \begin{pmatrix} h_{qk}^0 & h_{qk}^1 & \dots & h_{qk}^{N-1} \end{pmatrix}^T$ is the impulse response between the k:th transmitter and the q:th receiver and is assumed to be stationary during the transmission. $\mathbf{A}^H$ denotes the complex conjugate transpose of $\mathbf{A}$. The signal vector for transmitter k and time point n is given by $\mathbf{x}_k(n) = \begin{pmatrix} x_k(n) & x_k(n-1) & \dots & x_k(n-N+1) \end{pmatrix}^T$, and $v_q(n)$ is the noise on the q:th receiver, which is assumed to be a white, zero mean, and gaussian distributed process. By writing the received signals on the Q receivers as a vector $\mathbf{y}(n) = \begin{pmatrix} y_1(n) & y_2(n) & \dots & y_Q(n) \end{pmatrix}^T$, a more compact notation gives

$$\mathbf{y}(n) = \mathbf{H}\mathbf{x}(n) + \mathbf{v}(n), \tag{2}$$

where

$$\begin{aligned} \mathbf{H} &= \begin{pmatrix} \mathbf{h}_{11}^H & \mathbf{h}_{12}^H & \dots & \mathbf{h}_{1K}^H \\ \mathbf{h}_{21}^H & \mathbf{h}_{22}^H & \dots & \mathbf{h}_{2K}^H \\ \vdots & \vdots & \ddots & \vdots \\ \mathbf{h}_{Q1}^H & \mathbf{h}_{Q2}^H & \dots & \mathbf{h}_{QK}^H \end{pmatrix} & (3) \\ \mathbf{x}(n) &= \begin{pmatrix} \mathbf{x}_1(n)^T & \mathbf{x}_2(n)^T & \dots & \mathbf{x}_K(n)^T \end{pmatrix}^T, & (4) \end{aligned}$$

and $\mathbf{v}(n)$ is the noise on all receivers to time-point n. The noise on the different receivers are considered to be mutually uncorrelated, such that $E[\mathbf{v}(n)\mathbf{v}^H(n)] = \sigma_v^2 \mathbf{I}^1$,where σ_v^2 is the variance of the system noise. The (windowed) least squares estimate (LSE) at time point l of the impulse response matrix $\mathbf{H}$ is [15]

$$\hat{\mathbf{H}}_{LS}(l) = \hat{\mathbf{R}}_{yx}(l)\hat{\mathbf{R}}_{xx}(l)^{-1}, \tag{5}$$

where

$$\hat{\mathbf{R}}_{xx}(l) = \sum_{n=l-L+1}^{l} \mathbf{x}(n)\mathbf{x}^H(n), \tag{6}$$

$$\hat{\mathbf{R}}_{yx}(l) = \sum_{n=l-L+1}^{l} \mathbf{y}(n)\mathbf{x}^H(n), \tag{7}$$

are the estimates of the auto correlation matrix of $\mathbf{x}(n)$ and the cross correlation matrix of $\mathbf{x}(n)$ and $\mathbf{y}(n)$, respectively. L determines how many observations are used to determine the estimate of $\mathbf{H}(l)$. $\hat{\mathbf{R}}_{xx}$ has to have full rank to identify the correct solution to (5). Since the dimensions of $\hat{\mathbf{R}}_{xx}$ are $KN \times KN$, there has to be at least KN linear independent signal vectors available. After one transmission there are $M+N-1$ observations of the process available. This gives the inequality

$$\begin{aligned} M+N-1 &\geq KN \\ &\Downarrow \\ M &\geq (K-1)N+1, \end{aligned} \tag{8}$$

---

[1] $E[\mathbf{Q}]$ denotes the expectancy value of $\mathbf{Q}$.

if the impulse responses are to be estimated in only one transmission, provided that the signal vectors are linear independent. The KN signal vectors can be made to be linear independent by choosing K different pseudo random sequences satisfying the code length condition given in (8).

III. BEAMFORMING

This section describes the beamforming, which has been applied to properly focus the data. By estimating the impulse response vectors $\mathbf{h}_{qk}$, it is in fact known what the received signal on the q:th receiver would look like if only the k:th transmitter was active and transmitting a delta function.This allows the synthetic aperture focusing technique described in [16] to be applied.

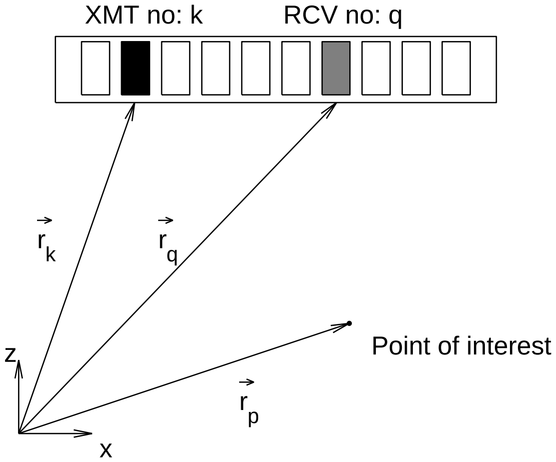

Fig. 3. Principles of synthetic aperture focusing for a point p for the k:th transmitter and the q:th receiver.

Since the system has access to defocused transmissions from all transmitters on the aperture, it is possible to focus in any arbitrarily chosen point of interest. The amplitude in a point p in the image is given by

$$A(\vec{r}_p) = \sum_{k=1}^{K} \sum_{q=1}^{Q} g_q h_{qk}(t_{pqk}), \tag{9}$$

where g_q is a weighting function (apodization) over the receiving aperture, and $h_{qk}(t)$ is the time signal corresponding to the identified impulse response between the q:th receiver and the k:th transmitter. Here t_{pqk} is the time corresponding to the geometrical travel distance from the k:th transmitter to the point p and back to the q:th receiver:

$$t_{pqk} = \frac{||\vec{r}_p - \vec{r}_k|| + ||\vec{r}_q - \vec{r}_p||}{c}, \tag{10}$$

where c is the speed of sound, and $\vec{r}_p - \vec{r}_k$ is the vector from the transmitter to the point p, and $\vec{r}_q - \vec{r}_p$ is the vector from the point p to the receiver as indicated in Fig. 3. Summing focused contributions from all transmitters and transmissions for all receiving elements, gives both dynamic transmit and receive focusing. In this paper the concept of virtual sources is applied. The virtual sources are created by grouping a number of transducer elements and focusing close to the transducer surface [5]. In this way a high energy defocused transmitter is created. In this paper, however, the focusing is made in front of the actual transducer surface. Each virtual source is considered as a single transmitter, and assigned an individual code. Since the virtual source is treated as a single transmitter, a time (depth) compensation has to be applied in the beamforming, to compensate for the displacement of the virtual source compared to the transducer surface.

IV. SIMULATIONS

In this section the proposed method is evaluated using simulations. The simulations are based on the simulation software Field II [17, 18]. In Section IV-A the PSF will be evaluated in three points, where the second point exhibits an axial movement of 1 m/s. In Section IV-B the method will be evaluated by simulating a blood vessel with a parabolic flow profile, where the flow profile is estimated.

A. Point spread function

A 7 MHz, 128 element transducer was simulated. The kerf was 0.035 mm, pitch 0.208 mm and height 4.5 mm. The transmitting aperture was created by grouping and focusing 64 of the central transducer elements, so that 4 virtual sources were formed. The reason for using only the 64 central elements was to minimize the spacing between the virtual sources, to reduce the effect of grating lobes. Each virtual source was created using 16 transducer elements, which were focused 2.5 mm in front of the transducer surface. The receiving aperture used all 128 elements with a Hanning weighting. The simulation sampling frequency was 120 MHz, but the output was downsampled to 40 MHz to reduce the amount of data. The transducer impulse response was set to be two cycles of a sinusoid at 7 MHz with a temporal Hanning weighting. Two different pseudo random sequences were generated by the Matlab function `randn` with a duration of 32.5 μs. This enabled the decoding of two simultaneously transmitting virtual sources, which implied that only two virtual sources could be active at the same time. The two outer most transmitters were excited and decoded in the first transmission, where after the two inner most transmitters were excited and decoded. In this way two low resolution images[2] could be formed in every transmission, which enables fully coherent summing of the two low resolution images. The pulse repetition frequency was set to 8 kHz. Three scatterers were positioned directly below the transducer at depths 30, 40 and 50 mm. The second scatterer was moved with a constant velocity of 1 m/s away from the transducer. The resulting PSF's can be seen in Fig. 5. The reference image was created using the same transducer setup, but the transmitters were excited separately. The excitation waveform was a 20 μs chirp with a center frequency of 7 MHz with a 75% bandwidth. The waveform was tapered using a Tukey window with 10 % tapering. The compression filter was the time reversed excitation waveform, mismatched using a Chebyshev window with a relative attenuation of 70 dB. The mismatching was done to suppress axial sidelobes [9]. The resolution for the proposed method was for the moving scatterer: axially 0.249 mm (-3dB), 0.291 mm (-6dB) and laterally 0.521 mm (-3dB), 0.748 mm (-6dB) and the lateral sidlobe level was below -45 dB. The corresponding resolution for the reference method was: axially 0.260 mm (-3dB), 0.611 mm (-6dB) and laterally 0.489 mm (-3dB), 0.643 mm (-6dB) and the lateral sidlobe level was below -45 dB.

---

[2] The term low resolution image represents the beamformed echoes from only one single transmitter, by summing beamformed data from several transmitters a large aperture can be synthesized creating a high resolution image [16]

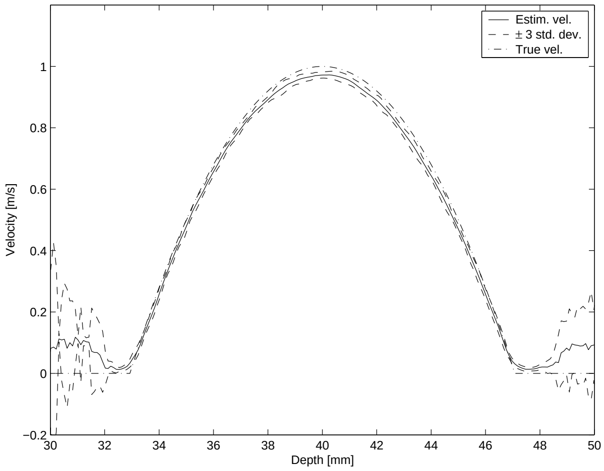

Fig. 4. The estimated flow as a function of depth. The dash dotted line indicates the true flow profile with a peak velocity of 1 m/s. The solid line indicates the mean estimated profile. The dashed line shows the interval of ± 3 standard deviation of the estimated flow profile

B. *Blood flow estimation*

A flow simulation was also performed using Field II. The same transducer setup and excitation was used as in Section IV-A. The vessel was positioned at a depth of 40 mm with a diameter of 10 mm. The flow profile was parabolic with a peak velocity of 1 m/s. The angle between the flow and the acoustic axis was 45°. Since it has been shown previously that it is possible to automatically detect the angle of the flow [19], it was assumed to be known. The beamforming described in Section III was applied to beamform image lines in the direction of the flow. The lateral spatial sampling frequency corresponded to $\frac{\lambda}{40}$. Lines beamformed along the flow direction from one given image were correlated with the corresponding lines from the previous image. The length of the lines were 20 λ. The cross correlation of the lines were used to find the velocity of the flow [19, 20]. The shift in the peak in the cross correlation function indicates the spatial shift of the speckle pattern between two images. Thus, dividing by the time for acquiring the two images yields the velocity estimate. To further improve the velocity estimate, 10 successive cross-correlations were averaged. The estimated velocity as function of depth can be seen in Fig. 4. The mean bias was 2.57% and the mean relative standard deviation was 0.505%. The mean profile and the standard deviation was found from 20 successive velocity estimates. The results are comparable to those found in [20].

V. CONCLUSION

In this paper a method for making the image acquisition faster has been proposed. It is possible to decode the information originating from different transmitters instantaneously, which means that the image can be created faster. The proposed method has been analyzed in simulations of the PSF, where movement of 1 m/s was present. A flow simulation has also been performed with a vessel with an angle of 45° to the acoustic axis. The velocity was estimated with a mean bias of 2.57% and a mean standard deviation of 0.505%. Future work will include

- Impact on signal to noise ratio for the proposed method.
- Feasibility in a physical system.
- Relaxation of the demand on code length

ACKNOWLEDGMENT

This work was supported by grant 9700883, 9700563 and 26-01-0178 from the Danish Science Foundation and by B-K Medical A/S, Denmark.

REFERENCES

[1] M. O'Donnell and L. J. Thomas, "Efficient synthetic aperture imaging from a circular aperture with possible application to catheter-based imaging," *IEEE Trans. Ultrason., Ferroelec., Freq. Contr.*, vol. 39, pp. 366–380, 1992.

[2] M. Karaman, P. C. Li, and M. O'Donnell, "Synthetic aperture imaging for small scale systems," *IEEE Trans. Ultrason., Ferroelec., Freq. Contr.*, vol. 42, pp. 429–442, 1995.

[3] C. Passmann and H. Ermert, "A 100-MHz ultrasound imaging system for dermatologic and ophthalmologic diagnostics," *IEEE Trans. Ultrason., Ferroelec., Freq. Contr.*, vol. 43, pp. 545–552, 1996.

[4] C. H. Frazier and W. D. O'Brien, "Synthetic aperture techniques with a virtual source element," *IEEE Trans. Ultrason., Ferroelec., Freq. Contr.*, vol. 45, pp. 196–207, 1998.

[5] M. O'Donnell, "Coded excitation system for improving the penetration of real-time phased-array imaging systems," *IEEE Trans. Ultrason., Ferroelec., Freq. Contr.*, vol. 39, pp. 341–351, 1992.

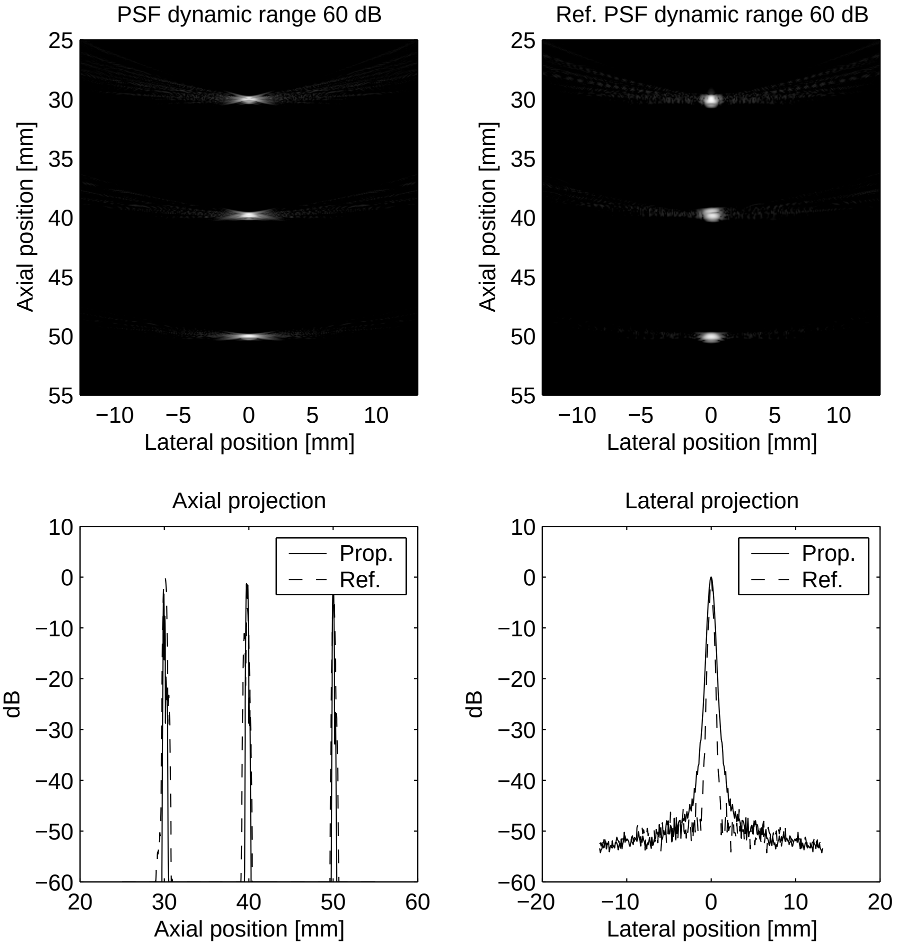

Fig. 5. The PSF's of the proposed method at depths 30, 40 and 50 mm can be seen in the left top figure, whereas the PSF's of the reference method can be seen in the right top figure. The axial an lateral projections can be seen in the left and right bottom figures respectively. (Solid line indicates proposed method, dashed line indicates reference method) The second scatterer is moving with a velocity of 1 m/s.

[6] T. X. Misaridis, K. Gammelmark, C. H. Jørgensen, N. Lindberg, A. H. Thomsen, M. H. Pedersen, and J. A. Jensen, "Potential of coded excitation in medical ultrasound imaging," *Ultrasonics*, vol. 38, pp. 183–189, 2000.

[7] T. X. Misaridis, M. H. Pedersen, and J. A. Jensen, "Clinical use and evaluation of coded excitation in B-mode images," in *Proc. IEEE Ultrason. Symp.*, 2000, vol. 2, pp. 1689–1693.

[8] T. X. Misaridis and J. A. Jensen, "An effective coded excitation scheme based on a predistorted FM signal and an optimized digital filter," in *Proc. IEEE Ultrason. Symp.*, 1999, vol. 2, pp. 1589–1593.

[9] T. Misaridis, *Ultrasound imaging using coded signals*, Ph.D. thesis, Ørsted●DTU, Technical University of Denmark, Lyngby, Denmark, 2001.

[10] R. Y. Chiao, L. J. Thomas, and S. D. Silverstein, "Sparse array imaging with spatially-encoded transmits," in *Proc. IEEE Ultrason. Symp.*, 1997, pp. 1679–1682.

[11] T. Misaridis and J. A. Jensen, "Space-time encoding for high frame rate ultrasound imaging," *Ultrasonics*, vol. 40, pp. 593–597, 2002.

[12] R. Y. Chiao and L. J. Thomas, "Synthetic transmit aperture using orthogonal golay coded excitation," in *Proc. IEEE Ultrason. Symp.*, 2000, pp. 1469–1472.

[13] Jian Shen and Emad S. Ebbini, "A new coded-excitation ultrasound imaging system-part 1: Basic principles," *IEEE Trans. Ultrason., Ferroelec., Freq. Contr.*, vol. 43, no. 1, pp. 131–140, 1996.

[14] Jian Shen and Emad S. Ebbini, "A new coded-excitation ultrasound imaging system-part 2: Operator design," *IEEE Trans. Ultrason., Ferroelec., Freq. Contr.*, vol. 43, no. 1, pp. 141–148, 1996.

[15] S. Haykin, *Adaptive Filter Theory*, Prentice-Hall, Englewood Cliffs, New Jersey, 1986.

[16] S. I. Nikolov, *Synthetic aperture tissue and flow ultrasound imaging*, Ph.D. thesis, Ørsted●DTU, Technical University of Denmark, 2800, Lyngby, Denmark, 2001.

[17] J. A. Jensen and N. B. Svendsen, "Calculation of pressure fields from arbitrarily shaped, apodized, and excited ultrasound transducers," *IEEE Trans. Ultrason., Ferroelec., Freq. Contr.*, vol. 39, pp. 262–267, 1992.

[18] J. A. Jensen, "Field: A program for simulating ultrasound systems," *Med. Biol. Eng. Comp.*, vol. 10th Nordic-Baltic Conference on Biomedical Imaging, Vol. 4, Supplement 1, Part 1, pp. 351–353, 1996b.

[19] J. A. Jensen, "Velocity vector estimation in synthetic aperture flow and B-mode imaging," in *IEEE International Symposium on Biomedical imaging from nano to macro*, 2004, pp. 32–35.

[20] J. A. Jensen and S. I. Nikolov, "Directional synthetic aperture flow imaging," *IEEE Trans. Ultrason., Ferroelec., Freq. Contr.*, pp. 1107–1118, 2004.

6.9 Journal paper: Spatial encoding using a code division technique for fast ultrasound imaging

Submitted to IEEE Transactions on Ultrasonics, Ferroelectrics and Frequency control, May 2005

Spatial encoding using a code division technique for fast ultrasound imaging

Fredrik Gran and Jørgen Arendt Jensen, *Senior Member, IEEE*

Abstract

This paper describes a method for spatial encoding in synthetic transmit aperture ultrasound imaging. This allows several ultrasonic sources to be active simultaneously. The method is based on transmitting pseudo-random sequences to spatially encode the transmitters. The data can be decoded after only one transmission using the knowledge of the transmitted code sequences as opposed to other spatial encoding techniques such as Hadamard or Golay encoding. This makes the method less sensitive to motion, and data can be acquired using fewer transmissions. The aim of this paper is to analyze the underlying theory and to test the feasibility in a physical system. The method has been evaluated in simulations using Field II where the point spread functions were simulated for different depths for a 7 MHz linear array transducer. A signal to noise ratio (SNR) simulation was also included in the study where an improvement in SNR of $\sim$1.5 dB was attained compared to the standard STA firing scheme. Considering the amount of energy transmitted, this value is low. A plausible explanation is given which is verified in simulation. The method was also tested in the experimental ultrasound scanner RASMUS and compared to a synthetic transmit aperture ultrasound imaging scheme using a sinusoidal excitation. The performance of the proposed method was comparable to the reference with an axial resolution of 0.384 mm (-3dB), 0.551 mm (-6dB) and a lateral resolution of 0.938 mm (-3dB), 1.238 mm (-6dB).

I. INTRODUCTION

A conventional ultrasound image consists of a number of lines. A line is measured by a focused transmission in a given direction, and the received signals can be beamformed using either fixed or dynamic focusing. If dynamic focusing in transmit is desirable, several transmissions have to be made per image line. To form a complete high quality image a large number of transmissions have to be made which imposes a severe restriction on stationarity.

In synthetic transmit aperture ultrasound imaging (STA) [1, 2], one transmitting element is active in every transmission, and one or several receiving elements are actively listening for echoes only from this transmitting element. Since only one element is active, the received echoes can be beamformed with dynamic receive focusing to yield several in parallel created receive lines. A larger transmit aperture can be synthesized by changing the physical location of the active element in the next transmission, beamforming the echoes, and combining the results from the two transmissions. This assumes that the object under investigation is fully stationary. The approach can be extended to cover a large amount of transmissions as long as this condition is not violated. STA therefore provides means for both dynamic transmit and receive focusing with a faster acquisition rate since several receive lines are created in parallel.

Two problems arise associated with the STA method.

- Motion leads to non-coherent summation of the data from different transmissions.
- The use of only one transducer element results in poor signal to noise ratio (SNR)

The use of virtual sources [3–6] has been suggested to increase the SNR. This method relies on using a focused sub-array, and treats the focus point as a virtual transmitting element. In [7–11]

Fredrik Gran (fg@oersted.dtu.dk) and Jørgen A. Jensen (jaj@oersted.dtu.dk) are both from the Center for Fast Ultrasound Imaging, Ørsted•DTU, Building 348, Technical University of Denmark, 2800 Kgs. Lyngby, Denmark

the use of linear frequency modulated signals (chirps) was suggested to increase the SNR. These signals make it possible to transmit longer signals with more energy by increasing (or decreasing) the instantaneous frequency of the signal linearly. By matched (or mismatched) filtration, the same axial resolution as with a short excitation waveform can be achieved. A combination of the two approaches can give a significant increase in penetration depth [12].

Spatial encoding has been suggested as means of increasing the SNR. By spatial encoding, several transmitters[1] can be excited simultaneously and separated at the receiver. In this way more acoustic energy can be transmitted with an increase in SNR as a result. Chiao et al. [13] and later also Misaridis and Jensen [14] suggested to use Hadamard encoding to spatially encode the transmitters. The excitation waveforms on the individual transmitters are multiplied by the coefficients of a row (or column) of the Hadamard matrix of the same dimension as the number of transmitters. The decoding is done by adding and subtracting the echoes from transmissions which have been premultiplied by different rows of the Hadamard matrix. Naturally, the same number of transmissions have to be made as the number of active transmitters before the echoes can be decoded. This imposes a restriction on the object under investigation to be fully stationary for the decoding to be done without any artifacts. Chiao and Thomas [15] suggested another method for spatially encoding the transmitters using Golay codes. This method, however, also requires the same number of transmissions as number of active transmitters and suffers from the same drawbacks as Hadamard encoding.

Yet another method for spatial encoding was suggested in [16] and was further developed in [17]. The method is based on dividing the available transducer bandwidth into several sub-bands with ideally disjoint spectral support. In every transmission each transmitter is assigned an individual band. Therefore, the information from a specific transmitter can be separated from the other transmitters instantaneously at the receiver with a simple filtering operation. However, to cover the full bandwidth with all transmitters, several transmissions have to be done to synthesize a broad band spectrum.

A problem for all these approaches, however, is that the decoding is based on data acquired from several transmissions. In this paper this issue is addressed. The purpose is to investigate a method for spatial encoding where the different signals can be decoded with data from one single transmission. A method for spatial encoding based on the findings in [18, 19] using pseudo-random sequences is proposed. Full bandwidth decoding can be performed instantaneously at the receiver using only one transmission. Pseudo random codes have been suggested previously in [20, 21], for spatial encoding purposes. The received signal was modeled as the weighted sum of the system impulse response for certain scatterer positions. A fixed grid of scatterers is defined, and the weights (scatterer strengths) in the image are estimated. In this paper, however, several transmitters are excited simultaneously and are decoded instantaneously at the receiver by estimating the scattering functions between the transmitters and the receivers. The scattering functions are modeled as FIR filters and no scatter map is defined which means that no assumptions on the geometry is made. The decoded echoes are then beamformed using a synthetic transmit aperture focusing technique. The aim of this paper is to explain the theory of the method and to test the feasibility in a physical system.

The paper is organized as follows: in Section II the underlying theory is explained and analyzed, in Section III the beamforming associated with the simulations and measurements is reviewed. Simulations of the point spread functions (PSF) for different depths are given in Section IV along with an analysis of the (peak) SNR. In Section V the PSF is measured in a water tank and in Section VI concluding remarks are given along with a discussion of future work.

II. THEORY

In this section, the theoretical framework for the approach will be derived.

---

[1] The term transmitter can either represent a single transducer element or virtual source.

A. System model

Consider a system with K transmitters and Q receivers. The k:th transmitter is transmitting the code sequence $x_k(t)$. It is assumed that the system is fully linear and that the interaction between the ultrasonic wave and the medium can be described by a linear process. The contribution from transmitter k of the scattered and received signal on receiver q can be written [22]

$$y_q^k(t) = \left\{ \sum_{p=0}^{P} s_p(\vec{r}_p) h_e(\vec{r}_k, \vec{r}_p, t) \star h_r(\vec{r}_p, \vec{r}_q, t) \right\} \star x_k(t). \tag{1}$$

Here P is the total number of scatters in the medium (may be infinite), and $s_p(\vec{r}_p)$ is the scatter strength of the p:th scatterer. $h_e(\vec{r}_k, \vec{r}_p, t)$ is the spatial impulse response from the k:th transmitter to the p:th scatterer, $h_r(\vec{r}_p, \vec{r}_q, t)$ is the spatial impulse response from the scatterer to the q:th receiver, and $\star$ denotes the convolution operator in the time domain. $\vec{r}_p$ is the position of the p:th scatterer, $\vec{r}_k$ is the position of the k:th transmitter and $\vec{r}_q$ is the position of the q:th receiver. The spatial impulse response represents all phenomena which effects the acoustic wave such as the electro-mechanical impulse response of the transducer and attenuation. A scattering function between the k:th transmitter and the q:th receiver is now defined as

$$h_{kq}(t) = \sum_{p=0}^{P} s_p(\vec{r}_p) h_e(\vec{r}_k, \vec{r}_p, t) \star h_r(\vec{r}_p, \vec{r}_q, t). \tag{2}$$

Note that the spatial dependence of this function has been totally incorporated in the sub indexes kq. The total received signal on the q:th receiver can now be written as

$$y_q(t) = \sum_{k=1}^{K} h_{kq}(t) \star x_k(t). \tag{3}$$

This signal is digitized for the purpose of applying digital signal processing. Now, the digitized received signal under influence of noise is written

$$y_q(n) = \sum_{k=1}^{K} h_{kq}(n) \star x_k(n) + v_q(n), \tag{4}$$

where $v_q(n)$ is the digitized noise process on the q:th receiver, and is assumed to be a zero mean and Gaussian distributed process. $h_{kq}(n)$ is the digitized version of the scattering function $h_{kq}(t)$ and $x_k(n)$ is the digitized version of $x_k(t)$ with a duration of N samples. The attenuation in the medium makes the received signal decay over time [23], therefore, it is reasonable to assume that the scattering function is well modeled as a (possibly long) finite impulse response (FIR) process, such that the transfer function of the scattering function can be written

$$H_{kq}(z^{-1}) = \sum_{m=0}^{M-1} h_{kq}(m) z^{-m}, \tag{5}$$

where M is the length of the impulse responses and z^{-1} is the unit backward-shift operator. The output at the q:th receiver can be written

$$y_q(n) = \sum_{k=1}^{K} \sum_{m=0}^{M-1} h_{kq}(m) x_k(n-m) + v_q(n). \tag{6}$$

The network structure of (6) can be seen in Fig. 1.

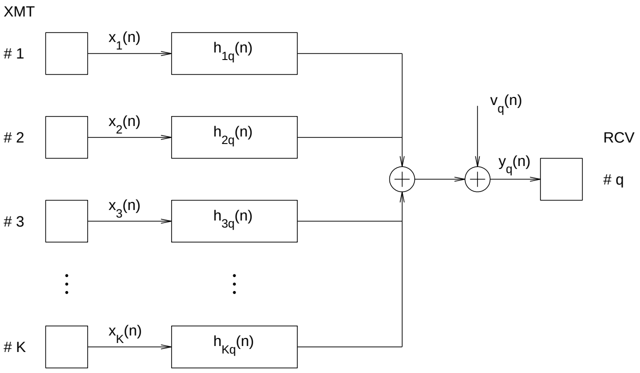

Fig. 1. The network structure of the input/output model of (6).

B. *Decoding and separation by estimation*

The sampled received signal in (6) is now written as a column vector $\mathbf{y}_q = \begin{pmatrix} y_q(0) & y_q(1) & \dots & y_q(N+M-2) \end{pmatrix}^T$ which implies that the convolution between the transmitted waveform and the corresponding scattering function can be written as a matrix operation,

$$\mathbf{y}_q = \sum_{k=1}^{K} \mathbf{X}_k \mathbf{h}_{kq} + \mathbf{v}_q, \tag{7}$$

where

$$\mathbf{h}_{kq} = \begin{pmatrix} h_{kq}(0) & h_{kq}(1) & \dots & h_{kq}(M-1) \end{pmatrix}^T \tag{8}$$

and

$$\mathbf{X}_k = \begin{pmatrix} x_k(0) & 0 & \cdots & 0 \\ x_k(1) & x_k(0) & \ddots & 0 \\ \vdots & \ddots & \ddots & \vdots \\ x_k(N-1) & \ddots & \ddots & x_k(0) \\ 0 & x_k(N-1) & \ddots & x_k(1) \\ \vdots & \ddots & \ddots & \vdots \\ 0 & 0 & \cdots & x_k(N-1) \end{pmatrix}, \tag{9}$$

and $\mathbf{v}_q$ is a zero mean noise process with Gaussian probability distribution and auto-covariance matrix $E[\mathbf{v}_q \mathbf{v}_q^T] = \mathbf{Q}_v$.[2] The result in (7) can be written using a more compact notation by grouping the signal matrices $\mathbf{X}_k$ and the scattering function vectors $\mathbf{h}_{kq}$,

$$\mathbf{y}_q = \underbrace{\begin{pmatrix} \mathbf{X}_1 & \mathbf{X}_2 & \dots & \mathbf{X}_K \end{pmatrix}}_{\mathbf{X}} \underbrace{\begin{pmatrix} \mathbf{h}_{1q} \\ \mathbf{h}_{2q} \\ \vdots \\ \mathbf{h}_{Kq} \end{pmatrix}}_{\mathbf{h}_q} + \mathbf{v}_q. \tag{10}$$

The Maximum Likelihood estimate of the scattering function vector $\mathbf{h}_q$ in (10) is found by first defining the probability distribution of receiving the output $\mathbf{y}$ given a set of scattering functions.

[2] $\mathbf{A}^T$ denotes the transpose of $\mathbf{A}$ and $E[\mathbf{Q}]$ denotes the expectancy value of $\mathbf{Q}$.

The probability distribution under the assumption that the scattering function vector is given only depends on the noise characteristics since this is the only part which is stochastic. Since the noise is assumed Gaussian distributed, the probability distribution is given by

$$\begin{aligned} p_{\mathbf{y}_q|\mathbf{h}_q}(\mathbf{y}_q|\mathbf{h}_q) &= \frac{1}{\sqrt{(2\pi)^{N+M-1}\det(\mathbf{Q}_v)}} \times \\ &\times \exp(-\frac{1}{2}(\mathbf{y}_q - \mathbf{X}\mathbf{h}_q)^T \mathbf{Q}_v^{-1}(\mathbf{y}_q - \mathbf{X}\mathbf{h}_q)). \end{aligned} \tag{11}$$

The objective is to find the set of scattering functions $\mathbf{h}_q$ which maximizes the probability distribution in (11), such that

$$\hat{\mathbf{h}}_q = \arg\max_{\mathbf{h}_q} p_{\mathbf{y}_q|\mathbf{h}_q}(\mathbf{y}_q|\mathbf{h}_q). \tag{12}$$

The solution to this well known optimization problem is given by [24]

$$(\mathbf{X}^T\mathbf{Q}_v^{-1}\mathbf{X})\hat{\mathbf{h}}_q = \mathbf{X}^T\mathbf{Q}_v^{-1}\mathbf{y}_q. \tag{13}$$

The solution to (13) is especially tractable when the noise process is white with variance σ_v^2, such that $\mathbf{Q}_v = \sigma_v^2\mathbf{I}$, where $\mathbf{I}$ is the identity matrix. The linear system of equations in (13) is then reduced to

$$(\mathbf{X}^T\mathbf{X})\hat{\mathbf{h}}_q = \mathbf{X}^T\mathbf{y}_q. \tag{14}$$

Further, the MISO (*multiple-input-single-output*) model in (10) can be generalized to the MIMO (*multiple-input-multiple-output*) case by writing

$$\underbrace{\begin{pmatrix} \mathbf{y}_1^T \\ \mathbf{y}_2^T \\ \vdots \\ \mathbf{y}_Q^T \end{pmatrix}}_{\mathbf{Y}} = \underbrace{\begin{pmatrix} \mathbf{h}_1^T \\ \mathbf{h}_2^T \\ \vdots \\ \mathbf{h}_Q^T \end{pmatrix}}_{\mathbf{H}} \mathbf{X}^T + \underbrace{\begin{pmatrix} \mathbf{v}_1^T \\ \mathbf{v}_2^T \\ \vdots \\ \mathbf{v}_Q^T \end{pmatrix}}_{\mathbf{V}}, \tag{15}$$

where each column in the matrix $\mathbf{Y}$ represents one (multi-dimensional) output sample of the receiving array (Q receiving transducer elements). The set of linear equations corresponding to (14) is for the MIMO case found to be

$$\hat{\mathbf{H}}(\mathbf{X}^T\mathbf{X}) = \mathbf{Y}\mathbf{X}. \tag{16}$$

C. *Identifiability*

The solution to both (14) and (16) are uniquely defined if and only if $\mathbf{X}$ has full column rank [25]. This means that the system of equations must not be under-determined. By analyzing the dimensions of the matrix $\mathbf{X}$, a lower bound on the code length can be derived. The dimensions of $\mathbf{X}$ are $M + N - 1 \times KM$, implying that

$$\begin{aligned} M + N - 1 &\geq KM \\ &\Downarrow \\ N &\geq (K-1)M + 1. \end{aligned} \tag{17}$$

The minimum code length is, thus, dependent on the number of active transmitters in every transmission and the length of the scattering functions which should be estimated.

D. Estimation error

The derivation of the mean square estimation error follows the derivation in [26]. The model is given in (10) and the noise is assumed white with zero mean. If $\mathbf{X}$ has full rank, the Maximum Likelihood Estimate of $\mathbf{h}_q$ can be written

$$\begin{aligned} \hat{\mathbf{h}}_q &= (\mathbf{X}^T\mathbf{X})^{-1}\mathbf{X}^T\mathbf{y}_q \\ &= \underbrace{(\mathbf{X}^T\mathbf{X})^{-1}\mathbf{X}^T\mathbf{X}\mathbf{h}_q}_{\mathbf{h}_q} + \underbrace{(\mathbf{X}^T\mathbf{X})^{-1}\mathbf{X}^T\mathbf{v}_q}_{\mathbf{e}_q}, \end{aligned} \tag{18}$$

where $\mathbf{e}_q$ is the estimation error on the q:th receiving transducer element. The covariance matrix of the estimation error is defined as

$$\begin{aligned} E\left[\mathbf{e}_q\mathbf{e}_q^T\right] &= E\left[(\mathbf{X}^T\mathbf{X})^{-1}\mathbf{X}^T\mathbf{v}_q\mathbf{v}_q^T\mathbf{X}(\mathbf{X}^T\mathbf{X})^{-1}\right] \\ &= (\mathbf{X}^T\mathbf{X})^{-1}\mathbf{X}^T E\left[\mathbf{v}_q\mathbf{v}_q^T\right]\mathbf{X}(\mathbf{X}^T\mathbf{X})^{-1} \\ &= (\mathbf{X}^T\mathbf{X})^{-1}\mathbf{X}^T\mathbf{Q}_v\mathbf{X}(\mathbf{X}^T\mathbf{X})^{-1} \\ &= (\mathbf{X}^T\mathbf{X})^{-1}\sigma_v^2. \end{aligned} \tag{19}$$

If it is assumed that the chosen codes have perfect auto-covariance with a peak E_x corresponding to the energy of the codes, and that the codes are mutually uncorrelated [3], the matrix $\mathbf{X}^T\mathbf{X}$ will simply be a diagonal matrix with the energy of the codes on the diagonal. The result in (19) will, thus, be reduced to

$$\begin{aligned} E\left[\mathbf{e}_q\mathbf{e}_q^T\right] &= (\mathbf{X}^T\mathbf{X})^{-1}\sigma_v^2 \\ &= (E_x\mathbf{I})^{-1}\sigma_v^2 = \frac{\sigma_v^2}{E_x}\mathbf{I}. \end{aligned} \tag{20}$$

This can be interpreted as if the estimation error acts as a white noise process with variance $\frac{\sigma_v^2}{E_x}$ on the actual scattering function. The mean square error of the estimate for the m:th sample in a given scattering function $\{h_{kq}(m)\}_{m=0}^{M-1}$ is therefore given by

$$E\left[|h_{kq}(m) - \hat{h}_{kq}(m)|^2\right] = \frac{\sigma_v^2}{E_x}. \tag{21}$$

The variance of the observed noise will effectively be reduced with a factor corresponding to the energy of the transmitted code sequences.

III. BEAMFORMING

This section describes the beamforming which has been applied to properly focus the data. When the data from one specific transmitter is available, either by applying spatial encoding and separating the signals from the different transmitters at the receiver, or using only one transmitter at a time, it is possible to determine where on the aperture the acoustic wave was transmitted, and where it was received. This allows the synthetic aperture focusing technique described in [2] to be applied.

Since the system has access to defocused transmissions from all transmitters on the aperture, it is possible to focus the acoustic energy on any arbitrarily chosen point of interest. The amplitude in a point p in the image is given by

$$H(\vec{r}_p) = \sum_{k=1}^{K}\sum_{q=1}^{Q} g_q(t_{pkq})h_{kq}(t_{pkq}), \tag{22}$$

---

[3] This will not be the case, however, this assumption will simplify the calculations and provide a lower bound on the estimation error as explained in [26].

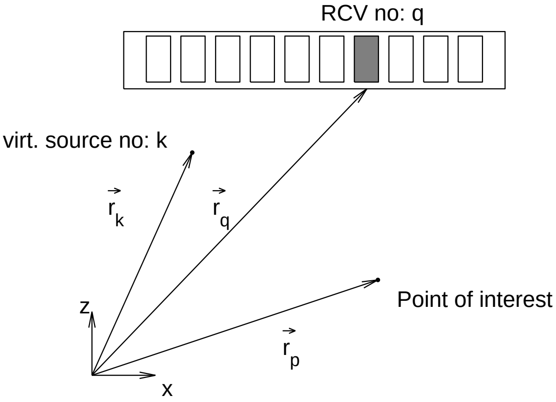

Fig. 2. Principles of synthetic aperture focusing for a point p for the k:th transmitter and the q:th receiver.

where $g_q(t_{pkq})$ is a weighting function (apodization) over the receiving aperture which ideally would be changing with spatial coordinates. However, in this paper the apodization is constant over space and is chosen as a Hanning window over all 128 receiving elements. The time signal $h_{kq}(t)$ is the received (and possibly filtered) echo on the q:th receiver, originating from the k:th transmitter. Here t_{pkq} is the time corresponding to the geometrical travel distance from the k:th transmitter to the point p and back to the q:th receiver:

$$t_{pkq} = \frac{||\vec{r}_p - \vec{r}_k|| + ||\vec{r}_q - \vec{r}_p||}{c}, \tag{23}$$

where c is the speed of sound, and $\vec{r}_p - \vec{r}_k$ is the vector from the transmitter to the point p, and $\vec{r}_q - \vec{r}_p$ is the vector from the point p to the receiver as indicated in Fig. 2. Summing contributions from all transmissions for all receiving elements gives both dynamic transmit and receive focusing.

IV. SIMULATIONS

A simulation study was conducted to compare the method to conventional STA imaging. For this purpose the simulation tool Field II [27, 28] was used. A 7 MHz linear array transducer was simulated. The pitch of the transducer was 0.208 mm, the kerf was 0.035 mm, and the height of the transducer elements was 4.5 mm. The simulated transducer consisted of 128 transducer elements, and the transducer impulse response was approximated by a two cycle sinusoid at 7 MHz with a temporal Hanning weighting. The transmitting aperture consisted of 64 transmitters where one transmitter was created by grouping two transducer elements. This was done to correspond to the succeeding experiments where it is desirable to transmit more acoustic energy to increase SNR. Transmitter one will, thus, represent transducer element one and two, transmitter two will represent transducer element three and four and so on. The spacing between the transmitters will, thus, be twice the distance between the individual transducer elements. The target was four point scatterers positioned at depths 30, 35, 40, and 45 mm.

A. Reference simulation

The reference simulation was created by exciting the transmitters sequentially. The excitation waveform was a four cycle sinusoid at 5 MHz with a temporal Hanning window. The received echoes from each transmission were matched filtered with the time reversed version of the excitation waveform and thereafter beamformed using the approach given in Section III. The image resulting from the 64 transmissions can be seen as the three plots to the left in Fig. 4.

B. Spatially encoded simulation

The spatially encoded simulation was created by exciting transmitter one and thirty-three in the first transmission, transmitter two and thirty-four in the second transmission and so on. Two transmitters were, thus, active in every transmission. In total 32 transmission were made. To separate the echoes originating from the two different transmitters, two binary code sequences were used. The codes were created from a zero mean Gaussian distributed stochastic process. The code sequence was given the value 1 if the result was greater than zero and -1 if the value was less or equal to zero. However, the actual transmitted waveform was the result of the convolution between the code sequence and a secondary sequence applied to decrease the bandwidth of the excitation waveform. The secondary sequence was chosen to be a four cycle 5 MHz sinusoid with temporal Hanning weighting. This can formally be written as

$$s_k(n) = x_k(n) \star c(n), \tag{24}$$

where $s_k(n)$ denotes the transmitted waveform for transmitter k, $x_k(n)$ the code sequence, $c(n)$ the secondary waveform and $\star$ the convolution operator. The distance between succeeding nonzero samples of the code sequences was chosen to be twice the duration of the $c(n)$. The codes and the resulting excitation waveforms can be seen in Fig. 3. The received echoes were first decoded using the decoding approach described in Section II. The separated echoes were thereafter matched filtered using the time reversed version of $c(n)$. Finally, the echoes were beamformed as if both transmitters had been excited separately. The resulting PSFs at 30, 35, 40 and 45 mm can be seen as the three plots to the right in Fig. 4. It can be seen that the spatially encoded approach finds the same response for the four point targets as the reference method. The result is ,however,

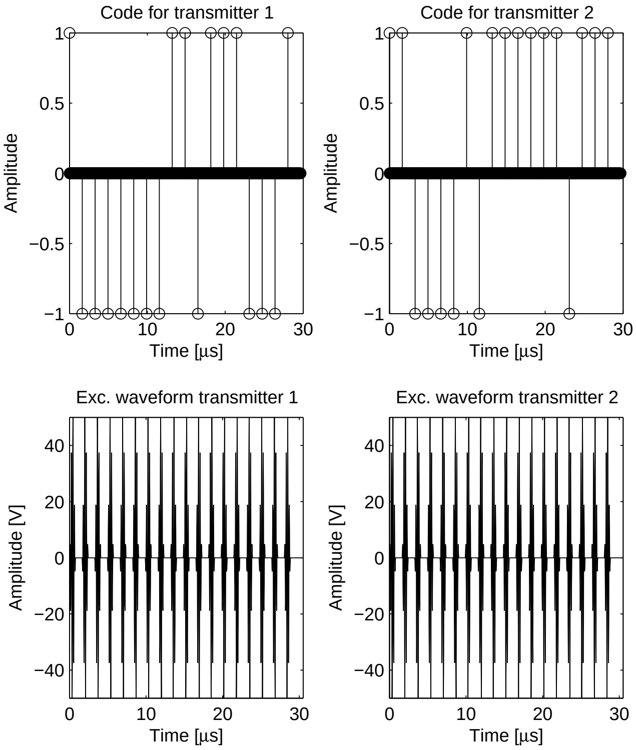

Fig. 3. The binary codes for the two transmitters are given in the top figures, whereas the two lower figures show the actual transmitted waveforms. The coding was generated with a distance between succeeding nonzero samples corresponding to twice the duration of the $c(n)$ waveform.

achieved in 32 transmissions, whereas the reference method uses 64 transmissions. The axial and lateral resolutions for the spatially encoded approach and the conventional STA using a sinusoid excitation can be seen in Table I and II respectively. It can be seen that the resolution is identical. This was, however, expected since the spatially encoded approach should find the true scattering functions for the different transmitters in a situation where the medium is linear and there is no noise present.

	Axial res. mm		Lateral res. mm	
depth	-3dB	-6dB	-3dB	-6dB
30 mm	0.300	0.430	0.170	0.306
35 mm	0.301	0.430	0.221	0.360
40 mm	0.300	0.430	0.251	0.425
45 mm	0.300	0.429	0.295	0.458

TABLE I

RESOLUTION AS A FUNCTION OF DEPTH, SPATIALLY ENCODED IMAGING

	Axial res. mm		Lateral res. mm	
depth	-3dB	-6dB	-3dB	-6dB
30 mm	0.300	0.430	0.170	0.306
35 mm	0.301	0.430	0.221	0.360
40 mm	0.300	0.430	0.251	0.425
45 mm	0.300	0.429	0.295	0.458

TABLE II

RESOLUTION AS A FUNCTION OF DEPTH, PULSED STA

C. *Signal-to-noise-ratio*

When the simulation is done without the influence of noise, the proposed method should find the exact scattering function since the simulation tool is fully linear. However, to evaluate the performance under the influence of noise, a signal-to-noise-ratio simulation was carried out. The same simulations were made as in Sections IV-A and IV-B, but a noise field was added to every set of received data before further processing. The noise fields were generated from a white, zero mean, Gaussian distributed process. By determining the maximum amplitude of the received signals for the spatially encoded approach the variance of the noise field was adjusted such that a SNR of 20 dB on the raw channel data was attained. The same variance was used for all transmissions both for the spatially encoded simulation and the reference simulation. The echoes from the spatially encoded simulation were first decoded using the approach described in Section II and then matched filtered using the time reversed version of $c(n)$. The processing of the echoes resulting from the reference simulation involved only matched filtering. The echoes from both simulations were beamformed in exactly the same way. Since the corresponding simulations without the influence of noise were available, the noise component of the images was found by simply subtracting the image influenced by noise by the corresponding image without noise. The (peak) SNR was then evaluated at the positions of the point targets. The noise variance was estimated by choosing an area of 3 mm×4 mm around the position of the point in the corresponding noise image

$$\hat{\sigma}^2(n_x, n_y) = \frac{1}{N_x N_y} \sum_{i=n_x}^{n_x+N_x} \sum_{j=n_y}^{n_y+N_y} n^2(i - \frac{N_x}{2}, j - \frac{N_y}{2}) \tag{25}$$

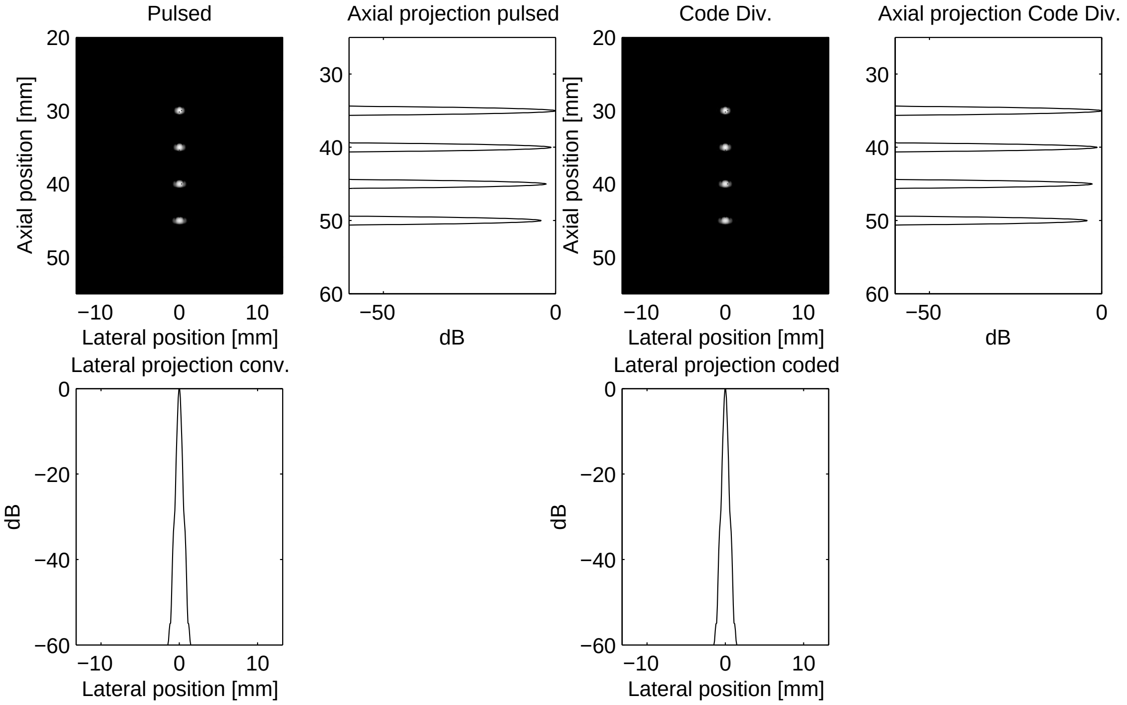

Fig. 4. The PSFs and axial and lateral projections for the two methods (left pulsed STA, right spatially encoded excitation). The two methods have comparable performance in terms of resolution and contrast. The image obtained using traditional STA used 64 transmissions, whereas the image obtained using spatial encoding only used 32 transmissions. The dynamic range of the B-mode images are 50 dB.

where (n_x, n_y) denotes the point position in samples, $N_x \times N_y$ the area over which the variance should be estimated in samples, and $n(i, j)$ the noise image. The SNR is then estimated by

$$SNR(n_x, n_y) = \frac{|s(n_x, n_y)|^2}{\hat{\sigma}^2(n_x, n_y)}, \tag{26}$$

where $s(n_x, n_y)$ is the amplitude in the image at the position of the point scatterers. The gain in SNR for the proposed method was then calculated by computing the ratio between the SNR for the spatially encoded approach and the SNR for the approach using a sinusoid excitation. The gain (in dB) is then

$$G = 10\log_{10}\Big(\frac{SNR_{code.div.}}{SNR_{pulsed}}\Big). \tag{27}$$

The result can be seen in Fig. 5 where it is compared to the ideal gain in SNR predicted in (21). It can be seen that the the ideal gain is ~12.5 dB whereas the actual gain is 1.66 dB. It should be noted that the predicted gain in SNR given in (21) was based on the assumption that the matrix $(\mathbf{X}^H\mathbf{X})^{-1}$ is diagonal. However, in this paper no attempts have been made to make this matrix diagonal, and therefore the ideal gain in SNR will not be achieved. To evaluate how the estimation process effects the variance of the noise, the diagonal elements of $(\mathbf{X}^H\mathbf{X})^{-1}$ should be analyzed. In Fig. 6 the diagonal elements are plotted. Each diagonal element corresponds to a specific sample in the impulse response estimate which means that the variance of the estimation error is a function of depth. The estimation error will act as a noise process in the images and scales linearly with the noise variance σ_v^2. The average variance of the estimation error can be estimated as

$$\tilde{\sigma}_v^2 = \sigma_v^2 \frac{1}{2M} \sum_{m=1}^{2M} \{(\mathbf{X}^H\mathbf{X})^{-1}\}_{m,m}, \tag{28}$$

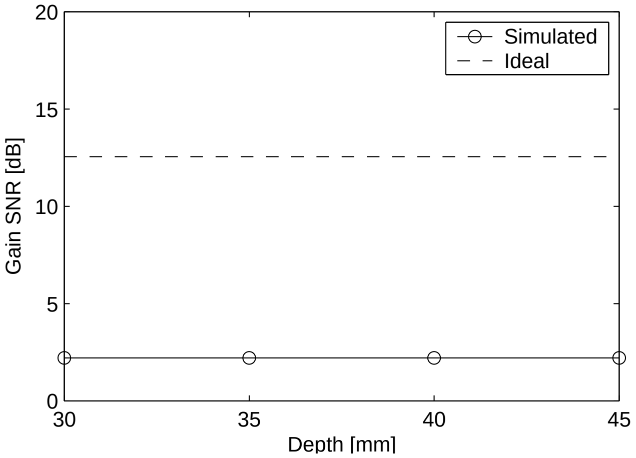

Fig. 5. The SNR as a function of depth. The dashed line indicates the ideal gain in SNR in dB as predicted in (21), whereas the solid line indicates the simulated result.

and gives an indication of the average noise level after decoding. In this paper for the code sequences chosen the quantity in (28) will be $\tilde{\sigma}_v^2 \approx 0.73\sigma_v^2$, which corresponds to an increase in SNR of approximately 1.4 dB. This also explains the discrepancy between the ideal gain in SNR and the actual gain in SNR simulated in Fig. 5.

V. MEASUREMENTS

This section describes the measurements which were done to demonstrate the method. The results in Section V-A show the principle performance of the proposed method with two simultaneously transmitting transmitters an a single receiver. In Section V-B the point spread function is measured and compared to a system using a sinusoidal excitation and sequential excitation and STA beamforming.

A. Simple estimation

The measurements were done using a BK8804 7 MHz linear array transducer(BK-Medical A/S Herlev Denmark). The experimental ultrasound scanner RASMUS [29] was used. RASMUS has access to 128 transmit channels which implied that the central 128 of the 192 existing transducer elements were used. Throughout Section V-A, transmitter one represents transducer element number 43 and 44, and the second transmitter represents element number 63 and 64. Every ”virtual” transmitter is, thus, created by two transducer elements. Transducer element number 64 was the active receiver. The experiments were carried out on a string phantom in water. A metal wire was positioned at 42 mm.

1) Reference: The reference was created by exciting each of the transmitters separately and recording the echoes from the metal wire. A four cycle sinusoid at a center frequency of 5 MHz with temporal Hanning weighting was used as excitation. The center frequency of the excitation waveform was chosen to coincide with the maximum in the system transfer function[4]. The received echoes were matched filtered using the time reversed version of the excitation waveform. The excitation voltage was ±50 V. This experiment was repeated 500 times, and the echoes from the individual experiments were averaged to reduce the noise and give good estimates of the scattering functions for this given excitation. The envelope in logarithmic scale can be seen Fig. 7 and 8 as the solid line.

---

[4] This includes both the transducer and the measurement system.

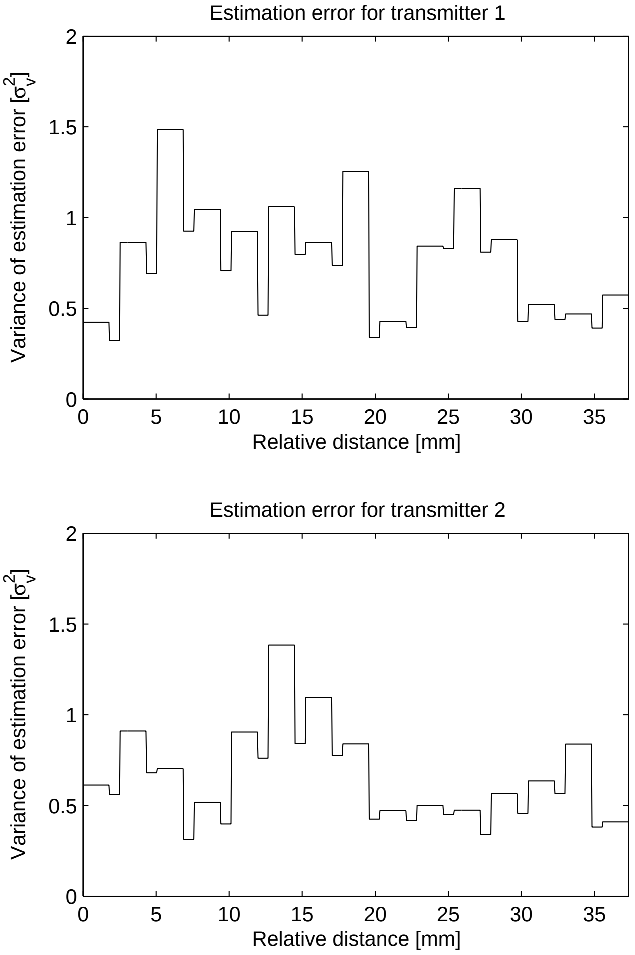

Fig. 6. The variance of the estimation error as a function of depth for the two transmitters. A value above one indicates that the SNR is worsened and a value below one indicates that the SNR is improved compared to the SNR on the raw RF data.

2) Spatially coded excitation: The spatially encoded method was tested experimentally using the same code sequences and excitation waveforms as in the simulations. The transmitters were excited simultaneously and the echoes from the wire were recorded. The excitation voltage was ±50 V. The estimation procedure given in (14) was used to find the scattering functions corresponding to the two transmitters. The decoded signals were then matched filtered with the time reversed version of $c(n)$. The envelope of the result in logarithmic scale can be seen in Fig. 7 and 8 as the dashed line. One realization of the reference experiment is given in Fig. 8 as the dotted line. It can be seen that the coded approach finds the scattering functions with approximately the same accuracy as if the transmitters had been excited separately.

B. Point spread function

The point spread function was measured using the same wire phantom as before. The same measurement system and transducer was used as in Section V-A. The central 128 transducer elements were used. The transducer elements were grouped in pairs, such that two neighboring elements emulated one transmitter. Transducer element one and two create transmitter one, and transducer element 65 and 66 create transmitter 2. Transmitter three represents element three and four, and transmitter four element 67 and 68 and so on. In total there will be 64 transmitters. All 128 transducer elements were used as the receiving aperture with a Hanning apodization.

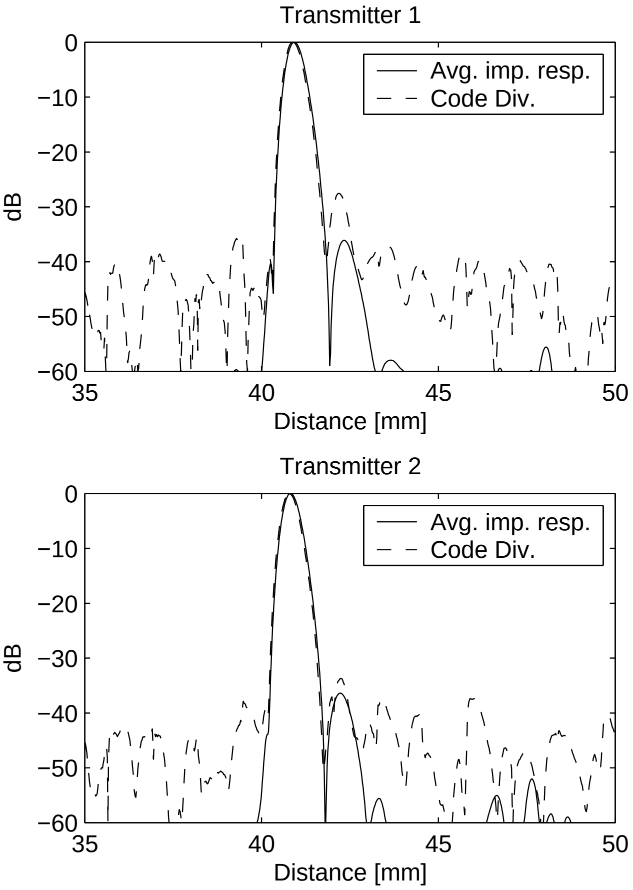

Fig. 7. The envelope of the estimate of the scattering functions for the two transmitters (dashed line). The axial sidelobe level is ∼40 dB. Estimates for the true scattering functions were found by exciting the transmitters separately 500 times and calculating the mean profile (solid line).

1) Reference experiment: For a reference the transmitters were excited sequentially using a 4 cycle sinusoid at 5 MHz with a temporal Hanning weighting. The resulting echoes were matched filtered with the time reversed version of the excitation waveform, and thereafter beamformed using the method described in Section III. The resulting point spread function with a dynamic range of 50 dB can be seen as the left most plot in Fig. 9. The axial and lateral projections was generated by taking the maximum of the rows and columns of the image data matrix, respectively and plotting the result.

2) Coded excitation: The point spread function was obtained by exciting two transmitters simultaneously. In the first transmission transmitter 1 and 2 were excited, in the second transmission transmitter 3 and 4 were used, and so on until all transmitters had been covered. The same code sequences and excitation waveforms as in Section V-A were used. The decoding and filtering performed on the received signals also follows the outline of Section V-A. Once the signals had been separated, the beamforming described in Section III was applied. The resulting point spread function with a dynamic range of 50 dB can be seen as the plot from the left in Fig. 9. The axial and lateral projections was generated by taking the maximum of the rows and columns of the image data matrix, respectively and plotting the result. The axial and lateral resolution can be seen in Table III. It can be seen that the resolution is comparable for the two methods. The axial contrast was also approximately the same with slightly poorer contrast in front of the string for the spatially encoded approach.

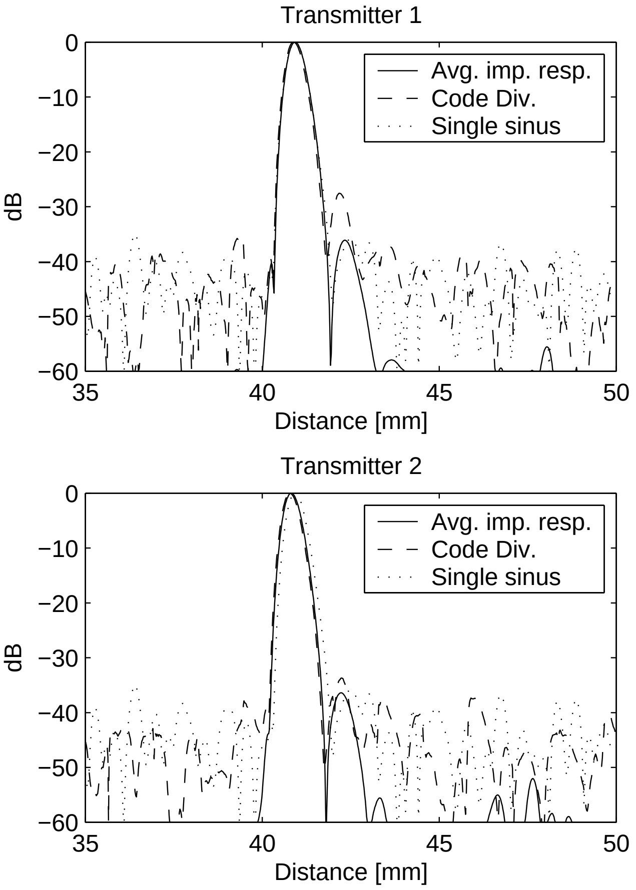

Fig. 8. The envelope of the estimate of the scattering functions for the two transmitters (dashed line). The axial sidelobe level is $\sim$40 dB. The dotted line represents the result from exciting the transmitters sequentially . Estimates for the true scattering functions were found by exciting the transmitters separately 500 times and calculating the mean profile (solid line).

	Axial res. mm		Lateral res. mm	
depth	-3dB	-6dB	-3dB	-6dB
Pulsed STA	0.382	0.549	0.919	1.215
Code. Div.	0.384	0.551	0.938	1.238

TABLE III

RESOLUTION AT 42 MM

VI. CONCLUSION

In this paper a method for spatial encoding was proposed. The method is based on a linear approximation, and the signals originating from different transmitters are separated using maximum likelihood estimation. The data can be separated after only one transmission which shows that fewer transmissions can be made to form a complete image. However, to solve the estimation problem uniquely, a lower limit on the code duration appears which depends on the number of active transmitters and the duration of the scattering functions. According to the theory, in the ideal case, the gain in SNR will be proportional to the energy of the code sequences. This was studied in simulation, where a gain in SNR was $\sim$1.5 dB compared to the pulsed case using a standard synthetic transmit aperture ultrasound imaging technique with twice the number of trans-

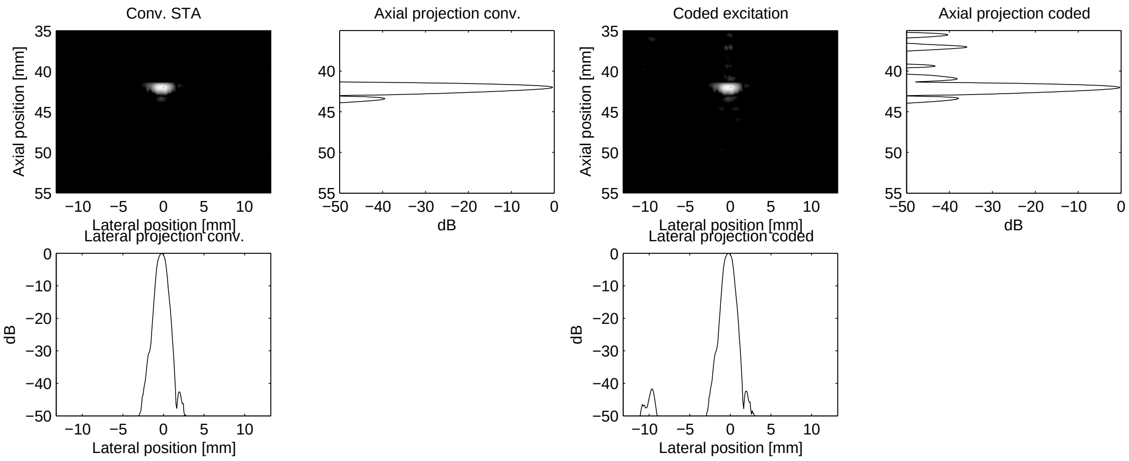

Fig. 9. The PSF of the method based on spatial encoding (two left plots), and the PSF of the reference experiment (two right plots). The dynamic range of the B-Mode images is 50 dB. The spatial encoding approach exhibits slightly poorer axial contrast.

missions. The expected gain in SNR was, however ∼12.5 dB and the discrepancy was traced to choice of code sequences. The PSFs at different depths were also simulated using Field II and were compared to conventional STA where the performance was identical. The method was also tested in a physical system (RASMUS). The PSF was measured in a water tank and was compared to a setup using conventional STA. The performance was comparable to the reference experiment with slightly poorer axial contrast. It shall be noted that the method is based on a linear assumption, and even though water is a strongly non-linear medium (since no attenuation is present), the method still performs acceptable. Future work will be focused on: code design, to achieve the theoretical SNR predicted in this paper, relaxing the demand on code duration, possibly by finding redundancies in the impulse response matrix **H**, and exploiting this.

ACKNOWLEDGMENT

This work was supported by grant 9700883, 9700563 and 26-01-0178 from the Danish Science Foundation and by B-K Medical A/S, Denmark.

REFERENCES

[1] S. Bennett, D. K. Peterson, D. Corl, and G. S. Kino, “A real-time synthetic aperture digital acoustic imaging system,” in *Acoust. Imaging*, P. Alais and A. F. Metherell, Eds., 1982, vol. 10, pp. 669–692.

[2] S. I. Nikolov, *Synthetic aperture tissue and flow ultrasound imaging*, Ph.D. thesis, Ørsted•DTU, Technical University of Denmark, 2800, Lyngby, Denmark, 2001.

[3] M. O’Donnell and L. J. Thomas, “Efficient synthetic aperture imaging from a circular aperture with possible application to catheter-based imaging,” *IEEE Trans. Ultrason., Ferroelec., Freq. Contr.*, vol. 39, pp. 366–380, 1992.

[4] M. Karaman, P. C. Li, and M. O’Donnell, “Synthetic aperture imaging for small scale systems,” *IEEE Trans. Ultrason., Ferroelec., Freq. Contr.*, vol. 42, pp. 429–442, 1995.

[5] C. Passmann and H. Ermert, “A 100-MHz ultrasound imaging system for dermatologic and ophthalmologic diagnostics,” *IEEE Trans. Ultrason., Ferroelec., Freq. Contr.*, vol. 43, pp. 545–552, 1996.

[6] C. H. Frazier and W. D. O’Brien, “Synthetic aperture techniques with a virtual source element,” *IEEE Trans. Ultrason., Ferroelec., Freq. Contr.*, vol. 45, pp. 196–207, 1998.

[7] M. O’Donnell, “Coded excitation system for improving the penetration of real-time phased-array imaging systems,” *IEEE Trans. Ultrason., Ferroelec., Freq. Contr.*, vol. 39, pp. 341–351, 1992.

[8] T. X. Misaridis, K. Gammelmark, C. H. Jørgensen, N. Lindberg, A. H. Thomsen, M. H. Pedersen, and J. A. Jensen, “Potential of coded excitation in medical ultrasound imaging,” *Ultrasonics*, vol. 38, pp. 183–189, 2000.

[9] T. X. Misaridis, M. H. Pedersen, and J. A. Jensen, “Clinical use and evaluation of coded excitation in B-mode images,” in *Proc. IEEE Ultrason. Symp.*, 2000, vol. 2, pp. 1689–1693.

[10] T. X. Misaridis and J. A. Jensen, “An effective coded excitation scheme based on a predistorted FM signal and an optimized digital filter,” in *Proc. IEEE Ultrason. Symp.*, 1999, vol. 2, pp. 1589–1593.

[11] T. Misaridis, *Ultrasound imaging using coded signals*, Ph.D. thesis, Ørsted•DTU, Technical University of Denmark, Lyngby, Denmark, 2001.

[12] K. L. Gammelmark and J. A. Jensen, “Multielement synthetic transmit aperture imaging using temporal encoding,” *IEEE Trans. Med. Imag.*, vol. 22, no. 4, pp. 552–563, 2003.

[13] R. Y. Chiao, L. J. Thomas, and S. D. Silverstein, “Sparse array imaging with spatially-encoded transmits,” in *Proc. IEEE Ultrason. Symp.*, 1997, pp. 1679–1682.

[14] T. Misaridis and J. A. Jensen, “Space-time encoding for high frame rate ultrasound imaging,” *Ultrasonics*, vol. 40, pp. 593–597, 2002.

[15] R. Y. Chiao and L. J. Thomas, “Synthetic transmit aperture using orthogonal golay coded excitation,” in *Proc. IEEE Ultrason. Symp.*, 2000, pp. 1469–1472.

[16] F. Gran and J. A. Jensen, “Multi element synthetic aperture transmission using a frequency division approach,” in *Proc. IEEE Ultrason. Symp.*, 2003, pp. 1942–1946.

[17] F. Gran and J. A. Jensen, “Spatio-temporal encoding using narrow-band linearly frequency modulated signals in synthetic aperture ultrasound imaging,” in *Proc. SPIE - Progress in biomedical optics and imaging*, 2005, p. Accepted for publication.

[18] F. Gran, J. A. Jensen, and A. Jakobsson, “A code division technique for multiple element synthetic aperture transmission,” in *Proc. SPIE - Progress in biomedical optics and imaging*, 2004, vol. 5373, pp. 300–306.

[19] F. Gran and J. A. Jensen, “Identification of spatial impulse responses for multi source transmission,” in *Thirty-Eighth Annular Asilomar Conference on Signals, Systems, and Computers*, 2004, p. Accepted for publication.

[20] J. Shen and E. S. Ebbini, “A new coded-excitation ultrasound imaging system-part 1: Basic principles,” *IEEE Trans. Ultrason., Ferroelec., Freq. Contr.*, vol. 43, no. 1, pp. 131–140, 1996.

[21] J. Shen and E. S. Ebbini, “A new coded-excitation ultrasound imaging system-part 2: Operator design,” *IEEE Trans. Ultrason., Ferroelec., Freq. Contr.*, vol. 43, no. 1, pp. 141–148, 1996.

[22] J. A. Jensen, “A model for the propagation and scattering of ultrasound in tissue,” *J. Acoust. Soc. Am.*, vol. 89, pp. 182–191, 1991a.

[23] J. A. Jensen, *Estimation of Blood Velocities Using Ultrasound: A Signal Processing Approach*, Cambridge University Press, New York, 1996.

[24] L. Ljung, *System Identification, theory for the user*, Prentice-Hall., New Jersey, 1987.

[25] S. H. Friedberg, A. J. Insel, and L. E. Spence, *Linear Algebra*, Prentice-Hall International Editions, 1992.

[26] G. Kang, E. Kosta, M. Weckerle, and E. Schulz, “Optimum channel estimation over frequency-selective fading channel in multiple antenna systems,” in *In Communication Technology Proceedings ICCT 2003*, 2003, pp. 1799–1803.

[27] J. A. Jensen and N. B. Svendsen, “Calculation of pressure fields from arbitrarily shaped, apodized, and excited ultrasound transducers,” *IEEE Trans. Ultrason., Ferroelec., Freq. Contr.*, vol. 39, pp. 262–267, 1992.

[28] J. A. Jensen, “Field: A program for simulating ultrasound systems,” *Med. Biol. Eng. Comp.*, vol. 10th Nordic-Baltic Conference on Biomedical Imaging, Vol. 4, Supplement 1, Part 1, pp. 351–353, 1996b.

[29] J. A. Jensen, O. Holm, L. J. Jensen, H. Bendsen, H. M. Pedersen, K. Salomonsen, J. Hansen, and S. Nikolov, “Experimental ultrasound system for real-time synthetic imaging,” in *Proc. IEEE Ultrason. Symp.*, 1999, vol. 2, pp. 1595–1599.

CHAPTER

SEVEN

Co-authored contributions

It is nearly impossible to carry out an entire Ph.D. project without interacting with other people and exchanging ideas across the boarders of the different research projects. The work presented in this chapter is based on publications where the author of this dissertation has contributed but is not the prime author. The publications herein, do not directly relate to the topic of spatial encoding, but offer an interesting alternative [73] (section 7.1) or an interesting application [74] (section 7.2) to the field.

In [73] all elements are excited simultaneously. The purpose is to emulate a plane wave, which spreads the acoustic energy over the region of interest, rather than focusing the energy in a single point. Hereby, several receive lines can be beamformed in parallel providing a very fast data acquisition rate. In the paper, the effects on spatial resolution, contrast and SNR compared to a conventional focused transmission are analyzed. When the SNR was analyzed, it was found that the system utilizing plane wave transmission attained a lower SNR compared to that of the focal point in the system based on focused transmission. To compensate for this, a linear FM signal was used to temporally encode the transmitting elements. The received signals were then compressed using a mismatched filter. The performance of the proposed imaging system as a blood velocity estimator was also analyzed. The fast data acquisition rate of the system is tractable in blood flow imaging, because it facilitates imaging of rapid fluctuations in the flow profile.

In [74] the synthetic transmit aperture ultrasound imaging is evaluated for 3D imaging. A rotating phased array transducer was used to analyze the performance of the method. The 3D synthetic transmit aperture was created by rotating the array around the elevation axis, and simultaneously transmitting with the array. The position of the active transmitter on the aperture was shifted during data acquisition. Also, the array it self was rotated during transmission and reception. To increase the SNR, a linear FM signal was utilized as excitation waveform. Virtual sources were created both in the transmitting aperture and the receiving aperture.

The full papers are given at the end of this chapter:

- Fast color flow mode imaging using plane wave excitation and temporal encoding.
  Jesper Udesen, **Fredrik Gran** and Jørgen Arendt Jensen
  Accepted for publication Proceedings of SPIE Medical Imaging meeting, Ultrasonic Imaging and Signal Processing, 2005

- Further development of synthetic aperture real-time 3d scanning with a rotating phased array.
  Svetoslav Nikolov, Borislav Tomov, **Fredrik Gran** and Jørgen Arendt Jensen
  Published in Proceedings IEEE Ultrason. Symp., pp 1899-1902, 2003

7.1 Conference paper: Fast color flow mode imaging using plane wave excitation and temporal encoding

Accepted for publication Proceedings of SPIE Medical Imaging meeting, Ultrasonic Imaging and Signal Processing, 2005

Fast color flow mode imaging using plane wave excitation and temporal encoding

Jesper Udesen[a,b], Fredrik Gran[a] and Jørgen Arendt Jensen[a]

[a]Center for Fast Ultrasound Imaging, Ørsted • DTU, Bldg. 348, Technical University of Denmark, DK-2800 Kgs. Lyngby, Denmark
[b]B-K Medical A/S, Mileparken 34, DK-2730 Herlev, Denmark

1. ABSTRACT

In conventional ultrasound color flow mode imaging, a large number (∼ 500) of pulses have to be emitted in order to form a complete velocity map. This lowers the frame-rate and temporal resolution. A method for color flow imaging in which a few (∼ 10) pulses have to be emitted to form a complete velocity image is presented. The method is based on using a plane wave excitation with temporal encoding to compensate for the decreased SNR, resulting from the lack of focusing. The temporal encoding is done with a linear frequency modulated signal. To decrease lateral sidelobes, a Tukey window is used as apodization on the transmitting aperture. The data are beamformed along the direction of the flow, and the velocity is found by 1-D cross correlation of these data. First the method is evaluated in simulations using the Field II program. Secondly, the method is evaluated using the experimental scanner RASMUS and a 7 MHz linear array transducer, which scans a circulating flowrig. The velocity of the blood mimicking fluid in the flowrig is constant and parabolic, and the center of the scanned area is situated at a depth of 40 mm. A CFM image of the blood flow in the flowrig is estimated from two pulse emissions. At the axial center line of the CFM image, the velocity is estimated over the vessel with a mean relative standard deviation of 2.64% and a mean relative bias of 6.91%. At an axial line 5 mm to the right of the center of the CFM image, the velocity is estimated over the vessel with a relative standard deviation of 0.84% and a relative bias of 5.74%. Finally the method is tested on the common carotid artery of a healthy 33-year-old male.

2. INTRODUCTION

In conventional ultrasound imaging used for blood flow estimation (CFM) an image of the flow velocities is formed by focusing a number (∼ 500) of beams. Each beam has a certain time of flight, since the sound has to travel forward and back through the tissue. Hence, the frame rate of a conventional CFM system is often low (∼ 10 Hz) and the temporal resolution in the velocity estimates is therefore poor. The problem becomes even more significant, when structures deep in the human body (e.g. the heart) are scanned. Here, fine temporal details in the blood flow will not be estimated due to the low frame rate. It is therefore of interest to develop methods, which combine a high frame rate with a relatively good performance in terms of bias and standard deviation on the velocity estimates.

The limiting factors on the frame rate can mainly be divided into two types. The first type is the factors connected to the electronics of the scanner. Here, the problem is the trade off between having fast expensive electronics and at the same time producing a scanner which is competitive on the scanner market. The second type of limitations, is the factors connected to the physics of the method implemented in the scanner. This paper addresses the latter type of limitations.

The method called plane wave excitation (PWE) presented in this paper uses different techniques to achieve a high frame rate ($\sim f_{prf}/10$) and a good performance on the velocity estimates.

- A chirp is used as excitation pulse to increase the signal to noise ratio (SNR)
- A plane wave is transmitted from the transducer. One image of the speckle pattern in the region of interest (ROI) is constructed from each transmitted plane wave. This method has previously been suggested for elastography,[1] but has not been used for blood velocity estimation. Mo et al.[2] have suggested a technique where a zone based imaging is performed, but this method does not use a single planewave in transmit, and the velocity estimation is performed using an autocorrelation method.

- Blood velocities are estimated using cross correlation along the lines of flow. This method has previously shown promising results for conventional and synthetic aperture flow.[3–5]

The paper is organized as follows: In Section 3 the theory behind the PWE method is introduced. In Section 4 the spatial resolution for the method is investigated and also the performance in terms of the intensities of the beamformed signals is compared to conventional focused flow imaging. In Section 5 the method is tested using the ultrasound simulation program Field II,[6, 7] where a virtual blood vessel with a parabolic velocity profile is scanned. In Section 6 the PWE method is tested on a circulating flowrig using the experimental ultrasound scanner RASMUS.[8] Finally, in Section 7 the method is tested in-vivo on the carotid artery of a healthy 33-year-old male.

3. THEORY

3.1. Excitation

The fundamental idea in the PWE method is to acquire an image of the whole ROI using only one transmission. This can be done, if the transmitted field is generated by a plane wave, where all transducer elements are excited at the same time. The acoustic energy will then be spread out in the tissue rather than be focused in one specific point. This enables the beamformation over several lines per transmission, but lowers the signal to noise ratio (SNR). To compensate for this degradation of SNR, a linear frequency modulated signal (chirp) is used which increases the (peak) SNR. The theoretical gain in SNR after matched filtration (in dB) is given by[9]

$$G = 10\log_{10}\Big(\frac{E_{chirp}}{E_{ref}}\Big), \tag{1}$$

where E_{chirp} is the energy of the chirp and E_{ref} is the energy of the waveform which is used as a reference. The theoretical gain calculated from (1) will be 20.8 dB. However, due to tapering of the chirp and the compression filter the actual gain will be 14 dB.[10] The excitation waveform is defined as

$$s(t) = a(t)\sin\Big\{2\pi(f_0 - \frac{B}{2})t + 2\pi\frac{B}{2T}t^2\Big\},\ 0 \le t \le T. \tag{2}$$

where $a(t)$ is a temporal weighting function, f_0 is the center frequency, B is the bandwidth, and T is the duration of the excitation waveform. The center frequency is 7 MHz, the bandwidth is 75% of the center frequency and the duration is 20 $\mu s.$ The temporal weighting function is chosen to be a Tukey window with 10% tapering. The compression filter is the corresponding matched filter version of the excitation waveform mismatched using a Chebyshev window with relative sidelobe attenuation of 70 dB. The temporal window applied to derive the mismatched filter is used in order to suppress axial sidelobes.[9]

To decrease lateral sidelobe level, apodization is applied on the transmitting aperture. A Tukey apodization with 70% tapering is used in order to get an acceptable contrast.

3.2. Receive beamforming

The basic principle in the receive beamforming is to beamform every point as a weighted sum of the received echoes. The echoes are delayed such that the delay for a specific receiving element corresponds to the shortest distance from the transducer surface to the point of interest and back to the receiving element. The beamforming principle can be seen in Fig. 1. The beamformed signal to a specific point for an array with Q receiving elements is given by

$$H(\vec{r}_p) = \sum_{q=1}^{Q} w_q s_q(t_q), \tag{3}$$

where $s_q(t)$ is the received echo on the q:th receiving element and w_q is the applied weighting function (apodization) on this element. The sample chosen from the filtered received signals corresponds to the time t_q which is given by

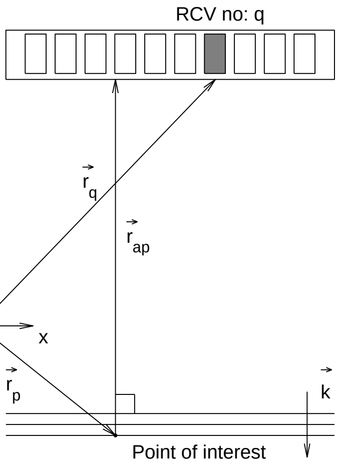

Figure 1. The principles of the beamforming method. Note that the applied delay for a specific received echo for a point in the image, is the shortest distance from the array to the point (which corresponds to the depth of the point) and back to the receiving element in question.

$$t_q = \frac{||\vec{r}_{ap}||}{c} + \frac{||\vec{r}_p - \vec{r}_q||}{c}, \tag{4}$$

where c is the speed of sound in the propagating medium, $\vec{r}_p - \vec{r}_q$ is the vector from the q:th receiving element and out to the field point. The vector $\vec{r}_{ap}$ is the vector which corresponds to the shortest distance from the array to the point. This vector is parallel to the wavevector $\vec{k}$ of the generated plane wave.

3.3. Velocity Estimation

Echo canceling is performed using a mean subtraction algorithm over a number of the acquired images. To estimate the velocity, the data are beamformed along the direction of the blood flow in the ultrasound plane. It has previously been shown that it is possible to find the direction of the flow automatically using one dimensional cross correlation.[5] It is therefore assumed, that the angle of the flow is known. The blood velocity is estimated using a one dimensional cross correlation method,[3] which estimates the velocity of the flow in the direction chosen. The number of plane wave beams used for one velocity frame is two for the simulations and flow rig experiments and 11 for the in-vivo experiments. It is thus possible to estimate a whole frame of independent velocity estimates with a rate of $\sim f_{prf}/10$ Hz.

4. RESOLUTION AND MAXIMUM INTENSITIES

Due to the broad lateral extend of the transmitted field, it is expected that the PWE method will perform worse than conventional flow imaging in terms of resolution. To quantify the resolution a simulation was performed using the ultrasound simulation program Field II.[6,7] A 7 MHz linear array transducer was simulated with 128 elements and the excitation pulse was a plane wave chirp as described in the previous section. The data for the transducer setup can be found in Table 1. The position of the transducer relative to the coordinate system is defined in Fig. 2 In Fig. 3 a point spread function for the PWE method is shown for a point at depth $z = 40$ mm and at lateral position $x = 0$ mm. The lateral and axial widths of the point spread functions are determined by estimating the maximum intensities in the lateral and axial directions. For comparison the corresponding PSF was simulated using a conventionally focused linear array approach (Fig. 4) with a one cycle pulse excitation, and the resolution was calculated. For the conventional linear array PSF the transmit and receive apodizations were changed to a boxcar function, and the transmit focus was situated at 40 mm. The number of elements used

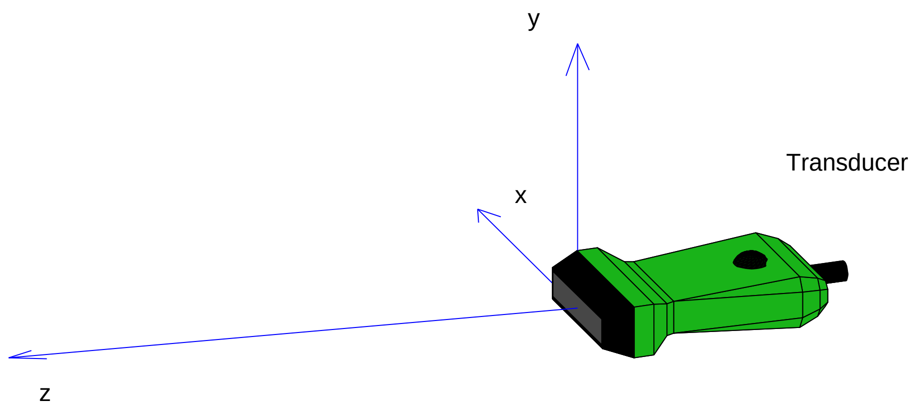

Figure 2. Definition of xyz-coordinate system.

Parameter	Value
Transducer	Linear array
Number of elements	128
Pitch	0.208 mm
Kerf	0.035 mm
Height	4.5 mm
Center frequency	7 MHz
Sampling frequency simulation	100 MHz
Sampling frequency experiments	40 MHz
Apodization in transmit	Tukey
Apodization in receive	Hamming

Table 1. Transducer set-up

for the conventional case are 64. In Fig. 4 it can be seen that the lateral width of the mainlobe is approximately the same for the PWE method compared to the conventional scan.

To get a quantitative measure of the resolution at different depths, the simulation was repeated for point scatters placed at depth between 5 mm and 100 mm, where consecutive points were separated by 2.5 mm. The lateral positions of the points were respectively $x = -5$ mm and $x = 0$ mm. Lateral and axial widths of the 3 dB contours were then determined by estimating the maximum intensities in the lateral and axial directions. The resolution for the PWE method was then compared to a conventional scan with transmit focus at 40 mm, dynamic receive focus and boxcar apodization. The result can be seen in Fig. 5. It can be seen that the lateral resolution is decreased by approximately a factor two at all depths when transmit focusing is not present, i.e. when using the PWE method. However, the axial resolution does not seem to be affected by the lack of transmit focusing in the PWE method.

Due to the broad lateral extend of the transmitted beam in the PWE method it is expected that the maximum intensities in the beam will be significantly lower compared to a focused beam. To quantify the intensities of the PWE method a simulation was performed using the transducer setup from Table 1, but with a one cycle sinusoid as excitation pulse. The maximum intensities in the resulting PSFs were compared to the corresponding case, when the beam was focused in transmit at the point of interest. In Fig. 6 the intensities for the two cases are shown. It is seen that the intensities are approximately 15 dB lower for the PWE method at 40 mm. However, when a chirp is used as excitation pulse in the PWE the intensities will be increased by 14 dB. It should therefore be expected that the signal intensities, and hence the signal to noise ratio, in the PWE method is comparable to normal focused imaging, when a chirp is used as excitation pulse.

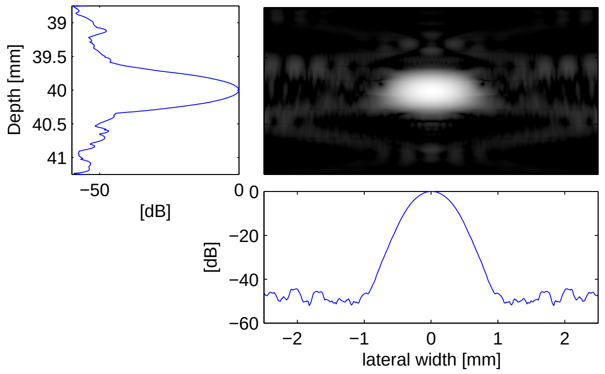

Figure 3. Point spread function (PSF) for the PWE method. Dynamic range is 60 dB.

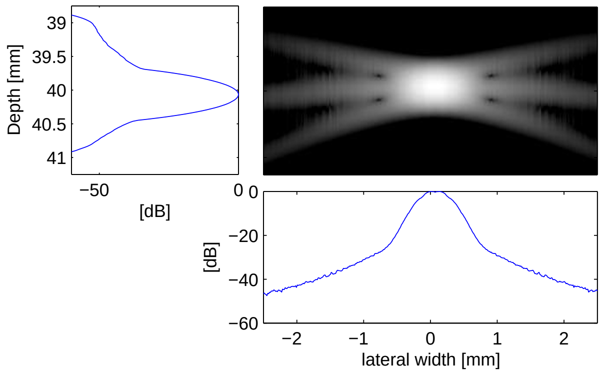

Figure 4. Point spread function (PSF) for conventional focused imaging. Dynamic range is 60 dB.

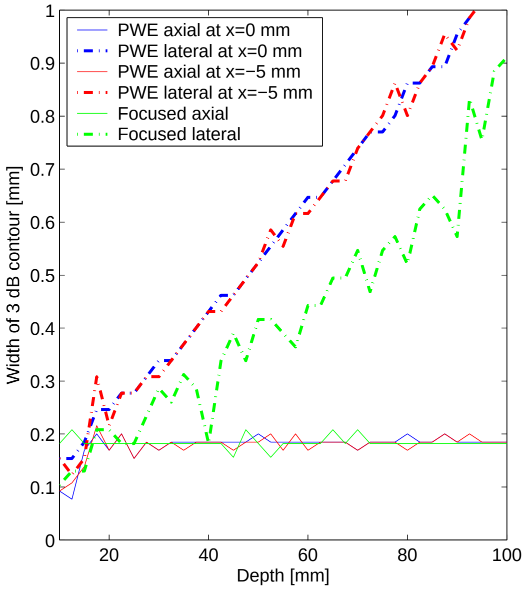

Figure 5. The resolution for the PWE method compared to conventional focused imaging. The axial and lateral widths at -3 dB are shown when a point scatter is located at $x = 0$ mm or $x = -5$ mm. For comparison, the corresponding resolution for a conventional focused scan with transmit focus at 40 mm is also shown.

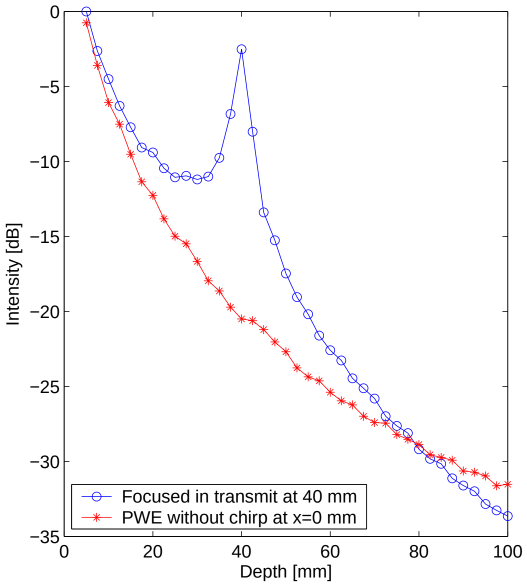

Figure 6. The maximum intensity in the PSFs for the conventional focused beam with transmit focus at 40 mm and for the PWE method without using chirp. The chirp gives an additional 14 dB to the PWE method.

5. FLOW SIMULATIONS

A cylindrical virtual blood vessel situated at a depth of 40 mm with a length of 45 mm and radius of 5 mm was simulated using the Field II program[6, 7] and the transducer described in Table 1. The number of point scatters used to model the vessel was 66,384, to ensure fully developed speckle signals. A beamformed B-mode image of the vessel using the PWE method is shown in Fig. 8. Note that this is acquired using only one pulse emmision. All scatters were moved between consecutive pulse emissions with $f_{prf} = 8$ kHz using a parabolic velocity profile with maximum velocity of 0.5 m/s in the center of the vessel (Fig. 7). The flow angle with respect to the emitted beam was 45°. Two images were acquired using the beamforming described in Section 3.2 and the resulting images were divided into a grid of 250 × 250 points. At these points cross correlation was performed along the lines of flow, where each line to be cross corelated had a length of 10 times the wavelength of the emitted pulse at the center frequency. The spatial sampling interval was 0.1 times the wavelength of the emitted pulse at the

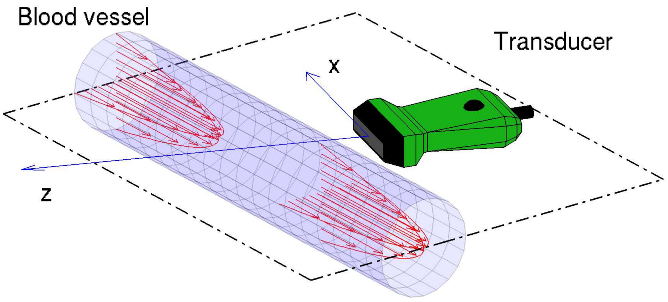

Figure 7. The setup of the virtual blood vessel.

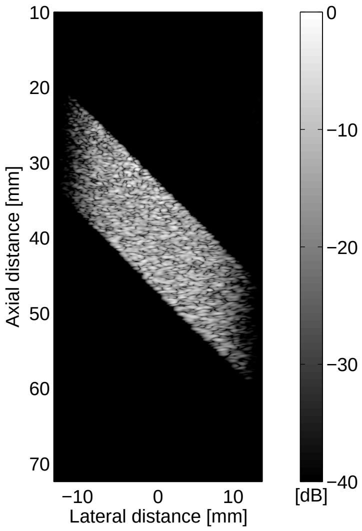

Figure 8. B-mode image of 66,384 point scatters using the Field II program and a single transmission (PWE method).

center frequency, i.e each line to be correlated consisted of 100 samples. The resulting CFM image is shown in Fig. 9 and the velocity at the line $x = 0$ mm is shown in Fig. 10 . Note that these images are acquired using only two pulse emissions.

6. FLOW PHANTOM EXPERIMENTS

The PWE method was evaluated on a circulating flowrig, which pumps blood mimicking fluid around a closed circuit. To avoid entrance effects in the flow, the fluid was first led through a 1.2 m long inflow pipe with radius $R = 6.4$ mm. At the end of the inflow pipe the fluid was led through a heat shrink tube submerged in a water container and scanned. The tube had an internal radius of 6.7 mm and the walls were 0.5 mm thick. The fluid volume flow Q was measured using a Danfoss MAG 1100 flow meter, which was situated after the heat shrink tube.

To drive the fluid around the closed circuit, a Cole Parmer (Vernon Hills, IL) 75211-60 centrifugal pump was used. The blood mimicking fluid consisted of water, glycerol, orgasol, Triton x-100, NaBenzoat and K_2EDTA diluted 10 to 1 with demineralized water. Viscosity was $\mu = 2.6 \cdot 10^{-3}$ kg/(m s), density $\rho = 10^3$ kg/m^3, and temperature during scanning was $T_0 = 24°C$.

The experimental ultrasound scanner RASMUS[8] and a 7 MHz linear array transducer characterized by the parameters in Table 1 and $f_{prf} = 2$ kHz, was used to scan the blood mimicking fluid and store the data for off-line processing. The Reynolds number of the flow was below 2000, hence the flow was assumed laminar and parabolic.[11] The maximum velocity in the center of the pipe was 0.32 m/s.

The blood vessel was situated at a depth of 40 mm at an angle of 60° with respect to the ultrasound beam. For each pulse emission a beamformed image of the ROI was created and echo canceling was performed by subtracting the mean value of all the 50 images acquired. The echo canceled images were divided into 150 × 150 points where the velocity was estimated at each point using 1D cross correlation along the direction of flow. Each line to be cross correlated had a spatial sampling interval of 0.15 times the wavelength of the emitted pulse at the center frequency and a length of 15 times the wavelength of the emitted pulse at the center frequency.

Using two echo canceled images a CFM mode image was created (Fig. 11). Due to the low number of correlated data (two images), false peaks are present in the CFM image. The image can be improved by using more pulse transmissions. In Fig. 12 the CFM image is made from 11 pulse transmissions.

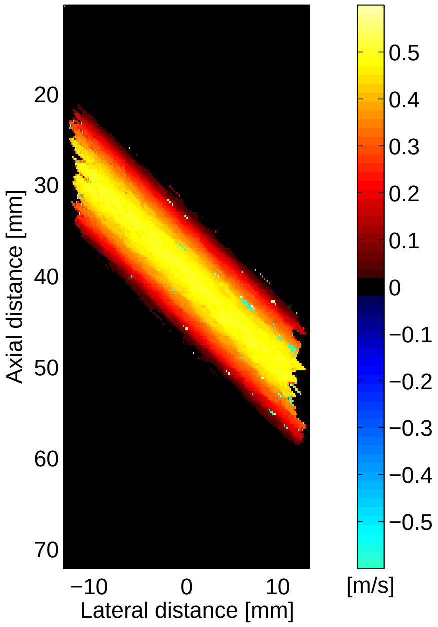

Figure 9. CFM-mode image of a virtual blood vessel. Two emissions with a plane wave chirp was simulated using the Field II program. The velocity was estimated using 1D cross correlation along the direction of flow. The direction of the flow is from the upper left corner to the lower right.

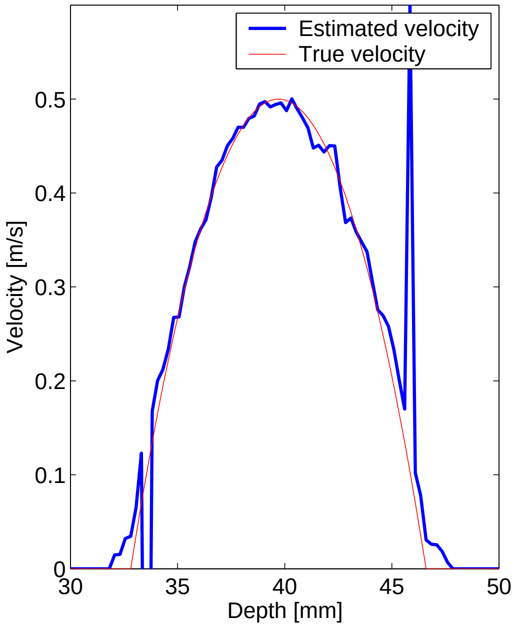

Figure 10. The velocity estimated at the line given by x=0 mm.

To verify that the derived CFM image is in agreement with the actual flow in the pipe, the velocity was estimated at two cross sections through the scanned area, where the lateral position x was $x = 0$ mm and $x = 5$ mm. 50 CFM images were used to find the mean velocity and standard deviation. The resulting mean velocity profile and standard deviation for $x = 0$ mm is shown in Fig. 13 together with the theoretical parabolic velocity profile. The velocity is estimated over the vessel with a mean relative standard deviation of 2.64% and a mean relative bias of 6.91%.

In Fig. 14 the profiles for $x = 5$ mm are shown. The velocity is estimated over the vessel with a relative standard deviation of 0.84% and a relative bias of 5.74%. This performance is comparable to conventional flow imaging.[12]

7. IN VIVO MEASUREMENT

An in vivo experiment was performed on a healthy 33-year-old male using the RASMUS scanner connected to the transducer defined by the parameters from Table 1 and with a pulse repetition frequency of $f_{prf} = 2$ kHz. The common carotid artery was scanned for two seconds and data were saved for off-line beamforming.

Echo canceling was performed by subtracting the mean value from 11 consecutive images. The echo canceled images were then divided into 150 × 150 points where the velocity was estimated at each point using 1D cross correlation along the direction of flow. Each line to be cross correlated had a spatial sampling interval of 0.3 times the wavelength of the emitted pulse at the center frequency and a length of 15 times the wavelength of the emitted pulse at the center frequency. To decrease the standard deviation on the estimates 11 lines were cross correlated and averaged before the maximum was estimated. This means that completely independent velocity images of the artery are acquired every $11/f_{prf} = 5.5$ ms.

In Fig. 15 the resulting CFM image is shown when data are acquired at the peak systolie. The B-mode image is estimated from one plane wave pulse transmission and no filtration of the velocity image has been performed.

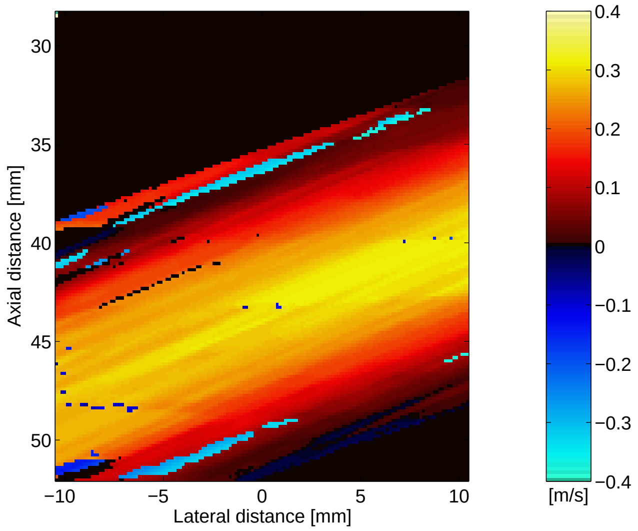
Axial distance [mm]
30
35
40
45
50
−10
−5
0
5
10
Lateral distance [mm]
0.4
0.3
0.2
0.1
0
−0.1
−0.2
−0.3
−0.4
[m/s]

Figure 11. Data from two pulse emissions were used to make a CFM-mode image of flow in an experimental flowrig. The experimental RASMUS scanner was used to acquire data. The velocity is only estimated in the tube containing the blood mimicking fluid.

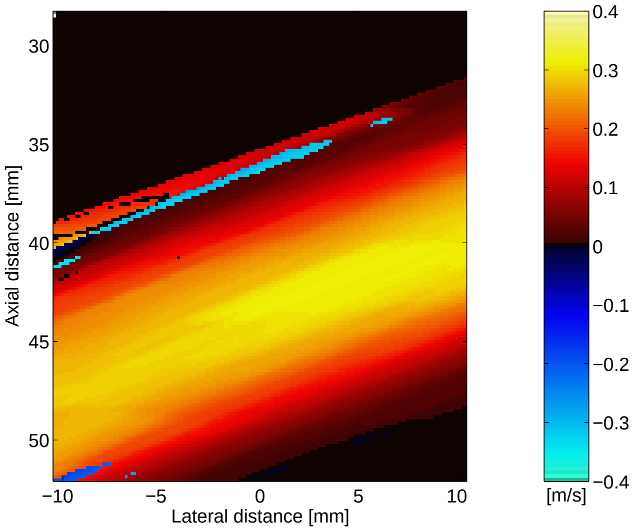
Axial distance [mm]
30
35
40
45
50
−10
−5
0
5
10
Lateral distance [mm]
0.4
0.3
0.2
0.1
0
−0.1
−0.2
−0.3
−0.4
[m/s]

Figure 12. Data from 11 pulse emissions were used to make a CFM-mode image of flow in an experimental flowrig. The velocity is only estimated in the tube containing the blood mimicking fluid.

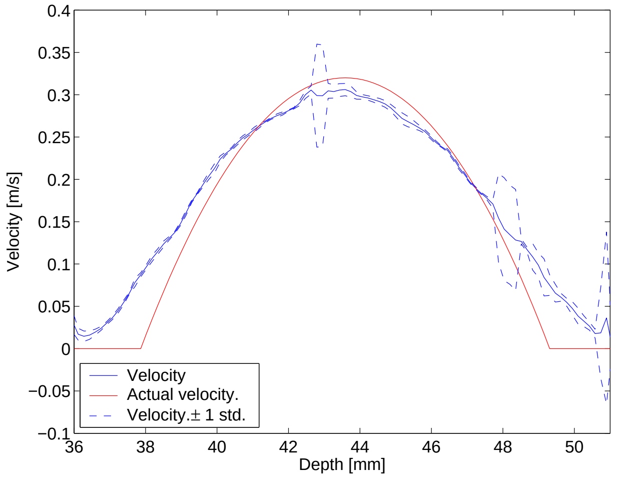

Figure 13. The mean velocity and standard deviation as a function of depth for the line defined at $x = 0$ mm from Fig. 11. Two pulse emissions used for each estimate.

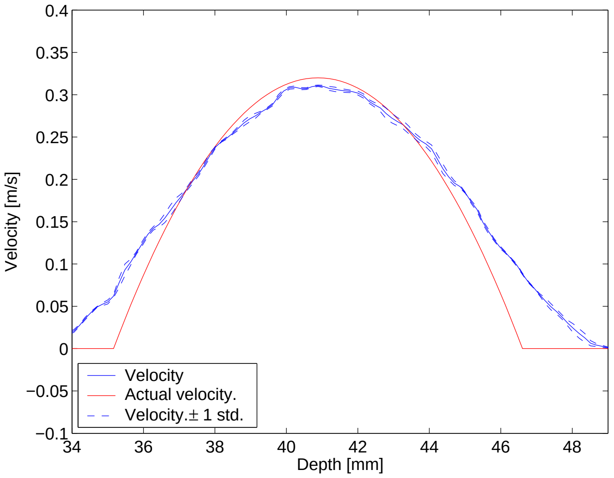

Figure 14. The mean velocity and standard deviation as a function of depth for the line defined at $x = 5$ mm from Fig. 11. Two pulse emissions used for each estimate.

8. DISCUSSION

It has been verified in simulations and experiments, that it is possible to obtain a CFM-mode image using less than 12 pulse emissions, when plane wave chirps are used as excitation pulses. If fast accelerating flow (e.g. in the heart) is to be estimated, the PWE method, thus, has the potential of showing temporal variations in the flow, which could not be estimated using a conventional method.

Furthermore, we believe that the PWE method also has potentials for 3D flow estimation using a 2D linear array transducer. Conventional methods for 3D flow based on focused transmit beams will have to compromise performance if a high frame rate is desired. This is due to the high (> 100) number of beams needed to cover the

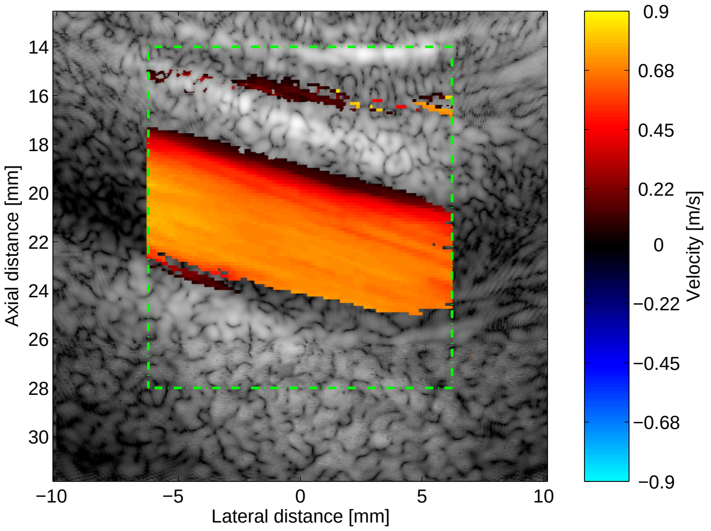

Figure 15. In vivo measurement of the common carotid artery of a healthy 33-year-old male at the time of the peak systolie. The velocity image is estimated from 11 plane wave pulse transmissions and the B-mode image is estimated from one plane wave pulse transmission. The B-mode image has a dynamic range of 40 dB and no filtration of the velocity data has been performed other than echo canceling. The velocity is only estimated within the green dashed line.

whole 3D ROI. The PWE method can cover the 3D ROI in only one pulse emission and in principle maintain the same performance as in the 2D case.

REFERENCES

1. M. Tanter, J. Bercoff, L. Sandrin, and M. Fink, "Ultrafast Compound Imaging for 2-d Motion Vector Estimation: application to Transient Elastography," *IEEE Trans. Ultrason., Ferroelec., Freq. Contr.* **49**, pp. 1363–1374, 2002.
2. L. Y. L. Mo, T. L. Ji, C. H. Chou, D. Napolitano, G. W. McLaughlin, and D. DeBusschere, "Zone-based color flow imaging," in *Proc. IEEE Ultrason. Symp.*, pp. 29–32, 2003.
3. J. A. Jensen, "Directional velocity estimation using focusing along the flow direction: I: Theory and simulation," *IEEE Trans. Ultrason., Ferroelec., Freq. Contr.* , pp. 857–872, 2003.
4. J. A. Jensen and R. Bjerngaard, "Directional velocity estimation using focusing along the flow direction: II: Experimental investigation," *IEEE Trans. Ultrason., Ferroelec., Freq. Contr.* , pp. 873–880, 2003.
5. J. A. Jensen, "Velocity vector estimation in synthetic aperture flow and B-mode imaging," in *IEEE International Symposium on Biomedical imaging from nano to macro*, pp. 32–35, 2004.
6. J. A. Jensen and N. B. Svendsen, "Calculation of pressure fields from arbitrarily shaped, apodized, and excited ultrasound transducers," *IEEE Trans. Ultrason., Ferroelec., Freq. Contr.* **39**, pp. 262–267, 1992.
7. J. A. Jensen, "Field: A program for simulating ultrasound systems," *Med. Biol. Eng. Comp.* **10th Nordic-Baltic Conference on Biomedical Imaging, Vol. 4, Supplement 1, Part 1**, pp. 351–353, 1996b.
8. J. A. Jensen, O. Holm, L. J. Jensen, H. Bendsen, H. M. Pedersen, K. Salomonsen, J. Hansen, and S. Nikolov, "Experimental ultrasound system for real-time synthetic imaging," in *Proc. IEEE Ultrason. Symp.*, **2**, pp. 1595–1599, 1999.

9. T. Misaridis, *Ultrasound imaging using coded signals.* PhD thesis, Ørsted•DTU, Technical University of Denmark, Lyngby, Denmark, 2001.
10. T. X. Misaridis and J. A. Jensen, “An effective coded excitation scheme based on a predistorted FM signal and an optimized digital filter,” in *Proc. IEEE Ultrason. Symp.*, **2**, pp. 1589–1593, 1999.
11. D. J. Acheson, *Elementary Fluid Dynamics*, Clarendon Press, Oxford, 1990.
12. J. A. Jensen, *Estimation of Blood Velocities Using Ultrasound: A Signal Processing Approach*, Cambridge University Press, New York, 1996.

7.2 Conference paper: Further development of synthetic aperture real-time 3d scanning with a rotating phased array

Published in Proceedings IEEE Ultrason. Symp., pp 1899-1902, 2003

FURTHER DEVELOPMENT OF SYNTHETIC APERTURE REAL-TIME 3D SCANNING WITH A ROTATING PHASED ARRAY

Svetoslav Ivanov Nikolov, Borislav Guerguiev Tomov, Fredrik Gran and Jørgen Arendt Jensen
Center for Fast Ultrasound Imaging, Bldg 348, Ørsted•DTU, Technical University of Denmark
DK-2800 Kgs. Lyngby, Denmark

Abstract - In a previous paper we have presented an approach combining synthetic transmit aperture imaging with a rotating phased array. The method is implemented on a specially made Vermon transducer capable of rotating at 5 Hz. The center frequency of the transducer is 3.2 MHz, and the pitch is 0.22 mm. The array active diameter is 16 mm and the number of elements is 64. The method is capable of scanning 10 volumes/sec. The order in which the transmit elements were fired made it possible to achieve lateral resolution of a 0.94 mm at 45 mm depth, which is comparable to a standard B-mode scan.

The penetration depth was $>$10 cm due to the use of 20 μs long frequency modulated (FM) pulses. The dynamic range was limited to 45 dB because of the non-optimized FM pulse and grating lobes.

This paper presents the work on improving the image quality of the approach: (1) instead of defocusing conventional focusing with an f-number of 1 is used in transmit to create spherical waves, (2) virtual receive elements are synthesized to decrease noise and grating lobes, (3) the compression filter for the FM pulses was modified to suppress the range lobes (4) additional hardware for synchronization is built.

I OVERVIEW

Real-time 3-D ultrasound imaging has been the goal of many researchers for over a decade. The main question is how to avoid the tradeoff between speed of acquisition and image quality. Lockwood et al. suggested the use of synthetic *transmit* aperture ultrasound imaging combined with mechanical motion of a phased array to scan 3-D volumes [1]. In that method, the array is ”rocking”, and the planes are scanned and beamformed independently one from another using only a few emissions. The use of such a sparse aperture results in high side-lobes.

In 2002, we presented a new approach for acquiring the volume [2]. The transducer is not rocking, but instead it is rotating. The advantage of this method is that more pulse-echo events can be used for the beamformation of a single point, thus yielding lower side- and grating-lobes. Figure 1 illustrates the acquisition method. A transducer is continuously rotating at a constant angular velocity. A cylindrical wave (such as the wave transmitted by a single element) is transmitted by a group of elements. This is symbolized on the figure with a dark filling color. All elements are used in receive. A point in the volume is formed by a simple delay-and-sum beamformation:

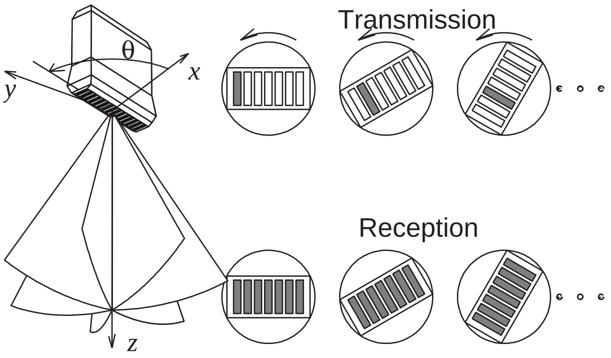

Figure 1: Acquisition and beamformation.

$$\mathbf{H}(\vec{x}) = \sum_{i\in\Omega_{xmt}(\vec{x})} \sum_{j=1}^{N} a_{ij}(\vec{x}) r_{ij}(t(\vec{x},\vec{x}_i,\vec{x}_j)), \qquad (1)$$

where $\vec{x}$ are the coordinates of the point being formed, $\Omega_{xmt}(\vec{x})$ is the set of transmissions, in which the cylindrical wave has passed through the imaged point, $\vec{x}_i$ is the center of the transmitted spherical wave, $\vec{x}_j$ is the position of the receiving element j, $r_{ij}(t)$ is the signal received by element j at transmission i, and N is the number of elements in the transducer. The time instance $t(\vec{x},\vec{x}_i,\vec{x}_j)$, at which a sample for the sum is taken, corresponds to the propagation time from the center of transmission $\vec{x}_i$ to the beamformed point $\vec{x}$ and back to the transducer element $\vec{x}_j$:

$$t = \frac{1}{c}(|\vec{x}-\vec{x}_i| + |\vec{x}_j - \vec{x}|), \qquad (2)$$

where c is the speed of sound.

The created images have a spatial resolution in the azimuth plane comparable to that of a standard B-mode scan [2]. The dynamic range, however, was limited to 45 dB, which is less than conventional images. In order for a scan method to be adopted for imaging, it must not only offer new advantages, but must perform in all other aspects at least as good as the existing methods. Several areas were identified as candidates for optimization:

- The generation of spherical waves. When the method was first implemented, the spherical waves were created by defocusing [1, 2, 3]. A similar effect could be achieved with focusing instead [4, 5].
- Optimization of the FM chirps. The pulses and filters used in [2] were not designed using the impulse response of the system as suggested in [6].
- The synchronization. The scans relied on the simultaneous start of the scan and the rotation of the transducer. Additional hardware for synchronization was to be built
- Reduce the grating-lobe level by creating virtual *receive* elements, whose directivity pattern has a narrow main lobe.

These topics are considered in the same order in the following sections of the paper.

II SPHERICAL WAVE GENERATION

Creating spherical waves is essential for the proposed method. There are two ways of generating spherical waves - using defocused or focused transmission. A defocused transmission with 13 transmit elements and a 20 μs chirp was used in [2]. This resulted in a penetration depth of up to 120 mm. Using a focused transmission has the advantage of increasing the energy sent into the body, thus increasing the penetration depth. Fig. 2 (left) shows the propagation path which must be used in the delay calculation for the beamfomration process [4]. The time at which a sample must be taken becomes (2):

$$t = \frac{1}{c}\left(|\vec{x}_i - \vec{x}_o| + |\vec{x} - \vec{x}_i| + |\vec{x}_j - \vec{x}|\right), \tag{3}$$

where the focal point is considered to be the virtual element $\vec{x}_i$, and $\vec{x}_o$ is the center of the aperture.

The result of using focused transmits is shown in the Fig. 2 (right). The spherical wave was created using 15 transmit elements. The focusing is at a depth of 5 mm in front of the transducer. A *conventional* 2 cycles sine pulse is used as an excitation in transmit. The cysts are detectable up to a depth of 140 mm, which is an increase of more than 20 mm compared to [2].

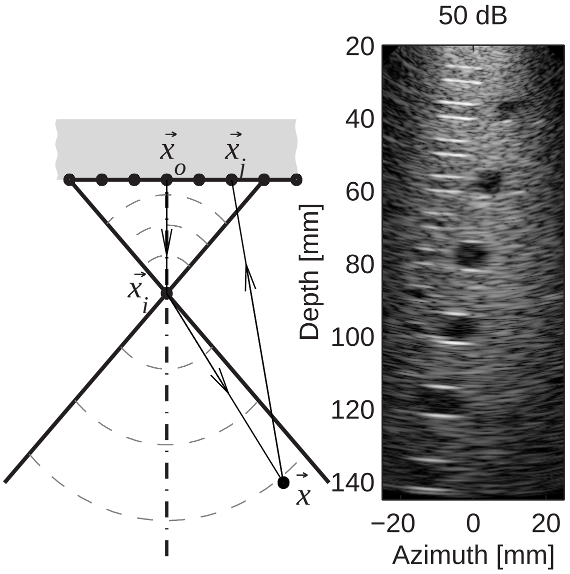

Figure 2: Delay calculations geometry (left). A B-mode slice created with a conventional pulse (right).

III OPTIMIZATION OF CHIRPS

In order to attain a better SNR codes are deployed. Coded excitation has previously been investigated in [6]. A linear FM chirp has been used as excitation,

$$s(t) = a(t)\sin\left(2\pi f_0 t + \frac{B}{2T}t^2\right), \; -\frac{T}{2} \le t \le \frac{T}{2}, \tag{4}$$

where $a(t)$ is a temporal weighting function, f_0 is the center frequency, B is the bandwidth being swept and T is the duration of the chirp. To achieve an acceptable axial resolution, a compression filter has to be used. Normally a matched filter with a temporal weighting function is applied

$$f(t) = g(t)s(-t). \tag{5}$$

However, the signal which is received at the transducer is in fact given by

$$r(t) = s(t) * h_{ti}(t) * h_{tr}(t), \tag{6}$$

where $h_{ti}(t)$ is the pulse echo impulse response of the interrogated tissue and $h_{tr}(t)$ is the pulse echo impulse response of the transducer. If the transducer pulse echo impulse response is known, one can compensate for it and replace (5) with,

$$\tilde{f}(t) = g(t)\tilde{s}(-t), \tag{7}$$

where $\tilde{s}(t) = s(t) * h_{tr}(t)$. The side lobes are then reduced below -50 dB as shown in Fig. 3.

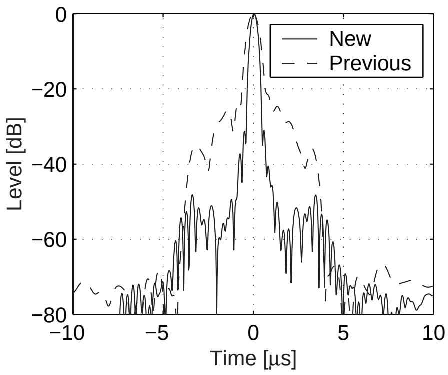

Figure 3: Reduction of the range side lobes with the new filter design.

IV SYNCHRONIZATION

The Vermon (Cedex, France) phased array rotating transducer is driven by a DC motor and controller supplied by Maxon Motor AG (Sachseln, Germany). The position of the rotating block is indicated by a rotation encoder and an end switch. The two sensors in the encoding block generate differential signals. An illustration of the positive signals from both sensors is shown in Fig. 4 (top part). The direction of rotation determines which signal precedes the other.

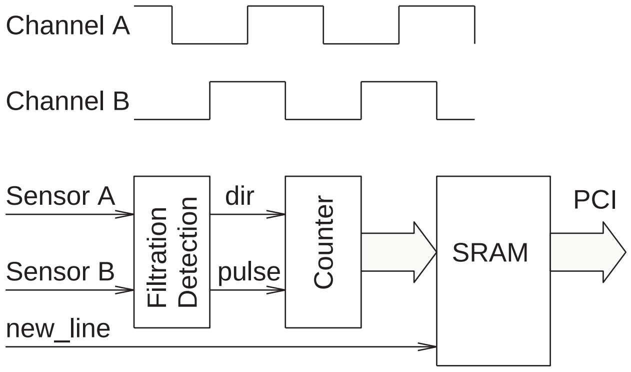

Figure 4: Rotary encoder sensor signals

An angle detector was built using the XC2S_EVAL board form CESYS GmbH (Herzogenaurach, Germany). The board features a PCI interface, Xilinx Spartan-2 FPGA and a SRAM block. The structure of the detector is shown in Fig. 4 (bottom part).

In that setup, the `new_line` signal is provided by a detection logic connected to one of the transmitter channels. The positive signals from both sensors are monitored and their relation is used to determine the position and the increment of a counter. Whenever a new image line acquisition is initiated, the present value of the counter is stored in the SRAM. After the end of the acquisition, the stored values are read through the PCI interface in a Linux environment. The error in the recorded position is less than ±0.3°.

V VIRTUAL RECEIVE ELEMENTS

For the different points in the image, a different number of transmissions is used as shown in Eq. 1. The points, which are close to the axis of rotation will be formed using a larger number of transmit events, and the points lying at the outskirts will be created with a smaller number of transmissions. The transmission order can be arranged such that the resolution of the image at all points is the same [4]. The side- and grating-lobe levels are, however, higher, when the number of emissions is less.

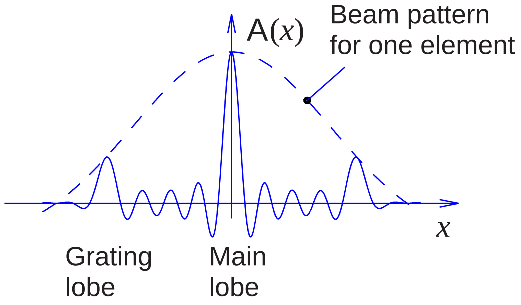

Figure 5: Illustration of suppression of the grating lobes

Fig. 5 shows how the grating lobes are suppressed. The distance between the grating lobes and the main lobe is inversely proportional to the number of elements in the aperture. The level of the grating lobes is suppressed by the radiation pattern of a single element. The bigger the element is, the lower the grating lobe level is.

One way to decrease the grating lobes is to *synthesize* receive elements, which are large and have a narrow directivity pattern. The distance between the centers of the receive elements must be maintained at $\lambda/2$. The synthesis of receive elements is done by summing the signals from a number of elements prior to the beamformation. In order to maintain the sensitivity for the different directions in the image, the signals are delayed such that the synthesized element ”looks” along scan line which will be beamformed (very much like a sunflower). Fig. 6 illustrates how a virtual receive element is synthesized. The dark dots mark the positions of the physical elements. The pale lines are the synthesized receive elements. The delays of the active elements, which are used to create one of the virtual receive elements are adjusted so as to align on the lines symbolizing the receive elements. If the currently beamformed line is perpendicular to the transducer

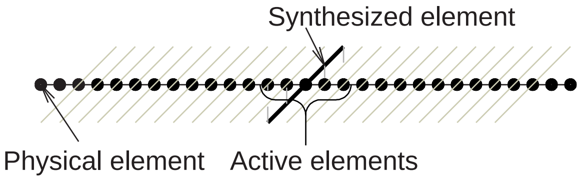

Figure 6: Illustration of the virtual receive elements

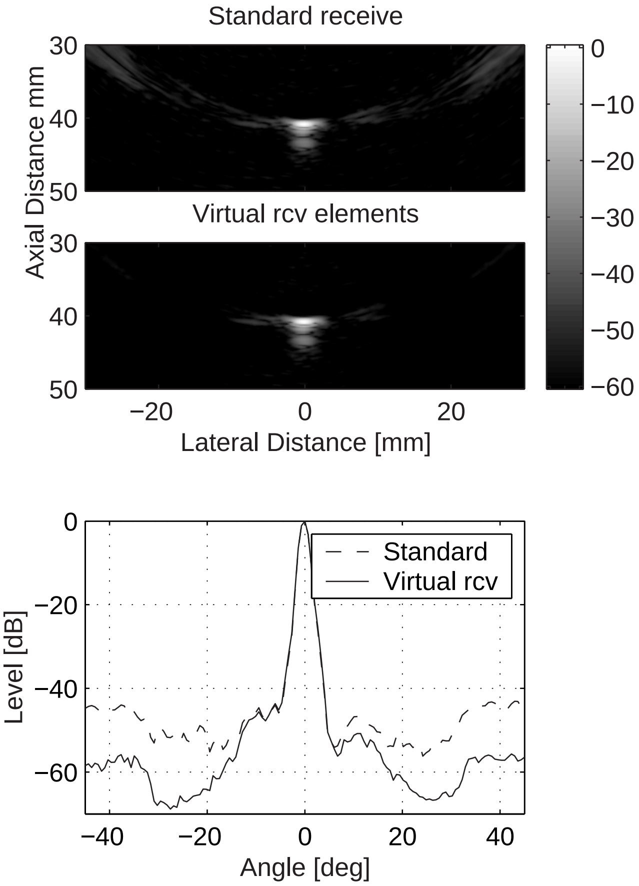

Figure 7: Sidelobe reduction using virtual receive elements.

surface, then synthesizing the receive elements is simply summing the received signals. If the beamformed line is tilted at an angle, then the signals must be appropriately delayed.

Figure 7 shows the reduction in the side lobe level when virtual receive elements are used. The image is created using only 13 emissions, which is the number of emissions normally used to create the points at the outskirts of the volume. Five elements were used in receive to generate a virtual receive element. The plot shows that the side- and grating-lobe level is reduced with more than 10 dB, which will correspondingly increase the contrast of the acquired images.

VI CONCLUSION

The 3D synthetic aperture imaging technique with a rotating array is capable of scanning 10 volumes per second. Previously it was shown that the images had resolution as the conventional B-mode images.

This paper presented the work on increasing the dynamic range and penetration depth of the images. The use of focused transmits allows to scan up to 140 mm with conventional sinusoidal pulses. The use of chirps increases the scan depth. The careful filter design suppresses the range side lobes to below -50 dB. The use of virtual receive elements reduces the grating lobes for the points at the edge of the volume with more than 10 dB. The method, thus, has the ability of generating 3D scans whose quality matches the quality of the conventional 2D scans.

VII ACKNOWLEDGMENTS

This work was supported by grant 9700883, 9700563 and 26-01-0178 from the Danish Science Foundation and by B-K Medical A/S Denmark.

VIII REFERENCES

[1] G. R. Lockwood, J. R. Talman, and S. S. Brunke. Real-time 3-D ultrasound imaging using sparse synthetic aperture beamforming. *IEEE Trans. Ultrason., Ferroelec., Freq. Contr.*, 45:980–988, 1998.

[2] S. I. Nikolov, R. Dufait, A. Schoisswohl, and J. A. Jensen. Three-dimensional real-time synthetic aperture imaging using a rotating phased array transducer. In *Proc. IEEE Ultrason. Symp.*, pages 1545–1548, 2002.

[3] M. Karaman, P. C. Li, and M. O'Donnell. Synthetic aperture imaging for small scale systems. *IEEE Trans. Ultrason., Ferroelec., Freq. Contr.*, 42:429–442, 1995.

[4] S. I. Nikolov and J. A. Jensen. Virtual ultrasound sources in high-resolution ultrasound imaging. In *Proc. SPIE - Progress in biomedical optics and imaging*, volume 3, pages 395–405, 2002.

[5] M. H. Bae and M. K. Jeong. A study of synthetic-aperture imaging with virtual source elements in B-mode ultrasound imaging systems. In *IEEE Trans. Ultrason., Ferroelec., Freq. Contr.*, volume 47, pages 1510–1519, 2000.

[6] T. X. Misaridis and J. A. Jensen. An effective coded excitation scheme based on a predistorted FM signal and an optimized digital filter. In *Proc. IEEE Ultrason. Symp.*, volume 2, pages 1589–1593, 1999.

CHAPTER

EIGHT

Conclusion

This dissertation has investigated the possibility of utilizing spatial encoding in medical ultrasound imaging. The purpose of spatial encoding is to let several transmitters be active simultaneously and separate the signals at the receiver. By doing so, the information originating from a specific transmitter can be processed independently of the signals from the other transmitters, even if the data was acquired at the same time. The potential benefits are twofold:

- More acoustic energy can be transmitted in every transmission and the signals from the different transmitters can still be separated in receive. This makes it possible to maintain good focusing but by increasing the transmitted energy the SNR is increased.
- More information can be acquired per transmission. If data acquired at different instances in time are processed to yield a combined result, relative motion between the data acquisitions will degrade the processing and result in motion artifacts. By acquiring more data per transmission this effect can be reduced.

Primarily, a method based on frequency division has been investigated. The available transducer bandwidth is divided into a number of frequency bands with approximately disjoint spectral support by designing waveforms with spectral support in the desired frequency range. During transmission each transmitter is assigned one of the narrow band waveforms. The signals representing a specific transmitter can be separated at the receiver using a simple filtering operation (matched- or bandpass filtering).

To show that the method works, it has been tested experimentally. The performance in terms of contrast and resolution of the frequency division approach is comparable to that of a conventional STA system with a linear FM signal as excitation waveform. Improvement in SNR and penetration depth was also documented when comparing the frequency division approach to conventional STA. Future work should be focused on to demonstrate that the method actually works invivo. Therefore a clinical study should be initiated. Code design is also a topic which requires further work.

Secondly, as an offspring from the frequency division approach, a method for spatial encoding inspired from tele-communication was developed. Here, the transmitters are encoded using pseudo-random sequences. The signals are separated at the receiver using an estimation based approach. By using this method, it is possible to separate the signals after only one transmission.

The code division approach has been tested experimentally where it displayed similar performance in terms of contrast and resolution as a conventional STA system.[1] However, several theoretical challenges still remain. Foremost, the requirement on a minimum code duration to solve the estimation problem must be eliminated. A possible path is to look into code sequences which are cyclically orthogonal. The periodic cross-correlation between such sequences is zero, and this could potentially be exploited. Moreover, the code design should be optimized so that the SNR reaches the theoretical limit.

---

[1] In the reference experiments, a sinusoid excitation was used.

Bibliography

[1] L. E. Kinsler, A. R. Frey, A. B. Coppens, and J. V. Sanders, *Fundamentals of Acoustics*, John Wiley & Sons, New York, third edition, 1982.

[2] A. D. Pierce, *Acoustics, An Introduction to Physical Principles and Applications*, Acoustical Society of America, New York, 1989.

[3] J. A. Jensen, "A model for the propagation and scattering of ultrasound in tissue," *J. Acoust. Soc. Am.*, vol. 89, pp. 182–191, 1991a.

[4] J. A. Jensen and N. B. Svendsen, "Calculation of pressure fields from arbitrarily shaped, apodized, and excited ultrasound transducers," *IEEE Trans. Ultrason., Ferroelec., Freq. Contr.*, vol. 39, pp. 262–267, 1992.

[5] J. A. Jensen, *Estimation of Blood Velocities Using Ultrasound: A Signal Processing Approach*, Cambridge University Press, New York, 1996.

[6] D. H. Johnson and D. E. Dudgeon, *Array signal processing. Concepts and techniques.*, Prentice-Hall., Englewood Cliffs, New Jersey, 1993.

[7] J. W. Goodman, *Introduction to Fourier optics*, McGraw Hill Inc., New York, second edition edition, 1996.

[8] S. W. Flax and M. O'Donnell, "Phase-aberration correction using signals from point reflectors and diffuse scatterers: basic principles," *IEEE Trans. Ultrason., Ferroelec., Freq. Contr.*, vol. 35, pp. 758–767, 1988.

[9] G. E. Trahey and D. Zhao, "Quality factors for phase aberration correction in medical ultrasound," in *Proc. SPIE - Int. Soc. Opt. Eng.*, 1990, vol. 1231, pp. 40–49.

[10] M. Karaman and H. Koymen, "A phase aberration correction method for ultrasound imaging," *IEEE Trans. Ultrason., Ferroelec., Freq. Contr.*, vol. 40, pp. 275–282, 1993.

[11] H. Baba, R. Shinomura, Y. Miwa, N. Nakata, and J. Harada, "Clinical evaluation of real-time phase-aberration correction system," in *Proc. IEEE Ultrason. Symp.*, 2000.

[12] Y. Li and B. Robinson, "Phase aberration correction using near-field signal redundancy-two-dimensional array algorithms," in *Proc. IEEE Ultrason. Symp.*, 2000.

[13] G. R. Lockwood and F.S. Foster, "Design of sparse array imaging systems," in *Proc. IEEE Ultrason. Symp.*, 1995, pp. 1237–1243.

[14] G. R. Lockwood, P-C. Li, M. O'Donnell, and F. S. Foster, "Optimizing the radiation pattern of sparse periodic linear arrays," *IEEE Trans. Ultrason., Ferroelec., Freq. Contr.*, vol. 43, pp. 7–14, 1996.

[15] G. R. Lockwood, J. R. Talman, and S. S. Brunke, "Real-time 3-D ultrasound imaging using sparse synthetic aperture beamforming," *IEEE Trans. Ultrason., Ferroelec., Freq. Contr.*, vol. 45, pp. 980–988, 1998.

[16] M.I. Skolnik, *Introduction to Radar Systems*, McGraw-Hill, New York, 1980.

[17] M.I. Skolnik, *Radar Handbook*, McGraw-Hill, New York, second edition, 1990.

[18] M. Soumekh, *Synthetic aperture radar. Signal processing with MATLAB algorithms*, John Wiley & Sons, Inc., New York, 1999.

[19] J. T. Ylitalo and H. Ermert, "Ultrasound synthetic aperture imaging: monostatic approach," *IEEE Trans. Ultrason., Ferroelec., Freq. Contr.*, vol. 41, pp. 333–339, 1994.

[20] J. T. Ylitalo, "Synthetic aperture ultrasound imaging using a convex array," in *Proc. IEEE Ultrason. Symp.*, 1995, pp. 1337–1340.

[21] J. T. Ylitalo, "A fast ultrasonic synthetic aperture imaging method: application to NDT," *Ultrasonics*, pp. 331–333, 1996.

[22] S. I. Nikolov, K. Gammelmark, and J. A. Jensen, "Recursive ultrasound imaging," in *Proc. IEEE Ultrason. Symp.*, 1999, vol. 2, pp. 1621–1625.

[23] S. I. Nikolov and J. A. Jensen, "Application of different spatial sampling patterns for sparse array transducer design," *Ultrasonics*, vol. 37, no. 10, pp. 667–671, 2000.

[24] S. I. Nikolov, *Synthetic aperture tissue and flow ultrasound imaging*, Ph.D. thesis, Ørsted•DTU, Technical University of Denmark, 2800, Lyngby, Denmark, 2001.

[25] J. A. Jensen and S.I. Nikolov, "Velocity estimation in synthetic aperture imaging, International patent," Priority date: September 2001.

[26] J. A. Jensen and S.I. Nikolov, "Recursive ultrasound imaging, International patent," Priority date: April 2000.

[27] J. A. Jensen, O. Holm, L. J. Jensen, H. Bendsen, H. M. Pedersen, K. Salomonsen, J. Hansen, and S. Nikolov, "Experimental ultrasound system for real-time synthetic imaging," in *Proc. IEEE Ultrason. Symp.*, 1999, vol. 2, pp. 1595–1599.

[28] J. A. Jensen, S. I. Nikolov, T. Misaridis, and K. L. Gammelmark, "Equipment and methods for synthetic aperture anatomic and flow imaging," in *Proc. IEEE Ultrason. Symp.*, 2002, pp. 1518–1527, (Invited).

[29] J. A. Jensen and S. I. Nikolov, "Directional synthetic aperture flow imaging," *IEEE Trans. Ultrason., Ferroelec., Freq. Contr.*, p. Submitted for publication, 2003.

[30] J. A. Jensen and S. I. Nikolov, "A method for real-time three-dimensional vector velocity imaging," in *Proc. IEEE Ultrason. Symp.*, 2003, pp. 1582–1585.

[31] J. T. Ylitalo, "On the signal-to-noise ratio of a synthetic aperture ultrasound imaging method," *Eur. J. Ultrasound*, pp. 277–281, 1996.

[32] M. O'Donnell and L. J. Thomas, "Efficient synthetic aperture imaging from a circular aperture with possible application to catheter-based imaging," *IEEE Trans. Ultrason., Ferroelec., Freq. Contr.*, vol. 39, pp. 366–380, 1992.

[33] M. Karaman, P. C. Li, and M. O'Donnell, "Synthetic aperture imaging for small scale systems," *IEEE Trans. Ultrason., Ferroelec., Freq. Contr.*, vol. 42, pp. 429–442, 1995.

[34] C. H. Frazier and W. D. O'Brien, "Synthetic aperture techniques with a virtual source element," *IEEE Trans. Ultrason., Ferroelec., Freq. Contr.*, vol. 45, pp. 196–207, 1998.

[35] M. H. Bae and M. K. Jeong, "A study of synthetic-aperture imaging with virtual source elements in B-mode ultrasound imaging systems," in *IEEE Trans. Ultrason., Ferroelec., Freq. Contr.*, 2000, vol. 47, pp. 1510–1519.

[36] S. I. Nikolov and J. A. Jensen, "Virtual ultrasound sources in high-resolution ultrasound imaging," in *Proc. SPIE - Progress in biomedical optics and imaging*, 2002, vol. 3, pp. 395–405.

[37] K. L. Gammelmark and J. A. Jensen, "Multi-element synthetic transmit aperture imaging using temporal encoding," in *Proc. SPIE: Progress in biomedical optics and imaging*, 2002, vol. 3, pp. 25–36.

[38] K. L. Gammelmark and J. A. Jensen, "Experimental study of convex coded synthetic transmit aperture imaging," in *Proc. IEEE Ultrason. Symp.*, 2002, pp. 1573–1576.

[39] K. L. Gammelmark and J. A. Jensen, "Multielement synthetic transmit aperture imaging using temporal encoding," *IEEE Trans. Med. Imag.*, vol. 22, no. 4, pp. 552–563, 2003.

[40] M. H. Pedersen, K. L. Gammelmark, and J. A. Jensen, "Preliminary in-vivo evaluation of convex array synthetic aperture imaging," in *Proc. SPIE - Progress in biomedical optics and imaging*, 2004, pp. 33–43.

[41] M. H. Pedersen, K. L. Gammelmark, and J. A. Jensen, "In-vivo evaluation of convex array synthetic aperture imaging," *Ultrasound Med. Biol.*, p. Submitted, 2004.

[42] K. Gammelmark, *Improving the Image Quality of Synthetic Transmit Aperture Ultrasound Images*, Ph.D. thesis, Ørsted•DTU, Technical University of Denmark, 2800, Lyngby, Denmark, 2004.

[43] FDA, "Information for manufacturers seeking marketing clearance of diagnostic ultrasound systems and transducers," Tech. Rep., Center for Devices and Radiological Health, United States Food and Drug Administration, 1997.

[44] S. Haykin, *Communication Systems*, John Wiley & Sons, Inc., 2001.

[45] M. Schwartz, *Information transmission, modulation, and noise*, McGraw-Hill, 1959.

[46] T. X. Misaridis and J. A. Jensen, "An effective coded excitation scheme based on a predistorted FM signal and an optimized digital filter," in *Proc. IEEE Ultrason. Symp.*, 1999, vol. 2, pp. 1589–1593.

[47] T. X. Misaridis, K. Gammelmark, C. H. Jørgensen, N. Lindberg, A. H. Thomsen, M. H. Pedersen, and J. A. Jensen, "Potential of coded excitation in medical ultrasound imaging," *Ultrasonics*, vol. 38, pp. 183–189, 2000.

[48] T. X. Misaridis, M. H. Pedersen, and J. A. Jensen, "Clinical use and evaluation of coded excitation in B-mode images," in *Proc. IEEE Ultrason. Symp.*, 2000, vol. 2, pp. 1689–1693.

[49] T. Misaridis, *Ultrasound imaging using coded signals*, Ph.D. thesis, Ørsted•DTU, Technical University of Denmark, Lyngby, Denmark, 2001.

[50] T. Misaridis and J. A. Jensen, "Use of modulated excitation signals in ultrasound, Part I: Basic concepts and expected benefits," *IEEE Trans. Ultrason., Ferroelec., Freq. Contr.*, p. Submitted for publication, 2002.

[51] T. Misaridis and J. A. Jensen, "Use of modulated excitation signals in ultrasound, Part II: Design and performance for medical imaging applications," *IEEE Trans. Ultrason., Ferroelec., Freq. Contr.*, p. Submitted for publication, 2002.

[52] T. Misaridis and J. A. Jensen, "Use of modulated excitation signals in ultrasound, Part III: High frame rate imaging," *IEEE Trans. Ultrason., Ferroelec., Freq. Contr.*, p. Submitted for publication, 2002.

[53] R. Y. Chiao and L. J. Thomas, "Synthetic transmit aperture using orthogonal golay coded excitation," in *Proc. IEEE Ultrason. Symp.*, 2000, pp. 1469–1472.

[54] R. Y. Chiao and X. Hao, "Coded excitation for diagnostic ultrasound: a system developer's perspective," *IEEE Trans. Ultrason., Ferroelec., Freq. Contr.*, vol. 52, pp. 160–170, 2005.

[55] J. A. Jensen, D. Gandhi, and W. D. O'Brien, "Ultrasound fields in an attenuating medium," in *Proc. IEEE Ultrason. Symp.*, 1993, pp. 943–946.

[56] R. Y. Chiao, L. J. Thomas, and S. D. Silverstein, "Sparse array imaging with spatially-encoded transmits," in *Proc. IEEE Ultrason. Symp.*, 1997, pp. 1679–1682.

[57] J. Shen and E. S. Ebbini, "A new coded-excitation ultrasound imaging system–part I: Basic principles," *IEEE Trans. Ultrason., Ferroelec., Freq. Contr.*, vol. 43, pp. 131–140, 1996.

[58] J. Shen and E. S. Ebbini, "A new coded-excitation ultrasound imaging system–part II: Operator design," *IEEE Trans. Ultrason., Ferroelec., Freq. Contr.*, vol. 43, pp. 141–148, 1996.

[59] M.K. Jeong and E.S. Ebbini, "Optimal transmit/receive beam synthesis for coded-excitation pulse-echo imaging," in *Proc. IEEE Ultrason. Symp.*, 2000, pp. 1219–1222.

[60] S. Haykin, *Adaptive Filter Theory*, Prentice-Hall, Upper Saddle River, New Jersey, 2002.

[61] F. Gran and J. A. Jensen, "Multi element synthetic aperture transmission using a frequency division approach," in *Proc. IEEE Ultrason. Symp.*, 2003, pp. 1942–1946.

[62] A. V. Oppenheim and R. W. Scafer, *Digital Signal Processing*, Prentice Hall, 1975.

[63] J. A. Jensen, O. Holm, L. J. Jensen, H. Bendsen, S. I. Nikolov, B. G. Tomov, P. Munk, M. Hansen, K. Salomonsen, J. Hansen, K. Gormsen, H. M. Pedersen, and K. L. Gammelmark, "Ultrasound research scanner for real-time synthetic aperture image acquisition," *IEEE Trans. Ultrason., Ferroelec., Freq. Contr.*, vol. 52 (5), May 2005.

[64] F. Gran and J. A. Jensen, "Frequency division transmission and synthetic aperture reconstruction," *IEEE Trans. Ultrason., Ferroelec., Freq. Contr.*, vol. Submitted for publication, 2004.

[65] F. Gran and J. A. Jensen, "Spatio-temporal encoding using narrow-band linearly frequency modulated signals in synthetic aperture ultrasound imaging," in *Proc. SPIE - Progress in biomedical optics and imaging*, 2005, p. Accepted for publication.

[66] J. A. Jensen and S. I. Nikolov, "Transverse flow imaging using synthetic aperture directional beamforming," in *Proc. IEEE Ultrason. Symp.*, 2002, pp. 1488–1492.

[67] F. Gran and J. A. Jensen, "Directional velocity estimation using a spatio-temporal encoding technique based on frequency division for synthetic transmit aperture ultrasound," *IEEE Trans. Ultrason., Ferroelec., Freq. Contr.*, vol. Submitted for publication, 2005.

[68] G. Kang, E. Kosta, M. Weckerle, and E. Schulz, "Optimum channel estimation over frequency-selective fading channel in multiple antenna systems," in *In Communication Technology Proceedings ICCT 2003*, 2003, pp. 1799–1803.

[69] L. Ljung, *System Identification, theory for the user*, Prentice-Hall., New Jersey, 1987.

[70] F. Gran, J. A. Jensen, and A. Jakobsson, "A code division technique for multiple element synthetic aperture transmission," in *Proc. SPIE - Progress in biomedical optics and imaging*, 2004, p. Submitted for publication.

[71] F. Gran and J. A. Jensen, "Identification of pulse echo impulse responses for multi source transmission," in *Conference Record of Thirty-Eighth Annular Asilomar Conference on Signals, Systems, and Computers*, 2004, vol. 1, pp. 168–172.

[72] F. Gran and J. A. Jensen, "Spatial encoding using code division for fast ultrasound imaging," *IEEE Trans. Ultrason., Ferroelec., Freq. Contr.*, vol. Submitted for publication, 2005.

[73] J. Udesen, F. Gran, and J. A. Jensen, "Fast color flow mode imaging using plane wave excitation and temporal encoding," in *Proc. SPIE - Progress in biomedical optics and imaging*, 2005, p. Accepted for publication.

[74] S. I. Nikolov, B. Tomov, F. Gran, R. Dufait, and J. A. Jensen, "Further development of synthetic aperture real-time 3d scanning with a rotating phased array," in *Proc. IEEE Ultrason. Symp.*, 2003, pp. 1899–1902.